AN EXPERIMENTAL AND THEORETICAL STUDY OF DENSITY-WAVE OSCILLATIONS IN TWO-PHASE FLOW

George Yadigaroglu
Arthur E. Bergles

Report No. DSR 74629-3
(HTL No. 74629-67)

Contract Nonr-3963(15)

Engineering Projects Laboratory
Department of Mechanical Engineering
Massachusetts Institute of Technology
Cambridge, Massachusetts 02139

December 1969

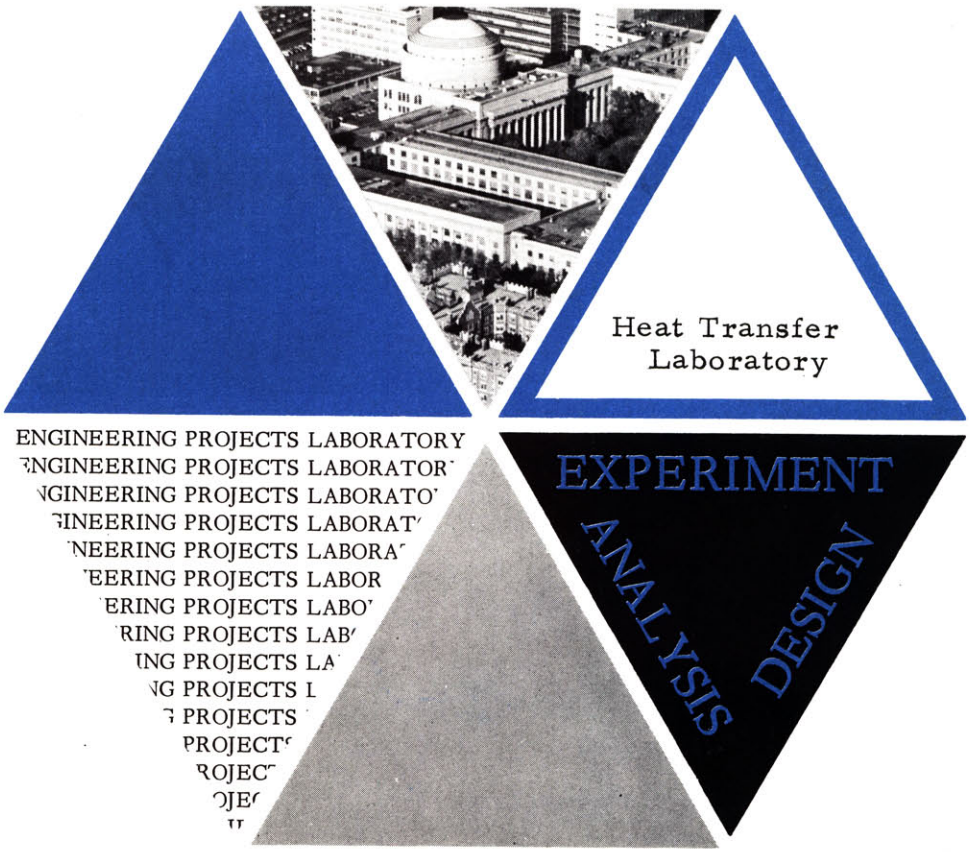

AN EXPERIMENTAL AND THEORETICAL STUDY OF DENSITY-WAVE OSCILLATIONS IN TWO-PHASE FLOW

George Yadigaroglu

Arthur E. Bergles

prepared for

Power Branch
Office of Naval Research
Department of the Navy
Washington, D.C.

under

Contract Nonr-3963 (15)

Engineering Projects Laboratory
Department of Mechanical Engineering
Massachusetts Institute of Technology
Cambridge, Massachusetts 02139

Report DSR 74629-3

ERRATA

p. 39 Title of Table 2.3: replace *Sections* by *Lengths*

p. 62 16th line: replace *required* by *specified*

p. 139 2nd line: replace *boiling channel* by *single-phase region*

Fig. 3.4 Ordinate should be *6* instead of *66*

Fig. 4.1 Solid lines refer to *UNIFORM* and dotted lines to *COSINE* heat flux distribution

Fig. 5.2 Labeling of curves in lower figure: Replace $\arg Q^*$ and $\arg H^*$ by $2\pi - \arg Q^*$ and $2\pi - \arg H^*$, respectively

Fig. 5.6 4th line of caption: delete *Eq. (5.38)*

Fig. 5.12b Labeling of the curves:
label *0.75* the curve labeled *0.125*
label *0.125* the unlabeled curve

Fig. 5.14 Label horizontal axes z
Replace δh by δh°_{bb}
Delete ° from δz°_{bb}
Delete the ' from $\delta h'_{bb}$
Replace δh_f by δh°_{fbb}

Fig. 5.15 Replace δh by δh°_{bb}
Delete the ° from δz°_{bb}

Fig. 7.7 4th line of caption: *model* should be *mode*

Fig. 8.2 Label δw_o the arrow entering block P_2

2 5 70

Abstract

A theoretical and experimental investigation of fundamental aspects of density-wave oscillations was undertaken. The experimental Freon-113 loop was operated at atmospheric pressure level with constant pressure drop across a single test channel. A wide range of inlet temperatures, flows and heat inputs was covered. The regions of unstable operation of the channel were mapped for both uniform and "cosine" heat flux distributions. The effect of the cosine distribution was stabilizing. The period of the oscillations was approximately equal to twice the "transit time", defined as the sum of one half the residence time of a fluid particle in the single-phase region plus the vapor transit time in the two-phase region.

At high subcoolings and low power levels unexpected "higher-order" oscillations were detected. These were characterized by frequencies that were multiples of the expected values. When the regions of unstable operation were classified according to the "order" of the oscillation, a coherent stability map emerged. The order of the oscillation is related to the number of nodes in the standing enthalpy waves generated by oscillating flow in the single-phase region.

Analytically the stability of the channel is investigated by oscillating the inlet flow. The linearized dynamics of the single-phase region account for heat storage in the channel walls and for the effects of the static and dynamic pressure variations on the movements of the boiling boundary. The description of oscillatory two-phase flow is Lagrangian and distributed in space. Considerable simplification in the calculation of the pressure drop is achieved via subdivision of the channel into intervals separated by points of constant enthalpy. The space variations of the fluid properties are taken rigorously into account while the variations of the saturation enthalpy and the relative velocity between the phases are treated approximately.

The theoretical procedures used for predicting the steady-state condition in the boiling channel were tested by extensive pressure drop measurements. The predictions of the stability model are compared to the experimental observations.

Acknowledgements

This investigation was sponsored by the Power Branch of the Office of Naval Research under Contract Nonr-3963 (15).

Thanks are due to Professors E.A. Mason, P. Griffith and H. Fenech for discussion of various aspects of this work.

The Engineering Projects Laboratory staff gave technical assistance. The machine computations were performed at the M.I.T. Information Processing Center and at the Mechanical Engineering Department Computer Facility. Acknowledgement is also due to Miss Anne Hsu for her diligent typing of the manuscript.

TABLE OF CONTENTS

LIST OF FIGURES

LIST OF TABLES

NOMENCLATURE

Symbols which occur only infrequently and are explained in immediate context have not been included in this list. A coherent system of units is assumed; the conversion factors that are necessary when British units are used were not included in the formulas.

Latin Alphabet

A	flow area
A(z)	coefficient, Eq. (5.29)
a	coefficient defined by Eq. (5.9)
B	coefficient, Eq. (5.30)
C	coefficient, Eq. (5.13)
c	specific heat of the liquid
D	inside diameter of the channel
d	thickness of the channel wall
E(z)	coefficient, Eq. (5.14)
F(s)	complex expression, Eq. (5.20)
f	Fanning friction factor
G	mass flux
g	acceleration of gravity
H(z,s)	flow-to-local-enthalpy transfer function, Eq. (5.34)
h	enthalpy
h_c	forced convection heat transfer coefficient (Chapter 5)

h_{fg}	latent heat of vaporization
j	imaginary unit
j	volumetric flux density (Chapter 6)
j_ζ	volumetric flux density in the moving frame of reference (Chapter 6)
K(s)	complex expression, Eq. (5.32)
k	thermal conductivity of the wall
L_h	length of the channel from Station 1 to exit, Fig. 2.2
L(s)	complex expression, Eq. (5.33)
ℓ	length
P	heated perimeter of the channel
Pr	Prandtl number
$P_{lw}(s)$	flow-to-pressure-drop-in-the-single-phase-region transfer function, Eq. (5.51)
P_{lz}	position-of-the-boiling-boundary-to-pressure-drop-in-the-single-phase-region transfer function, Eq. (5.50)
p	pressure
Q(z,s)	flow-to-heat-flux transfer function, Eq. (5.36)
q	total heat input rate
q_i	heat input rate per test length (i = 1,7)
q'	linear heat input rate
q"	heat flux
q'''	volumetric power density
Re	Reynolds number
s	complex frequency, Laplace variable (Chapter 5)
s	slope, Section 6.2.4

T	temperature
t	time
V	velocity
v	specific volume
v_{fg}	$v_g - v_f$
$W(s)$	open loop transfer function, Chapter 8
w	mass flow rate
$Z(s)$	flow-to-position of-the-boiling boundary transfer function, Eq. (5.48)
z	axial coordinate, measured from Station 1, Fig. 2.2
z'	axial coordinate, measured from exit, $z' = L_h - z$
z_{bb}	coordinate of the boiling boundary, measured from Station 1
z°_{in}	equivalent inertia length, Section 5.4.1

Greek Alphabet

α	void fraction
α	thermal diffusivity (Chapter 5) of the wall
ζ	coordinate in the moving frame of reference, Section 6.2
λ	wavelength, Section 5.2.1.2
μ	viscosity
ρ	average density of the liquid-gas mixture, $\rho_g \alpha + \rho_f (1-\alpha)$
σ	surface tension
τ	period of the oscillation
τ_c	time constant, Eq. (5.39)

τ_h	convective time constant, Eq. (5.38)
τ_k	wall conduction time constant, Eq. (5.37)
$\phi^2_{\ell tt}$	Lockhart-Martinelli, two-phase friction multiplier (relative to liquid phase)
ϕ^2_{gtt}	Lockhart-Martinelli two-phase friction multiplier (relative to gas phase)
Ω	coefficient, Eq. (6.3)
ω	angular frequency, $2\pi/\tau$

Operators

d	differential operator
∂	partial derivative
Δ	difference
δ	small perturbation
Σ	sum
$\bar{}$	average

Subscripts

ac	acceleration
b	bulk (mixed-mean)
bb	boiling boundary
d	point of net vapor generation, Section 3.5
e	segment exit
ex	channel exit
f	liquid phase
f	feedback (Chapter 8)

fg	transition from liquid to vapor
fr	friction
g	gas phase
gr	gravity
i	inlet of segment
i	enthalpy mesh point (Chapter 6)
in	inlet of heated section
in	inertia (Chapters 5 and 8)
ℓ	liquid phase
sat	saturation
subb	subcooling with respect to the boiling boundary, Section 7.4
suin	subcooling with respect to the heated channel inlet, Section 7.4
o	average value at inlet (Station 0 or 1)
1	single-phase region
2	two-phase region
00, 0, 1, ..., 8, ex	Stations along the channel, Fig. 2.2

Supercripts

k	center-of-volume-plane index, Section 6.4.2
o	reference steady state
*	dimensionless quantity
^	peak amplitude

Chapter 1

INTRODUCTION AND SUMMARY

The study of instabilities occurring in two-phase flow systems was initiated approximately thirty years ago. Greatly increased attention was given to these problems in the last fifteen to twenty years with the advent of high power density boilers and boiling water reactors (BWR). Review articles that appeared in this period follow the historical developments [1-6]*.

The particular subject of this work, the so-called "density-wave oscillations," will be outlined in this introductory chapter within the larger framework of two-phase stability phenomena. A brief preview of the subsequent chapters is given in Sections 1.4 and 1.5.

Chapter 2 describes the experimental apparatus. Chapters3 and 4 deal with the prediction and the measurement of the steady-state conditions in the channel. They need little introduction and can be left aside without loss of continuity by the reader more interested in the stability problems. Chapter 5 treats the dynamics of the single-phase region. A model for the dynamics of the two-phase region is developed in Chapter 6. The stability experiments are described in Chapter 7. The dynamic models developed in Chapters 5 and 6 are then assembled in Chapter 8 to predict the threshold of stability. The work is concluded in Chapter 9. Each chapter can be read independently as cross references

*Numbers in square brackets designate references listed in pages 168-174

provide the necessary links to other sections.

1.1 Definition of the Problem

It is first necessary to make the distinction between microscopic instabilities which occur locally at the liquid-gas interface, for example the well known Helmholtz and Taylor instabilities, bubble collapse, etc., and macroscopic instabilities which involve the entire two-phase flow channel. Acoustic waves, shock waves, and critical flow phenomena constitute another important family of two-phase dynamics problems characterized by relatively high frequencies. Only macroscopic channel instabilities, involving relatively slow transients (time constants of the order of a few seconds) will be considered here. These can be essentially categorized as instabilities of flow distribution among several parallel channels and flow instabilities in a single channel. The first, is beyond the scope of this work which deals only with one important class of single-channel flow instabilities. The major distinction between single and parallel channels stems from the formulation of the boundary conditions. For example, consider a BWR core. To study the redistribution of flow among the subassemblies in the case of some large external disturbance, it is necessary to examine the entire primary loop. On the contrary, when the stability of the hot channel alone is investigated, it is sufficient to specify the pressure at the inlet and exit plenums, as flow changes in a single channel will not affect significantly the total flow, and consequently the pressure drop, across the core. Therefore, whenever the conditions at the channel limits are sufficiently specified at all

times, the problem reduces to a single-channel instability.

There has been considerable confusion in the past as many experiments were designed without making an effort to clearly define the boundaries of the unstable part of the system. In particular, system-induced instabilities have often interfered with more fundamental oscillation modes. Furthermore, the term "parallel channels" has been used frequently to recall a constant-pressure-drop boundary condition, while it might have been used more properly to denote flow distribution phenomena.

It is clear that it is necessary to solve first the stability problems in a single channel before attempting to synthesize the parallel-channel solutions. The discussion that follows is limited to single channels.

The thermo-hydrodynamic instabilities occurring in a boiling channel can be classified in several ways. According to the circulation mode, it is possible to make the distinction between instabilities occurring with natural and forced convection. Considering, however, the similarity of the appropriate boundary conditions this distinction is removed. Only the range of certain parameters will differ in the two cases.

A more fundamental approach would be to characterize the instabilities by the nature of the phenomena taking place. Few investigators have explicitly done so in the past. The general term of "two-phase flow instabilities" was used for dissimilar phenomena. Recent publications [5,7] have finally brought some order and clarity, and, most importantly, categorized the various kinds of possible instabilities.

The distinction will be made first between static or excursive and

dynamic or oscillatory instabilities. The Ledinegg instability is the classical example of the first type. Stenning and Veziroglu [7], in their experiments with Freon-11, have encountered two major modes of dynamic instabilities, which they have termed "density-wave oscillations" and "pressure-drop oscillations." Their findings are believed to be representative of the general situation. They have also reported the occurrence of "thermal oscillations" in their experimental apparatus, and postulated a mechanism for these based on a relatively rare combination of flow and heat transfer characteristics. Instabilities generated by particular phenomena (flow regime transitions, nucleation, etc.) that for some reason acquire a major importance under unusual conditions, for example these thermal oscillations, seem to defy à priori classification. Therefore, the list of instability mechanisms should be left open to include these minor types.

Pressure-drop oscillations occur (like the Ledinegg instability) when the pressure drop across the channel decreases with increasing flow. They contrast, however, the Ledinegg instability by their oscillatory nature. Their frequency is governed by the volume and compressibility of the system, and they occur in the low exit quality region only, where the pressure drop - flow rate characteristic exhibits a negative slope.

1.1.1 Density Wave Oscillations - The Physical Phenomenon

The density-wave oscillations that constitute the subject of this work are due to the multiple regenerative feedbacks between the flow rate, the vapor generation rate, and the pressure drop. Inlet flow fluctuations

create enthalpy perturbations in the single-phase region. When these reach the boiling boundary they are transformed into void fraction perturbations that travel with the flow along the channel, creating a dynamic pressure drop oscillation in the two-phase region. Since the total pressure drop is imposed upon the channel externally, this two-phase pressure perturbation produces a perturbation of the opposite sign in the single-phase region, which in turn creates further inlet flow variations. It is evident that with correct timing, the perturbations can acquire appropriate phases and become self sustained. Therefore, transportation delays in the channel are of paramount importance for the stability of the system, although inertia effects are also responsible for the generation of phase shifts. This led to the suggestion that these oscillations be called "time-delay" oscillations. Emphasizing the feedback mechanism, Neal and Zivi [5] named them "flow-void feedback instabilities".

Oscillation of any physical system requires a mechanism for intermittent storage and release of some particular form of energy. In the present case, for constant heat input, the total energy contained within the channel varies according to the mass flow rate. At high flow rates little energy is stored; when the flow diminishes the amount of energy contained in the channel increases. Transient heat storage in the channel walls, variation of the saturation temperature with pressure, compressibility effects, and thermal non-equilibrium constitute auxiliary energy storage and release mechanisms, that can create additional phase shifts.

Many other secondary phenomena also contribute to the fundamental feedback mechanism described above, e.g.: variable heat transfer, flow

regime changes, the relative velocity between the phases, etc. Although none of these is the cause of density-wave oscillations, they might acquire under certain conditions a controlling role.

The class of instabilities considered here will be further specialized by the boundary condition that the pressure drop across the boiling channel is maintained constant. This is approximately the case when the pressure drop-flow rate characteristic of the system is sufficiently "stiff." The boundary condition is even closer approximated in the most unstable channel (probably the hot channel) of a large array of parallel channels. Furthermore a natural circulation loop can be described in this fashion if the cold leg is included as part of the channel [5].

1.2 Density-Wave Oscillations in Boiling Water Reactors

The safety and operational evaluation of the BWR's provided the main incentive for the numerous two-phase flow stability studies. Although the first investigators attempted to explain the flow instabilities in BWR's in terms of the rather unique reactivity-void coupling, e.g. [8], it was soon realized that these phenomena could usually be accounted for by purely hydrodynamic considerations. The void-reactivity feedback plays an incidental, but contributing, role in the overall reactor stability. It is now generally believed that the thermo-hydrodynamics can be profitably studied independently of the dynamics of the reactor. On this premise several theoretical investigations [9-18] and test loop stability experiments [19-24] followed.

The early BWR's operated at relatively low pressure levels, and consequently their power density was limited by flow stability considerations. The large commercial BWR's built or planned in the United States in the late sixties, operate at higher pressures and have overcome the stability problems. Their thermal output is limited by the critical heat flux ratio. There is, however, no assurance that new, economically improved designs will not bring back the concern about the thermo-hydrodynamic stability. Futhermore, flow stability is an important consideration in the design of pressure-tube reactors and will probably be the limiting factor in the design of large scale low-pressure desalination plants.

The typical BWR has a closed box subassembly. It stands therefore between the open lattice core and the single tube channel. It is suspected that two-dimensional effects in the rod bundle do somehow alleviate the stability problems. No theoretical work has been reported on the stability of rod bundles. This is not surprising as the difficulties of predicting even the steady-state operation are considerable. The reactor designers have to rely on full-scale tests of pressure tubes and rod bundles to verify their stability, e.g. [25,26].

1.3 Previous Work at M.I.T.

A number of previous investigations prepared the ground for the present work. Steady-state experiments with fluorocarbons in heated glass tubes provided the necessary experience with such systems [27,28]. Early stability experiments [29] gave very valuable indications and guided the conception of the present experiment. Extensive surveys of the two-phase flow literature [30] and a detailed survey of the stability

problems [31] provided for the collection and classification of the background information.

Crowley, Deane and Gouse [32] reported the first experimental results obtained with the present equipment. The experimental part of this investigation is essentially an expansion and completion of their work.

1.4 Experimental Work

The primary goal of the present experimental work was to produce a complete stability map that could be used to test various analytical models. The experimental facility, described in Chapter 2, was designed [33] to produce density wave oscillations under well defined conditions, without interference from other kinds of instabilities. The constant-pressure-drop boundary condition was assured by a large bypass in parallel with the test channels and a sufficient condenser volume. Although the facility had three vertical, identical parallel test channels, all the experiments were run, as described in Chapter 7, with a single channel in order to avoid any possible coupling between channels.

In practice, the independent variables were easily controllable; thus the system could be operated at any point within its range. This contrasts the experiments conducted with natural circulation, e.g. [19,20,21,23], where only certain curves could be followed in the operational space.

With Freon-113 as the test fluid, the experiments could be pursued safely inside the unstable region without encountering excessive heated wall temperatures. The instabilities where thus dissociated from the

burnout phenomena, and valuable information on the limit cycle could be gathered.

In many similar experiments a primary fluid loop was used to transfer heat to the test channel. The use of easily controllable electric heating in the present experiment eliminated potential coupling of the test channel dynamics with the primary heat source dynamics.

Glass was used extensively to permit visualization of the flow. Visual observations of the oscillating test channels provided valuable insight into the problem. Operation at atmospheric pressure levels emphasized phenomena that would have been unimportant at higher pressures.

The effect of the axial heat flux distribution has been recognized earlier [9,20] but very little experimental data are available. Segmentation of the heated test sections permitted simulation of non-uniform heat flux distributions and evaluation of their effect on the stability of the channel.

1.4.1 Higher-Mode Oscillations

The occurrence of "higher-mode" oscillations and transitions from mode to mode inside the unstable region was observed during the experiments, and is described in Section 7.5.1. As no published reports on such behavior could be found in the literature, part of the experimental program was reoriented to examine closely these phenomena. The higher-mode oscillations were characterized by periods that were equal to a fraction only of the expected period. In fact, for density-wave oscillations, it has been well established that the period is approximately

equal to twice the "transit time", i.e. the time required for a fluid particle to travel through the channel. This can be intuitively understood by considering the fact that the perturbations travel with the flow and that the inlet flow perturbation is approximately 180° out of phase with the pressure perturbations. Examination of the single-phase dynamics (Chapter 5) and a series of ad hoc experiments (Section 7.9) established that these higher modes were associated with the presence of "standing enthalpy waves" in the single-phase region.

1.5 Analytical Models

Analytical investigations of stability in two-phase flow start with the fundamental mass, momentum, and energy conservation equations [6,34], augmented by semi-empirical relations such as heat transfer rate equations, pressure drop correlations, etc. Obviously if enough detail is built into a model, it should be possible to predict all excursions and oscillations. This is, however, impractical in general, and the models must be specialized to suitably treat certain classes of problems. Care must be exercised then to include all features essential to the phenomena being considered.

The equations of the present problem are space and time dependent. Direct integration of these is impossible unless drastic simplifications are made. The possible solutions can be classified according to the methods used to eliminate the space and time dependences and arrive to a stability criterion [37]. The models are termed lumped if the space variable is eliminated by integration along the channel, assuming à priori some approximate space dependence. They are called distributed when the

space dependence is derived rigorously from the equations. In the time domain, the equations are either linearized, to permit application of the well-developed control theory, or treated numerically in a non-linear fashion.

Although the notion of the boiling boundary, i.e. the point of the channel where the mixed-mean enthalpy reaches saturation, is rather artificial, it will be used extensively throughout this work. In fact, it is necessary to treat separately the single-phase and the two-phase regions in order to incorporate in each formulation all the essential features; the boiling boundary provides a convenient separation. Moreover, a number of experimental observations can be explained by considering the dynamics of the boiling boundary alone.

The existing analytical stability models fall into two categories. In the first, the models, in taking into account all possible effects evolve into complex computer codes, e.g. [12] or inextricable algebra, from which little physical understanding can be extracted. There are also relatively cumbersome or expensive to use for preliminary survey calculations.

In the second category, the models are reduced to a simple form, which either limits their applicability or compromises seriously their accuracy. Credit must be given, however, to some models in this category for contributing to the physical understanding of the stability phenomena.

A middle course was taken here. Fragmentation of the model into smaller, independent blocks permitted retention of enough detail without

loosing touch with the physics of the problem. The stability model presented can be characterized as hybrid, in the sense that it makes use of both linear, frequency-domain and non-linear, time-domain solutions.

As described in Chapter 8, given the steady-state conditions at some point, the approximate frequency of a potential oscillation can be obtained. Indeed it is shown in Chapter 7 that the frequency of the oscillation is uniquely correlated to channel variables. The stability of the channel is then tested by oscillating the inlet flow around this frequency. For these calculations, the single-phase region and the two-phase region are dealt with separately.

1.5.1 Single-Phase Region

The single-phase region is treated in Chapter 5 in a rather conventional fashion; the equations are linearized and solved in the frequency domain. It is indeed generally agreed that linearized models predict adequately the threshold of stability. The variations of the saturation enthalpy with pressure, at the boiling boundary are taken into account, while they were neglected in previous formulations. Subcooled boiling, however, is ignored for lack of an adequate dynamic description.

The importance of heat storage in the channel wall and variable heat transfer have been recognized and the dynamics of the heated wall were incorporated in the formulations of the single-phase region. As shown in Section 5.2.3, the often neglected wall dynamics might play under certain conditions an important role.

Solution of the equations of Chapter 5 yields the oscillations of the boiling boundary and the variations of the single-phase pressure drop when the inlet flow is oscillated. These two are then used as inputs to the two-phase dynamics model.

1.5.2 Two-Phase Region

The treatment of the two-phase region is novel. A Lagrangian description was used and exact distributed solutions were obtained with a minimum of simplifying assumptions. The resulting "Enthalpy Trajectory Model" is described in detail in Chapter 6. Use of a Lagrangian approach limits, however, the applicability of the model to channels with axially uniform cross-section and heat flux. Variations of the heat transfer from the wall are less important in the boiling region where the heat transfer coefficient is weakly dependent on velocity and quality. The structure of the model does not permit an accounting of these effects. Thermodynamic equilibrium between the phases was assumed and, although the treatment of the two-phase region is non-linear, the application of the equations is confined to small and medium flow perturbations. Flow reversals, for example, cannot be dealt with.

The various existing models that deal with the dynamics of two-phase flow are oriented toward high pressure systems as they do not take into account the variations of the saturation temperature and other properties with pressure in space. Moreover, incorporation of time dependent property variations increases the difficulty of obtaining numerical solutions by an order of magnitude [35]. A compromise was reached here by using a reference pressure profile which takes into account the space variations of the properties. This reference profile is provided exter-

nally with any available degree of accuracy. The time dependence of the saturation enthalpy is taken approximately only into account (Chapter 8).

The stability model does not make use of the various semi-empirical correlations required for the steady-state calculations but rather uses a fundamental technique to determine the deviations from the reference state. The enthalpy trajectory model is used in Chapter 8 to predict the pressure drop in the two-phase region with oscillating flow.

1.5.3 Stability Criterion

Once the pressure oscillations in the two distinct regions of the channel are obtained, use of the constant-pressure-drop boundary condition allows the stability criterion to be written in its simplest form

$$\delta\Delta p_1 + \delta\Delta p_2 \rightarrow 0$$

where the two terms are the pressure perturbations in the single-phase and the two-phase regions, respectively. In Chapter 8 this criterion is put into a more convenient form for use in the stability analysis.

The procedure of predicting the threshold of stability outlined above allows one to follow the calculations step by step. Physical understanding of the phenomena and the effect of parametric variations can be easily extracted from the model.

As a test of the theory, a computer program was written to investigate the stability of the present experimental system. In Chapter 8, the theoretical predictions of this code are compared to the experimental data.

Although the stability model exhibited a qualitatively correct behavior, the predicted threshold of stability was not in agreement with the experimental observations. As discussed in detail in Chapters 8 and 9, effects that could not be included in the theory, for example lack of thermodynamic equilibrium and radial heat transport effects in the single-phase region, seemed to be mainly responsible for the discrepancy. It is recommended that the model is further tested under different experimental conditions, including high pressure water systems.

Chapter 2

EXPERIMENTAL APPARATUS

The basic experimental apparatus used in this work was described in detail in previous publications that originated from the project [32 - 33]. A brief description will be repeated here for completeness, and numerous innovations that were made in the instrumentation will be discussed.

The equipment evolved from previous designs [29], and was designed with flexibility and simplicity in mind. The vital part of the loop, the test-section assembly, consists of three parallel heated glass channels in parallel with a large bypass whose function is to maintain a constant pressure drop across the heated channels. The test fluid enters the three channels at the bottom and flows, while evaporating, vertically upward. Use of glass in the loop permits visualization of the flow, but limits the attainable pressure level.

Subdivision of each channel into seven individually powered test lengths permitted simulation of non-uniform heat flux distributions, similar to those encountered in boiling water reactors. The rig was designed for Freon-113, although other test fluids can be used. Freon-113 was well suited for the test program since it has a boiling point of 118°F at atmospheric pressure, a low vapor pressure, and a latent heat of vaporization about one tenth that of water. It is thus possible to produce any exit quality and even superheated vapor with modest power, at low temperature and without any fear of burnout. Moreover, Freon-113 is

relatively inexpensive, and exhibits the desirable properties of fluorocarbons, i.e. it is non-corrosive, non-toxic, electrically non-conductive, non-flammable, and chemically stable. It has, however, several potentially undesirable properties: a very low thermal conductivity, high air solubility, and high degree of wettability. These properties may significantly influence the heat transfer behavior relative to that obtained, for example, with water.

2.1 Description of the Loop

Figures 2.1 and 2.2 are schematic diagrams of the loop. Figure 2.1 describes in detail the hardware and general instrumentation, while Fig. 2.2 gives exact test section dimensions and codes important components. The basic flow system consists of: the pump, located well below the entrance of the test sections to avoid cavitation; the main flow lines; the pump bypass that permits isolation of the test sections; the total flow metering lines; the main (HX1) and test section (HX2) preheaters; the test-section assembly in parallel with the large bypass; the condenser and after-condenser; the downcomer; and the precoolers used to lower the fluid temperature before reaching the pump. Glass was extensively used to permit visual observations of the boiling phenomena and to monitor system performance. Two preheaters were necessary in order to be able to keep the temperature in the bypass below saturation, while still independently varying the test-section inlet temperature.

The flow is divided between the pump bypass and the test sections by adjusting valves V1, V6 and V3 or V2. The test-section bypass valve, V9, controls the pressure drop across the test sections.

Two condensers were thought to be necessary to eliminate non-condensible gases from the main condenser; the idea was to maintain the condenser pressure slightly above atmospheric and allow a slow leakage of vapor to the after-condenser. This, however, did not provide a sufficiently constant exit pressure when the vapor generation rate was varied during the experiments. For this reason, after an initial degassing, sufficient cooling was provided to the main condenser to keep the pressure at atmospheric level (see also 4.1). The condenser volume and cooling were sufficient to eliminate any dynamic pressure variations.

The flow area in the test section preheater HX2 was large enough so that there was essentially no frictional pressure drop across it for the range of flows passed through the heated sections. There was, however, an inertial pressure drop in this leg (see 5.4.1). The constant-pressure-drop region therefore extended from point 00 (Fig. 2.2) or to a lesser approximation point 0, to the channel exit (ex). The heated region between points 1 and 8, is described in more detail below. Table 2.1 gives more general information about the loop. Table 2.2 summarizes a few important properties of the test fluid for convenient reference.

Table 2.1

Characteristics of the Experimental Loop

Construction Materials	Brass, copper and glass.
Pump	40-hp centrifugal pump, manufactured by Buffalo Forge. "Chem-rated" AVS size 50. Double mechanical carbon seals. 150 gal/min at 235 ft of water head.

Table 2.1 Concluded

Heat Exchangers and Condensers	Tube and shell type, manufactured by American-Standard. Cooling and heating by mixture of steam and water.
Charge of Freon-113	Approximately 700 lbm.
Electric power to the test sections	Seven* General Radio Variac W20G2 autotransformers, 220 V primary/0 to 330 V secondary.
Total power available	Approximately 12 kW maximum (limited by autotransformer load).

* An eighth autotransformer could be used to power all seven Variacs at reduced load in order to preserve the power distribution while changing the total input.

Table 2.2

Selected Physical Properties of Freon-113 [41,42,43]

Chemical name and formula	trichlorotrifluoroethane, $CCl_2F\text{-}CClF_2$
Boiling point	117.6°F at 14.7 psia
Liquid density	97.7 lbm/ft^3 (1.565 g/cm^3) at 77 °F
Critical Point	417.4 °F; 495.0 psia
Latent heat of vaporization	63.1 Btu/lbm at 14.7 psia
Specific heat of the liquid	0.213 Btu/lbm at 70 °F
Prandtl number of the liquid	7.3 at 100°F
Liquid-to-vapor density ratio	195 at 15.4 psia, 137 at 20.5 psia

See also Appendix B

2.1.1 Heated Test Section Assembly

The test channels were made of Pyrex EC electrically conducting glass tubing. Seven test lengths, each 15-in. long, stacked and coupled with 0.5-in. thick coupling plates, comprised the heated portion of a test section. Figure 2.2 gives the important dimensions and Fig. 2.3 shows the details of the coupling. The three test channels were connected to a common header at the inlet, to a large transparent riser at the exit. A short unheated length of copper tubing was provided at the end of each test section to bring the channel exits above the liquid level in the riser. The liquid from the riser was directly drained to the downcomer (Fig. 2.1), while the vapor was passed to the condenser. Structural rigidity and alignment were provided by three metal rods running along the test sections, through the plastic couplings.

Two instrument taps were provided in each coupling for each of the channels: a 0.042-in. dia. pressure tap and a 0.062-in. dia. thermocouple well.

The glass tubes were coated with a thin, optically transparent, electrically conductive film. Heat was supplied to the tubes by passing an electric current through this resistive coating. The temperature coefficient of resistivity of the coating was estimated to be of the order of 10^{-4}/°C. Thus, in contrast with other investigations where a second fluid was used to supply heat, the heat supply was essentially constant in time (except for the negligible effect of time-varying heat losses) and easily controllable. Each Variac was powering all three test lengths at one level; the power was equally distributed by means of adjustable trimmer resistors.

The factory tin oxide coating was somewhat uneven resulting in a rather consistent, slightly non-uniform axial resistance distribution. Typically, the linear resistivity curve presented two humps situated at 1/3 and 2/3 of the total length. The peak to average ratio was 1.15 for the few tubes measured (1.33 if the unheated length is taken into account). The actual heat flux distribution would be slightly flattened by axial heat conduction. Electric power was supplied to the tubes by wire braid power leads coiled around a heavier coating at each tube end. The presence of the couplings, the coupling plates and the power leads leaves an unheated length of 2 to 2.5 in. at each experimental station, referred to in later chapters as cold spot.

The physical properties of the glass test sections are summarized in Table 2.3.

Table 2.3

Physical Characteristics of the Test Sections

Geometry:	Overall length	15 in.
	Heated length	13 in.
	Diameters	0.510 in. OD, 0.430 in. ID.
	Flow area	0.0010085 ft^2
Material		7740 Pyrex Glass (Corning Glass Works)
Physical Properties of the glass [44,45]:		
	density	162 lbm/ft^3
	heat capacity	0.21 Btu/lbm°F at 250°F
	thermal conductivity	0.75 Btu/hrft°F at 250°F
	thermal diffusivity	0.022 ft^2/hr at 250°F
	safe operating temperature	480°F
Conductive coating:		
	thickness	approximately 16 x 10^{-6} in.
	optical transparency	70 percent
	total resistance	100 to 200 Ω

2.1.2 Operating Range

As noted earlier, the pressure level is limited by the glass portions of the loop. The maximum heat input to the test sections is given by the acceptable autotransformer load or the permissible safe heat flux. The mass flow rate was limited by the liquid evacuation capability of the riser, which had an inadequate liquid drain; at exit liquid flow rates in excess of 4000 lbm/hr flooding of the riser occurred. The temperature of the city water determined the lowest inlet temperature obtainable (38°F during the coldest winter days). The range of variables, as summarized in Table 2.4, was generally sufficient for the present experiment.

Table 2.4

Operating Range of the Independent Variables

Pressure level (condenser)	0 to 20 psig
Maximum average* "safe" heat flux (inside diameter)	16000 Btu/hrft^2 # corresponding to 680 W/test length or to a linear heat rate of 1800 Btu/hrft
Flow rate (per tube)	up to 4000 lbm/hr
Inlet velocity	up to 12ft/s
Exit quality	subcooled liquid to superheated vapor
Inlet subcooling	0 to 100 °F

* averaged including the unheated lengths at the experimental stations

successful operation at 50,000 Btu/hrft^2 has been reported [27]

2.2 Instrumentation

The loop was equipped with a large number of instruments as shown in Fig. 2.2. Channel C, which was generally the only channel used, was equipped with thermocouples and pressure transducers at all couplings.

Although the primary measuring elements (venturis, pressure transducers, and thermocouples) were the same for both the steady-state and the stability runs, different recording instrumentation was used for each type of experiment. The millivolt transducer signals were measured with a precision d.c. vacuum tube volt meter (Hewlett-Packard, Model 412A) during the steady-state runs. A direct-writing oscillograph (Visicorder, Model 906B, manufactured by Honeywell; 12 recording channels) was used during the stability runs to record all the rapid transients.

2.2.1 Pressure Measurements

Bourdon type precision pressure gauges were used to monitor the condenser pressure (P95) and the pressure at the bottom of the test sections (P93). An open mercury manometer was connected to the inlet header (Station 0). During the blowdown experiments (Section 7.1.1) the level of the liquid in the graduated bypass was also used to determine the inlet pressure.

Transducers were connected to the pressure taps at stations 0 to 8. A variety of "unbonded strain gauge" differential and gauge pressure transducers were used. Their usable ranges extended from 1 psi to 30 psi. They had been calibrated individually and their calibrations were often checked using the liquid level in the test sections as a reference.

The reference side of the differential pressure transducers was either connected to the condenser or left open to the atmosphere. Occasionally, to extend the range of the differential transducers, a liquid Freon head was applied as reference.

Regulated d.c. voltage excitation to the transducers and passive signal adjustments were provided by a set of eight strain gauge bridge adapters supplied by the Ramapo Instrument Co. (Model SGA-100B). Whenever necessary, simple RC filters were installed between the bridges and the recording instruments to eliminate the 60 Hz pickup.

During a single run, the total observed transducer drifts were generally below 0.1 psi, typically between 0.03 and 0.1 psi, depending on the range of the individual transducer. This drift, caused by thermals and introduction of vapor into sensing lines, was considered in the data reduction.

2.2.2 Flow Measurements

Three venturis in the unheated inlet section of the channels provided both the static and the dynamic flow measurements. The calibration and characteristics of these units, designed to produce a minimal pressure drop, are given in Ref. [32]. Pressure lines, approximately one foot long, were used to feed the pressure signals to three differential pressure transducers (± 1 psid), in parallel with three inverted U-tube Freon manometers used for static measurements only. Great care was exercised in eliminating trapped gas from the pressure lines.

The transducer signal was read with the d.c. VTVM during the steady-state runs. As this signal is approximately proportional to the square

of the flow, it was necessary to further process it in order to readily interpret transient flow recordings. An amplifier having a square-root response was built to perform this function and is shown schematically in Fig. 2.4. This unit had provisions for variable gain and convenient calibration.

Unfortunately the pressure transducers available had a resonant frequency in the vicinity of 10 Hz. It was therefore necessary to follow the square-root amplifier by a RLC low-pass filter. After a few trials, a satisfactory filter having a 60 db/decade attenuation after a cutoff frequency of 6 Hz (10 percent drop at 1.2 Hz, 60 percent at 5 Hz) was obtained.

Finally, an integrating circuit was built to provide the average flow value during the flow oscillations. The average flow was obtained from the average slope of the integral signal, recorded over a few oscillation cycles. The entire flow measuring instrumentation shown in Fig. 2.4 performed quite satisfactorily at moderate flow oscillations. However, when flow blockage, reversals or vapor flowback from the heated sections occurred, large discrepancies were observed. The venturi, being non-symmetric, gave an erroneous reading for reverse flow even without vapor entrainment. As mentioned above, the large diameter ratio venturi was chosen to minimize the pressure losses and was delivering a very weak signal at low flow (0.04 psi at 1 ft/s). It might have been beneficial to use instead a simple orifice to get identical calibration in both directions and a larger, direction-sensitive pressure signal (a venturi gives a pressure signal of the same sign regardless of the flow direction).

The response of the square-root amplifier was excellent, except in the lower 5 percent of its full scale, where there were significant deviations from the theoretical characteristic. At these low velocities the output was also sensitive to pressure signal drift, although the drift was generally quite low (typically 0.001 psi). It was, however, necessary to zero the transducer very carefully. For these reasons, the venturi flowmeter was used mainly at high velocities and in the stable region. At low velocities, below about 0.8 ft/s for oscillating flow during the blowdown experiments, the flow was metered by volume as explained in 7.1.2.

The total flow to the test sections and the bypass was measured by two orifices, connected to mercury manometers. All flow measurements were estimated to be accurate to a few percent.

2.2.3 Electric Power Measurements

The electric power supplied to each test length was monitored by a set of seven panel wattmeters. Provisions were also made for the external connection of an accurate (Westinghouse, class 0.5%) laboratory wattmeter whenever accurate measurements were desired. The line voltage was checked frequently during the experiments to detect and correct drifts.

2.2.4 Temperature Measurements

Copper-constantan thermocouples were used throughout the loop. The test-section thermocouples were steel sheathed, 0.062 in. in diameter. Ordinary thermocouple wire in dry wells was used at other locations. All thermocouples were connected to a 144-point Honeywell-Brown potentiometric recorder. Switching of any thermocouple to a Visicorder channel for dynamic recordings was also possible. The recorder was calibrated

frequently and was accurate to approximately 0.2°F.

2.2.5 Other Measurements

Occasionally, a hot wire probe, consisting of a 0.001 in. dia. stainless steel wire, inserted through a thermocouple hole and stretched across the flow area, was used as an inexpensive, average void fraction gauge [46] to detect flow regimes and dynamic void fraction variations. Its operation was quite successful and gave valuable qualitative results.

An attempt was also made to detect the dynamic variations of the outside surface temperature of the test sections. A measure of the resistance variations of the conductive coating of the test sections by a carrier frequency Wheatstone bridge failed for lack of sensitivity (low temperature coefficient of resistivity) in the 300 V power environment. It would have been much better to use a resistance thermometer (e.g. a thin insulated wire wrapped around the tube). In any case, the temperature variations were very small, of the order of 1 or 2°F even during the most violent oscillations.

Chapter 3

PREDICTION OF THE STEADY-STATE OPERATING CONDITIONS IN THE BOILING CHANNEL

The stability analysis that will be undertaken in Chapters 5, 6, and 8 will require, like any stability analysis, knowledge of conditions throughout the boiling channel. Steady-state prediction methods presented in this chapter will be experimentally verified in Chapter 4 in order to ascertain that the steady-state foundations of the stability analysis are sound.

More specifically, a calculation procedure was developed in order to predict the pressure, temperature, quality, and void fraction profiles along the channel at steady state. In essence, the whole procedure centers around the pressure drop prediction; the additional parameters are required inputs to the pressure drop calculation. The independent variables required are the inlet (all liquid) mass flow rate, the inlet temperature, the exit (or condenser) pressure and the heat flux distribution along the channel. A computer code (PRESDROP) was written in FORTRAN IV to carry out the calculations on an IBM-360 computer. The code was written with the specific experimental geometry and fluid in mind; however, it can be easily modified to accomodate any single channel geometry and fluid. In this code, turbulent flow at thermodynamic equilibrium is assumed, the relative velocity between the phases is taken into account, the fluid properties are variable with pressure, and the effects of subcooled boiling are considered.

An outline of the various correlations used in developing this procedure is given in this chapter. A description of the code and its FORTRAN IV listing can be found in Appendix A. A parametric study of the pressure drop predicted under the present experimental conditions is undertaken in the last section of this chapter.

3.1 General Calculation Procedure

The pressure drop along a single channel is calculated for a smooth, constant diameter, round pipe and for vertical upward flow. Reflecting the experimental setup, the channel was subdivided into seven heated lengths and a short unheated exit section, the heat inputs to each test length being individually adjustable. To further take into account in the calculations the variations of the fluid properties with pressure and the continuous variation of the quality, each test length was subdivided into a number of segments, depending on the accuracy desired.

The input information is:

the inlet (all liquid) mass flow rate, w [lbm/hr]
the inlet temperature, T_o [°F]
the exit or condenser pressure, p_{ex} [psia] or p_{cond} [in. Hg]
the heat input distribution, q_{wi}, i = 1,7 ordered from inlet to exit [Watts per test length]

The total net heat input is then given by

$$q_{tn} = \sum_{i=1}^{7} (q_i - q_{i\ loss}) \qquad [Btu/hr]$$

where the losses are estimated from a previous iteration, Section 3.7. The inlet enthalpy and the total enthalpy rise are given by

$$h_{in} = h_f(T_o) \ , \qquad \Delta h = q_{tn}/w \qquad [Btu/lbm]$$

The exit quality can then be calculated as follows:

$$x_{ex} = \frac{h_{in} + \Delta h - h_f(p_{ex})}{h_{fg}(p_{ex})}$$

The conditions now being known at the exit, the pressure drop is calculated for each segment, marching upstream until the channel inlet is reached. The two possible cases of subcooled and two-phase flow as well as the special case of the segment around the bulk boiling boundary are treated in the following sections. All properties are evaluated at the saturation pressure or temperature unless otherwise specified.

3.2 Pressure Drop

The pressure drop at steady state is given by the sum of the frictional, gravitational, and acceleration pressure drop terms:

$$\Delta p = \Delta p_{fr} + \Delta p_{gr} + \Delta p_{ac}$$

It becomes necessary at this point to define rigorously a few terms that will be used extensively throughout this work. The (bulk) boiling boundary (BB) is defined as the point in the channel where the bulk or mixed-mean enthalpy of the flow reaches saturation. The subcooled region extends from the inlet to the BB, and will occasionally be referred to as single-phase region (subscript 1), ignoring the occurrence of subcooled boiling. The boiling region starts at the point of net vapor generation (NVG) and is divided by the BB into a subcooled boiling and a (bulk) boiling region, otherwise referred to as two-phase region (subscript 2), whenever the presence of vapor in the subcooled region is ignored. The superheated vapor region is not considered in this work.

3.2.1 Frictional Pressure Drop

3.2.1.1 Single-Phase Region

For a single-phase diabatic flow, according to Sieder and Tate [47],

$$\Delta p_{1fr} = -4\ f\ \frac{\Delta L}{D}\ \frac{G^2}{2\rho_r}\ (\mu_w/\mu_b)^{0.14}$$

where $f = f(Re_b)$ and $Re_b = \frac{G\ D}{\mu_b}$

The friction factor for smooth pipes is formulated as a function of the Reynolds number for use in the program (Appendix C). The temperature of the wall is obtained using the familiar McAdams correlation for the heat transfer coefficient

$$\frac{h\ D}{k_b} = 0.023\ (Re_b)^{0.8}\ (Pr_b)^{0.4}$$

There might be some question concerning the validity of the wall-to-bulk temperature correction when the wall temperature exceeds saturation temperature. Radial property variations might also be expected to influence the heat transfer coefficient; however, this was not considered since some uncertainty in the wall temperature could be tolerated. With this procedure, the predicted pressure drop slope agreed well with the observed one in the single-phase region, even under extreme wall temperature conditions (Figs. 4.4 and 4.5). Finally note that, lacking an adequate correlation for Freon, the effect of subcooled boiling on the frictional pressure drop is ignored.

3.2.1.2 Two-Phase Region

A number of more-or-less sophisticated empirical and semi-empirical models exist for the calculation of the frictional pressure drop in the two-phase region (e.g. [49,50,51,52]). The Lockhart-Martinelli model [49] was used here because of its wide acceptance and the similarity of the experiments from which it was derived to the present one. The calculation procedure is outlined below:

$$\Delta p_{fr2} = \Phi^2_{\ell tt} \, \Delta p_\ell$$

$$\Delta p_\ell = -4f \frac{\Delta L}{D} \frac{[G(1 - \bar{x})]^2}{2\rho_f}$$

$$f = f(Re_\ell)$$

$$Re_\ell = \frac{G(1 - \bar{x}) \, D}{\mu_f}$$

The Lockhart-Martinelli two-phase friction multiplier

$$\Phi^2_{\ell tt} = \Phi^2_{\ell tt} \, (X_{tt})$$

is obtained numerically from a polynomial which was fitted to the recommended curve as a function of the parameter X_{tt}

$$X_{tt} = X_{tt}(\bar{x}, p) = \left(\frac{1 - \bar{x}}{\bar{x}}\right)^{0.9} \left(\frac{\rho_g}{\rho_f}\right)^{0.5} \left(\frac{\mu_f}{\mu_g}\right)^{0.1}$$

See Appendix C. Both phases are assumed to be in the turbulent regime, which is not strictly correct for the gas phase near zero quality and for the liquid phase at low flow rates and high qualities. Practically, however, it does not make any difference as these regions cover only a short channel length. In the above formulas, the evaluation of the

quantities at the average quality for each segment

$$\bar{x} = \frac{1}{2}(x_e + x_i)$$

requires knowledge of the segment inlet quality x_i, which is obtained by iteration.

3.2.2 Gravitational Pressure Drop

This term is given simply by

$$\Delta p_{gr} = -[\rho_f(1 - \bar{\alpha}) + \rho_g \bar{\alpha}]\, g\, \Delta L$$

The difficulty resides in the estimation of the average void fraction, $\bar{\alpha}$, in the boiling region. The Lockhart-Martinelli void fraction correlation

$$\alpha = \alpha(X_{tt})$$

was used throughout this work, where again the empirical function was approximated numerically by a polynomial (Appendix C) and all quantities were evaluated at the average quality $\bar{x}$.

The Lockhart-Martinelli void fraction correlation was, however, compared to other correlations as discussed in Section 3.4. Section 3.5 describes the evaluation of the true quality in the subcooled boiling region, which can be used with the Lockhart-Martinelli correlation to estimate the subcooled voids. The expression reduces to the usual hydrostatic expression in the region prior to subcooled boiling.

3.2.3 Acceleration Pressure Drop

Assuming that each phase is flowing separately with uniform velocity throughout the flow cross-section, the acceleration pressure drop is given by [53]

$$\Delta p_{ac} = B(x_e,p_e) - B(x_i,p_i)$$

with

$$B(x,p) \equiv -G^2 \left[\frac{(1 - x)^2}{(1 - \alpha)\rho_f} + \frac{x^2}{\alpha\rho_g}\right]$$

In the single-phase region, B(x,p) reduces to

$$B(T) = \frac{-G^2}{\rho_f}$$

3.3 The Segment Containing the Bulk Boiling Boundary

It is noted that since there is a large pressure drop at the bulk boiling boundary due to the sudden acceleration of the fluid, it becomes necessary to treat separately the segment that contains the zero quality point. This effect is especially pronounced at low pressures where the equilibrium void fraction rises from zero to 50 or 75 percent in a few inches of heated length.

It is then necessary to determine the zero quality point by successive iterations, calculate separately the pressure drops in the non-boiling and boiling lengths, and add them to get the total pressure drop. Although the solution to the problem seems trivial, considerable numerical difficulties were encountered. The difficulties are significantly alleviated when subcooled boiling is taken into account, due to smoothing of the void fraction distribution around the bulk boiling point. Appendix A discusses this problem in more detail.

3.4 Prediction of the Void Fraction

Among the numerous existing void fraction correlations, four were chosen to be compared here:

a.) The Lockhart-Martinelli empirical correlation [49]

$$\alpha = \alpha(X_{tt}) \qquad \text{with} \quad X_{tt} = X_{tt}(x,p)$$

neglects the effects of mass flux, pipe diameter, and flow regime but has given satisfactory results for a variety of fluids and conditions.

b.) A correlation proposed by Zuber and Findlay [54] for the "churn-turbulent" flow regime, which takes into account the flow regime and the mass flux effect, is given by

$$\alpha = \frac{x}{\rho_g}\left\{1.13\left[\frac{x}{\rho_g} + \frac{1-x}{\rho_f}\right] + \frac{1.18}{G}\left[\frac{\sigma g(\rho_f - \rho_g)}{\rho_f^2}\right]^{1/4}\right\}^{-1}$$

c.) The slug flow model proposed by Griffith and Wallis [55], which takes into account tube diameter, flow regime and mass flux,

$$\alpha = \frac{Q_g/A}{1.2\left(\frac{Q_g + Q_f}{A}\right) + 0.35(gD)^{1/2}}$$

with

$$Q_g = \frac{w\,x}{\rho_g} \qquad \text{and} \qquad Q_f = \frac{w(1-x)}{\rho_f}$$

d.) The simple homogeneous model given by

$$\alpha = \frac{x}{x + (1-x)\rho_g/\rho_f}$$

These four models were compared at typical experimental conditions of this investigation as shown in Fig. 3.1. The dotted lines indicate that the model is probably used outside its intended range of flow regime. The Lockhart-Martinelli extension towards the low quality region is an arbitrary one, as noted in Appendix C. The comparison shows that in the range of interest, i.e. for $x = 0.01$ to 0.30, the first three models agree closely, while the homogeneous model overestimates the void fraction. It was felt that this comparison justified use of the Lockhart-Martinelli void fraction correlation throughout this work. The effect of variation in the predicted void fraction on the pressure drop is discussed in Section 4.5.

3.5 Void Fraction in the Subcooled Boiling Region

The void profile in the subcooled region is essentially determined by the position of the point of NVG. This is considered to be the point in the channel where the void fraction increases rapidly with position. Upstream of NVG, the subcooled voids are on the wall and two-phase effects are small. Levy [56] and Staub [57] have somewhat similar approaches to prediction of this point. They consider NVG to be coincident with bubble departure which is due to unbalance of forces on the bubble. Staub takes into account surface tension, buoyancy and shear drag terms, while Levy considered only surface tension and buoyancy effects. Both models have "adjustable constants" which have been evaluated mainly from high pressure water data, and there is no assurance that they should apply equally well to Freon-113 at low pressures.

The two models were compared for the present experimental conditions

using the following recommended values of the constants.

Staub: $f(\beta) = 0.030$

Levy: $C = 0.015$ and $C' = 0$

The subcooling at the point of NVG, as predicted by the two models, is plotted in Fig. 3.2 versus the mass flux, for various heat fluxes. As expected, Levy's model gives unrealistic estimates at very low velocities where the buoyancy effects dominate or at least play an important role, but the models agree otherwise. Staub's model with $f(\beta) = 0.030$ was used in most of this work, although some earlier calculations were done using Levy's model.

Once the point of NVG is known (given by the models as subcooling with respect to the local saturation temperature ΔT_d) a relation is postulated between the "true" local vapor quality x_{tr} and the corresponding equilibrium value x. Levy proposes:

$$x_{tr} = x - x_d \exp(x/x_d - 1) \qquad \text{for } x \geq x_d$$

$$x_{tr} = 0 \qquad \text{for } x < x_d$$

where:

$$x_d = - \frac{c\, \Delta T_d}{h_{fg}} < 0$$

The void fraction is then calculated from the appropriate relationship (in the present case the Lockhart-Martinelli correlation) using this true quality.

The computer subroutines (SUBBOL) that perform these calculations are listed in Appendix A. The effect of the subcooled boiling void fraction on the pressure drop is examined in Section 4.4.

3.6 Temperature Profile

In the subcooled region, the local bulk temperature is directly related to the fluid enthalpy. A correction is, however, necessary to account for subcooled boiling:

$$T_b = T_f[h - x_{tr}h_{fg}(p)]$$

In the bulk boiling region the local temperature is equal to the saturation temperature.

3.7 Heat Losses

The glass channel was not insulated in order that continuous visual observations of the boiling phenomena could be made. The heat loss from the outer wall was small, of the order of 5 percent, but not negligible. Gouse and Hwang [27] under almost identical experimental conditions have measured these losses and tested the accuracy of the correlation used to predict them. The good agreement they obtained justified the use of similar methods to predict the heat losses here.

The film temperature drop is calculated, neglecting the heat loss as a first approximation. The McAdams correlation is used in the forced convection region and the heat transfer coefficient is set equal to 1000 Btu/hrft^2°F in the boiling region. Then the wall temperature drop is estimated for an average glass temperature. These two temperature drops added to the average bulk temperature yield the average outside wall temperature, T_{out}. The natural convection losses are then given by [58]

$$q''_{nc} = 0.29\ \Delta T_a^{5/4}/L^{1/4} \qquad [\text{Btu/hr ft}^2]$$

with

$$\Delta T_a = T_{out} - T_{room} \qquad [°F]$$

$$L = \text{test length} \qquad [ft]$$

Adding the radiation loss, assuming a view factor of 1.0 and emissivity of 0.95, the total heat loss is obtained. The FORTRAN listing of the subroutine LOSSES in Appendix A provides additional details.

3.8 Parametric Study of the Pressure Drop

As all the stability predictions depend closely on the steady-state pressure and quality distributions at the threshold of stability and on the relative magnitude of the three terms in the pressure drop equation, it will be useful to examine here the parametric effects of mass flow rate, inlet temperature, heat input, and quality under the present experimental conditions.

3.8.1 Effects of the Inlet Temperature and the Mass Flow Rate

Figure 3.3 shows the variations of the total pressure drop, $\Delta p_{l\ ex}$, when the inlet temperature is changed, while all the other independent variables are maintained constant. Figure 3.4 shows the effect of the mass flow rate. The subcooled boiling and the heat losses were not taken into account in these calculations. The pressure at the boiling boundary, p_{bb}, the exit quality, x_{ex}, the length of the single-phase region, z_{bb}, and the subcooling with respect to the boiling boundary, $\Delta T_{subb} = T_{sat}(p_{bb}) - T_o$ are also shown in these figures, as they all have some importance in the stability analyses. A detailed discussion of these parametric trends is not

required here since the explanation for the behavior is quite simple and the plots will be considered later.

3.8.2 Relative Importance of Friction, Gravity, and Acceleration Terms

For a given geometry, fluid, and pressure level, the local differential frictional and gravitational pressure drops are functions of the mass flux and the quality only. It is thus possible to compare them in the (G,x) plane. The acceleration term depends on the rate of vapor generation, or the rate of quality increase with length and therefore will also be dependent on the heat input.

The three terms were calculated for a matrix of values in the (G,x) plane and for three different heat fluxes. Contour maps were than produced by computer for lines of constant ratios. Figure 3.5 shows such a contour map. The plot has a background of lines of equal gravity-to-friction ratio. Superimposed on these are the three unity ratio curves: gravity = friction = acceleration (for q' = 792 Btu/hrft, 300 W/test length). They subdivide the entire plane into three major regions. Gravity is dominant in the upper left region, acceleration is larger than the two other terms in the lower left corner and friction is the major term in the rest of the plane.

The 264 and 1320 Btu/hrft (100 and 500 W/test length) lines, also shown on this plot, permit to evaluate the effect of the heat flux on the acceleration term: as the heat flux is increased, the "triple point" moves upwards along the gravity = friction line, enlarging the acceleration dominated area. This figure will be referred to frequently in subsequent chapters.

Chapter 4

MEASUREMENT OF STEADY-STATE PRESSURE AND TEMPERATURE PROFILES AND COMPARISON WITH PREDICTIONS

Detailed pressure and temperature profile measurements at steady-state were undertaken in order to verify the validity of the computational methods developed in the preceding chapter. The range covered in the 21 experimental runs was:

inlet temperature, T_o	95 and 115 °F
gross average heat flux, q"	0, 4700, 9400 and 14,100 Btu/hrft^2
	(0, 200, 400 and 600 W/test length)
inlet velocity, V_o	approximately 0.5 to 10 ft/s
condenser pressure, p_{cond}	atmospheric
heat flux distribution	uniform, cosine, and "rooftop"

Heat flux distributions are given in Table 4.1.

Table 4.1

Definition of the Heat Flux Distributions Used Throughout This Work

Local to Average Heat Inputs (per Test Length)

Test Length Number		1	2	3	4	5	6	7
Distribution	Uniform	1	1	1	1	1	1	1
	Chopped Cosine	0.43	0.98	1.35	1.48	1.35	0.98	0.43
	"Rooftop"	0.875	1.75	1.458	1.165	0.875	0.585	0.291

The experimental procedure is outlined in the following section. The effect of the various uncertainties in the theoretical models on the calculated pressure drop and the effect of the heat flux distribution are also discussed in this chapter.

4.1 Experimental Procedure

All experiments were conducted with a single channel (Channel C). The other two channels were isolated during the measurements using valves V11 and V12 (see Fig. 2.1).

After slowly heating up the system, the Freon at an inlet temperature close to saturation was circulated in all three channels at full power for approximately one hour to extract dissolved air. During this period the main condenser water was shut off and most of the condensation occurred in the small after-condenser which was left permanently open to the atmosphere during these experiments. This technique resulted in a partial purge of the air from the system. Then the inlet temperature was set by adjusting the steam and water flows to heat exchangers HX1 and HX2. The pressure transducer lines were carefully purged and the transducers electrically zeroed at the nominal run temperature with a negligibly small flow in the test section, which was necessary to maintain a constant head and to purge any bubbles. Valve V13 was then completely opened and the flow was controlled using valves V10 (common inlet to the test sections), V9 (bypass), and V1 (pump outlet). Since some of the data were taken in regions which would normally be unstable, the oscillations were damped out by using inlet throttling provided by valve V10. It was generally necessary to supply some cooling to the main condenser during the measure-

ments in order to achieve a constant channel exit pressure.

The experiments began at a flow rate as low as the stability of the system would permit, then the flow was increased in small increments. Flooding of the riser, which had an insufficient liquid drain, defined the maximum flow rate.

For each data point, the inlet flow, w, the inlet pressure, p_o, the pressure at stations 1 to 8, p_1 to p_8, the inlet temperature, T_o, and occasionally the temperature at the remaining stations, T_2 to T_8, were recorded. The instruments were checked frequently for drift, and corrections to the data were made whenever necessary as described in Chapter 2.

As preliminary measurements with isothermal single-phase flow had shown that the thermocouples were disturbing the flow and the pressure measurements (probably by creating turbulence at the diametrically opposed pressure taps), they were retracted flush to the wall for most of the steady-state experiments.

4.2 Measured Pressure and Temperature Profiles

Typical data are presented and compared to the theoretical predictions in Figs. 4.1 - 4.7. To make the local slope changes in the pressure profile visible, the hydrostatic, all liquid, pressure head at nominal run temperature was substracted from the absolute pressure. The plotted value therefore corresponds exactly to the pressure transducer signal. Appendix D gives a summary of the experimental runs and a tabulation of the data.

Figures 4.1 to 4.3 show the dependence of the total pressure drop across the heated section, $p_1 - p_{ex}$, on the mass flow rate, for two

different inlet temperatures at three power levels. Both the uniform and the chopped cosine heat flux distribution results are plotted in these figures. In one instance, the "rooftop" distribution is also included. Figures 4.4 to 4.6 are randomly selected pressure profiles along the channel.

4.2.1 Total Pressure Drop at the Threshold of Stability

The accurate prediction of the steady-state pressure drop at the threshold of stability and at other dynamically interesting points is of paramount importance in this work. A final test of the calculation methods developed in the preceding chapter is made here by comparing the total pressure drops $(p_1 - p_{ex})$, measured during the stability experiments described in the following chapter, to PRESDR predictions. This comparison given in Fig. 4.7 includes all threshold and transition points of runs D4 to D21. For the PRESDR calculations the channel was subdivided into 14 segments, the heat losses and subcooled boiling according to Levy's model were taken into account, and one major iteration was required for each experimental point.

4.3 Accuracy of the Predictions

The accuracy of the steady-state pressure drop predictions was generally good to excellent. Some discrepancies that were noted are analyzed below.

4.3.1 Pressure Drop Predictions

Table 4.2 gives the average predicted to measured total pressure drop ratios and associated rms errors for all the points plotted in Fig. 4.7.

There is apparently a systematic but small error in the predictions as the average ratio is 0.97. The 6% rms error is otherwise quite satisfactory.

Table 4.2

Accuracy of the Total Pressure Drop Predictions at the Threshold of Stability and the Transition Points

Runs	Heat Flux Distribution	Number of points	Ave. predicted to measured ratio	rms error
D4-D23	uniform	77	0.974	0.062
D4-D23	cosine	25	0.970	0.053
TR, E	uniform	23	0.955	0.066
E	unheated inlet	12	0.985	0.025
All	-	137	0.971	0.059

See also Fig. 4.7

Inspection of Figs. 4.1 to 4.3 indicates that the agreement between the measured and predicted total pressure drops is similar to that exhibited by the data of Fig. 4.7. The only noticeable disagreements are in the low exit quality, high velocity region (x = 0.01 to 0.05) where the experimental curves show an accentuated hump.

The pressure profiles plotted in Figs. 4.4 to 4.6 show invariably a disagreement between the predicted and measured pressure increment near the channel exit at low exit qualities and sufficiently high mass fluxes. The experimental profiles do not exhibit the predicted sharp pressure drop (caused by the acceleration term at the BB or the point of NVG), suggesting thermal non-equilibrium due to poor nucleation. Thermal non-

equilibrium could also arise from an insufficient rate of vapor generation when the flow is leaving the channel before reaching thermal equilibrium. In fact, as the friction and acceleration terms are dominant in this region (Fig. 3.5), a lower true exit quality, resulting from either mechanism, would produce a significantly smaller pressure drop at the exit, shifting the entire pressure profile downwards. The same trend is evident in Fig. 4.7 where the predicted-to-measured pressure drop ratio is generally larger than one at small exit qualities. At higher qualities and lower mass fluxes the flow is given sufficient time in the channel to reach equilibrium and these effects disappear. The effects of poor nucleation were dramatically exhibited in a hysteresis phenomenon that was observed and is reported in Section 4.6.

Figure 4.6 shows an opposite effect. PRESDROP exit pressure drop predictions are low for all but the highest and the lowest mass fluxes. Three different and opposing effects must be considered here:

a.) The separated flow model used here systematically underestimates the very important acceleration pressure drop in this region (page 74 of [59]; Table 4.3).

b.) The almost uncontrollable air content of the Freon has an important effect on the void fraction, as a recent investigation has shown [60].

c.) Void fraction measurements with Freon-22, reported by Zuber et al. [61] reveal a discrepancy of the Lockhart-Martinelli correlation, which was derived from adiabatic flow data and, moreover, does not account for the mass flux effect. The measured void fractions were always below the Lockhart-Martinelli predictions, the error being largest for the lowest mass fluxes.

It appears that in Fig. 4.6 the first two effects (especially the air content of the Freon) were overwhelming. Excluding the high mass flux points (where poor nucleation at the exit is evident), the measured exit pressure drops are higher for all points except at 0.92 ft/s. Inspection of Fig. 3.5 will confirm that only this point is in the gravity dominated region. There are almost no discrepancies of this nature in Figs. 4.4 and 4.5.

4.3.2 Temperature Predictions

Acceptable agreement between the measured and the predicted temperature profiles was obtained, considering that no particular care was taken to minimize the thermocouple errors in this investigation.

The hypothesis of a deficient vapor formation near the exit at high mass flow rates, made in the previous section, seemed at first to be in disagreement with the temperature readings at station 8 which were lower than the saturation temperature, suggesting excess vapor formation. It was found however that this discrepancy was entirely due to a thermocouple error. In contrast to the other test stations which were made of plexiglass, station 8 was made of a massive brass block having a much larger heat capacity and conductivity, and rather large diameter insulated thermocouples were used. This resulted in a temperature reading at station 8 that was consistantly below

the saturation temperature by as much as 10 to 15 °F. When, however, the 0.062 in. OD insulated thermocouple was replaced by a 0.001 in. bare thermocouple, the discrepancy disappeared and temperatures slightly in excess or equal to the saturation temperature were recorded.

4.4 Effect of Subcooled Boiling

Visual observations have shown that, at low flow rates, detached bubbles, approximately 1/32 to 1/16 in. in diameter, were produced from discrete nucleation centers of the heated wall, only a few inches from the inlet, regardless of the heat flux intensity. At higher velocities, approximately above 1 or 1.5 ft/s, the first nucleation centers were generally pushed downstream up to an experimental station where numerous small geometry defects provided good nucleation centers. Both Levy's and Staub's predictions of the point of net vapor generation (see 3.5) were always well downstream of the visually observed values and there was no way to fit the data by any reasonable change of the model constants. Despite these facts, the pressure drop predictions in the subcooled region were good, suggesting that the opposite effects of the subcooled voidage on the gravity and frictional terms probably balance.

Figures 4.4 and 4.6 show the effect of the two models on the calculated pressure profile. Again, the differences are small and confined to a narrow region extending from the point of net vapor generation to the bulk boiling boundary.

4.5 Choice of the Void Fraction Correlation

As shown in Fig. 3.1 there is little difference in the predictions of

the three void fraction correlations that do take into account the relative velocity between the phases. To estimate the effect of the slip on the pressure drop, values calculated with the Lockhart-Martinelli void fraction correlation (L-M) are compared here to predictions made using the homogeneous void fraction model. The respective void fractions were used to evaluate the acceleration and gravitational pressure drop formulas of Sections 3.2.2 and 3.2.3. The frictional pressure drop term was calculated in both cases using the L-M method.

A few representative points at the threshold of stability were used for this comparison and the results are summarized in Table 4.3. The reported pressure drops are as usual measured from the entrance of the heated section to the channel exit ($p_1 - p_{ex}$).

For the few points tested here, the predicted to measured pressure drop ratio averaged 0.932 for the homogeneous and 0.992 for the L-M correlation. The deviations from the average, as characterized by the rms error were 9.2 percent for the homogeneous and only 5.7 percent for the L-M method.

4.6 Observed Hysteresis in the Pressure Drop Characteristic

As described in 4.1, the pressure-drop - flow-rate characteristics were generated by gradually increasing the flow rate. When, however, at the end of a run, the flow was reduced again to repeat a few points as a check, it was observed that very often these points would not lie on the increasing flow characteristic. The explanation that this behavior was due to suppression of the nucleation at high mass flow rates was advanced to explain the discrepancies. When the flow is reduced there is a

Table 4.3

Effect of the Relative Velocity Between the Phases (As Predicted by the L-M Correlation) on the Gravitational and Acceleration Pressure Drop

Point	q_{wi}	T_o	w	x_{ex}	Lockhart-Martinelli*			Homogeneous Model*			Calculated to measured total pressure drop ratio	
					Δp_{gr}	Δp_{ac}	Δp_{fr}	Δp_{gr}	Δp_{ac}	Δp_{fr}	L - M	Homog.
	[W/TL]	[°F]	$[\frac{lb_m}{hr}]$		[psi]			[psi]				
D20-194	500	41.7	396	0.196	4.344	0.352	0.908	4.088	0.774	0.900	0.978	1.006
D20-181	400	43.0	192	0.496	2.899	0.358	0.937	2.539	0.526	0.942	0.922	0.881
D19-191	300	40.0	234	0.203	4.227	0.132	0.412	3.914	0.290	0.416	0.992	0.961
D19-986	300	42.0	119	0.663	2.370	0.237	0.645	2.017	0.297	0.649	1.121	1.022
D4 -299	300	120.3	387	0.293	1.849	0.608	2.415	1.314	1.165	2.408	0.961	0.964
D4 -917	200	118.0	281	0.260	1.846	0.267	1.311	1.214	0.537	1.331	0.946	0.852
D17-296	100	85.3	154	0.117	4.103	0.028	0.140	3.687	0.068	0.145	1.024	0.935
D4 -294	100	116.6	286	0.120	2.759	0.100	0.622	2.034	0.241	0.653	1.006	0.846

*Small differences in the friction terms are due to change of properties with pressure

substantial delay before normal nucleation resumes. The main effect should be localized towards the channel exit.

The suspected hysteresis was revealed by making careful measurements at both increasing and decreasing flow rates, together with bulk temperature measurements. Figure 4.8 shows the measured pressure characteristics at stations 1 and 6. The effect is obviously at the exit, as the station 6 characteristic shows. The measured temperature profiles for two points lying on the two distinct branches of the curve are plotted in Fig. 4.9 which clearly shows that, on the decreasing flow rate curve, the flow was superheated toward the channel exit (the drop in temperature at the exit is a thermocouple error as pointed in 4.3.2). Figure 4.8 also shows that it was necessary to go above a certain velocity to induce the hysteresis cycle. Note that it was practically impossible to obtain any data on the negative slope part of the decreasing-flow branch: The return to normal nucleation was abrupt. There was, however, also a very slow time recovery that would take place in several minutes; points on the lower part of the curve would very slowly drift towards the upper curve.

A similar but much more violent phenomenon was observed during a later experiment in which the flow in the unheated channel was at a temperature close to saturation. There was absolutely no voidage in the test sections until the entire channel voided suddenly, in less than a second. Such sudden flashing can be explained by the strong dependence of the saturation temperature on pressure at the low pressures of these experiments. Apparently there was an avalanche effect, the voided upper parts of the channel reducing the pressure at lower points and creating further voids.

The occurrence of such nucleation instabilities should be kept in mind when examining other types of flow oscillations as they might trigger and enhance them. Unfortunately, they are practically unpredictable.

4.7 Effect of the Heat Flux Distribution on the Pressure Drop

The effect of the heat flux distribution will be discussed now by examining one-by-one the three terms of the pressure drop equation.

The acceleration pressure drop depends only on the inlet and exit qualities and therefore is completely independent of the heat flux distribution within the channel.

The gravity contribution comes mostly from the single-phase region. Any distribution that would result in downstream shift of the boiling boundary should therefore increase the gravity head.

The frictional pressure drop term becomes dominant near the exit of the channel, where the flow attains large velocities. In most cases, all the frictional pressure drop is concentrated near the exit. It follows that a downstream movement of the boiling boundary will reduce the frictional pressure drop slightly as a two-phase portion of the channel will be replaced by a single-phase portion which has a smaller friction contribution. The net effect will of course depend on the relative importance of gravity and friction (Fig. 3.5), but it is obvious that for relatively smooth distributions the change will be small. The calculated and experimental results of Figs. 4.1 and 4.2 confirm this observation.

4.8 The Pressure Drop in the Unheated Entrance Piping

An accurate estimate of the pressure drop between stations 0 and 1

(including the flow venturis and the valves) will become necessary for the dynamic predictions, later in this work. Using all the available data from the steady-state runs the following correlation was obtained:

$$\Delta p_{01gr} = (1.5 \text{ ft})\ \rho/144 \tag{4.1}$$

$$\Delta p_{01fr} = 0.00177\ \rho^{0.8}\ \mu^{0.2}\ V^{1.8}$$

$$= 7.01 \times 10^{-10}\ G^{1.8}\ \mu^{0.2}/\rho \tag{4.2}$$

where the pressure drop is in psi, ρ in lbm/ft^3, μ in lbm/hrft, V in ft/s and G in $lbm/hrft^2$.

The frictional pressure drop from the bypass to the inlet of the test sections through the preheater (HX2) is negligible.

4.9 Conclusions

The data presented in this chapter show that an accurate prediction of the pressure drop in low pressure systems is possible when well established correlations are used, the channel is subdivided into a relatively small number of segments, and the variations of the fluid properties with pressure are taken into account. The predictions were good in a relatively wide range of variables and particularly good (average error 3%, rms error 6%) in the region of interest for dynamic tests (for exit qualities mostly around 30 percent). The only discrepancies were due to unpredictable deviations from thermodynamic equilibrium. Subcooled boiling was shown to have only a small local effect on the pressure drop. The Lockhart-Martinelli void fraction correlation gave systematically better results than a void fraction based on the homogeneous model.

The heat flux distribution was shown to have only a minor effect on the total pressure drop.

Given the good agreement at steady-state it is felt that the dynamic calculations could be tackled with some confidence.

Chapter 5

DYNAMICS OF THE SINGLE-PHASE REGION

The single-phase region is defined here as the channel length extending from the inlet plenum (station 0) to the boiling boundary (BB), i.e. to the point where the mixed mean enthalpy is at saturation. It includes the unheated upstream portion of the channel between stations 0 and 1. Any occurrence of subcooled boiling in this region is neglected in this chapter. The length of the single-phase region will vary in time when the flow oscillates.

The linearized coolant energy equation, governing the time variation of enthalpy in the single-phase region under oscillating flow conditions, will be coupled with the transient conduction equation of the heated wall to yield the flow-to-local-enthalpy transfer function, $H(z,j\omega)$, at any axial position. The two sets of equations mentioned above will be linked by a flow-dependent heat transfer coefficient. Although the heat input to the wall will be maintained constant, there will be time varying heat input to the coolant because of heat storage in the wall.

A number of investigators [62,63,65,66,67] have considered the problem of heated wall dynamics. The incentive was generally to predict the thermal behavior of the fuel in a nuclear reactor under transient conditions, and especially during oscillator tests when some variable, generally the power, is externally oscillated in order to measure the dynamic characteristics of the reactor. The transfer functions obtained vary in complexity in inverse proportion to the number of simplifying

assumptions made in their derivation. In the present study, almost all simplifying assumptions were avoided. The solution is identical to the one obtained by Smets [63] for the case of oscillating flow. However, a simpler derivation is presented here; the resulting transfer function is put into a much more compact and meaningful form, and the solution is specialized to represent the exact experimental conditions.

Once the wall temperature and the enthalpy variations along the channel have been determined, it is relatively easy to deduce the time-varying position of the boiling boundary, again using a linearized model for simplicity. In the present work, some effects that had been neglected in previous analyses, because they were relatively unimportant in high pressure systems, are considered and shown to be of some importance in low pressure systems. These are the pressure variations at the instantaneous position of the boiling boundary due to the gravity head, to the frictional losses in the single-phase region, and to the inertia of the subcooled liquid column. Finally, knowing the instantaneous position of the boiling boundary and the instantaneous flow, the pressure drop variations in the single-phase region will be obtained in a straightforward manner.

In this chapter, all the formulations will be treated in a completely linearized form. In fact, the wall conduction equation is inherently linear. An exact non-linear solution for the coolant energy equation can be obtained numerically when a steady and uniform heat input to the coolant is assumed (Section 5.2.4.1). This solution was not used, however, in order to save computation time and to facilitate the incorporation of the wall dynamics into the model. The comparison with the exact solution will confirm, as expected, the validity of the linear solution at the small

relative amplitudes, which occur at the threshold of stability.

The linearized equations will be Laplace-transformed in time and then integrated in space. Although, in the sections that follow, the Laplace variable, s, and its imaginary part, $j\omega$, the imaginary angular frequency, are used interchangeably, it is understood that the transfer functions will be evaluated along the imaginary frequency axis $j\omega$. Subroutine DZDWTF was written in FORTRAN IV to perform the numerical computations on the IBM-360 and is listed in Appendix F.

5.1 Dynamics of the Heated Wall

The transient conduction equation of the heated wall will be solved in this section. It is recalled that heat is supplied to the test sections by means of the electrically conductive external coating. The following assumptions are made:

a.) The heat generation rate is constant. Since the temperature coefficient of resistivity of the oxide coating is of the order of $10^{-4}/°C$, this assumption is fully justified.

b.) The coating can store no significant amount of energy. This is reasonable for the 16 μin. coating.

c.) The heat losses are either negligible or time independent. In Section 3.7 it was noted that the losses are less than 5 percent.

d.) The thin cylindrical glass tube wall is approximated by a plate of equal thickness. Although the solution for a cylindrical geometry can be obtained at small additional complication (namely, replacement of the hyperbolic functions that will appear in the solution by the corresponding

Bessel functions), the plane solution was retained to simplify the numerical work.

e.) The axial heat conduction in the wall is neglected.

f.) Average values of the thermophysical properties of the glass wall are used.

g.) The heat generation and the heat transfer to the coolant are circumferentially uniform (one dimensional problem).

h.) The heat transfer at the wall-fluid interface will vary according to the instantaneous value of the flow.

i.) Any axial heat flux distribution is permitted.

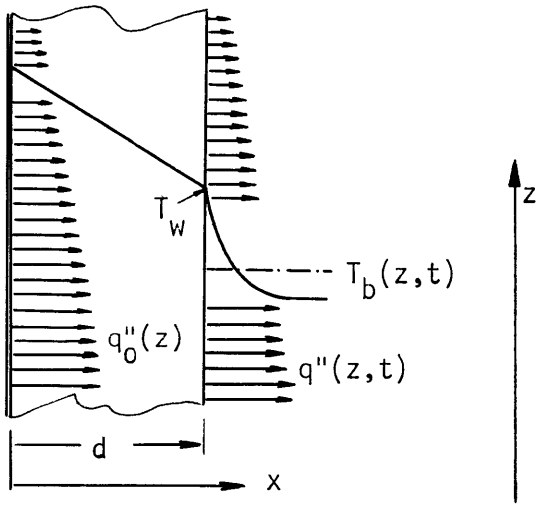

FIG. 5.1 THE HEATED WALL

The conduction equation at axial position z, for the geometry shown in Fig. 5.1 becomes

$$\frac{\partial^2 T(z,x,t)}{\partial x^2} = \frac{1}{\alpha} \frac{\partial T(z,x,t)}{\partial t} \qquad (5.1)$$

where $\alpha = (k/\rho c)_w$ is the thermal diffusivity of the wall. In accordance with assumptions a.) to c.) the boundary condition at the heated side is

$$- \frac{\partial T(z,x,t)}{\partial x}\bigg|_{x=0} = \frac{q''_o(z)}{k} \tag{5.2}$$

where $q''_o(z)$ is the applied constant heat flux. At the cooled side, the boundary condition is

$$- \frac{\partial T(z,x,t)}{\partial x}\bigg|_{x=d} = \frac{h_c(t)}{k} \left[T(z,d,t) - T_b(z,t)\right] \tag{5.3}$$

where $T(z,d,t)$ is the surface temperature at axial position z, $T_b(z,t)$ the corresponding fluid bulk temperature, and $h_c(t)$ the time-dependent (flow dependent) convective heat transfer coefficient.

It is convenient to write

$$T(z,x,t) = T^\circ(z,x) + \delta T(z,x,t) \tag{5.4}$$

$$T_b(z,t) = T^\circ_b(z) + \delta T_b(z,t) \tag{5.5}$$

$$h_c(t) = h^\circ_c + \delta h_c(t) \tag{5.6}$$

where the superscript $^\circ$ denotes the steady-state conditions satisfying the time-independent equations

$$\frac{\partial^2 T^\circ(z,x)}{\partial x^2} = 0 \tag{5.7}$$

$$q''_o(z) = h^\circ_c \left[T^\circ(z,d) - T^\circ_b(z)\right] = - k \frac{\partial T^\circ(z,x)}{\partial x}\bigg|_{x=d} \tag{5.8}$$

and the δ denotes small perturbations from equilibrium.

As stated in assumption h.) above, if the heat transfer coefficient

can be expressed as

$$h_c^\circ = \text{constant} \cdot w_o^a$$

for small flow variations,

$$\frac{\delta h_c(t)}{h_c^\circ} = a \frac{\delta w(t)}{w_o} \tag{5.9}$$

Lacking a better discription of the transient convective boundary condition, it is hoped that this formulation will be valid, at least at low frequencies [69,70].

Inserting definitions (5.4) to (5.6) into Eqs. (5.1) to (5.3), eliminating the steady-state terms from these equations, and neglecting the only second-order term in Eq. (5.8) yields

$$\frac{\partial^2 \delta T(z,x,t)}{\partial x^2} = \frac{1}{\alpha} \frac{\partial \delta T(z,x,t)}{\partial t} \tag{5.10}$$

$$- \frac{\partial \delta T(z,x,t)}{\partial x}\bigg|_{x=0} = 0 \tag{5.11}$$

$$- \frac{\partial \delta T(z,x,t)}{\partial x}\bigg|_{x=d} = \frac{C}{d} [\delta T(z,d,t) - \delta T_b(z,t)] + E(z)\, \delta w(t) \tag{5.12}$$

where $$C \equiv \frac{h_c^\circ}{k/d} \tag{5.13}$$

and $$E(z) = \frac{a}{k} \frac{q_o''(z)}{w_o} \qquad \left[\frac{^\circ F/ft}{lbm/hr}\right] \tag{5.14}$$

Notice that in the equations written above the axial coordinate z is merely a parameter introduced through the boundary condition, in particular T_b.

Eqs. (5.10) to (5.12) will be now Laplace-transformed in time*, with the initial condition $\delta T(z,x,0) = 0$:

$$\frac{\partial^2 \delta T(z,x,s)}{\partial x^2} = \frac{s}{\alpha} \delta T(z,x,s) \tag{5.15}$$

$$- \left.\frac{\partial \delta T(z,x,s)}{\partial x}\right|_{x = 0} = 0 \tag{5.16}$$

$$- \left.\frac{\partial \delta T(z,x,s)}{\partial x}\right|_{x = d} = \frac{C}{d} [\delta T(z,d,s) - \delta T_b(z,s)] + E(z)\ \delta w(s) \tag{5.17}$$

The general solution of Eq. (5.15) is

$$\delta T(z,x,s) = m(z,s) \cosh\left(\sqrt{\frac{s}{\alpha}}\, x\right) + n(z,s) \sinh\left(\sqrt{\frac{s}{\alpha}}\, x\right)$$

Boundary condition (5.16) forces n(z,s) to zero and the remaining boundary condition (5.17) is used to determine m(z,s). The final result is

$$\delta T(z,x,s) = \frac{C\ \delta T_b(z,s) - d\ E(z)\ \delta w(s)}{d \sqrt{\frac{s}{\alpha}} \sinh\left(\sqrt{\frac{s}{\alpha}}\, d\right) + C \cosh\left(\sqrt{\frac{s}{\alpha}}\, d\right)} \cdot \cosh\left(\sqrt{\frac{s}{\alpha}}\, x\right) \tag{5.18}$$

Then, for x = d, the inner wall temperature $\delta T_w(z,s) = \delta T(z,d,s)$ becomes

$$\delta T_w(z,s) = \frac{C\ \delta T_b(z,s) - d\ E(z)\ \delta w(s)}{F(s) + C} \tag{5.19}$$

where

$$F(s) \equiv \sqrt{\tau_k s} \tanh \sqrt{\tau_k s} \tag{5.20}$$

---

*To avoid overburdening the notation, the same symbols are used for the transformed variables, with t replaced by the complex frequency s.

with

$$\tau_k \equiv d^2/\alpha$$

5.2 The Flow-to-Local-Enthalpy Transfer Function

In this section the coolant energy equation, together with the wall temperature equation derived in the previous section, will be used to determine the time variations of the bulk temperature or enthalpy at any position along the single-phase region. The general solution, for any heat flux distribution, will be obtained first and then specialized for three particular cases of interest here. Some approximations to the "exact" solution will be discussed too.

5.2.1 Solution for Arbitrary Heat Flux Distribution

The following assumptions are made:

a.) The temperature and velocity gradients in the fluid are not taken into account and perfect mixing and "plug flow" are postulated. These assumptions, probably acceptable in turbulent water flow, become very poor in the extreme case of laminar flow, especially for Freon which has a low thermal conductivity. A pure conduction calculation using standard methods [58] has shown that 100 seconds were required for the temperature change at the center of a Freon column filling the test section, initially at uniform temperature, to reach approximately 50 percent of a step change in wall temperature. Akcasu [68] proposes an averaged transfer function to take into account the transit time spread, and Shotkin [14] makes a "heat source correction" based on a stationary-

fluid conduction and diffusion relation to account for the temperature profile.

b.) The flow is incompressible; length average values of other fluid-properties are used.

c.) There is no subcooled boiling.

d.) The kinetic and potential energy terms in the energy equation are, as usual, neglected.

With these assumptions, the energy equation for the coolant becomes

$$\rho_f \cdot \frac{\partial h(z,t)}{\partial t} + G(t) \frac{\partial h(z,t)}{\partial z} = \frac{q'(z,t)}{A} \tag{5.21}$$

with $$\delta h(z,t) = c\delta T_b(z,t) \tag{5.22a}$$

and $$q'(z,t) = h_c(t)\, P\, [T_w(z,t) - T_b(z,t)] \tag{5.22b}$$

where P is the heated perimeter, and $q'(z,t)$ is the linear heat input rate to the coolant. Assuming no inlet temperature perturbation

$$T_b(0,t) = T_b^\circ(0) = \text{constant} \tag{5.23}$$

The linearized form of Eqs. (5.21), and (5.23) utilizing Eqs. (5.22), is

$$\frac{1}{V_o} \frac{\partial \delta T_b(z,t)}{\partial t} + \frac{\partial \delta T_b(z,t)}{\partial z} = -\frac{q_o'(z)}{w_o\, c} \left[(1-a) \frac{\delta w(t)}{w_o} - \frac{\delta T_w(z,t) - \delta T_b(z,t)}{T_w^\circ(z) - T_b^\circ(z)}\right] \tag{5.24}$$

$$\delta T_b(0,t) = 0 \tag{5.25}$$

where the steady-state terms denoted by the superscript $^\circ$ satisfy the

reference conditions

$$\frac{dT_b^\circ(z)}{dz} = \frac{q_o'(z)}{w_o\ c}$$

$$q_o'(z) = h_c^\circ\ P\ [T_w^\circ(z) - T_b^\circ(z)]$$

and V_o is the reference coolant velocity $w_o/A\ \rho_f$.

The Laplace transforms of Eqs. (5.24) and (5.25), obtained with the initial condition

$$\delta T_b(z,0) = 0 \tag{5.26}$$

are

$$\frac{\partial \delta T_b(z,s)}{\partial z} + \frac{s}{V_o}\ \delta T_b(z,s) = -A(z)\ \delta w(s) + B\ [\delta T_w(z,s) - \delta T_b(z,s)] \tag{5.27}$$

and

$$\delta T_b(0,s) = 0 \tag{5.28}$$

where the coefficients are defined as follows:

$$A(z) \equiv \frac{q_o'(z)\ (1 - a)}{w_o^2\ c} \qquad [\frac{hr^\circ F}{ftlbm}] \tag{5.29}$$

$$B \equiv \frac{P\ h_c^\circ}{c\ w_o} \qquad [\frac{1}{ft}] \tag{5.30}$$

When the expression of δT_w as a function of δw and δT_b from Eq. (5.19) is substituted into Eq. (5.27), a first-order linear differential equation in δT_b with frequency-dependent coefficients is obtained

$$\frac{\partial \delta T_b(z,s)}{\partial z} + K(s)\ \delta T_b(z,s) = -\frac{q_o'(z)}{\bar{q}_o'\ c} L(s)\ \ \delta w(s) \tag{5.31}$$

where $\bar{q}_o'$ is some reference (average) linear heat rate,

$$K(s) \equiv \frac{s}{V_o} + B\,\frac{F(s)}{F(s)+C} \qquad [\frac{1}{ft}] \tag{5.32}$$

$$L(s) \equiv \frac{\bar{q}_o'}{\frac{2}{w_o}}\left[(1-a) + a\,\frac{C}{F(s)+C}\right] \qquad [\frac{Btu/lbm}{(lbm/hr)\,ft}] \tag{5.33}$$

Equation (5.31) with the boundary condition (5.26) can be solved by a Laplace transformation in z or by conventional means to yield the flow-to-local-enthalpy and the flow-to-local-bulk-temperature transfer functions

$$H(z,s) \equiv \frac{\delta h(z,s)}{\delta w(s)} = -L(s)\ e^{-K(s)z} \int_0^z \frac{q_o'(z')}{\bar{q}_o'}\ e^{K(s)z'}\ dz' \qquad [\frac{Btu/lbm}{lbm/hr}] \tag{5.34}$$

$$\frac{\delta T_b(z,s)}{\delta w(s)} = \frac{1}{c}\ H(z,s) \qquad [\frac{^\circ F}{lbm/hr}] \tag{5.35}$$

Knowing $\delta T_b(z,s)$ it is interesting to calculate the modulation of the heat flux to the fluid. From the conduction equation of the wall and from the convective heat transfer equation

$$\delta q''(z,s) = -k\,\frac{\partial \delta T(z,x,s)}{\partial x}\bigg|_{x=d}$$

$$= h_c^\circ\,[\delta T_w(z,s) - \delta T_b(z,s)] + \delta h_c\,[T_w^\circ(z) - T_b^\circ(z)]$$

Either equation yields the flow-to-heat-flux transfer function

$$Q(z,s) \equiv \frac{\delta q''(z,s)}{\delta w(s)} = \left[-\frac{h_c^\circ}{c} H(z,s) + k\, E(z)\right] \frac{F(s)}{F(s)+C} \quad \left[\frac{Btu/hrft^2}{lbm/hr}\right] \tag{5.36}$$

5.2.1.1 Non-dimensional Form of the Transfer Functions

It is sometimes convenient to use the transfer functions in a non-dimensional form by normalizing the enthalpy variations to h_{fg} (evaluated preferably at the boiling boundary) and the other perturbations to the corresponding average values:

$$H^*(z,s) \equiv \frac{\delta h(z,s)/h_{fg}}{\delta w(s)/w_o} = \frac{w_o}{h_{fg}} H(z,s)$$

$$Q^*(z,s) \equiv \frac{\delta q''(z,s)/q_o''(z)}{\delta w(s)/w_o} = \frac{w_o}{q_o''(z)} Q(z,s)$$

$$= \left[-\frac{h_{fg}\, h_c^\circ\, P}{c\, q_o'(z)} H^*(z,s) + a\right] \frac{F(s)}{F(s)+C}$$

These two transfer functions are plotted in Fig. 5.2* for a set of representative conditions with a uniform heat flux distribution (5.2.2.1). Notice that in this figure, and in general in this work, the phase delay rather than the phase angle is used as a more representative quantity. Figure 5.3 is intended to remove any ambiguity on this point.

*The waviness of the lines of this and following plots is due to the limited resolution of the digital plotter used to produce these figures directly from computer output.

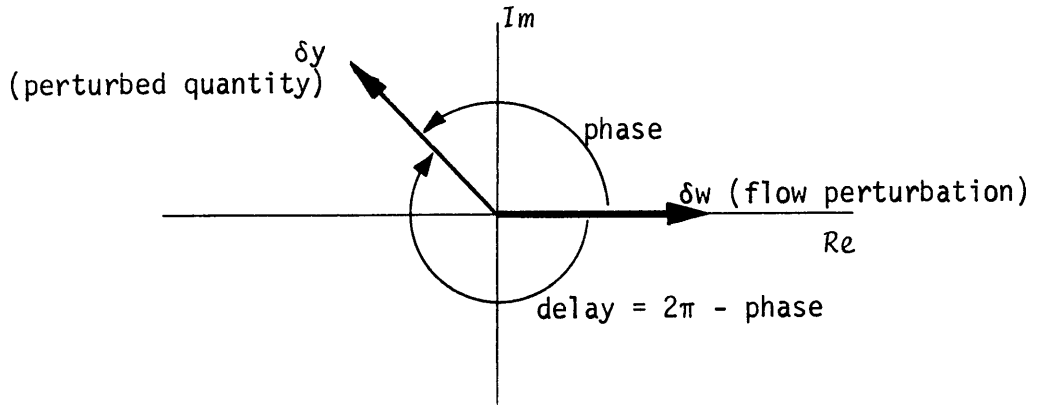

FIG. 5.3 DEFINITION OF THE DELAYS AS USED IN THIS WORK

It is also more practical to plot the transfer functions versus the period, which is a directly measurable quantity and has convenient units rather than the circular frequency $\omega = 2\pi/\tau$.

One immediate observation regarding $Q^*(z,s)$ is that at high frequencies, as the storage effects become negligible, the heat flux variations are in phase with the flow variations, while at low frequencies, where the wall heat storage plays an important role, $\delta q''$ is leading δw by 90°.

Figure 5.4 shows the parametric variations of $H^*(z,j\omega)$ in the complex plane, around some arbitrarily chosen representative point. The effects of G, q_o' and z are included in this plot.

5.2.1.2 Characteristic Constants

The equations derived above can be characterized in the time domain by two constants, namely the wall conduction time constant

$$\tau_k \equiv \left(\frac{d\rho c}{k/d}\right)_w = \frac{d^2}{\alpha} \qquad (5.37)$$

the convective time constant

$$\tau_h \equiv \frac{(d\rho c)_w}{h_c^\circ} = \frac{d\,k}{\alpha h_c^\circ} \tag{5.38}$$

and their ratio

$$C \equiv \frac{\tau_k}{\tau_h} = \frac{h_c^\circ}{k/d} \quad , \quad \text{already defined.}$$

The conduction time constant controls the temperature gradient in the wall, while the convection time constant affects the transient heat transfer to the coolant. The values of these constants for this particular experimental setup are given in Fig. 5.2.

The wavelength $\lambda = V_o \tau$ determines the space dependence of the solutions, which also have a periodic character in space. In Chapter 7 the regions of unstable operation will be characterized by the values of the ratio z_{bb}°/λ, where z_{bb}° is the single-phase length. The largest integer not exceeding z_{bb}°/λ, will be called the order of oscillation.

5.2.1.3 High Frequency Approximation

At large frequencies, i.e. when the period gets much shorter than the conduction time constant, $\tau << 2\pi\tau_k$,

$$F(j\omega) \rightarrow \sqrt{\tau_k \omega}\ (1 + j)$$

$$L(j\omega) \rightarrow \frac{\bar{q}_o'}{w_o^2}\ (1 - a)$$

$$K(j\omega) \rightarrow \frac{j\omega}{V_o} + B \rightarrow \frac{j\omega}{V_o} \quad \text{provided that } 2\pi\tau_c >> \tau \text{ where}$$

$$\tau_c \equiv \frac{\rho A c}{P\, h_c^\circ} \tag{5.39}$$

For a uniform heat flux distribution, evaluation of the integral in Eq. (5.34) with K and L as given above yields

$$H^*(z,j\omega) \rightarrow \frac{\bar{q}_o'(1 - a)\, V_o}{w_o\, h_{fg}} \cdot \frac{e^{-j\omega\frac{z}{V_o}} - 1}{j\omega} \rightarrow 0$$

at ω sufficiently large, and

$$Q^*(z,j\omega) \rightarrow a$$

Stenning and Veziroglu [7], in a similar derivation, did not consider the wall dynamics but did account for flow-dependent heat flux by writing $\delta q''/q_o'' = a\, \delta w/w_o$ in the energy equation. This results in the high frequency approximation presented above. Figure 5.2 shows that this high frequency approximation is a rather poor one in the range of interest in this work (2 to 10 second periods). The approximation is even worse in the case of Stenning and Veziroglu's apparatus [7] which had a conduction time constant of only about 0.1 sec. It is suspected that this discrepancy might have been partly responsible for the lack of agreement between their analytical predictions and test data.

5.2.1.4 Case of Negligible Heat Storage in the Wall - Low Frequency Approximation

It can be shown by a series expansion of the hyperbolic functions that when the product $d\rho c\omega$ tends towards zero, the following approximations can be made:

$$K(j\omega) \rightarrow \frac{s}{V_o}$$

$$L(j\omega) \rightarrow \frac{\bar{q}_o'}{w_o^2}$$

$$F(j\omega) \rightarrow 0$$

In practice this occurs when the period of interest becomes much larger than $2\pi\tau_k$ ($d\rho c\omega << k/d$) and $2\pi\tau_h$ ($d\rho c\omega << h_c^\circ$), i.e. when, for equal corresponding temperature perturbations, the heat flux "retained" in the wall becomes negligible with respect to the conduction and convection heat flux perturbations. The heat flux perturbation in this case naturally disappears, $\delta q''(z,j\omega) \rightarrow 0$. Notice that the low and high frequency approximations are identical except for the (1-a) attenuation factor at high frequencies.

5.2.1.5 Case of Highly Conductive Wall

If the wall is an excellent heat conductor ($k \rightarrow \infty$) but still has a substantial heat capacity ($d\rho c \neq 0$), i.e. when $\tau >> 2\pi\tau_k$,

$$K(j\omega) \rightarrow \frac{j\omega}{V_o} + B\,\frac{j\omega}{j\omega + 1/\tau_h}$$

$$L(j\omega) \rightarrow \frac{\bar{q}_o'}{w_o^2}\left[(1-a) + \frac{a/\tau_h}{j\omega + 1/\tau_h}\right]$$

and again $F(j\omega) \rightarrow 0$. But now the heat flux perturbation becomes

$$\delta q''(z,j\omega) = j\omega\, a\, q_o''(z)\, \tau_h \cdot \frac{\delta w(j\omega)}{w_o}$$

5.2.2 Solutions for Given Heat Flux Distributions

Once the heat flux distribution $q_o'(z)$ is specified, the integral

in Eq. (5.34) can be evaluated to yield explicitly the flow-to-local-enthalpy transfer function, $H(z,s)$. The solutions for three cases of particular interest in this work are given below.

5.2.2.1 Uniform Heat Flux Distribution

When $q_o'(z) = q_o'$ = uniform along the channel,

$$H(z,s) = \frac{L(s)}{K(s)} \left(e^{-K(s)z} - 1\right)$$

5.2.2.2 Exact Chopped Cosine Heat Flux Distribution

For the heat flux distribution shown in Fig. 5.5

$$q_o'(z) = \bar{q}_o' \frac{\ell}{N} \sin\left(\pi \frac{\ell_1+z}{\ell_o}\right)$$

where $$N = \frac{\ell_o}{\pi}\left\{\cos\left[\frac{\pi\ell_1}{\ell_o}\right] - \cos\left[\frac{\pi(\ell+\ell_1)}{\ell_o}\right]\right\}$$

is a normalized factor and $\bar{q}_o'$ is the average heat flux.

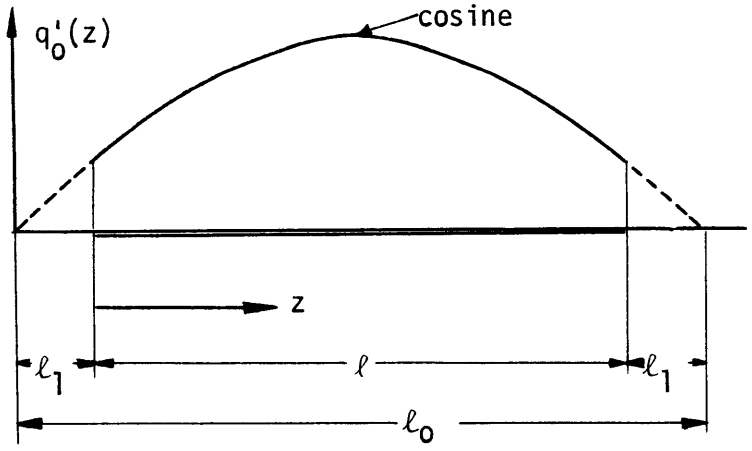

FIG. 5.5 CHOPPED COSINE HEAT FLUX DISTRIBUTION

Utilizing these expressions Eq. (5.34) yields

$$H(z,s) = - L(s)\, e^{-K(s)z} \frac{N}{[K(s)]^2 + [\frac{\pi}{\ell_o}]^2} \cdot$$

$$\left\{ e^{K(s)z} [K(s) \sin (\pi \frac{\ell_1+z}{\ell_o}) - (\frac{\pi}{\ell_o}) \cos (\pi \frac{\ell_1+z}{\ell_o})] \right.$$

$$\left. - [K(s) \sin (\pi \frac{\ell_1}{\ell_o}) - (\frac{\pi}{\ell_o}) \cos (\pi \frac{\ell_1}{\ell_o})] \right\}$$

5.2.2.3 Stepwise Varying Heat Flux Distribution

This case is of special importance in this work as it approximates closely the experimental conditions. If the heat flux distribution is given by

$$q'_o(z) = q'_{io} \quad \text{for} \quad z_i < z < z_{i+1}, \quad i = 1,N$$

piecewise evaluation of the integral in Eq. (5.34) yields

$$H(z,s) = - \frac{L(s)}{K(s)}\, e^{-K(s)z} \left\{ \sum_{j=1}^{J-1} (\frac{q'_{jo}}{q'_o}) [e^{K(s)z_{j+1}} - e^{K(s)z_j}] \right.$$

$$\left. + (\frac{q'_{Jo}}{q'_o}) [e^{K(s)z} - e^{K(s)z_J}] \right\}$$

where J is the segment in which z lies: $z_J < z < z_{J+1}$.

5.2.3 Heat Flux Distribution and Wall Heat Storage Effects

As it will become evident in subsequent chapters, the time delays in

the single-phase region, especially the delay between the inlet flow peak and the peak of the enthalpy at the boiling boundary are of paramount importance for the stability of the system. In this section, the effect of the heat flux distribution on the flow-to-local-enthalpy transfer function, $H(z,s)$ is examined and the effect of the heat capacity of the wall is brought out by comparing the transfer functions with and without the wall effect.

5.2.3.1 Importance of the Wall Heat Storage

Figures 5.6 to 5.8 show the enthalpy variations along the channel, in amplitude and phase, for three experimental points covering the observed ratios of single-phase length to wavelength z°_{bb}/λ (orders 0, 1, and 4). Both the complete solution and the high frequency approximations are shown. These three figures emphasize the fact already noted that the wall dynamics plays an important role, at least under the present experimental conditions, in determining the enthalpy variations along the channel. For all cases there are significant differences both in amplitude and in phase between curves 2 (with wall effect), 3 (high frequency approximation) and 4 (no wall heat storage at all).

5.2.3.2 Importance of the Unheated Portions of the Wall

As explained in Section 2.1.1 there are unheated portions, approximately 2 in. long between test lengths. When these cold spots were taken into account in the transfer function calculations, using the formulas given in Section 5.2.2.3, their importance became evident. The effect is significant, even for first-order oscillations. Substantial differences are noted at higher modes, when the wavelength approaches the

unheated length. Curves 1 of Figs. 5.6 to 5.8 show these results.

5.2.3.3 Uniform Versus Cosine Power Distribution

As both a uniform and a chopped cosine power distribution (as defined in Table 4.1) were used for the stability experiments, it is of interest to examine their effect on the flow-to-local-enthalpy transfer function. In the comparative calculations, the flow rate, period, and average temperature, referring to an experimental point obtained with a uniform power distribution, were used for both cases. The power input for the cosine case was adjusted to give the same total heat input in the single-phase region (same position of the boiling boundary). Figures 5.9 and 5.10 show the results obtained. In both cases the amplitude distribution seems to follow the heat flux distribution; however, for the cosine case, the entire phase curve is shifted downstream because of the low heat flux at the channel inlet.

5.2.3.4 Effects of Channel Segmentation

Finally, in order to test the validity of the simulation of a continuous power profile by a small number of stepwise variations of the heat flux, as was done in this experiment, the transfer functions for the exact chopped cosine and the simulated chopped cosine were compared. The heat flux distribution of Fig. 5.5 with ℓ_1 = 0.25 ft and ℓ = 9.04167 ft represents the case that was stepwise simulated by the "cosine" distribution used throughout this work. The exact cosine solution is given as the dotted line in Fig. 5.9 for a zero-order case. The two curves are practically superimposed, both in amplitude and in phase.

When the test was repeated for the fourth order case of Point D18A-196, a large difference in the results was revealed. The exact cosine distri-

bution gave almost no wavy structure, while large space oscillations existed in the simulated, stepwise cosine solution. In order to ascertain that the difference was not due to some computational error, the calculations were repeated with the entire channel length subdivided into 14, 28, and 56 segments instead of the original 7. The heat flux assigned to each segment was the average value at the corresponding portion of the exact cosine curve. Figure 5.11 shows how the solutions, although widely different for 7 segments, converge very rapidly to the exact cosine result. For 28 segments, the two solutions are almost undistinguishable.

The two tests described above, namely the cold spot and the segmentation tests, showed that small discontinuities of the heat flux distribution might have unexpectedly large effects on the enthalpy variations along the channel, especially at high frequencies and with multiple-mode oscillations. The combined effects of the cold spots, the discontinuous power distribution and the wall heat storage might produce strange variations of $H(z,j\omega)$ along the channel and even "resonances" when the test-section-length-to-wavelength ratio assumes particular values (Chapter 7). The effect of the uneven heat generation in the conductive coating (Section 2.1.1) is certainly minor compared to the effect of the cold spots.

5.2.4 Understanding the Physical Phenomena - A Lagrangian, Non-Linear Solution

An attempt will now be made to gain some understanding of the physical phenomena governing the variations of enthalpy along the channel.

The fact that, for a uniform and steady heat input, the enthalpy gained by a fluid particle is directly proportional to its residence time in the heated channel suggests that a Lagrangian description might be appropriate. Assuming a sinusoidal variation of the flow

$$V(t) = V_o + \hat{\delta V} \sin \omega t \tag{5.40}$$

the axial position, z, of a particle that spent a time Δt in the heater will in general depend on Δt and on the time t' at which it entered the heated section

$$z(\Delta t, t') = \int_{t'}^{t'+\Delta t} V(t)\, dt = V_o\, \Delta t - \frac{\delta \hat{V}}{\omega} [\cos\omega\, (t'+\Delta t) - \cos\omega\, t'] \tag{5.41}$$

It is obvious that if Δt is chosen to be equal to the period τ, all particles will reach the same point z in Δt, regardless of their entrance time, and therefore pick up the same amount of enthalpy on the way. Therefore, the enthalpy variations will resemble a standing wave with nodes equally spaced by a wavelength $\lambda = V_o \tau$, as clearly shown in Figs. 5.7 and 5.8 (curves without wall effect). The same effect is evident in the Bode plot of $H(z, j\omega)$ at a fixed location (Fig. 5.2). Nodes appear whenever $\tau = z/n\, V_o$, with n taking integer values.

Furthermore, the slope of the linear phase relationship, given in Figs. 5.6 to 5.8 for the case of uniform and steady heat input, indicates that the enthalpy perturbation travels along the channel at twice the average flow velocity. Considering, for example, the enthalpy variations at $z = \lambda/2$, where they are most pronounced, this simply means that the

enthalpy-wise most perturbed particle is not the one that enters at the peak of the flow. It is actually the one that entered a quarter of a cycle before and has felt the effect of higher velocity (lower transit time, lower enthalpy gain) all the way up to $z = \lambda/2$. The particle will reach this location in approximately half a cycle, but only a quarter of a cycle after the peak of the flow.

Any unsteadiness or non-uniformity in the heat input to the fluid will tend to blunt the sharp nodes. The heat storage in the walls produces such an effect by delaying the heat input (Figs. 5.7 and 5.8). A similar effect is produced by the cold spots of the heated wall. Notice that the delay increases twice as fast in the unheated regions, where the enthalpy perturbation travels at the flow velocity rather than at twice the flow velocity. Therefore, even a short unheated length can produce significant changes, especially when the effects accumulate, as shown in Fig. 5.8. The slow attenuation of the amplitude of δh in the unheated regions is due to the real part of $K(s)$ (Eq. 5.32) or, physically speaking, to heat losses to the wall. The effect disappears when, without the wall effect, $\exp K(s)$ becomes a pure delay.

Notice also that unheated or poorly heated regions, as considered in Figs. 5.7, 5.8 and 5.11, can also produce delays between 0 and 180°, which are otherwise unattainable in the uniform heat flux case which has the delay oscillating between 180 and 360°.

5.2.4.1 An exact Non-Linear Lagrangian Solution

An exact non-linear solution will be developed now for the case of uniform and steady heat input to the fluid, in order to evaluate the

effects of the non-linearities. For a sinusoidal oscillation of the flow (Eq. 5.40), $z(\Delta t, t')$ is given by Eq. (5.41). Taking the enthalpy at the heater inlet as zero, $h(0,t) = 0$, the particle at z will have gained an enthalpy

$$h(z,t) = q''' \frac{\Delta t}{\rho}$$

where q''' is the heat input per unit volume of coolant ($Btu/hrft^3$). Subtracting the steady-state enthalpy rise

$$h^\circ(z,t) = q''' \frac{\Delta t^\circ}{\rho} \quad , \quad \text{where} \quad \Delta t^\circ = \frac{z}{V_o} \, ,$$

$$\delta h(z,t) = \frac{q'''}{\rho} \left(\Delta t - \frac{z}{V_o}\right) \tag{5.42}$$

with $$t = t' + \Delta t \tag{5.43}$$

Equations (5.41) to (5.43), solved simultaneously for various values of the entrance time t', will provide the variations of δh at any axial location z. The non-dimensional form of these equations will be used below:

$$z^*(\Delta t^*, t^*) = \Delta t^* + \frac{\delta \hat{V}}{\pi V_o} \sin(2\pi t^* - \pi \Delta t^*) \sin(\pi \Delta t^*) \tag{5.44}$$

$$\delta h^*(z^*, t^*) = \Delta t^* - z^* \tag{5.45}$$

where

$$t^* = \frac{t}{\tau} \, , \quad \Delta t^* = \frac{\Delta t}{\tau} \, , \quad z^* = \frac{z}{\lambda} \, , \text{ and } \quad \delta h^* = \delta h \frac{\rho}{q'''\tau}$$

Equation (5.44) is used to generate values of z^* for a fixed value of t^* and variable Δt^*, and Eq. (5.45) provides the corresponding δh^*.

Figures 5.12 and 5.13 show the results obtained in this way for

$\delta\hat{V}/V_o$ equal to 0.1 and 1.0 . Parts a.) of these figures show the enthalpy perturbation profiles at various times. Thermocouples, at fixed locations measuring the average fluid temperature would have produced the temperature traces shown in parts b.). At $\delta\hat{V}/V_o = 0.1$ the curves are quasi-sinusoidal and coincide with the linear solution obtained previously, while they deviate completely from sinusoids at $\delta\hat{V}/V_o = 1$.

Notice the progression in space and time of the enthalpy perturbation waves in the part a.) of these figures. Due to the linear relationship of Eq. (5.45), points of equal transit time lie on straight lines in the $(\delta h^*, z^*)$ plane. These lines are almost vertical at small $\delta\hat{V}/V_o$. At larger relative flow oscillations, they progressively rotate around their intersections with the $\delta h^* = 0$ axis and distort the characteristic wave pattern.

The perturbation velocity can be obtained from the $(\delta h^*, t^*)$ plane by cross-plotting the z^* of each curve versus the time at which δh^* reaches its peak value. The slope of such a plot is the perturbation velocity, which is twice as large as the flow velocity. This slope is constant at small $\delta\hat{V}/V_o$, and the points deviate only slightly from a straight line, even at $\delta\hat{V}/V_o = 1$ which denotes a constant propagation velocity.

Another interesting observation from these plots is that the non-linearities, by distorting the sine waves, introduce additional time delays; the peaks and valleys of the curves are shifted in time when the relative oscillation amplitude changes.

5.3 The Position of the Boiling Boundary

The time-varying position of the boiling boundary, $z_{bb}(t)$, is primarily determined by the enthalpy variations $\delta h(z^{\circ}_{bb},t)$ at the steady-state location, z°_{bb} of the BB. In a low pressure system, however, the movements of the BB are also affected by the pressure variations in the single-phase region. All of these effects will be considered in the derivation that follows. Starting with the simplest description, the degree of sophistication will be increased gradually in order to separate the various effects.

5.3.1 Effect of the Enthalpy Variations

Figure 5.14A shows the enthalpy, h, and the saturation enthalpy, h_f, profiles (assumed flat in this case) around the BB, at steady state and at some time t during the oscillation. It is evident that, neglecting second order terms,

$$\delta z_{bb} = -\frac{\delta h^{\circ}_{bb}}{(\frac{dh^{\circ}}{dz})_{bb}}$$

5.3.2 Effect of the Pressure Variations

The static pressure variations will tilt the saturation enthalpy profile, while the dynamic pressure oscillations will displace it, both causing a corresponding movement of the BB. The static and dynamic effects are considered now separately.

5.3.2.1 Static Pressure Effects - Variable Saturation Enthalpy Along The Channel

With reference to Fig. 5.14B, in this case

$$\delta z_{bb} = - \frac{\delta h^{\circ}_{bb}}{\left(\frac{dh^{\circ}}{dz}\right)_{bb} - \left(\frac{dh^{\circ}_f}{dz}\right)_{bb}}$$

the superscript $^{\circ}$ and the subscript bb meaning again that the quantities are evaluated at the steady-state location of the BB.

5.3.2.2 Dynamic Pressure Effects

Changes in flow will produce a change in the frictional component of the pressure drop in the single-phase region and will add an inertial component. At the instantaneous position of the BB, z_{bb},

$$p_{bb}(z_{bb}) = p^{\circ}(z_{bb}) + \delta p_{fr} + \delta p_{in}$$

where assuming that $\Delta p^{\circ}_{lfr} = \text{constant} \cdot w^{1.8}$,

$$\delta p_{fr} = \frac{\partial p_{bb}}{\partial w} \delta w \approx \frac{\partial p^{\circ}_{bb}}{\partial w} \delta w = 1.8 \, \Delta p^{\circ}_{lfr} \frac{\delta w}{w_o}$$

and Δp°_{lfr} (< 0) is the total steady-state frictional pressure drop in the single-phase region. The inertia term is given by

$$\delta p_{in} = - z_{in} \frac{\partial G}{\partial t} \approx - z^{\circ}_{in} \frac{\partial G}{\partial t} = - \frac{z^{\circ}_{in}}{A} \frac{\partial w}{\partial t}$$

where z°_{in} is an equivalent inertia length for the single-phase region (Section 5.4.1). In both cases, the second-order terms $(\delta w \cdot \delta z)$ were neglected.

Figure 5.14C shows how the combined effect of the two dynamic terms will displace the pressure profile, and consequently the saturation enthalpy profile, by

$$\delta h^{\circ}_{fbb} = \left(\frac{dh_f}{dp}\right)_{p^{\circ}_{bb}} (\delta p^{\circ}_{fr} + \delta p^{\circ}_{in})$$

causing a final movement of the boiling boundary equal to

$$\delta z_{bb} = \frac{-\delta h^{\circ}_{bb} + \delta h^{\circ}_{fbb}}{\left(\frac{dh^{\circ}}{dz}\right)_{bb} - \left(\frac{dh^{\circ}_f}{dz}\right)_{bb}} \tag{5.46}$$

5.3.3 The Flow-to-Position-of-the-Boiling-Boundary Transfer Function

Equation (5.46) can be written in more detail as

$$\delta z_{bb} = \frac{-\delta h^{\circ}_{bb} + \left(\frac{dh_f}{dp}\right)_{p^{\circ}_{bb}} \left[1.8\ \Delta p^{\circ}_{1fr} \frac{\delta w}{w_o} - z^{\circ}_{in} \frac{\partial G}{\partial t}\right]}{\frac{q'_o(z^{\circ}_{bb})}{w_o} - \left(\frac{dh_f}{dp}\right)_{p^{\circ}_{bb}} \left(\frac{dp^{\circ}_1}{dz}\right)_{z^{\circ}_{bb}}} \tag{5.47}$$

where $\delta h^{\circ}_{bb} = \delta h(z^{\circ}_{bb}, t)$

$\left(\frac{dh_f}{dp}\right)_{p^{\circ}_{bb}}$ = derivative of the liquid saturation enthalpy evaluated at p°_{bb} (fluid property)

$\left(\frac{dp_1}{dz}\right)_{z^{\circ}_{bb}}$ = total differential pressure drop at z°_{bb} (< 0)

The variations of enthalpy at the time-varying position of the BB are given by

$$\delta h_{bb} = h(z_{bb}) - h^{\circ}(z^{\circ}_{bb}) = \delta h^{\circ}_{bb} + \left(\frac{dh^{\circ}}{dz}\right)_{bb} \cdot \delta z_{bb}$$

and can amount to a substantial fraction of δh°_{bb}, or even become larger than δh°_{bb} when the dynamic terms dominate.

The dynamic corrections are generally small or even negligible, except when the non-boiling length becomes very large and the period is short. This is the case for the higher-order oscillations.

Cast as a transfer function, Eq. (5.47) becomes

$$Z(j\omega) \equiv \frac{\delta z_{bb}(j\omega)}{\delta w(j\omega)} = \frac{-H(z^{\circ}_{bb}, j\omega) + \left(\frac{dh_f}{dp}\right)_{p^{\circ}_{bb}} \cdot P_{lw}(j\omega)}{\frac{q'_o(z^{\circ}_{bb})}{w_o} - \left(\frac{dh_f}{dp}\right)_{p^{\circ}_{bb}} \left(\frac{dp_l}{dz}\right)_{z^{\circ}_{bb}}}$$

$$\left[\frac{ft}{lbm/hr}\right] \qquad (5.48)$$

where

$$P_{lw}(j\omega) \equiv 1.8 \frac{\Delta p^{\circ}_{lfr}}{w_o} - \frac{z^{\circ}_{in}}{A} j\omega \qquad \left[\frac{1}{fthr}\right]$$

Figure 5.15 shows δh and δz_{bb} in the complex plane. As seen in the previous section, δh is generally located, except for some "pathological" cases, in the upper half plane; δz_{bb} will therefore always be in the lower half plane. The dynamic terms will always increase the delay in δz_{bb} if this vector is located in the fourth quadrant (Fig. 5.15B), while if it is located in the third quadrant, the outcome will depend on the relative magnitudes of the friction and inertia terms (Fig. 5.15A). The static pressure term has only an important attenuating effect on δz_{bb}.

5.3.3.1 Remarks

Continuous variations of the two enthalpy profiles, h° and h_f°, around the BB, were assumed in the derivation of the transfer function presented above. As this is not the case at the limits of the heated and unheated segments, the solutions obtained are obviously not applicable there. Moreover, as within the unheated segments dh°/dz is zero, the amplitude of $Z(j\omega)$ is limited only by the remaining lesser term dh_f°/dz. Therefore, if the steady-state position of the BB happens to be in an unheated segment, its oscillation will be greatly amplified.

5.4 The Pressure Drop in the Single-Phase Region

It is important to recall here that the single-phase region, as defined in this chapter has a time-varying length. The pressure drop variations will be due to the change in length and to the dynamic effects already mentioned in 5.3.2.2. Summing these effects:

$$\delta\Delta p_1 = \delta\Delta p_{1z} + \delta\Delta p_{1w}$$

$$= \left(\frac{dp_1^\circ}{dz}\right)_{z_{bb}^\circ} \delta z_{bb} + \left[1.8\ \Delta p_{1fr}^\circ - \frac{w_o}{A}\ z_{in}^\circ\ \frac{\partial}{\partial t}\right] \frac{\delta w}{w_o} \qquad (5.49)$$

It is of course implied here that the friction factor, obtained from steady-state experiments, is applicable to a dynamic situation. There is recent evidence that this assumption is justifiable at low frequencies, when the dimensionless parameter $R^2\omega/\nu$ is smaller than approximately 1000 (R is the pipe radius and ν the kinematic viscosity) [71].

Using transfer-function notations

$$\delta\Delta p_1(j\omega) = P_{1z}\,\delta z_{bb} + P_{1w}\,\delta w$$

where

$$P_{1z} = \frac{\delta\Delta p_{1z}}{\delta z_{bb}} = \left(\frac{dp_1^\circ}{dz}\right)_{z_{bb}^\circ} \tag{5.50}$$

is the position-of-the-boiling-boundary-to-pressure-drop-in-the-single-phase-region transfer function, and

$$P_{1w}(j\omega) = \frac{\delta\Delta p_{1w}}{\delta w} = 1.8\,\frac{\Delta p_{1fr}^\circ}{w_o} - \frac{z_{in}^\circ}{A}\,j\omega \tag{5.51}$$

is the flow-to-pressure-drop-in-the-single-phase-region transfer function. Both of these transfer functions appear in Eq. (5.48).

5.4.1 The Equivalent Inertia Length

It is convenient to define an equivalent inertia length for the single-phase region by writing

$$\frac{z_{in}^\circ}{A} = \sum_i \frac{z_i^\circ}{A_i}$$

where z_i° and A_i are the lengths and cross-sections of the various channel segments contributing to the inertial pressure drop.

Although there were practically no frictional losses in the preheater (HX2), pressure recordings at station 0 (inlet plenum) during violent flow oscillations showed perturbations of the order of 0.1 psi, obviously due to the inertia of the fluid in the preheater and associated piping. Correlation of the peak pressure perturbation to the maximum

rate of increase of the flow $(dw/dt)_{max}$ was consistent and permitted the assignment of an equivalent inertia length of 0.8 ft to this part of the rig. Adding the length of the unheated region between stations 0 and 1, z°_{in} becomes

$$z^{\circ}_{in} = 2.3 \text{ ft} + z^{\circ}_{bb} \tag{5.52}$$

Chapter 6

DYNAMICS OF THE TWO-PHASE REGION - THE LAGRANGIAN ENTHALPY TRAJECTORY MODEL

The purpose of this chapter is to establish the basic hydrodynamic equations that will permit calculation of the pressure drop in the two-phase region under time-dependent flow conditions. The method developed here together with the single-phase dynamics derived in Chapter 5, will be used in Chapter 8 to investigate the stability of the entire boiling channel.

A new method of subdividing the channel by points of constant enthalpy, and a Lagrangian description lead to a model that permits considerable economy in computation time. The mass and energy conservation equations of the model are formulated in Section 6.2, the pressure drop formulas are derived in Section 6.3, and a complete calculation procedure is outlined in Section 6.4.

6.1 Introduction

Several models that treat time dependent two-phase flow have been proposed in the past, and have been shown to predict with various degrees of accuracy the transient conditions in a boiling channel [5,13,37,38]. The common characteristic of these models is that they subdivide the boiling length into a number of space nodes and solve the three basic equations (mass, momentum and energy conservation) for each node, thus

providing a basically Eulerian description of the flow. A novel approach will be taken here. The channel will not be subdivided by space points, but rather by discrete constant enthalpy points, and an essentially Lagrangian description of the flow will be used. This procedure follows the example of Wallis and Heasley [10], who appear to be the only investigators to utilize a Lagrangian description. However, they did not sectionalize the channel. The present procedure of sectionalizing the channel provides for considerable simplification in the calculation of the pressure drop.

The model assumes locally incompressible flow; however, changes of the fluid properties according to some reference steady-state pressure profile are taken into account. The dynamic calculations do not rely on any particular procedure for prediction of the steady state: therefore the reference profile can be provided with any available degree of accuracy. Furthermore, the use of a reference profile permits consideration of the relative velocity between phases. Incorporation of space and time dependent fluid properties (especially saturation enthalpy) and vapor compressibility into such a model is desirable for low pressure systems, but it represents at least another order of complexity, and was not considered. The following discussion will justify the particular formulation of the model and delineate its advantages.

Stability considerations limit the time steps that can be taken in numerical applications of hydrodynamic models, which assume incompressible flow, to about the transit time in the segment. Since velocities increase rapidly with quality, it becomes evident that the length of a node can be proportionally increased downstream. It would be natural, then, to

define nodes of equal transit time. This is a first hint in favor of a Lagrangian description. Moreover, as was pointed out by Meyer and Rose [13] in their comparison of various hydrodynamic models, such a description has the distinct advantage that exact solutions are obtained for the continuity and energy equations.

An inspection of the two-phase pressure drop correlations shows that, for given geometry and fluid, the pressure drop in a segment is a function of the mass flow rate, the length of the segment, the average quality, and the pressure, this last dependence being a weak one. When the Lockhart-Martinelli correlation is used, for example, the longest part of the computation involves the determination of the friction multiplier and the void fraction. Both of these quantities are essentially functions of the quality alone. In the pressure drop formula the mass flow rate and length act as multipliers. It follows then that, numerically, it would be very efficient to deal with segments of constant average quality. This second observation leads the suggestion that it might be convenient to subdivide the boiling length at all times by points of constant enthalpy.

The limitations and possible extensions of the method will be discussed in Section 6.5.

6.2 Derivation of the Basic Equations

Consider a uniformly heated boiling channel of constant cross-sectional dimensions. As shown in Fig. 6.1, the upstream boundary or inlet (i) of a "translating and expanding control volume" is defined at any instant of time as the plane at which the enthalpy of the flowing

mixture has a given constant value h_i. An example of such a constant enthalpy plane is the boiling boundary at high system pressures (i.e. when the saturation temperature remains essentially constant along the channel).

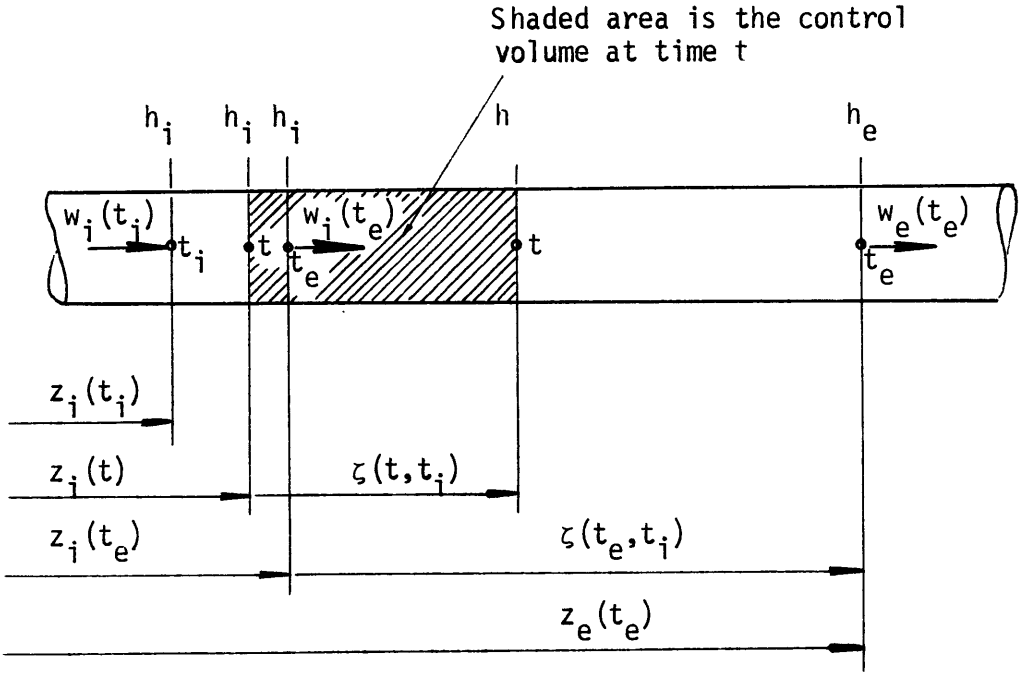

FIG. 6.1 DEFINITION OF COORDINATES

Denote $z_i(t)$ the inlet coordinate of the control volume in an absolute frame of reference (e.g. measured from the heated length inlet) and ζ the relative coordinate with respect to a moving frame of reference attached to the upstream boundary of the control volume. Then the absolute coordinate of any plane is given by

$$z(t) = z_i(t) + \zeta(t)$$

Following Zuber's nomenclature [72-74] a "center of volume" plane is defined as the plane from which a moving observer sees no net volume flow. The velocity of this plane is then the velocity of the center of volume or volumetric flux density, j, which also happens to be the unique velocity of the homogeneous model:

$$j = (1 - \alpha)V_f + \alpha V_g$$

In the Lagrangian description that follows such planes and the quantities associated with them will be identified by two variables, the time t and the entrance time t_i, the time at which the plane was coincident with the upstream boundary.

6.2.1 The Continuity Equation

Consider now a center-of-volume plane that passed by the upstream boundary at time t_i (entrance time). At time $t > t_i$, this plane will be at some point $\zeta(t,t_i)$, having sweeped or generated a volume $A\zeta$. At any instant of time t, the total rate of increase of this volume equals the net volumetric flow entering at the inlet boundary (i) plus the expansion due to evaporation

$$A \frac{\partial}{\partial t} \zeta(t,t_i) = A\, j_{\zeta i}(t) + \frac{\zeta(t,t_i)\, q'\, v_{fg}}{h_{fg}} \qquad (6.1)$$

where j_ζ is the center-of-volume velocity in the moving frame of reference

$$j_{\zeta i}(t) = j_i(t) - \left.\frac{dz_i}{dt}\right|_t \qquad (6.2)$$

It is important to notice here the fundamental underlying assumptions made in writing Eq. (6.1). It was assumed that the heat supply rate to the fluid is constant and that this heat is immediately used for evaporation. Thus, the effects of the heat storage in the walls, variable heat transfer, and thermal non-equilibrium are not taken into account. Thermal non-equilibrium, however, might be accounted for approximately by the use of a corrected v_{fg}/h_{fg} ratio.

Defining*

$$\Omega \equiv \frac{q' v_{fg}}{h_{fg} A} \tag{6.3}$$

Eq. (6.1) takes the form

$$\frac{\partial}{\partial t} \zeta(t,t_i) - \Omega\zeta(t,t_i) = j_{\zeta i}(t) \tag{6.4}$$

Given the inlet center-of-volume velocity $j_i(t)$ and the position of the inlet boundary at any instant of time, $z_i(t)$, integration of this equation gives ζ as a function of time

$$\zeta(t,t_i) = e^{\Omega t} \int_{t_i}^{t} e^{-\Omega t'} j_{\zeta i}(t')\, dt' \tag{6.5}$$

The term $\partial\zeta/\partial t$ in equation (6.4) represents the relative center-of-volume velocity, j_ζ. To get the absolute center-of-volume velocity, j, at any location z at time t, the velocity of the moving frame of reference, dz_i/dt, must be added, resulting in

---

* The same notation is used by Zuber [72-74] to define a characteristic reaction frequency.

$$j(t,t_i) = \Omega\zeta(t,t_i) + j_i(t) \tag{6.6}$$

6.2.2 The Energy Equation

Besides the usual approximations of replacing energy by enthalpy and neglecting the potential and kinetic energy of the flowing mixture, a "quasi-steady-state" approximation is made here in order to obtain a simple expression relating the quality seen by an observer traveling at the velocity of the center of volume, j, to time. Therefore it is necessary to consider time intervals short enough so that the flow does not vary appreciably. The enthalpy variation across an infinitesimal, stationary control volume at a quasi-steady state is

$$dh = \frac{dq}{w} = \frac{q'\,dz}{w} = \frac{q'\,j\,dt}{w} = \frac{q'}{w}\frac{w}{A}\left[(1-x)v_f + xv_g\right]dt$$

$$= \frac{q'\,dt}{A}\left(v_f + x\,v_{fg}\right) \tag{6.7}$$

In the bulk boiling region, neglecting locally the changes in saturation enthalpy with pressure

$$dh = h_{fg}\,dx \tag{6.8}$$

Combining Eqs. (6.7) and (6.8),

$$\frac{dx}{dt} = \Omega\left(x + \frac{v_f}{v_{fg}}\right) \tag{6.9}$$

For a homogeneous flow, Wallis and Heasley [10] obtained the same equation without making any approximations. They considered a mass Δm, occupying instantaneously a volume

$$\Delta v = A\,\Delta\ell = \Delta m\left(v_f + x\,v_{fg}\right)$$

and flowing along the channel; its enthalpy rise dh during dt is given by

$$dh = \frac{\text{heat input during } dt}{\Delta m} = \frac{q' \, \Delta \ell \, dt}{\Delta m}$$

$$= \frac{q' \, \Delta m \, (v_f + x \, v_{fg}) \, dt}{\Delta m}$$

which is identical to Eq. (6.7).

In the case of slip flow there are no identifiable mass lumps that can be followed along the channel. The trajectories of volumes bounded by two "no net mass through" planes (planes moving with the velocity of the "center of mass"*) could be considered, but enthalpy is exchanged through such planes. Similarly mass is exchanged through planes traveling at the velocity of the "center of enthalpy"*. As both these definitions lead to cumbersome corrective terms that spoil the simplicity of the description, they were abandoned in favor of the approximate but simple description given above.

Solution of Eq. (6.9) with the initial condition $x(t_i,t_i) = x_i$ yields

$$x(t,t_i) = x_i \, e^{\Omega(t-t_i)} + \frac{v_f}{v_{fg}} \left(e^{\Omega(t-t_i)} - 1\right) \qquad (6.10)$$

Then integrating Eq. (6.8) with the corresponding initial condition, $h(t_i,t_i) = h_i$,

$$h(t,t_i) = h_i + h_{fg} \left(x_i + \frac{v_f}{v_{fg}}\right) \left(e^{\Omega(t-t_i)} - 1\right) \qquad (6.11)$$

Finally, using the definition of the flowing specific volume or its

---

* These definitions are modeled on the definition of the velocity of the center of volume; they are respectively the mass weighted (area fraction times density) and enthalpy weighted (area fraction times density times specific enthalpy) mean velocities.

inverse, the flowing density

$$1/\rho(t,t_i) = v(t,t_i) = v_f + x(t,t_i)\, v_{fg}$$

$$= v_{fg}\left(x_i + \frac{v_f}{v_{fg}}\right) e^{\Omega(t-t_i)} = (1/\rho_i)\, e^{\Omega(t-t_i)} \qquad (6.12)$$

where

$$\frac{1}{\rho_i} = v_f + x_i\, v_{fg}$$

The control volume will be further specified now by requiring that it be at all times bounded downstream by another plane of constant enthalpy h_e. Inspection of Eq. (6.11) shows that given h_i and h_e there is a unique "residence time" $\Delta t = (t_e - t_i)$ satisfying this condition. The instantaneous length of the control volume is then given by Eq. (6.5) for $t = t_e$. The time-dependent position of the exit boundary,

$$z_e(t_e) = z_i(t_e) + \zeta(t_e,t_i), \qquad (6.13)$$

is used to calculate its absolute velocity:

$$\left.\frac{dz_e}{dt}\right|_{t_e} = \left.\frac{dz_i}{dt}\right|_{t_e} + \left.\frac{\partial\zeta}{\partial t}\right|_{t_e - t_i = \Delta t} \qquad (6.14)$$

The last term is readily obtained by differentiation of Eq. (6.5):

$$\left.\frac{\partial\zeta}{\partial t}\right|_{t_e - t_i = \Delta t} = e^{\Omega t_e}\left[e^{-\Omega t_e} j_{\zeta i}(t_e) - e^{-\Omega t_i} j_{\zeta i}(t_i)\right]$$

$$+ \Omega\zeta(t_e,t_i)$$

Substitution into Eq. (6.14) gives

$$\left.\frac{dz_e}{dt}\right|_{t_e} = \left.\frac{dz_i}{dt}\right|_{t_e} + \Omega\zeta(t_e,t_i) + j_{\zeta i}(t_e) - j_{\zeta i}(t_i)\, e^{\Omega\Delta t} \qquad (6.15)$$

the entrance time t_i now being arbitrary, but the residence time, $\Delta t = t_e - t_i$, is fixed. With this requirement in mind, the entrance time index (t_i) can be dropped from the exit quantities and replaced by the subscript e.

The exit mass flux at time $t = t_e$, at $z = z_e$, is immediately available:

$$G_e(t_e) = G(t_e,t_i) = G(t_e,z_e) = \rho_e\, j_e(t_e) \qquad (6.16)$$

where j_e is given by Eqs. (6.6), (6.5), and (6.4), and ρ_e is given by Eq. (6.12) for $t = t_e$.

6.2.3 Summary of the Solutions

Given:

the time interval, Δt

the time-dependent position of the inlet boundary, $z_i(t)$

the inlet volumetric flux density, $j_i(t)$, or the inlet mass flux, $G_i(t)$

the inlet quality, x_i or enthalpy, h_i

the solutions for any time t are:

$$x_e = x_i\, e^{\Omega\Delta t} + \frac{v_f}{v_{fg}}\,(e^{\Omega\Delta t} - 1) \qquad (6.17)$$

$$h_e = h_i + h_{fg}\left(x_i + \frac{v_f}{v_{fg}}\right)\left(e^{\Omega\Delta t} - 1\right) = h_f + x_e\, h_{fg} \tag{6.18}$$

$$\rho_e = \rho_i\, e^{-\Omega\Delta t} \tag{6.19}$$

$$j_{\zeta i}(t) = j_i(t) - \left.\frac{dz_i}{dt}\right|_t \tag{6.20}$$

$$G_e(t) = j_e(t)\ \rho_e \tag{6.21}$$

$$j_e(t) = \Omega\zeta_e(t) + j_i(t) \tag{6.22}$$

$$\zeta_e(t) = e^{\Omega t}\int_{t-\Delta t}^{t} e^{-\Omega t'}\, j_{\zeta i}(t')\, dt' \tag{6.23}$$

$$z_e(t) = z_i(t) + \zeta_e(t) \tag{6.24}$$

$$\left.\frac{dz_e}{dt}\right|_t = \left.\frac{dz_i}{dt}\right|_t + \Omega\zeta_e(t) + j_{\zeta i}(t) - j_{\zeta i}(t-\Delta t)\, e^{\Omega\Delta t} \tag{6.25}$$

Notice that Eqs. (6.21) to (6.25) specify all the input information necessary for undertaking the solution for the next enthalpy-time step.

6.2.4 First-Order Approximation

The solutions summarized above, though complete, are somewhat cumbersome to use, as the evaluation of $\zeta_e(t)$ requires a numerical integration. Equation (6.23) can be further simplified without great loss of accuracy

by expanding linearly the inlet relative volumetric flux density, $j_{\zeta i}(t)$, around $t_i = t - \Delta t$ as follows:

$$j_{\zeta i}(t) = j_{\zeta i}(t_i) + s(t - t_i) \tag{6.26}$$

where

$$s = \left.\frac{dj_{\zeta i}}{dt}\right|_{t_i}$$

This first-order expansion is further justified by the previous assumption of small variations of the inlet flow during the time interval. Introducing Eq. (6.26) into Eq. (6.23) and performing the integration,

$$\zeta_e(t) = \frac{j_{\zeta i}(t-\Delta t)}{\Omega}\left(e^{\Omega\Delta t} - 1\right) + \frac{s}{\Omega^2}\left(e^{\Omega\Delta t} - 1 - \Omega\Delta t\right) \tag{6.27}$$

Introducing this expression into Eq. (6.25) yields

$$\left.\frac{dz_e}{dt}\right|_t = \left.\frac{dz_i}{dt}\right|_t + \frac{s}{\Omega}\left(e^{\Omega\Delta t} - 1\right) \tag{6.28}$$

6.2.5 Zero-Order Approximation

In some cases where even a zero-order approximation of $j_{\zeta i}(t)$ could be adequate,

$$j_{\zeta i}(t) = j_{\zeta i}(t - \tfrac{1}{2}\Delta t) = \text{constant during } \Delta t$$

Eqs. (6.27) and (6.28) reduce to

$$\zeta_e(t) = j_{\zeta i}(t - \tfrac{1}{2}\Delta t)\ \frac{e^{\Omega\Delta t} - 1}{\Omega}$$

and

$$\left.\frac{dz_e}{dt}\right|_t = \left.\frac{dz_i}{dt}\right|_t$$

6.2.6 A Remark on the Character of the Model

It is instructive at this point to calculate the change in mass flux from inlet to exit of the control volume at time t,

$$\Delta G_{ei}(t) = G_e(t) - G_i(t) = [j_e(t)\ \rho_e - j_i(t)\ \rho_i]$$

Using Eqs. (6.19), (6.22) and (6.23):

$$\Delta G_{ei}(t) = -\left[j_i(t)\ (1 - e^{-\Omega\Delta t}) + \Omega \int_o^{\Delta t} e^{-\Omega\Delta t'} \left(j_i(t') - \left.\frac{dz_i}{dt}\right|_{t'}\right) dt' \right] \rho_i \tag{6.29}$$

Approximated to the first order, i.e. using the definition of Eq. (6.26), Eq. (6.29) reduces to

$$\Delta G_{ei}(t) = \left[\frac{s}{\Omega}\ (1 - \Omega\Delta t - e^{-\Omega\Delta t}) + \left.\frac{dz_i}{dt}\right|_t (e^{-\Omega\Delta t} - 1)\right] \rho_i \tag{6.30}$$

With the zero-order approximation, Eq. (6.29) reduces to

$$\Delta G_{ei}(t) = \left.\frac{dz_i}{dt}\right|_t (e^{-\Omega\Delta t} - 1)\ \rho_i \tag{6.31}$$

Equations (6.29) to (6.31) confirm the fact that the model is accounting for the important transient mass accumulation and space distributed flow

variations. As expected, all three expressions reduce to zero at steady-state when $j_i(t) = \text{constant}$ or $s = 0$ and $dz_i/dt = 0$.

6.3 Calculation of the Pressure Drop

The steady-state pressure drop for a segment of length $\Delta\zeta^\circ$, a mass flux G°, and an average quality $\bar{x}^\circ = \frac{1}{2}(x_i^\circ + x_e^\circ)$ is given in Chapter 3 as

$$\Delta p^\circ = \Delta p^\circ_{fr} + \Delta p^\circ_{gr} + \Delta p^\circ_{ac}$$

where the superscript $^\circ$ was added here to denote steady-state conditions. Under time-dependent conditions for a segment of length $\Delta\zeta$, an instantaneous average mass flux $\bar{G} = \frac{1}{2}(G_i + G_e)$, the <u>same</u> average quality $\bar{x} = \bar{x}^\circ$ and at the same pressure level, the pressure drop can be written as

$$\Delta p = \left[\left(\frac{\Delta p^\circ_{fr}}{\Delta\zeta^\circ}\right) \left(\frac{\bar{G}}{G^\circ}\right)^{1.8} + \left(\frac{\Delta p^\circ_{gr}}{\Delta\zeta^\circ}\right) - \frac{\partial \bar{G}}{\partial t} \right] \Delta\zeta + \Delta p^\circ_{ac} \left(\frac{\bar{G}}{G^\circ}\right)^2 \qquad (6.32)$$

Once the time-independent values have been calculated, the computation of the time-dependent pressure drop is reduced to the evaluation of the simple expression above. It is the fact that Eq. (6.17), giving the exit quality as a function of the residence time, is independent of the mass flux that makes the evaluation of the total pressure drop extremely simple. First the mass fluxes at all mesh points at all times and the segment lengths are established, using the equations of Section 6.2.3. Then the total pressure drop at any point at any time is obtained using Eq. (6.32), by summation of the corresponding pressure drop increments at this time up to this point. The procedure is further clarified in the next section.

6.4 Computation Procedure

The application of the theory outlined in the preceeding sections will be described now in some detail. The FORTRAN subroutine DYNPR2 that performs these calculations is listed in Appendix F.

6.4.1 Reference Steady State

It is first necessary to determine the quality, enthalpy, density and pressure drop distributions at a reference steady-state (values with superscript °). The time step Δt can be either chosen arbitrarily or by subdividing the total reference transit time in the boiling length into an arbitrary number of segments, N. Starting at the boiling boundary (BB), the segments and their boundaries are numbered as shown in Fig. 6.2. The inlet/exit subscripts i/e are replaced by the mesh point numbers i/i+1.

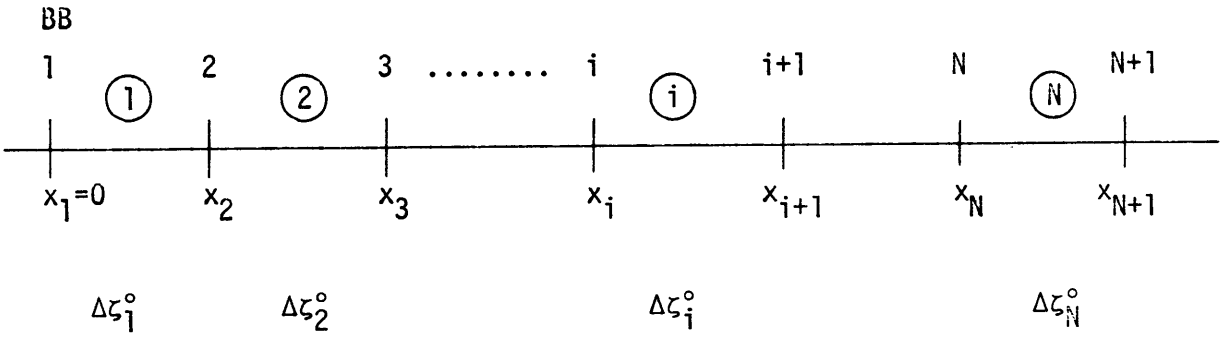

Fig. 6.2. Time-Independent Reference Conditions in the Boiling Channel

The general equations (6.17 - 6.19) could be used to determine the quality, enthalpy, and density distributions at steady state. In these calculations, properly defined local average values of the fluid

properties should be used. The length of the segments would be given by Eq. (6.23)

$$\Delta\zeta_i^\circ = j_i^\circ \; E_i$$

where

$$E_i \equiv \frac{e^{\Omega_i \Delta t} - 1}{\Omega_i} \tag{6.33}$$

and the pressure drops would be estimated using some appropriate model. This procedure, although theoretically correct, does not give good results when the fluid properties v_{fg} and h_{fg} vary rapidly along the channel. The deficiency comes from the exponential extrapolation required to obtain the exit quantities from the inlet quantities. Small discrepancies in the spatial averaging of v_{fg}/h_{fg} produce large propagating errors. It was found that a much better procedure was to calculate first the pressure profile by conventional means (Chapter 3), then determine the mesh points using the constant transit time requirement and calculate the densities at these points, ρ_i. Effective Ω values are then defined by

$$\Omega_i = \frac{1}{\Delta t} \; \ln\left(\frac{\rho_i}{\rho_{i+1}}\right) \tag{6.34}$$

and the coefficients E_i can be calculated using Eq. (6.33). Subroutine STAPR2 was written to perform the steady-state calculations and is listed in Appendix F.

6.4.2 Time-Dependent Hydrodynamic Calculations

The trajectories of center-of-volume planes that enter the boiling length at equally spaced times $t_2, t_3, \ldots, t_k, \ldots t_M$ will now be considered, the time step being again Δt. The superscript k in the equations will refer to the plane that entered at time t_{k+1}. Figure 6.3 shows the progression in time and space of these planes. Notice that all points having the sum of their subscript i and superscript k equal to m refer to the same time t_m and are situated on a diagonal line. The regular pattern of these lines at steady state is distorted during transients.

The following recursive relations, directly derived from the formulas of Section 6.2.3, specify the solution of the problem; in this first-order, machine-oriented solution, the differentials were further approximated by finite differences.

$$j_{\zeta i}^{k} = j_i^{k} - \left(\frac{dz}{dt}\right)_i^{k} \tag{6.35}$$

$$j_{\zeta i}^{k+1} = j_i^{k+1} - \left(\frac{dz}{dt}\right)_i^{k+1} \tag{6.36}$$

$$s_i^{k} = \frac{j_{\zeta i}^{k+1} - j_{\zeta i}^{k}}{\Delta t} \tag{6.37}$$

$$\Delta\zeta_i^{k} = E_i\, j_{\zeta i}^{k} + B_i\, s_i^{k} \tag{6.38}$$

where E_i, as defined by Eq. (6.33), and

$$B_i \equiv \frac{e^{\Omega_i \Delta t} - 1 - \Omega_i\ \Delta t}{\Omega_i^2} = \frac{E_i - \Delta t}{\Omega_i} \tag{6.39}$$

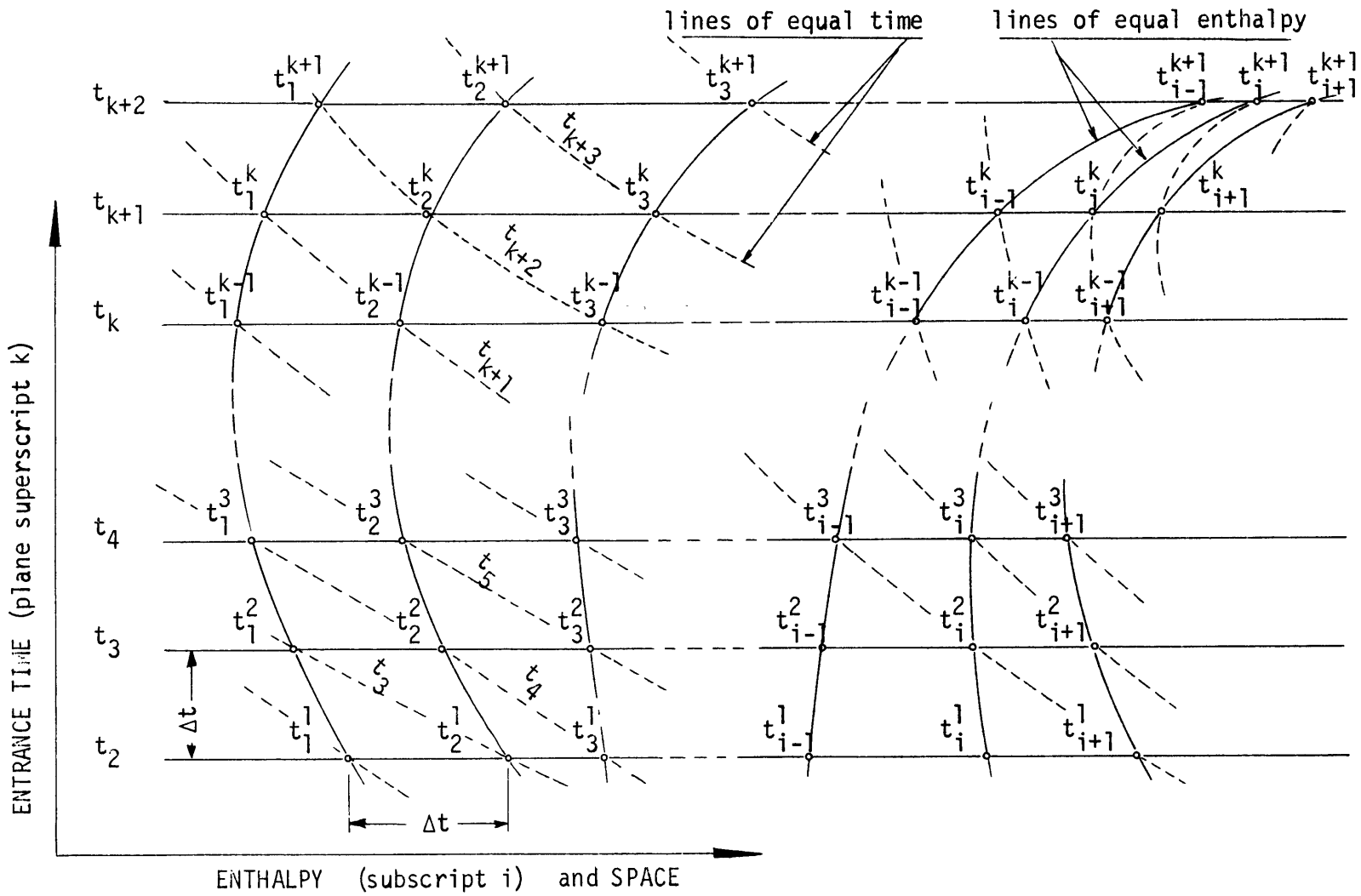

FIG. 6.3 TRAJECTORIES OF THE CENTER-OF-VOLUME (AND CONSTANT-ENTHALPY) PLANES

are time-independent coefficients.

$$j_{i+1}^{k} = j_{i}^{k+1} + \Omega_i \, \Delta\zeta_i^k \tag{6.40}$$

$$G_{i+1}^{k} = \rho_{i+1} \, j_{i+1}^{k} \tag{6.41}$$

$$\bar{G}_i^k = \frac{1}{2} (G_{i+1}^{k} + G_i^{k+1}) \tag{6.42}$$

$$\Delta p_i^k = \left[\left(\frac{\Delta p^\circ_{fri}}{\Delta\zeta^\circ_i}\right) \left(\frac{\bar{G}_i^k}{G^\circ}\right)^{1.8} + \left(\frac{\Delta p^\circ_{gri}}{\Delta\zeta^\circ_i}\right) - \frac{\bar{G}_i^{k+1} - \bar{G}_i^k}{\Delta t} \right] \Delta\zeta_i^k + \Delta p^\circ_{aci} \left(\frac{\bar{G}_i^k}{G^\circ}\right)^2 \tag{6.43}$$

$$\left(\frac{dz}{dt}\right)_{i+1}^{k} = \left(\frac{dz}{dt}\right)_{i}^{k+1} + E_i \, s_i^k \tag{6.44}$$

$$z_{i+1}^{k} = z_i^{k+1} + \Delta\zeta_i^k \tag{6.45}$$

$$p_{i+1}^{k} = p_i^{k+1} + \Delta p_i^k \tag{6.46}$$

The following three rules specify the time in the variables above:

I. For quantities referring to a point (j, j_ζ, G, z, and dz/dt) the time index is obtained by adding the superscript to the subscript.

II. For quantities referring to a segment (s, $\Delta\zeta$, $\bar{G}$, and Δp), unity must be added to the sum of the subscript and superscript.

III. Time-independent quantities have no superscript (or superscript °).

Inspection of the set of equations shows that all the information needed to undertake the next, (i+1)th enthalpy step is provided by

Eqs. (6.40), (6.41), (6.44), (6.45), and (6.46).

6.5 Comments on the Method

By now the reader will be aware of the fact that the enthalpy trajectory model, as presented in this chapter, has no built-in provision for feedback. Given the inlet variations, boundary conditions can be rigorously specified at the boiling boundary only. Then the conditions are calculated at any other point downstream.

The few limiting assumptions made during the derivation of the basic equations, namely the assumption of slow flow rate variations and the non-dependence of the local saturation enthalpy on dynamic pressure variations, suggest that the model will probably be most useful for moderate flow transients around an equilibrium point. Such conditions prevail at the incipience of flow oscillations. An increase of the system pressure is certainly beneficial to the performance of the model. However, the model is better than other existing models for low pressure systems, as it takes into account at least the steady-state pressure profile.

Notice that when the position of the BB, as determined by the analysis of Chapter 5, is used as the first mesh point, the pressure dependence of the saturation enthalpy is automatically taken into account at this point, and approximately at points downstream. Indeed, statically, an increase of the pressure level shifts the entire pattern of enthalpy mesh points downstream. A similar effect is produced by the correction of the position of the BB according to the static and

dynamic pressure variations. Obviously, the validity of this correction deteriorates with distance from the BB, and reverses into an error at the channel exit, where the pressure is externally fixed. A correction that was applied to the pressure drop calculation near the exit of the channel is discussed in Chapter 8. It is believed that with the two refinements mentioned above, the model is also capable of approximately considering the time variations of the saturation enthalpy.

Unfortunately, it is impossible to account for variable channel geometry, non-uniform heat flux profile, time-dependent heat input, or, in general any space distributed input variable, without spoiling the inherent simplicity of the equations. On the other hand, the effect of local flow restrictions can be superimposed easily on the uniform geometry channel results.

The necessity to determine the conditions at a given space point indirectly, by interpolation of values at bracketing points, constitutes another minor disadvantage of the method. It should also be noted here that to be able to determine the conditions at the channel exit it is necessary to virtually extend the boiling length.

In spite of these relatively minor limitations the model seems to be well-suited for calculations of pressure variations for small or medium amplitude flow oscillations and transients.

Chapter 7

PRESENTATION AND DISCUSSION OF THE STABILITY EXPERIMENTS

One of the primary goals of the project for which this investigation was initiated was to produce a complete and reliable stability map that could be used to test various existing or new analytical models such as the model described in Chapters 5, 6 and 8. In fact, most of the stability data presented in the literature are either isolated points or small collections of points that do not permit thorough testing of a model. Moreover many experiments were conducted with poorly defined systems, having uncertain or varying boundary conditions. Because of the risks of physical damage to the test sections, generally the experiments were terminated near the threshold of stability without entering deep into the unstable region. Therefore, few limit cycle data are available.

Crowley, Deane, and Gouse [32] obtained the stability boundaries of the present system at four power levels with a uniform heat flux distribution. The frequencies of the phenomena they observed confirmed that these were density wave oscillations. Relative to the previous work, the purpose of the present stability experiments was to:

a) extend and complete the uniform heat flux stability map toward lower power levels and higher subcoolings,

b) produce a corresponding map with a cosine heat flux distribution, and

c) enter deep into the unstable region and study the characteristics of the limit cycle.

Section 7.1 describes the experimental procedure. The difficulties encountered in the definition of the threshold of stability are discussed in Section 7.2. A short survey of the various ways of presenting the data is given in Section 7.3. Section 7.4 describes the data reduction methods used. Stability maps are presented and discussed in Section 7.5, and the period of the oscillations is considered in Section 7.6. The effect of the cosine heat flux distribution is examined in Section 7.7. The characteristics of the limit cycle are described in Section 7.8. Section 7.9 deals with a series of experiments that were designed especially to show the existance of standing enthalpy waves in the single-phase region. Conclusions are drawn in the last section of this chapter.

A total of 23 routine stability runs ("D" runs) were made. Excluding the first three trial runs, eight runs were made with cosine and the remaining twelve with uniform heat flux distribution. Another eight stability runs provided tape recordings of the flow signal that could be analyzed for frequency content ("TR" runs). Finally six special runs ("E" runs) demonstrated the existance of higher-mode enthalpy waves in the subcooled region (Section 7.9).

A total of 750 points, including 175 threshold and transition points, was recorded. This large amount of data required machine processing. The introduction of data handling programs, early in the data reduction phase, permitted the mainpulation of large amounts of data, with any desired degree of sophistication and with minimal numerical discrepancies. The raw stability data and relevant calculated parameters are tabulated in Appendix E.

7.1 Experimental Procedure

Crowley, Deane, and Gouse [32] have shown that the oscillation characteristics were practically independent of the number of channels operating in parallel. This is a direct consequence of the constant-pressure-drop boundary condition maintained by the large bypass. Dynamic pressure recordings at station 0 have, however, shown a small oscillation due to the inertia of the liquid in the preheater HX2 (Section 5.4.1). To eliminate the weak coupling introduced by this pressure drop, all stability experiments were conducted with a single channel, namely channel C. The other two channels were isolated using valves V11 and V12. Valves V10 and V13 were left wide open for all the stability runs.

For a given test fluid and geometry, the conditions in the boiling channel are determined by the five independent variables listed in Table 7.1.

Table 7.1

Range of the Independent Variables During the Stability Experiments

Channel exit pressure, p_{ex}	atmospheric
Total pressure drop, Δp_{oex}	approximately 7.5 to 3.5 psi
Gross average linear heat rate, $\bar{q}'_o$	265, 530, 795, 1060, and 1325 Btu/hrft (100, 200, 300, 400, 500 W/test length)
Heat flux distribution, $q'_o(z)$	uniform and cosine
Inlet temperature, T_o	40 to 125°F

The inlet average mass flow rate, w_o, the exit quality, x_{ex}, etc., as well as the limit cycle characteristics (frequency, τ, and peak flow amplitude, $\hat{w}$) are considered as dependent variables.

Crowley, Deane, and Gouse [32] conducted their experiments with a fixed pressure drop across the test channels, while varying the inlet temperature. The experimental path obtained in this way is parallel to the stability boundary over a large range of temperatures (Fig. 7.1 and Ref. [32]). In the present experiments, the inlet temperature was maintained constant while the pressure drop, and consequently the average flow rate, were varied. Thus a path perpendicular to the stability boundary was generated, except for the lowest subcoolings. Since previous studies, e.g. [9], have demonstrated that the stability of the system is independent of its history or the path followed in approaching some point, the two approaches are equivalent. The present approach, however, has operational advantages.

In the previous experiments, the power region from 380 W/test length up to the maximum safe heat flux had been covered. It became immediately clear that at lower power levels, with forced circulation, the system was stable. With forced circulation the minimum available Δp_{oex} is given by the hydrostatic head in the bypass. It was then necessary to change the operating procedure and conduct blowdown tests as described below.

7.1.1 Blowdown Tests

The loop was prepared for data collection by a procedure similar to that used for the steady-state experiments (Section 4.1). The steam and

water flow rates to the test section preheater HX2 were then adjusted, to bring the mixture to the desired nominal Freon inlet temperature. Data collection generally started with forced circulation. The bypass valve V9 was wide opened and the flow through the bypass was reduced to a minimum using valves V1, V2 or V3, and V6. Then valve V1 was completely closed so as to isolate the test sections, and the pump was stopped or simply circulated Freon in the pump bypass. The reserve of fluid in the large bypass was sufficient to maintain the flow in a single channel for 15 to 60 minutes, depending on the inlet temperature and the heat input. During this period the level in the bypass, and proportionally p_o, decreased continuously so that the system was led through an infinite number of quasi-steady states. The rate of decrease was slow enough to have no effect on the stability. This was verified by taking data with increasing p_o (slowly filling up the bypass). Moreover, the velocity through HX2 was so small that the Freon inlet temperature was indistinguishable from the heating water temperature and could be controlled very easily. Besides providing the necessary low inlet pressures and a way of continuously varying the flow, the blowdown procedure provided also for accurate flow rate measurements as explained in the following section.

7.1.2 Data Collection

During the experiments the inlet temperature, T_o, was continuously recorded on the thermocouple recorder. The linear flow signal, the integral flow signal (Section 2.2.2), and selected pressure signals from various stations along the channel were recorded on the Visicorder.

Occasionally the signals from void gauges (Section 2.2.5) and thermocouples were also recorded. An additional potentiometric strip-chart recorder (Hewlett Packard-Moseley Model 680) was used to produce a continuous trace of the inlet pressure, p_o. The signal fed to this recorder was provided by a 20-psig pressure transducer and amplified by a Statham Model UR5 readout unit. Two calibrated bias signals could be added to the pressure signal to keep the pen within the chart limits while using a large amplification. Since the cross-section of the bypass was constant (except at the top), the slope of the pressure trace was exactly proportional to the mass flow rate, regardless of the temperature in the bypass. The glass bypass was graduated to permit visual observation of the level. At steady state, the mass flow rates obtained "barometrically", as described above, agreed within 5 percent with the venturi readings. With large oscillations and at very low flow rates, only the "barometric" method was reliable. The top of the bypass had an irregular shape and made flow rate measurements impossible at the beginning of the blowdown. It was then necessary to use the downcomer level (valve V15 to the release tank shut) to volumetrically determine the flow. For this purpose, the transparent downcomer was also graduated and the liquid level was read and noted in short intervals. This method was less accurate because of the delay of the vapor in the condenser. The p_o trace was compared many times during every run to the manometer M3 level and the gauge P93 pressure readings (Fig. 2.2). The deviations were smaller than 0.05 psi and therefore negligible.

The three recorders and the manual readings were synchronized with appropriate time marks on the charts. During most of the runs (D4 - D16)

the rapidly varying signals were recorded intermittently with a large time scale to measure accurately the characteristics of the limit cycle. After the discovery of higher modes of oscillation, continuous recordings at a reduced paper speed were made in order to detect all the transition points (Runs D17 - D23, TR,and E).

7.2 Determination of the Threshold of Stability

When a boiling system is brought into the unstable region by a continuous variation of some independent parameter, the experimenter faces the difficult task of defining the threshold of stability. In theory, a system becomes unstable when infinitesimal oscillations around an equilibrium point are indefinitely sustained. As in a real boiling system the small oscillations are masked by random noise, such a criterion is generally not applicable unless the oscillations grow rapidly. Furthermore a train of decaying oscillations triggered by external events, near the threshold of stability can be easily mistaken for a steady oscillation. It becomes clear, then that some arbitrary criterion must be applied in defining the threshold of stability. Often the decision is made by simple visual examination of the traces; e.g. Berenson [22]. Massini et al. [24] also detected the threshold by visual inspection of pressure recordings. They note that "the theoretical threshold power is probably overestimated, but by no more than 1-2 percent as it appears from the diagrams of oscillations amplitude vs. power, extrapolating the amplitude to zero". There is no assurance, however, that the oscillations grow linearly. Various attempts have been made to systematize the

procedure. Jain [23] states that "in some cases the inception point is readily distinguished, ..., but in other cases, a clearcut threshold is not observed." The knee of the amplitude curve versus some independent variable can be used in the former case, while statistical methods are generally necessary in the latter. For example, Bogaardt et al. [21] plot the rms value of a fluctuating pressure signal, while Mathisen [40] defines the threshold by extrapolating toward zero the inverse of the flow-noise variance. Kjaerheim and Rolstad [26] define a "noise function" resembling an autocorrelation function and extrapolate the fast rising portion of this curve backwards toward zero.

For the present experiments, the threshold of stability was fairly well defined at moderate and high subcoolings as there was little flow noise and the amplitude of the oscillations grew very rapidly. (Fig. 7.16A). At low subcoolings, however, it was difficult to define the threshold by visual observation of the traces alone.

An attempt was made to define the threshold at low subcooling by statistically analyzing the flow signal. Tape recordings of the flow signal were made, the analog signal was sampled and converted to digital data, which was analyzed numerically for frequency content by computer. The elaborate analysis yielded no better definition of the threshold and therefore was not used extensively. The threshold of stability is defined in this work as the point where the decreasing flow trace exhibits for the first time sustained periodic oscillations with a characteristic frequency and a distinguishable amplitude. The subjectivity of this definition might be responsible for some scatter in the threshold points.

7.3 Similarity Considerations and Non-Dimensional Parameters

A brief survey of the various non-dimensional parameters involved in the thermal-hydraulic dynamics of the boiling channel will be made here to prepare the ground for presentation of the stability maps in terms of these parameters.

As a single fluid at atmospheric pressure was used throughout the present experiments, the fluid-related parameters need not be considered here. In more general studies these parameters include the ratio of the critical pressures, the liquid to vapor density ratios at a given pressure, the Lockhart-Martinelli parameter X_{tt} [49], or the Baroczy [52] property index $(\mu_f/\mu_g)^{0.2}\ (\rho_g/\rho_f)$. Moreover, the geometry ratio, L/D, is fixed. For small variations of the liquid viscosity, the inlet Reynolds number becomes a direct measure of the flow velocity.

Many authors agree on the importance of the relative position of the boiling boundary (BB). It seems then natural to use the single-phase length to total channel length ratio, L_1/L [75] or the single-phase enthalpy to total enthalpy ratio, $\Delta h_1/\Delta h$ [7], which is identical to L_1/L for a uniform heat flux distribution.

The exit quality is itself a non dimensional parameter [76], but it can be advantageously replaced by the inlet to exit density ratio, ρ_{in}/ρ_{ex} or the inlet to exit velocity ratio, V_{in}/V_{ex} [7].

The temperature of the fluid as it enters the heated channel can be replaced by the inlet subcooling or, better yet, by the subcooling with respect to the boiling boundary, which can also be represented by the ratio $\Delta h_1/h_{fg}$ [76,77].

All attempts made in non-dimensionalizing the heat input (e.g. [15,75,77]) lead to parameters that are proportional to $q/w_o h_{fg}$ where q is the total heat input. The analysis of section 5.3.2.1 showed that for low pressure systems, this ratio should be augmented by $\frac{L_h}{h_{fg}} \left(\frac{dh_f}{dp}\right)_{p^\circ_{bb}} \left(\frac{dp_1}{dz}\right)_{z^\circ_{bb}}$ to account for the vapor generation due to the change in saturation pressure. In the present case this corrective term is practically constant, and for this reason it is omitted.

All the parameters considered so far account mainly for thermal effects. The momentum effects are represented by the ratio of the pressure drop in the single-phase region to total pressure drop, $\Delta p_1/\Delta p$. Another parameter that emerged from the analysis of Chapter 5 (Eq. 5.49) is the ratio of the period of the oscillation to the characteristic single-phase inertia time constant

$$\frac{\tau}{\tau_{in}} = \frac{1.8}{2\pi} \frac{\Delta p^\circ_{ifr}\, \tau}{G^\circ\, z^\circ_{in}}$$

Stenning and Veziroglu used a similar parameter in their analysis [7].

The important time delays are discussed in detail in Section 7.6.1 For the single-phase region the "order of oscillation" is defined as

$$z^\circ_{bb}/V_o\tau$$

where $V_o\tau = \lambda$ is the enthalpy oscillation wavelength used in Chapter 5.

It seems that both the hydrodynamic and the thermodynamic similarity conditions, mentioned above, must be met in order to have two completely similar states of the boiling channel. As these are incompatible in general, there will be no single curve to represent, for example, the

threshold of stability, but rather a family of curves (recall that three independent variables define the system, namely p_o or w_o, T_o, and q). The dimensionless parameters actually used in reducing the experimental data are given in the following section.

7.4 Data Reduction

The raw experimental data, i.e. the atmospheric (condenser) pressure, the inlet pressure readings, the average flow rate, the inlet temperature, the power level and distribution, the period of the oscillation, and the peak flow (the last two from the Visicorder traces), were fed to computer programs that calculated:

the pressure at the inlet of the heated section, p_1

the inlet subcooling, $\Delta T_{suin} = T_{sat}(p_1) - T_o$

the average position of the boiling boundary, z°_{bb}

the average pressure at the BB, p°_{bb}

the average subcooling with respect to the BB, $\Delta T_{subb} = T_{sat}(p^\circ_{bb}) - T_o$

the average exit quality, x_{ex}

and various non-dimensional parameters of interest:

the enthalpy parameter, $q/w_o h_{fg}$ where $h_{fg} = h_{fg}(p_{ex})$

the single-phase length, z°_{bb}/L_h

the single-phase pressure drop, $\Delta p_1/\Delta p = \Delta p_{obb}/\Delta p_{oex}$

the single-phase enthalpy, $\Delta h_1/\Delta h$

the single-phase transit time or "order of the oscillation", $z^\circ_{bb}/V_o\tau$

The heat losses were not taken into account as they were small and approximately constant for each power level. Subcooled boiling was

ignored as it has been shown in Chapter 4 that it contributes very little to the pressure drop.

The following procedure was devised to determine the position of the BB: Using the measured inlet pressure as the starting point, the pressure drop and the corresponding temperature rise for each test length are calculated. When the mixed-mean temperature exceeds the local saturation temperature, successive linear interpolations permit the determination of the position of the BB. The method is reliable as the pressure drop in the single-phase region can be determined with sufficient accuracy. Subroutine SUBCBB performs these calculations and is listed in Appendix F. The cold spots were not taken into account for the experimental data reduction, since a simplified version of SUBCBB was used.

7.5 Stability Maps

The experimental threshold of stability data, tabulated in Appendix E, and some characteristics of the limit cycle will be presented graphically by means of stability maps. Figures 7.1 to 7.5 are typical stability maps in the $(\frac{q}{w_o h_{fg}}, \Delta T_{subb})$ plane. Each curve on these figures represents a run at constant inlet temperature. As the experiments were conducted with decreasing flow, data collection progressed from left to right. The first occurrence of oscillations or the "threshold of stability" is denoted by circles. The points where, at rare instances, the oscillations ceased are marked by a cross. The deviation of the points at very low subcoolings toward the left is due to the presence of air in the system. When the Freon was not exhaustively degassed, gas bubbles started

flowing out of the preheater (HX2) at temperatures approximately 10°F below the local saturation temperature and precipitated the occurrence of instability.

7.5.1 Higher-Mode Oscillations

At high subcoolings and low power levels the system exhibited an interesting behavior, named "higher-mode (or order) oscillations" for reasons that will be apparent later. No reports on similar phenomena were found in the literature. The following observations led to the detection of this peculiar behavior:

a) In the ($q/w_o\ h_{fg}$, ΔT_{subb}) plane, at high subcoolings, the threshold boundaries should normally curve toward the right [29]. Such a behavior was not observed; the stability boundaries remained vertical or even curved to the left.

b) It has been well established [7,24] that the period of the oscillation is approximately equal to twice the "transit time" in the channel. In the higher-mode region the measured periods were equal to a small, approximately constant fraction of the expected period (Fig. 7.11).

c) There were sudden changes in the oscillation pattern and period, named "transitions". Often the oscillations seemed to decay, only to diverge again with a different frequency. Figure 7.6A shows the flow trace for such a transition point. At other times the transition occurred without decay of the oscillation, by a mixture of the two modes over a few cycles (Fig. 7.6B).

d) The hypothesis that this behavior was due to nucleation instabilities alone was rejected in light of the complete explanation given later.

The analysis of Chapter 5 (particularly Section 5.2.4) showed the existence of enthalpy nodes in the boiling channel, i.e. points where the enthalpy variations are minimum when the flow is oscillating. For a spatially uniform heat input to the fluid, these nodes are separated by a wave-length $\lambda = V_o \tau$. The enthalpy perturbations resemble a standing wave in an organ pipe (Figs. 5.7 and 5.8). The oscillations were assigned an order according to the relative position of the BB. If the BB is in the first wavelength ($z^o_{bb}/\lambda < 1$), the oscillation mode will be called "zero-order" or "fundamental." In general

$$\text{order of oscillation} = \text{integer part of } \frac{z^o_{bb}}{\lambda}$$

It is clear that the enthalpy perturbations upstream of the last node before the BB do not contribute anything dynamically. Therefore this portion of the channel should not be taken into account for the calculation of the transit time. This explanation makes the presence of "unexpectedly" short periods legitimate. A series of experiments devised to confirm this behavior is discussed in Section 7.9.

When the ($q/w_o h_{fg}$, ΔT_{subb}) plane is divided into stable and unstable regions, and the unstable regions are further subdivided according to the order of the oscillations, a consistent stability map emerges. The transition points become threshold points for some adjacent region exhibiting a different order of instability. All the threshold boundaries curve, as expected, to the right (Figs. 7.1 to 7.5). For each mode, the period of the oscillation can be closely correlated with the subcooling as shown in Fig. 7.11.

Of course, what was said above does not explain why the system exhibits higher modes and why transitions from mode to mode occur. This question should be answered in the context of the stability analysis; a few remarks, however, will be made here.

The boiling channel is dynamically dissimilar for each mode. At higher modes the "inactive" wavelengths must be added to the length of the unheated inlet piping, changing the relative position of the BB in the effective heated length.

There seems to be a dynamically acceptable range of periods (approximately 2 to 10 s in the present case). At low subcoolings, and high power levels, as the transit time and consequently the fundamental period become short, the occurrence of higher modes with even shorter periods is prohibited. On the other hand, with very low heat inputs and inlet velocities, at high subcoolings, the transit time becomes excessively long and the fundamental period is divided into smaller fractions. The transitions from mode to mode are probably due to the combined effects of the spatial oscillations of the enthalpy along the channel, the cold spots of the heated wall, and they are possibly enhanced by nucleation instabilities. As the inlet flow is gradually decreased, the period, the wavelength and the position of the BB change and their combinations must be considered. When, for example, the BB reaches an enthalpy node, the oscillation might be no longer sustained and another mode might emerge. On the contrary, the oscillations will be amplified if the average position of the BB reaches a cold spot (Section 6.3.3.1). In one instance, at very low inlet velocity, it has been possible to observe visually a change of

mode. There seemed to be a sudden shift of the average position of the oscillating BB to a few inches upstream, suggesting that nucleation effects might be occasionally triggering the frequent transitions. It is evident, however, that the higher oscillation modes are not nucleation instabilities.

In the remainder of this work the oscillations are always assigned an order, as defined in Section 7.4. This simple parameter does not take into account the heat flux distribution and the wall heat storage effects. Both of these modify the spacing of the enthalpy minima as shown in Figs. 5.8 and 5.10. When the required corrections are kept in mind, the order of the oscillation can be very useful in categorizing the oscillations.

Extensive graphical search and cross-verification was used to draw the threshold lines of Figs. 7.1 to 7.5. All the experimental observations had to be used simultaneously to provide continuity of the boundaries from all points of view. Period versus subcooling plots (Fig. 7.11) were used extensively. In many instances, when there was doubt, the original recordings were reexamined. In the light of what was expected, features of the oscillations that were not noticed during the initial data reduction were found. Obviously the information in the higher-mode regions is limited and some extrapolation and speculation is necessary in order to plot all the boundaries. The information, as presented in Figs. 7.1 to 7.5, however, is consistent and all the small discrepancies can be justified on experimental or other grounds. Regions where extensive mixing of modes occurs are probably indifferent to the order of the oscillation.

7.5.2 Zero-Order Stability Boundaries - Uniform Heat Flux Distribution

The points at the first threshold of stability, regardless of mode, and the zero-order transition points were plotted in Fig. 7.7, together with the smoothed zero-order boundaries. Five power levels are represented on this figure, all with a uniform heat flux distribution. At 200 W/test length (W/TL) two boundaries are shown as no decision could be made regarding the mode of the oscillations in the region between these two curves. There seemed to be a continuous mixing of zero and first order modes, as shown in Fig. 7.6C, with the flow peaks grouped two by two. Similar behavior also occurred at other power levels. There is a single higher-mode threshold point at 400 W/TL and none at 500 W/TL.

The smoothed boundaries from the experiments by Crowley, Dean, and Gouse were also plotted on this figure and labeled "C-D-G". As the inlet pressure was not available for the points on these curves it had to be calculated using the methods of Chapter 3 in order to obtain ΔT_{subb}.

Figures 7.8 and 7.9 are the conventional stability plots in the inlet velocity - inlet subcooling plane. Only zero order points were plotted on these figures. The enlargement of the unstable region with increasing heat input is clearly visible. Figure 7.10 shows the threshold points in the $(\Delta p_1/\Delta p,\ q/w_o h_{fg})$ plane. The boundaries at all power levels are almost indistinguishable in this plane. When $\Delta p_1/\Delta p$ is replaced by $\Delta h_1/\Delta h$, a similar plot is obtained, but the boundaries are much further apart.

7.6 Period of the Oscillation

An analytical expression for the time delays in the channel will be developed first in this section, in order to provide a basis for discussion of the experimental data.

7.6.1 Time Delays in the Channel

The instabilities studied in this work are due to delayed feedbacks between the flow rate, the void fraction, and the resulting pressure drop. A small sinusoidal perturbation of the inlet flow will be considered now and its effects on the pressure drop will be determined. A uniform and constant heat input to the fluid will be assumed for simplicity.

The analysis of Section 5.2.4 has shown that, if the flow was maximum at time $t = 0$, the enthalpy perturbation at the BB will reach a maximum at time

$$\Delta t_1 = \frac{z^\circ_{bb}}{2V_o}$$

The ratio of this time to one half the period of the oscillation has been already used extensively as the order of the oscillation. In the two-phase region the enthalpy perturbations will create void perturbations. These, according to Zuber [72], propagate with the kinematic wave velocity which is approximately equal to the vapor velocity. Therefore, in the two-phase region, the appropriate transit time is

$$\Delta t_2 = \int_{z^\circ_{bb}}^{L_h} \frac{dz}{V_g(z)}$$

The maximum of the void perturbation will reach the exit after a time

$$\Delta t_{ex} = \Delta t_1 + \Delta t_2$$

The perturbation of interest, however, is the total pressure drop perturbation, which will depend in an integral fashion upon the local void and flow perturbations. The period will be approximately equal to twice the total delay, Δt_{ex}, since the delays in the two-phase region are short, due to the large mixture velocities. Other authors [7,24] have used the same assumption without, however, accounting for the fact that the enthalpy perturbations travel at twice the flow velocity.

The following expression for Δt_{ex} was derived assuming homogeneous flow, constant properties and uniform heat input to the fluid.

$$\Delta t_{ex} = \Delta t_1 + \Delta t_2 = \frac{1}{2} \frac{\rho_f}{q'''} \Delta h_1 + \frac{h_{fg}}{q''' v_{fg}} \ln\left(1 + \frac{v_{fg}}{v_f} x_{ex}\right)$$

Notice that Δt_{ex} is a linear function of the enthalpy rise in the single-phase region Δh_1, or of the subcooling with respect to the BB, $\Delta T_{subb} = \Delta h_1/c$. It increases logarithmically with the exit quality and is proportional to the inverse of the heat input.

7.6.2 Period of the Oscillation at the Threshold of Stability

The measured period of the oscillations ranged from approximately 2 to 10 seconds, increasing continuously with subcooling. Figure 7.11 is a typical plot of the periods measured at the first occurrence of oscillations and at the transition points, versus subcooling with respect to

the BB. (The periods measured after the transitions were plotted.) All the points taken at the power level of 200 W/TL, for both uniform and cosine heat flux distributions, are shown. The experimental points lie on a family of curves, grouped according to their order. Points shown with two successive order codes had values z°_{bb}/λ close to an integer. For instance, both orders two and three were assigned to points having a value of z°_{bb}/λ equal to 2.95 or 3.1 to account for experimental uncertainties.

All the zero-order period data are plotted in Figs. 7.12 and 7.13 for uniform and cosine heat flux distributions respectively. Trends anticipated in the previous section are evident. The period increases with subcooling and is roughly inversely proportional to the average heat input. There is generally little scatter of the data. Cross examination of these figures and Figs. 7.1 to 7.5 will show that the points lying off the smoothed threshold boundaries also lie off the period curves. Given the assumption that there is a unique possible frequency for each point on the stability map, this observation is not surprising.

7.6.3 Period of the Oscillations in the Unstable Region

In the unstable region, for constant average subcooling, the period of the oscillations varied very slowly. Figure 7.14 is a typical contour map showing the lines of equal frequency. The lines present inflection points situated approximately on a diagonal line. This line moves upwards at a higher heat input (500 W/TL). At lower power levels the inflections disappear. This behavior was tentatively attributed to non-linearities in the boiling region and/or to flow regime changes.

7.7 Cosine Versus Uniform Heat Flux Distribution

Figure 7.9 shows the zero-order stability boundaries obtained at three different power levels with the cosine heat flux distribution. Zero-order oscillations were not encountered at 100 W/TL. Comparison of these boundaries with the corresponding uniform heat flux threshold curves, shown in dotted lines, suggests that the effect of the cosine heat distribution was stabilizing at all but the lowest subcoolings. The comparisons made in Chapter 4 showed that there is little effect of the heat input distribution on the pressure drop. The major effect on stability must therefore come from the changes in the average position and dynamic behavior of the BB. The latter depends on the oscillation frequency. In fact, the period versus subcooling plot of Fig. 7.13 shows that the curves obtained with the cosine distribution always lie below the corresponding uniform heat flux curves. The explanation is given below.

The enthalpy along the channel, for both uniform and cosine heat flux distributions, is sketched in Fig. 7.15A. This figure shows that for identical inlet conditions and equal average heat input, the BB will be displaced toward the center of the channel in the case of the cosine power distribution. Consider now the enthalpy delay curve, (2π - arg$\delta h(z,j\omega)$, Fig. 5.9, redrawn in Fig. 7.15B). For any heat flux distribution peaked toward the center of the channel the δh delays are shortened. Figure 7.15B shows how the two effects tend to cancel in the first third of the channel, while they add up as the BB moves downstream. Since the boiling delays are small and approximately equal for the two cases, the period of the oscillation will follow the trends exhibited by the δh delay. These

trends are evident in Fig. 7.13 where the cosine curves depart progressively from the uniform heat flux curves as subcooling increases, moving the BB downstream. The stability of the channel is influenced accordingly, as shown in Fig. 7.9.

7.8 Oscillation Amplitude in the Unstable Region - The Limit Cycle

Figure 7.16A shows the growth of the oscillations at the threshold of stability at high subcooling. Only a few cycles and a small decrease in average flow rate were necessary to bring the system from a stable regime to the limiting oscillation cycle. The violence of the oscillations, measured by the peak to average flow rate, increased with subcooling. At low subcoolings the transition from stable to unstable flow was much more gradual as shown in Fig. 7.16B.

Figures 7.16C to F are typical recordings. They include traces from a hot wire void gauge and a thermocouple. Notice the phase differences between the flow, the pressure along the channel, and the void fraction. The pressures in the boiling region are minimum when the inlet flow is maximum confirming the dynamic nature of the instability. The pressure oscillations are more pronounced in the center of the channel. Notice also the resemblance of the temperature trace to the curves of Fig. 5.13B.

7.9 Experiments to Confirm the Mechanism of Higher-Order Oscillations

The statement that, in the case of higher-mode oscillations, the portion of the channel up to the last enthalpy node before the BB does not contribute to the enthalpy perturbation at the BB, was made in

Section 7.5.1. If this were correct, it should be possible to remove the power from this portion of the channel and provide the corresponding enthalpy rise by an increase of the inlet temperature without affecting the oscillations. A number of experiments (series E) were conducted to verify this hypothesis.

An experimental transition point with a wavelength approximately equal to the test length was chosen, in order to be able to cut the power for portions of the channel that were multiples of the wavelength. Obviously, such a procedure assures similitude of the enthalpy at a single point, as the relation

$$\Delta h = q/w_o = c \ \Delta T_{subb}$$

is true at a unique flow rate only. Four experimental runs were made (Runs E03 to E06) with the power shut off from the first 0, 1, 2, and 3 test lengths, respectively. The oscillation characteristics obtained (data tabulated in Appendix E) were very much similar for each run. Figure 7.17 shows the experimental points in the $(q^*/w_o h_{fg} , \Delta T^*_{subb})$ plane. The corrected (asterisked) quantities are

$$q^* = \frac{7}{7-n} \ q \ , \qquad \Delta T^*_{subb} = \Delta T_{subb} + \frac{n \ (q/7)}{w_o \ \bar{c}}$$

and the corrected order of the oscillation becomes

$$\frac{z^\circ_{bb} - n \ \Delta L}{\lambda} + n$$

where n is the number of test lengths ΔL without power and $\bar{c}$ the average heat capacity of the liquid in the non-heated length. The transition boundaries at the corresponding power level of 200 W/TL, from

Fig. 7.2, are shown in dotted lines.

The $(q^*/w_o h_{fg}$, $z^o_{bb}/L_h)$ plane is used in Fig. 7.18. Inspection of this plot shows that, to a first approximation, the transitions occurred whenever the BB was crossing particular points of the channel.

In general the experiments have shown a remarkable similarity in the dynamic behavior of the channel, confirming the initial hypothesis.

7.10 Summary and Conclusion

Two complete stability maps, one for uniform and one for cosine heat flux distribution were presented. The large number of threshold points taken permitted the drawing of stability boundaries with sufficient accuracy. The effect of the cosine heat flux distribution was stabilizing. Although it is generally not possible to completely describe the stability of the channel by a non-dimensional analysis, some non-dimensional parameters were very useful in presenting the data.

The presence of higher-mode oscillations was detected and when the unstable regions were characterized by the order of the oscillation, consistent stability boundaries emerged. Many observations could be explained by the dynamic behavior of the boiling boundary. The association of the higher-mode oscillations with standing enthalpy waves in the single-phase region was well established. The oscillation pattern was independent of the history or the path followed into the unstable region. Some characteristics of the limit cycle were presented.

There seems to be a limited range of possible oscillation frequencies. A unique correlation between the fundamental period of the oscillation and the steady-state conditions in the channel was shown to exist.

Chapter 8

STABILITY ANALYSIS

The theoretical models for the stability analysis undertaken in this chapter were developed in Chapters 5 and 6. The dynamics of the single-phase region were studied in Chapter 5 and a method for predicting oscillatory pressure drop in the two-phase region was developed in Chapter 6. Both analyses were based on the assumption of an oscillatory inlet flow. In this chapter, a stability criterion is developed and a block diagram for the system is presented. Then experimental data are used to test the model and the discrepancies observed are analyzed.

As already mentioned, the pressure at the time-dependent position of the BB, $p_{bb}(t)$, is used here rather than the pressure at the reference position of the BB, $p^{\circ}_{bb}(t)$. The pressure perturbation at the BB, $\delta p_{bb}(t)$, which is not a directly measurable quantity, is related to the single-phase and two-phase pressure drop perturbations:

$$\delta\Delta p_1 = \delta p_{bb} - \delta p_{oo} = \delta p_{bb}$$

$$\delta\Delta p_2 = \delta p_{ex} - \delta p_{bb} = -\delta p_{bb}$$

The second equality in these equations implies that there are no inlet and exit pressure perturbations.

8.1 Stability Criterion

Figure 8.1 shows the block diagram of a boiling channel. The single-phase dynamics are represented by three transfer functions, namely Z, P_{1z}, and P_{1w}, given by Eqs. (6.48), (6.50) and (6.51) respectively. As the treatment of the two-phase region is non-linear, the corresponding block will be called the describing function P_2. The fundamental component of the harmonic response of this block will be used in the linear stability analysis of the system. The pressure drop perturbations in the single-phase and the two-phase regions are summed to yield the total pressure drop perturbation

$$\delta\Delta p_1 + \delta\Delta p_2 = \delta\Delta p$$

Consider an approach to the unstable region by a variation of some parameter, e.g. the average mass flow rate. For the inlet flow oscillating with some frequency ω, the system will cross the threshold of stability whenever

$$\delta\Delta p_1(j\omega) + \delta\Delta p_2(j\omega) \rightarrow 0$$

The stability criterion is impractical to use in this form as it relies heavily on an accurate prediction of the perturbation amplitudes. To permit application of conventional control theory methods, the block diagram of Fig. 8.1 is transformed into the closed loop diagram of Fig. 8.2. As shown in this figure, the net inlet flow perturbation produces a movement of the BB, δz_{bb}, and a two-phase pressure drop perturbation, $\delta\Delta p_2$.

As there is no externally applied total pressure drop perturbation ($\delta\Delta p = 0$), $\delta\Delta p_2$ is transformed into a single-phase pressure drop perturbation, $\delta\Delta p_1$. After subtracting the static contribution $\delta\Delta p_{1z}$ (due to the change in position of the BB) the remaining dynamic single-phase perturbation, $\delta\Delta p_{1w}$, is used to generate the feedback inlet flow perturbation, δw_{fo} through the single-phase-pressure-drop-to-flow transfer function, P_{1w}^{-1}. The stability of the channel is then investigated by examining the open loop transfer function,

$$W(s) = \frac{\delta w_{fo}}{\delta w_o}$$

in a conventional manner. For any operational point W(s) must be evaluated for a range of frequencies and plotted in the complex plane. Since most physical aspects of the problem are understood, it will be simply stated that the channel is unstable whenever the locus of the open loop transfer function crosses the real axis to the left of the -1 point.

8.1.1 Range of Frequencies

As was shown in Section 7.6, excluding the higher mode oscillations, there is a unique correlation between the period of the oscillation and the average conditions in the channel. Therefore it will be sufficient to examine the stability of the system for a limited range of frequencies. An estimate of the period of the oscillation can be obtained from the "total transit time", Δt_{ex}, defined in Section 7.6.1. Figure 8.3 shows indeed that the period of the oscillation (at the threshold of stability)

is approximately equal to twice the total transit time Δt_{ex}. For higher mode oscillations this correlation is still true, provided that the integer order of the oscillation is subtracted from $2\Delta t_1$:

$$\frac{2\Delta t_1}{\tau} - \text{int}\left[\frac{z^\circ_{bb}}{\lambda}\right] + \frac{2\Delta t_2}{\tau} \sim 1$$

As there is no way of predicting à priori the order of the oscillations, the range of frequencies must be extended toward higher values whenever the occurrence of higher modes is suspected.

To account for the wall effect, $\Delta t_1/\tau$ should be replaced by $1 - \arg \delta h^\circ_{bb}/2\pi$. Unfortunately, the evaluation of δh°_{bb} requires à priori knowledge of the period of the oscillation.

8.2 Computer Program for Stability Analyses

A computer program was written in FORTRAN IV to carry out the numerical work necessary for the stability analysis. The program, listed in Appendix F, is described briefly here.

The required inputs are: the inlet temperature, the heat input, the mass flow rate, an estimate of the total pressure drop, the exit pressure, and the period of the oscillation. Subroutine SUBCBB determines the steady-state location of the BB and the pressure drop in the single-phase region. DZDWTF calculates the single-phase transfer functions, namely H, Z, P_{1z} and P_{1w}. Subroutine STAPR2 is then called to establish the reference pressure and enthalpy profiles in the two-phase region, according to the methods of Chapter 3. With this information and using the perturbations at the BB provided by DZDWTF as inputs, DYNPR2 performs

the dynamic calculations in the two-phase region according to the enthalpy trajectory model. As noticed in Chapter 6, the enthalpy trajectory model provides time-dependent information at the enthalpy mesh points, which do not necessarily coincide with the exit of the channel. The procedure devised to determine the pressure perturbations at the exit is described below.

8.2.1 Exit Pressure Perturbations

Knowing the pressure at two points bracketing the exit, the pressure variations at the exit can be obtained by linear interpolation (Chapter 6). This method fails to account for the true exit pressure as saturation enthalpy values relative to the reference profile are used at each mesh point, regardless of the magnitude of the time-dependent pressure. In order to improve this situation, the given exit pressure was used to evaluate the fluid properties in the virtually extended channel (Section 6.7). This assures that the correct value of the pressure is used around the exit when the mesh points situated at steady-state outside the physical channel are pulled back into the channel during the oscillations. Conversely, however, when interior mesh points are pushed outside the channel, no correction can be applied. Given the importance of the pressure drop near the exit of the channel in the present system, it became necessary to correct this behavior further. This was accomplished by recalculating the pressure drop with the time dependent value of the saturation enthalpy in the segment extending from some mesh point inside the channel to the channel exit. This method also provides an artifice for approximately taking into account

thermodynamic non-equilibrium. Assuming that thermodynamic non-equilibrium can be simulated by a change in the saturation enthalpy, a correction of the channel exit pressure might appropriately account for this effect. All features mentioned above were included in the computer program. Recalculation of the pressure drop near the exit accounted for up to 50 percent change in the total two-phase pressure drop perturbation. The linear interpolation scheme gave, as expected, larger perturbations except at high mass flow rates. Adjustment of the exit pressure to 18 psia accounted typically for an additional ten percent reduction in the pressure drop perturbation.

8.2.2 Phase of the Pressure Perturbations

The phase of the pressure perturbations is determined simply by searching for the maximum calculated value (Subroutine PRTPL3). This method evidently limits the available resolution. It might have been more accurate to fit the perturbations to a pure cosine in the least squares sense, and then determine analytically the phase of this function. For the present work the former method was sufficient.

8.2.3 Options and External Corrections

The computer program, being at this stage a research tool rather than a production code, was given sufficient flexibility to permit thorough testing of the theory. For example, various parameters non-essential to the stability analysis are calculated and printed. "Switches" allow bypassing certain calculations or repeating others with

partially different inputs. It is also possible to externally apply corrections to the amplitude and phase of the BB perturbation.

8.2.4 Performance of the Code

Despite of the serious burdening of the program with peripheral calculations and some lack of efficiency due to duplication of effort in various subroutines, the program was rather economical to run. A complete calculation of the open loop transfer function, for one frequency value (120 time steps, 16 enthalpy mesh points, limited printout) required approximately 1.5 seconds on the IBM-360/65 (FORTRAN Compiler G).

8.3 Prediction of the Threshold of Stability

The computer program described in the preceding section was used to predict the behavior of the channel for a number of experimental points. Figures 8.4 and 8.5 show the calculated open loop transfer functions. The frequency response obtained is similar to results reported in the literature [7,12]. The small loops in the figures occur when the wavelength approaches the single-phase length ($z^{\circ}_{bb}/V_o\tau \sim 1$). Similar results have been reported by Stenning and Veziroglu [7]. The gain of the open loop transfer function increases, as expected, with decreasing flow rate, as the unstable region is approached. The threshold of stability, however, as predicted by the frequency analysis was not in agreement with the experimental observations (see data included in Figs. 8.4 and 8.5). The curves cross the real axis for values of the period well below the measured ones. The agreement is, however, slightly better at low subcoolings.

8.3.1 Discussion of the Discrepancies

The origin of the disagreement between experimental observations and typical theoretical predictions is discussed with reference to Fig. 8.6. The two components of the dynamic pressure drop perturbation in the single-phase region, $\delta\Delta p_{lw}$, are shown separately in this figure; the frictional component, $\delta\Delta p_{lfr}$ is 180° out of phase* with δw, while the inertial component, $\delta\Delta p_{lin}$, leads the frictional component by 90°.

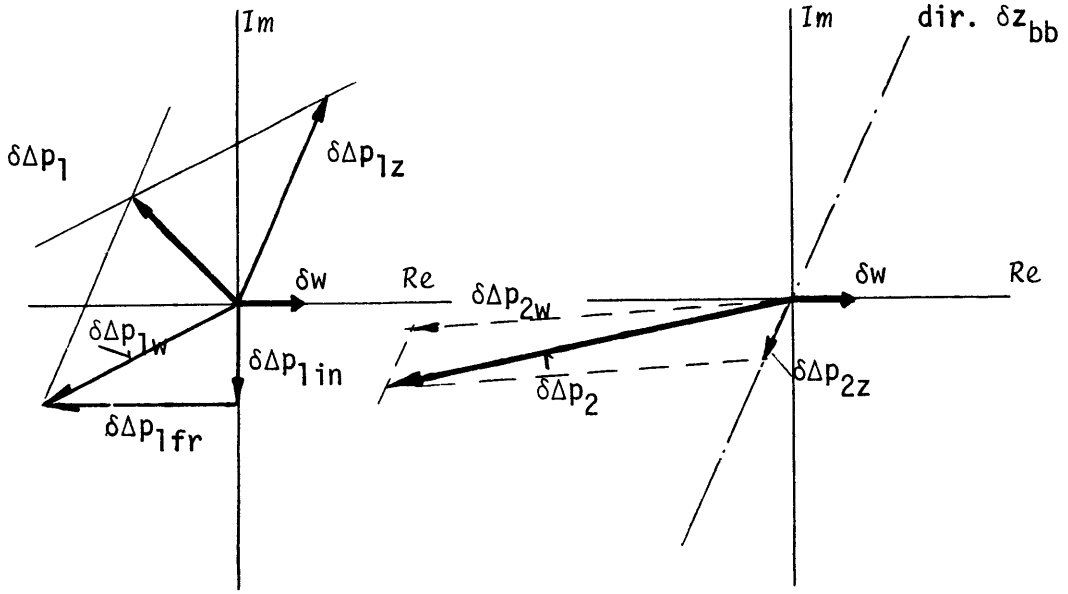

FIG. 8.6 VECTOR DIAGRAM OF PERTURBATIONS AS TYPICALLY PREDICTED BY THE MODEL

*Recall that Δp_1 and Δp_2 are defined here as negative quantities. In the computer program, however, the opposite convention was adopted and the pressure drops were treated as positive quantities.

In the two-phase region the pressure drop perturbation was approximately 180° out of phase with the flow perturbation, suggesting that the delays and the inertia effects were small. This plot shows also two components of $\delta\Delta p_2$, the static component $\delta\Delta p_{2z}$ and the dynamic component $\delta\Delta p_{2w}$, although the enthalpy trajectory model does not make such a distinction.

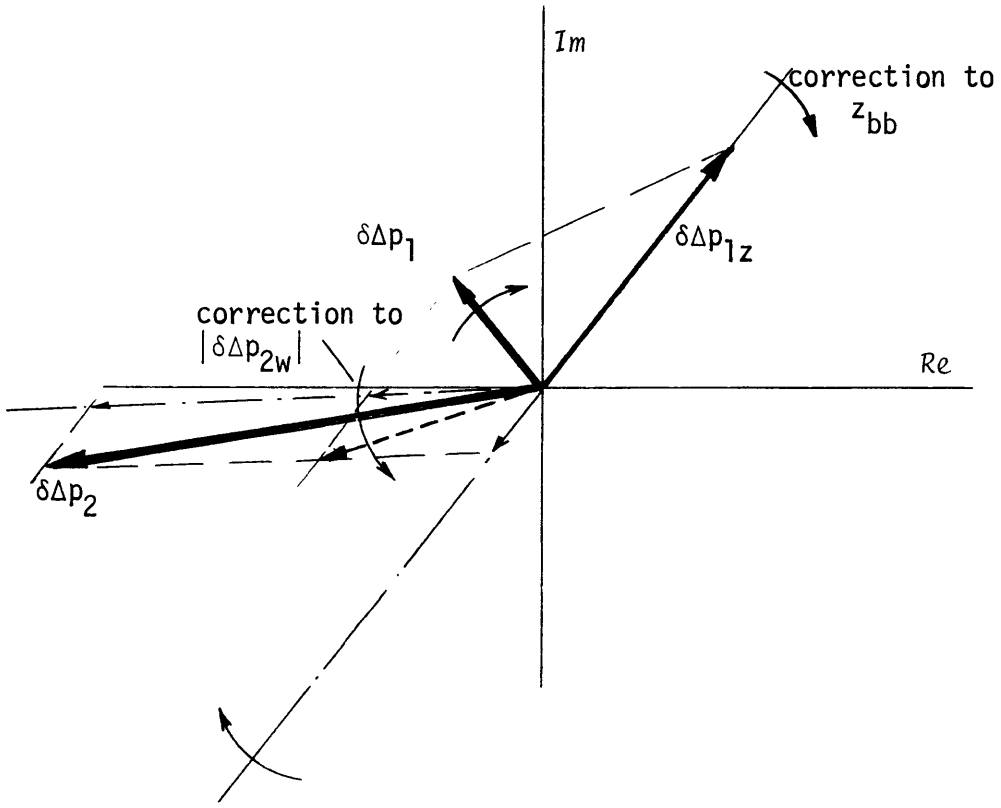

FIG. 8.7 CORRECTIONS TO PREDICTED PERTURBATIONS

Figure 8.7 shows the adjustments that would have been necessary to correct the results. These are analyzed below and their relation to physical phenomena is brought out. It is obvious, that in order to have

$\delta\Delta p_1 + \delta\Delta p_2 = 0$ it is necessary to rotate $\delta\Delta p_1$ clockwise and/or $\delta\Delta p_2$ counterclockwise. Assuming that $\delta\Delta p_{1w}$ is correctly estimated, the first correction can be accomplished by an increase in either the delay or the amplitude of δh°_{bb}. It is likely that the phase of δh°_{bb} is questionable. Indeed the analysis of Chapter 5 assumed a perfect mixing of the flow and flat radial temperature and velocity profiles. The validity of these assumptions for Freon is doubtful. Unfortunately, there is little information on transient convective heat transfer to undertake a rigorous examination of this complicated problem. Qualitatively, it seems that the enthalpy variations travel with a lesser velocity than expected. The heat generated in the wall has to be conducted through an almost stationary laminar sublayer to diffuse to the central core of the duct, from where it will be transported downstream. It can be deduced that the combined effects of the temperature and velocity profiles introduce significant additional delay.

A reduction of the amplitude of the dynamic two-phase pressure drop perturbation, $\delta\Delta p_{2w}$, will result in a counterclockwise rotation of $\delta\Delta p_2$. This dynamic perturbation has been generally overestimated by the enthalpy trajectory model and is responsible for the approximately 180° phase angle of $\delta\Delta p_2$. For the range of qualities under consideration, the frictional pressure drop is dominant in the two-phase region (Fig. 3.5). In addition, the transit time in the boiling region is also short (of the order of 0.5 s) compared to the order of the oscillation.

Therefore, little phase correction can be achieved by changes in the space - time distribution of the flow perturbations.*

Comparison of the dynamically obtained pressure drop perturbations with corresponding steady-state differences in the two-phase pressure drop showed that they were of the same order of magnitude. The exit pressure drop correction discussed earlier in Section 8.2.1 and eventual adjustments of the exit pressure to account for thermodynamic non-equilibrium provided insufficient reductions of the amplitude of $\delta\Delta p_2$. Therefore it can be argued that time-dependent heat transfer plays an important role in determining the amplitude of the two-phase pressure drop perturbation. The dependence of the heat transfer on the flow velocity will reduce the changes in the vapor generation rate and consequently diminish the pressure drop perturbation. Stenning and Veziroglu [7] came to the same conclusion. They had estimated the value of the coefficient a (Eq. 5.9) to be close to 0.4; a value of approximately 0.7 would have been required for their observations to agree with their theoretical predictions of the threshold of stability.

The importance of the effects mentioned above diminishes as the boiling region is extended upstream. This explains the closer agreement obtained at low subcoolings.

It can be concluded that two simultaneous corrections were necessary

---

*In the progress of the experimental work a short movie was made to study the space - time distribution of the flow perturbations. A system of mirrors was used to photograph simultaneously, on the same frame, the inlet and the exit of the channel.

to bring agreement between the theory and the experiments: a) a significant reduction of the amplitude of the dynamic two-phase pressure drop perturbation, and b) an increase of the delays in the single phase region. Both were explained on physical grounds but could not be incorporated in the model.

8.3.2 Higher-Mode Oscillations and Transitions

Examination of Figs. 8.4 and 8.5 suggests that the occurrence of transitions can be related to the presence of small loops in the locus of W(s). When the real axis intercepts the locus of the open loop transfer function at more than one point multiple modes of oscillation are possible. Moreover, the results of the frequency analysis shown in these figures are in agreement with the experimental fact that at high mass flow rates unstable operation is possible only at low periods. Unfortunately, the discrepancies discussed above did not encourage further analytical investigation of this problem.

Chapter 9

GENERAL CONCLUSIONS AND RECOMMENDATIONS

Partial conclusions drawn in previous chapters will be combined and summarized here and recommendations for future work will be made.

9.1 Steady-State Work

Methods for predicting the steady-state behavior of the boiling channel were presented and their validity was verified by an extensive series of experiments. An accurate prediction of the pressure drop in the channel was achieved using well established correlations. The calculated pressure drops were particulatly accurate in the dynamically interesting region. The only discrepancies were due to deviations from thermodynamic equilibrium between the phases. Thermodynamic non-equilibrium is at present under investigation in various laboratories. It is hoped that these studies will provide a theoretical basis for accounting for these phenomena.

Freon-113 seems to be particularly prone to thermodynamic non-equilibrium. It has also a high air solubility and a very low thermal conductivity. These undesirable properties must be kept in mind when future work with Freon is undertaken.

9.2 Stability Work

9.2.1 Experimental Results

The regions of unstable operation of the channel were mapped with sufficient accuracy to permit evaluation of parametric trends.

A number of dimensionless groups proved to be useful in correlating the data. These groups often contained integral parameters that were not directly measurable. Evaluation of these quantities required some numerical effort which was, however, justified by the improvements obtained in the presentation of the data. It is concluded that non-dimensional groups can be profitably used for interpolation or extrapolation of theoretical predictions and experimental measurements.

A close correlation between the period of the oscillation at the threshold of stability and the average conditions in the channel was established. The period of the oscillation is approximately equal to twice the total transit time in the channel. This quantity is rigorously defined below.

Two distinct propagation phenomena must be considered: the propagation of the enthalpy perturbations in the single-phase region and the propagation of the void perturbations in the two-phase region. The enthalpy perturbations travel at twice the flow velocity, while the void perturbations propagate approximately at the velocity of the vapor phase. Therefore, the total transit time is defined as the sum of one-half the physical transit time in the single-phase region plus the vapor transit time in the two-phase region.

At high subcoolings and low heat inputs the channel oscillated at frequencies that were a multiple of the expected frequency. Sudden changes in the period of the oscillation were also recorded in this region. The occurrence of these "higher-order" oscillations and transitions from mode to mode were shown to be associated with the existence of more than one node in the standing enthalpy waves of the single-phase region. The "order" of the oscillation was defined as the integer part of twice the ratio of the single-phase transit time to the period of the oscillation, and is equal to the number of enthalpy nodes minus one. When the regions of unstable operation were characterized by the order of the oscillation, a coherent stability map was obtained.

The effect of a chopped cosine heat flux distribution was investigated experimentally and was found to be stabilizing. Because the influence of the heat flux distribution on the pressure drop was small, the stabilizing effect of the cosine distribution was attributed to the dynamics of the boiling boundary. With the cosine heat flux distribution the period of the oscillations was shorter than with the uniform heat flux distribution. The difference could be explained by considering the delays in the single-phase region.

9.2.2 Theoretical Results

It was shown that heat storage in the channel walls can acquire under appropriate conditions a major importance in the single-phase dynamics. Under the present experimental conditions an exact treatment of the wall dynamics was necessary to account correctly for time-dependent heat flux. The distribution of the enthalpy perturbations along the channel is also

influenced by local discontinuities in the heat flux distribution, such as stepwise heat flux changes and cold spots in the wall. The effect is significant when the characteristic length of the discontinuities approaches the wavelength of the oscillation, $\lambda = V_o \tau$.

The movements of the boiling boundary were determined taking into account both the static and the dynamic pressure drop perturbations in the single-phase region. The relative importance of the generally neglected dynamic terms increases in proportion to the length of the single-phase region and also increases with the frequency of the oscillation.

A new method of calculating two-phase pressure drop under oscillatory flow conditions was developed and shown to have several advantages over conventional techniques in the calculation of the time-dependent pressure drop. The method, however, cannot account for time-dependent heat transfer from the wall. In the present case this seemed to be a limitation.

The single-phase and the two-phase dynamics models were used to predict the threshold of stability of the present experimental channel. Although the stability model exhibited a qualitatively correct behavior, the theoretically predicted thresholds of stability were not in agreement with the experimental observations. The causes of the disagreement were attributed mainly to three phenomena:

a) radial heat conduction and diffusion effects in the single-phase region that influence the propagation of the enthalpy perturbations;

b) lack of thermodynamic equilibrium; and

c) time-dependent heat transfer rates in the boiling region.

The prediction of excessively large two-phase pressure drop perturbations was probably due to effects b) and c).

9.3 Recommendations

9.3.1 Experimental Work

It would be interesting to investigate experimentally the progression of the enthalpy perturbations in the single-phase region. Detailed information on the radial temperature and velocity profiles under oscillating flow will be needed to test analytical models. Fluorocarbons will be suitable as test fluids, their low thermal conductivity enhancing the radial phenomena. Externally controlled oscillation of the flow will be necessary to eliminate dependence on the natural oscillations of the channel. Discontinuities in the heat flux distribution should be considered with caution in future experiments.

9.3.2 Analytical Work

It is recommended that the limits of applicability of the enthalpy trajectory model be determined by comparison to other well established hydrodynamics codes or to experimental data. The entire stability model developed here should be tested under more favorable conditions, e.g. using stability data obtained with water systems.

Two-dimensional treatment of the single-phase region is an extremely challenging problem and should be undertaken in order to evaluate the importance of the radial effects.

Analytical and experimental investigations of thermodynamic non-equilibrium are necessary.

REFERENCES

1. Lottes, P., et al., "Experimental Studies of Natural Circulation Boiling and Their Application to Boiling Reactor Performance," Proceedings of the Second International Conference on the Peaceful Uses of Atomic Energy, Geneva 1958, P/1983, 7, 784.

2. Anderson, R. and P. Lottes, "Boiling Stability," J. Nucl. Energy, 2, Reactor Technology, B, 13 (1962), also in

   Progress in Nuclear Energy, Series IV, vol. 4, Technology, Engineering and Safety, Pergamon Press, N.Y. (1961).

3. Lottes, P.A., et al., "Fluid Dynamics, Stability and Vapor-Liquid Slip in Boiling Water Reactor Systems," Proceedings of the Third International Conference on the Peaceful Uses of Atomic Energy, Geneva 1964, P/230, 8, 263-271.

4. Efferding, L.E., "Static and Hydrodynamic Stability of Steam-Water Systems Part I: Critical Review of the Literature," GA - 5555 (Oct. 1964).

5. Neal, L.G. and S.M. Zivi, "Hydrodynamic Stability of Natural Circulation Boiling Systems, Vol. I: A Comparative Study of Analytical Models and Experimental Data," STL-372-14(1) (June 1965), also

   "Stability of Boiling-Water Reactors and Loops," Nucl. Sci. Eng., 30, 25-38 (1967).

6. Zuber, N., "Flow Excursions and Oscillations in Boiling, Two-Phase Flow Systems With Heat Addition," Proceedings of the Symposium on Two-Phase Flow Dynamics, Euratom - The Technological University of Eindhoven (Sept. 1967).

7. Stenning, A.H. and T.N. Veziroglu, "'Density-Wave' Oscillations in Boiling Freon-11," ASME Paper 66-WA/HT-49 (1966), also

   "Oscillations in Two-Component Two-Phase Flow," vol. I, NASA CR-72121 (Feb. 1967), and

   "Flow Oscillations in Forced Convection Boiling," vol. II, NASA CR-72122 (Feb. 1967).

8. Thie, J.A., "Theoretical Reactor Statics and Kinetics of Boiling Reactors," Proceedings of the Second International Conference on The Peaceful Uses of Atomic Energy, Geneva 1958, P/638, 11, 440-446.

9. Quandt, E.R., "Analysis and Measurement of Flow Oscillations," Chemical Eng. Progress Symposium Series, No. 32, Heat Transfer, Buffalo, 111-126 (Aug. 1960).

10. Wallis, G.B. and J.H. Heasley, "Oscillations in Two-Phase Flow Systems," Trans. ASME, Series C, J. Heat Transfer, 83, 363 (1961).

11. Fleck, J.A., Jr., "The Influence of Pressure on Boiling Water Reactor Dynamic Behavior at Atmospheric Pressure," Nucl. Sci. Eng., 9, 271 (1961).

12. Jones, A.B./A.B. Jones and D.G. Dight, "Hydrodynamic Stability of a Boiling Channel," Part I: KAPL - 2170 (1961), Part II: KAPL - 2208 (1962), Part III: KAPL - 2290 (1963), Part IV: KAPL - 3070 (1964)

Jones, A.B. and W.M. Yarbrough/A.B. Jones, "Reactivity Stability of a Boiling Reactor," Part I: KAPL - 3072 (1964), Part II: KAPL - 3093 (1965).

13. Meyer, J.E. and R.P. Rose, "Application of a Momentum Integral Model to the Study of Parallel Channel Boiling Flow Oscillations," Trans. ASME, J. Heat Transfer, 85,1(1963).

14. Shotkin, L.M., "Flow of Boiling Water in Heated Pipes," Nucl. Sci. Eng., 26, 293-304 (1966).

15. Shotkin, L.M., "Stability Considerations in Two-Phase Flow," Nucl. Sci. Eng., 28, 317-324 (1967).

16. Craya, A. and J. Bouré, "Sur un Mécanisme de Mise en Oscillations dans les Ecoulements Disphasiques Chauffés," C.R. Acad. Sc., Paris, 263, A 477 (1966).

17. Bouré, J.A. and A. Mihaila, "The Oscillatory Behavior of Heated Channels," Proceedings of the Symposium on Two-Phase Flow Dynamics, Euratom - The Technological University of Eindhoven (Sept. 1967).

18. Davies, A.L. and R. Potter, "Hydraulic Stability: an Analysis of the Causes of Unstable Flow in Parallel Channels," The Proceedings of the Symposium on Two-Phase Flow Dynamics, Euratom - The Technological University of Eindhoven (Sept. 1967).

19. Levy, S. and E. Beckjord, "Hydraulic Instability in a Natural Circulation Loop with Net-Steam Generation at 1000 psia," GEAP-3215 (1959), also

ASME Paper 60-HT-27 (1960).

20. Becker, K.M. et al., "Hydrodynamic Instability and Dynamic Burnout in Natural Circulation Two-Phase Flow - An Experimental and Theoretical Study," Proceedings of the Third International Conference on the Peaceful Uses of Atomic Energy, Geneva 1964, P/607, 8, 325.

21. Bogaardt, M., C.L. Spigt, F.J.M. Dijkman and A.N.J. Verheugen, "On the Heat Transfer and Fluid Flow Characteristics in a Boiling Channel Under Conditions of Natural Convection," Proc. Inst. Mech. Engrs., 180, Part 3C, 77-87 (1965-1966) "Boiling Heat Transfer in Steam Generating Units and Heat Exchangers."

22. Berenson, P.J., "An Experimental Investigation of Flow Stability in Multitube Forced-Convection Vaporizers," ASME Paper No. 65-HT-61 (Aug. 1965).

23. Jain, K.C., et al., "Self Sustained Hydrodynamic Oscillations in a Natural-Circulation Boiling Water Loop," Nucl. Eng. Design, 4, 233-252 (Oct. 1966).

24. Masini, G., G. Possa and F.A. Tacconi, "Flow Instability Thresholds in Parallel Heated Channels," Energia Nucleare, 15, no. 12, 777 (1968).

25. Bowring, R.W., and C.L. Spigt, "Seven-Rod Bundle Natural-Circulation Stability and Burnout Test with Water at up to 28 Atmospheres Pressure," Nucl. Sci. Eng., 22, 1-13 (1965).

26. Kjaerheim, G. and E. Rolstad, "In-Pile Hydraulic Instability Experiments with a 7-Rod Natural Circulation Channel," Proceedings of the Symposium on Two-Phase Flow Dynamics, Euratom - The Technological University of Eindhoven (Sept. 1967).

27. Gouse, S.W., Jr., and C.C. Hwang, "Visual Study of Two-Phase One-Component Flow in a Vertical Tube with Heat Transfer," M.I.T., EPL Report DSR-8973-1 (June 1963).

28. Dickson, A.J. and S.W. Gouse, Jr., "Heat Transfer and Fluid Flow Inside a Horizontal Tube Evaporator," Phase III, Final Report, M.I.T. EPL Report DSR-9649-3 (Aug. 1966).

29. Gouse, S.W., Jr. and C.D. Andrysiak, "Flow Oscillations in a Closed Loop with Transparent, Parallel, Vertical, Heated Channels," M.I.T. EPL Report DSR-8973-2 (June 1963).

30. Gouse, S.W., Jr., "An Index to the Two-Phase Gas Liquid Flow Literature," M.I.T. Report No. 9, The M.I.T. Press (1966).

31. Zotter, B.C., "The Two-Phase Gas-Liquid Flow Oscillation Literature - A Critical Review," S.M. Thesis, Dept. of Mech. Eng., M.I.T. (Sept. 1966).

32. Crowley, J.D., C. Deane and S.W. Gouse, "Two-Phase Flow Oscillations in Vertical, Parallel, Heated Channels," Proceedings of the Symposium on Two-Phase Flow Dynamics, Euratom - The Technological University of Eindhoven (Sept. 1967), also

Gouse, S.W., Jr., R.G. Evans, C.W. Deane and J.C. Crowley, "Two-Phase Gas-Liquid Flow Dynamics: Part I - Flow Oscillations in Transparent, Parallel, Heated Channels, Part II - Acoustic Velocity in Two-Phase Flow," M.I.T., EPL Report No. DSR-74629-1 (Nov. 1967).

33. Deane, C.W., IV, "An Experimental Investigation of Flow Oscillations in Two-Phase Mixtures in a Closed Loop with Transparent, Parallel, Vertical, Heated Channels," S.M. Thesis, M.E. Dept., M.I.T. (Sept. 1966).

34. Meyer, J.E., "Conservation Laws in One-Dimensional Hydrodynamics," Bettis Technical Review, WAPD-BT-20, 61-72 (1960).

35. Meyer, J.E., "Hydrodynamic Models for the Treatment of Reactor Thermal Transients," Nucl. Sci. Eng., 10, 269 (1961).

36. Meyer, J.E. and E.A. Reinhard, "Numerical Techniques for Boiling Flow Stability Analyses," J. of Heat Transfer, Trans. ASME, Series C, 87, 311-312 (May 1965).

37. Grumbach, R., "A Systematic Comparison of Different Hydrodynamics Models," Nucl. Sci. Eng., 36, 429 (1969).

38. Bjørlo, T. et al., "Comparative Studies of Mathematical Hydrodynamic Models Applied to Selected Boiling Channel Experiments," Proceedings of the Symposium on Two-Phase Flow Dynamics, Euratom - The Technological University of Eindhoven (Sept. 1967).

39. Shotkin, L.M., "Effect of Slip Ratio on the Crucial Boiling Length in Two-Phase Instability," Proceedings of the Symposium on Two-Phase Flow Dynamics, Euratom - The Technological University of Eindhoven (Sept. 1967).

40. Mathisen, R.P., "Out of Pile Instability in the Loop Skälvan," Proceedings of the Symposium on Two-Phase Flow Dynamics, Euratom - The Technological University of Eindhoven (Sept. 1967).

41. Benning, A.F. and R.C. McHarness, "Thermodynamic Properties of 'Freon'-113. Trichlorotrifluoroethane, CCl_2F-$CClF_2$, with Addition of Other Physical Properties," E.I. du Pont de Nemours and Co., Inc., Bulletin T-113A (1938).

42. Downing, R.C., "Transport Properties of 'Freon' Fluorocarbons," Du Pont Technical Bulletin C-30 (1967).

43. "Freon, TF Solvent", Du Pont Technical Bulletin FST-1.

44. Goldsmith, A. et al., "Handbook of Thermophysical Properties of Solid Materials," The MacMillan Co., New York (1961).

45. Corning Glass Works, "Properties of Selected Commercial Glasses," Bulletin B-83.

46. Hsu, Y.Y., FF. Simon and R.W. Graham, "Application of Hot Wire Anemometry for Two-Phase Flow Measurements Such as Void Fraction and Slip Velocity," ASME Multi-Phase Flow Symposium, 26-34 (Nov. 1963).

47. Sieder, E.N. and G.E. Tate, "Heat Transfer and Pressure Drop of Liquids in Tubes," Ind. Eng. Chem, 28, 1429 (1936).

48. Pipe Friction Manual, Hydraulic Institute, New York (1954).

49. Lockhart, R.W. and R.C. Martinelli, "Proposed Correlation of Data for Isothermal Two-Phase Two-Component Flow in Pipes," Chemical Engineering Progress, 45, no. 1, 39-48 (1949).

50. Levy, S., "Steam Slip - Theoretical Prediction from Momentum Model," J. Heat Transfer, Trans. ASME, Series C, 82, 113 (1960).

51. Marchaterre, J.F., "Two-Phase Frictional Pressure Drop Prediction From Levy's Momentum Model," J. Heat Transfer, Trans. ASME, Series C, 83, 503 (1961).

52. Baroczy, C.J., "Correlation of Liquid Fraction in Two-Phase Flow with Application to Liquid Metals," Sixth National Heat Transfer Conference AIChE, ASME, Boston, Mass. (Aug. 1963), also in Chemical Engineering Progress Symposium Series, No. 57, 61, 179-191 (1965).

53. Lottes, P.A., M. Petrick and J.F. Marchaterre, "Lecture Notes on Heat Extraction from Boiling Water Power Reactors," ANL-6063 (Oct. 1959).

54. Zuber, N. and J.A. Findlay, "Average Volumetric Concentration in Two-Phase Flow Systems," J. of Heat Transfer, Trans. ASME, Series C, 87, 453 (1965).

55. Griffith, P. and G.B. Wallis, "Two-Phase Slug Flow," J. of Heat Transfer, Trans. ASME, Series C, 83, 307 (1961).

56. Levy, S., "Forced Convection Subcooled Boiling - Prediction of the Vapor Volumetric Fraction," Int. J. Heat Mass Transfer, 10, 951-965 (1967).

57. Staub, F.W., "The Void Fraction in Subcooled Boiling - Prediction of the Initial Point of Net Vapor Generation," J. of Heat Transfer, Trans. ASME, Series C, 90, 151 (1968).

58. Rohsenow, W.M. and H.Y. Choi, "Heat, Mass and Momentum Transfer," Prentice-Hall (1961).

59. Lottes, P.A., et al., "Boiling Water Reactor Technology, Status of the Art Report, Vol. I: Heat Transfer and Hydraulics," ANL-6561 (Feb. 1962).

60. Murphy, R., Personal communication, (1969), M.I.T., Heat Transfer Laboratory.

61. Zuber, N., F.W. Staub, G. Bijwaard, P.G. Kroeger, "Steady State and Transient Void Fraction in Two-Phase Flow Systems," GEAP-5147 (Jan. 1967), EURAEC - 1949.

62. Narin, F. and D. Langford, "Analytical Solutions for Transient Temperature Distributions in Two-Region Nuclear Reactor Fuel Elements," Nucl. Sci. Eng., 6, 386 (1959).

63. Smets, H.B., "Nuclear Power Plant Transfer Functions," M.Sc. Thesis, Chem. Eng. Dept., M.I.T., (Sept. 1957).

64. Gyftopoulos, E.P., "Transfer Function Representation of Nuclear Power Plants," ANL-6205, 18-44 (1960).

65. Gyftopoulos, E.P. and H.B. Smets, "Transfer Functions of Distributed Parameter Nuclear Reactor Systems," Nucl. Sci. Eng., 5, 405-414 (1959).

66. Storrer, F., "Temperature Response to Power, Inlet Coolant Temperature and Flow Transients in Solid Fuel Reactors," APDA 132 (1959).

67. Christensen, H.,"Power-to-Void Transfer Functions," ANL-6385 (1961).

68. Akcasu, A.Z., "Theoretical Feedback Analysis in Boiling Water Reactors," ANL-6221 (Oct. 1960).

69. Siegel, R. and M. Perlmutter, "Heat Transfer for Pulsating Laminar Duct Flow," J. of Heat Transfer, Trans. ASME, Series C, , 111 (1962).

70. Feiler, C.E. and E.B. Yeager, "Effect of Large-Amplitude Oscillations on Heat Transfer," NASA TRR-142 (1962).

71. Margolis, D., Personal communication (1969), Ph.D. Thesis to be published, M.E. Dept., M.I.T.

72. Zuber, N., F.W. Staub, "An Analytical Investigation of the Transient Response of the Volumetric Concentration in a Boiling Forced-Flow System," Nucl. Sci. Eng., 30, 268-278 (1967).

73. Staub, F.W., N. Zuber and G. Bijwaard, "Experimental Investigation of the Transient Response of the Volumetric Concentration in a Boiling Forced-Flow System," Nucl. Sci. Eng., 30, 279-295 (1967).

74. Zuber, N. and F.W. Staub, "The Propagation and the Wave Form of the Vapor Volumetric Concentration in Boiling, Forced Convection System Under Oscillatory Conditions," Int. J. Heat Mass Transfer, 9, 871-895 (1966).

75. Davidov, A.A., "Investigation of Flow Pulsations in Tubes of the Evaporation Section of Radiant Boilers," AEC-tr-4490 (1961)

76. Schuster, J.R. and P.J. Berenson, "Flow Stability of a Five-Tube Forced-Convection Boiler," ASME Paper 67-WA/HT-20 (1967).

77. Staniforth, R. and G.F. Stevens, "Experimental Studies of Burn-out Using Freon 12 at Low Pressure with Reference to Burnout in Water at High Pressure," Proc. Inst. Mech. Eng., London, 180, Part 3C, 216-225 (1965-1966).

Appendix A

PRESDROP, a Computer Code to Predict the Steady-State Operating Conditions in the Boiling Channel

This Appendix contains a schematic description of the program PRESDROP that calculates the steady-state operating conditions in the boiling channel according to the procedure presented in Chapter 3. A FORTRAN listing of PRESDROP is given at the end of this Appendix. This program was also used in subroutine form (PRESDR) for incorporation in any program to provide the steady-state information.

A.1 Structure of the Main Program

The program starts by reading in the general information, i.e. the inlet temperature (TIN), the condenser pressure (PCOND), the room temperature (TROOM), the heat input (QW(I), I=1,7) and the various convergence criteria and control parameters. These data are used to perform a few basic calculations.

Next, an inlet velocity (VIN) is read in together with a guess of the total pressure drop (PINEST). Calculations start based on the gross power input, and subroutine SUBBOL is called to estimate the point of NVG. The exit conditions are determined and the pressure drop in the unheated exit length is evaluated. Then a march upstream, segment by segment, is started: subroutine SUBLIQ for negative or MARNEL for positive exit equilibrium quality is called to perform the calculations

for a single segment. Both subroutines can take into account subcooled boiling. When the bulk boiling boundary is reached subroutine BOBDRY is called to determine accurately this point. With subcooled boiling the BOBDRY call is omitted and the zero quality point is determined by linear interpolation. At this point, the steady-state conditions along the channel are known in a first approximation. The heat losses are estimated by LOSSES and the location of the NVG point is found by linear interpolation on the basis of the bubble departure enthalpy provided by SUBBOL. The calculation is then repeated with the corrected heat input and NVG point as many times as desired. Finally, printout occurs at selected points by skipping intermediate nodes. The program then returns to read in another inlet velocity value (VIN).

The FUNCTION subprograms called in PRESDROP to evaluate the physical properties of Freon-113 are described in Appendix B. Appendix C deals with the auxiliary functions used in the two-phase pressure drop calculations. More information about the program can be found in the comment cards of the FORTRAN listing. A few convergence problems encountered during the debugging of the code are discussed in the following section.

A.2 Convergence Problems Around the Bulk Boiling Boundary

Subroutine BOBDRY, which is used to locate exactly the zero equilibrium quality point, occasionally presented serious convergence problems. At high mass fluxes and heat fluxes, there is a very large and sudden acceleration of the flow at the bulk boiling point, resulting in an almost stepwise pressure drop. This physical discontinuity,

coupled with the mechanics of the pressure drop and quality evaluations frequently produced numerical oscillations of the pressure and quality during the iterative process, when a narrow enough tolerance was specified for the zero quality point. The quality then jumped continuously from negative to positive values and vice-versa without ever approaching zero. To circumvent this annoying difficulty, the convergence algorithm was modified, a length rather than a quality tolerance was imposed, and the calculations were ended when a slightly negative "zero point" quality was obtained. The last consideration assured that the important acceleration term in the pressure drop was correct.

A similar problem appeared in subroutine MARNEL which calculates the pressure drop around the zero quality point when subcooled boiling is taken into account and the BOBDRY call is bypassed. The problem was dealt with in a similar fashion and to avoid expensive looping, a limit on the number of iterations was imposed. See the FORTRAN listings and comments for details.

A.3 Effect of the Segment Size and Error Criteria on the Code Accuracy

Test runs with variable segment sizes (the 15.5 inch test length was subdivided into as many as 24 segments) have shown that the pressure profile is rather insensitive to the segment size. Node lengths of a few inches, used with a pressure drop convergence criterion (ERROR) of 0.001 or 0.002 give quite satisfactory results. Even segment sizes above ten inches give errors of a few hundredths of a psi only, mainly concentrated around the zero quality point. A value of about 0.02 is

recommended for the boiling boundary position error (EBB). One major iteration is generally sufficient to accurately estimate the losses and the NVG point.

```
C
C      ********* P R E S D R O P  ************************ VERSION 2.1 *
C                                                            11/3/69
C      PRESDROP CALCULATES PRESSURE DROP IN TWO-PHASE FLOW WITH VARIABLE
C      PRESSURE DEPENDENT PROPERTIES.
C
C           INPUT INFORMATION ******************************************
C      VARIABLES AND FORMAT
C
C      **** TIN, INLET TEMP. (F), PCOND, CONDENSER PRESS.(IN HG),
C      *         TROOM, ROOM TEMPERATURE (F),
C      *         TITLE
C      *         IP, TO GET PRINTOUT FOR ALL ITERATIONS PUT IP .GT. 0
C      *                        /3F10.5, 12A4, I2
C      * QW(I), POWER DISTRIBUTION BOTTOM TO TOP (WATT) /7F10.5
C      * N, NUMBER OF SEGMENTS FOR EACH TEST LENGTH,  MUST BE MULT. OF NP
C      *   NP, NUMBER OF SEGMENTS BETWEEN PRINTOUTS,
C      *   ISUBC, SWITCH FOR SUBBOL (POS.IF WANTED),
C      *   LOSS, SWITCH FOR HEAT LOSS CALCULATION (POS. IF WANTED),
C      *   KITER, NUMBER OF MAJOR ITERATIONS,
C      *   ERROR, CONVERGENCE CRITERION FOR MARNEL (RELATIVE ERROR)
C      *   EBB, ERROR CRITERION FOR BOBDRY (USE .GT. 0.005) /5I2,2F10.5
C      *
C      * VIN, INLET VELOCITY (FT/SEC),PINEST, AN ESTIMATE OF THE INLET
C      *        PRESSURE (PSIA)        /2F10.5
C      *
C      * VIN, PINEST
C      * ETC
C      **** 0.0  END OF VELOCITY VALUES   /F10.5
C
C      **** TIN, PCOND,   ETC
C      *
C
C      *
C      ****0.0
C      0.0    END OF DATA     /F10.5
C
C           OUTPUT INFORMATION *****************************************
C      PRESSURE, TEMPERATURE, VOID FRACTION, QUALITY PROFILES ALONG THE CHANNEL
C      POINT OF NVG, BOILING BOUNDARY, HEAT LOSSES, ETC
C
C      MAIN PROGRAM ***************************************************VERSION-2
C
       REAL MUL, MUG, MULF, MUGF, MULTF
       INTEGER FIN
       DIMENSION QW(7), Q(7), HEATFL(7), P(175), X(175), H(175), T(175),
      1      FR(168), GR(168), AC(168), TOT(168), SUMFR(175), SUMGR(175)
      2      , SUMAC(175), PNET(175), A(175), SUMTOT(175), XTR(175),
      3      TBST(8), XST(8), QNETW(7), QNET(7), TTR(175), QLOSW(7),
      4      TITLE(12)
       COMMON D, DL, ERROR, G, DH, QTS, HE, HI, XE, XI, PE, PI,
      1     BE, BI, TRE, TBI, ALFA, DPFR, DPGR, DPAC, DPTOT, XITR, XD,
      2     TBITR
       COMMON /SUBSUB/ QNET
       COMMON /FLUID/ ROL, ROG, MUL, MUG
       COMMON /NNN/ N
C
 1     FORMAT(3F10.5, 12A4, I2)
 2     FORMAT (7F10.5)
 3     FORMAT (5I2, 2F10.5)
 4     FORMAT ('1', 20X,  'PRESSURE DROP CALCULATION   ***  ', 12A4///
      1      ' INLET TEMPERATURE = ', F7.2, '  DEG F',
      1           20X, 'ROOM TEMPERATURE =', F7.1  //
      2      ' CONDENSER PRESSURE = ', F7.3, '  IN HG'  //
      3      ' EACH TEST SECTION DIVIDED INTO ', I5, '  SEGMENTS'  //
      4      ' DATA PRINTED EVERY ', I5, '  POINTS'   //
      5      ' ERROR CRITERION = ', F10.8 //
      6      ' ERROR CRITERION IN BOBDRY = ', F10.8 ///)
 5     FORMAT ('0', 'POWER DISTRIBUTION' // ' TEST SECTION NUMBER',
      1      9X, '1',9X,'2',9X,'3',9X,'4',9X,'5',9X,'6',9X,'7'  //
      2      ' POWER (WATT)',10X, 7F10.1 //
      3      ' HEAT FLUX (BTU/HR FT2)', 7F10.1)
 6     FORMAT ('0', 'TOTAL POWER INPUT = ', F7.1, '  WATT')
 7     FORMAT ('0', 17X, 'PRESSURE DROP, QUALITY, VOID FRACTION AND BULK
      1TEMPERATURE ALONG THE TEST SECTION' ///    ' POINT', 1X, 'Z (IN)',
      2      5X,'X-EQ',5X,'X-TR',5X,'VOID FR.',3X,'T-EQ',4X,'T-TR',3X,
      3      'P (PSIA) P-RO*G*Z  FRICTION GRAVITY',3X,'ACCEL.',4X,'TOTAL'
      4 )
 9     FORMAT ('0',   'EXIT',3X,'0.0',4X,2F9.5,F10.5,1X,2F8.2,
      1      F9.3,3X,'0.0' )
 9     FORMAT ('0','EXIT LIQUID PHASE REYNOLDS NUMBER SMALLER THAN 2000,
      1  RE = ', F6.1)
10     FORMAT(79X,4F9.3 /3X,'8',4X,'3.125',2X,2F9.5,F10.5,1X,2F8.2,
      1      1X,2F8.3,2X,4F9.3 )
11     FORMAT(79X, 4F9.3 / I4, F9.3,2X,2F9.5,F10.5,1X,2F8.2,1X,2F8.3,
      1      2X, 4F9.3 )
13     FORMAT ('1','INLET LIQUID VELOCITY =', F7.3, ' FT/SEC', 5X,
      1      'MASS FLUX, G = ', F10.1, ' LBM/HR FT2',  5X,
      2      'MASS FLOW RATE, W = ', F7.1, ' LBM/HR' //)
14     FORMAT(//// ' BOILING BOUNDARY AT  Z =',        F8.3, '  INCHES FR
      1OM EXIT, OR AT' / 25X, F8.3, '  INCHES FROM INLET'/
      2      ' AT BOILING BOUNDARY : EQUIL.TEMP. =', F7.2, '  DEG. F,   '
      3     ,'TRUE TEMP. =', F7.2,'  DEG. F'/
      4      23X, 'PRESSURE =', F7.3, '  PSIA' /
      5      23X, 'INLET SUBCOOLING WITH RESPECT TO TEMP. AT BOILING ',
      6      'BOUNDARY,  TBB - TIN =', F7.2,  '  DEG. F' )
15     FORMAT(///' ***************** ERROR ****************************'/
      1      ' INLET TEMPERATURE ABOVE SATURATION POINT' /
      2      ' INLET TEMPERATURE SHOULD BE AT LEAST BELOW ', F6.1,
      3      'DEG F')
16     FORMAT(//'OFOR A PRESSURE OF',
      1        F8.2, '  PSIA THE BUBBLES DEPART AT TSAT-TBULK =',
      2      F6.1, '  DEG. F   '   , 'OR AT A QUALITY =', F10.5 ///)
17     FORMAT(//// ' BUBBLE DEPARTURE AT  Z =',        F8.3, '  INCHES FR
      1OM EXIT, OR AT' / 25X, F8.3, '  INCHES FROM INLET, IN TEST SECTION
      2 ', I3, '  (COUNTING FROM INLET)' /
      3      ' AT THE NET VAPOR GENERATION POINT THE EQUIL. TEMP. WAS',
      4      F7.2, '  DEG. F' /
      5      35X, 'THE TRUE BULK TEMPERATURE WAS', F7.2, '  DEG. F'  /
      6      35X, 'AND THE PRESSURE WAS', F7.2, '  PSIA' )
18     FORMAT('1', 20X, 'S U M M A R Y   O F   R E S U L T S' //)
19     FORMAT('0',' VIN (FT/SEC)', '  W  (LBM/HR)',    '  QWAV (WATT)',
      1      '   PEX (PSIA)',    '     XEX     ',    '    XEXTR    ',
      2      '    ALFAEX   ',    '    PI (PSIA)',   ' PI-RHO*G*Z  ',
      3      '  DPIEX (PSI)'   )
20     FORMAT( F13.3, 2F13.1, F13.3, 3F13.5, 3F13.3)
99     FORMAT ('0', 'EXIT QUALITY LARGER THAN 1.0 , XEX = ', F10.5)
C
C      PRESSURE DROP FUNCTIONS ****************************************
C
       RF(X) = (-1.6628E-11)*G*G*((1.0-X)**2/((1.0-ALFA)*ROL)+X**2/(ALFA
      1      *ROG))
       RELPF(X) = G*(1.0-X)*D/MUL
C
C      READING AND PRINTING INPUT INFORMATION *************************
C
       WRITE(8,18)                                                    SUMMARY
1111   READ(5,1) TIN, PCOND, TROOM, TITLE, IP
       IF(TIN .LE. 0.0) GO TO 999
       READ (5, 2) (QW(I), I = 1, 7)
       READ (5,3) N, NP, ISUBC, LOSS, KITER, ERROR, EBB
       WRITE(6,4) TITLE, TIN, TROOM, PCOND, N, NP, ERROR, EBB
       WRITE(8,4) TITLE, TIN, TROOM, PCOND, N, NP, ERROR, EBB         SUMMARY
       WRITE(8,19)                                                    SUMMARY
C
C      POWER INPUT ****************************************************
C
       QTOT = 0.0
       DO 100 J = 1, 7
       Q(J) = 3.412 * QW(J)
       HEATFL (J) = QW(J) / 0.04255
       QTOT = Q(J) + QTOT
100    CONTINUE
       QTOTW = QTOT / 3.412
       QWAV = QTOTW/7.0
       WRITE (6, 5) QW, HEATFL
       WRITE (6, 6) QTOTW
```

```
C
C     BASIC CALCULATIONS ************************************************
C
      D = 0.43 / 12.0
      ROLIN = ROLTF(TIN)
      HIN = HLTF(TIN)
      PEX = 0.4912 * PCOND
      HLEX = HLF(PEX)
      HFGEX = HFGF(PEX)
  111 READ(5,2) VIN, PINEST
      IF(VIN .LE. 0.0) GO TO 1111
      KCOMP = 0
      G = 3600.0 * VIN * ROLIN
      W = 0.0010095 * G
      WRITE (6,13) VIN, G, W
C
C     START CALCULATIONS WITH GROSS POWER INPUT **********************
C
      DO 119 I = 1,7
      QNET(I) = Q(I)
      QNETW(I) = QW(I)
  119 CONTINUE
      QTOTN = QTOT
      PIN = PINEST + PEX
      PNVG = PIN
      ITS = 1
C
  112 ZBB = 0.0
      ZBBIN = 111.625
      ZD = 0.0
      ZDIN = 111.625
      DHTOT = QTOTN / W
      HEX = HIN + DHTOT
      XEX = (HEX - HLEX) / HFGEX
      IF(XEX .GT. 1.0) GO TO 998
C
C     ESTIMATE POINT OF NET VAPOR GENEARATION, USING LEVY'S MODEL (ONLY
C     IF ISUBC SWITCH IS POSITIVE). NET VAPOR GENEARATION IS AT FIRST
C     ASSUMED TO TAKE PLACE IN FIRST TEST SECTION.
C
      XD = 1.0E-30
      XEXTR = XEX
      IF (ISUBC)121,121,122
  122 CALL SUBBOL (PNVG, ITS, DTD, XD)
      XIN = (HIN - HLF(PIN))/HFGF(PIN)
      IF(XD .LE. XIN) XD = XIN
      IF(XD .LE. XIN) ZD = 111.625
      IF((KCOMP+1 .GE. KITER) .OR. (IP .GT. 0))
     1WRITE (6,16) PNVG, DTD, XD
      IF(XD .GE.0.0) GO TO 121
      IF((XEX.GT.XD).AND.(XEX/XD.GT.-25.0))
     1                  XEXTR = XEX - XD*EXP(XEX/XD - 1.0)
      IF(XEXTR .GT. 1.0) GO TO 998
  121 IF((KCOMP+1 .GE. KITER) .OR. (IP .GT. 0))     WRITE(6,7)
C
C     UNHEATED EXIT LENGTH (3.125 INCHES) ****************************
C
      DL = 0.2604
      DH = 0.0
      XE = XEXTR
      HE = HEX
      PE = PEX
      QTS = 0.0
      IF (XEX .GT. 0.0) GO TO 200
C     CASE OF NEGATIVE EXIT QUALITY  . . . . . . . . . . . . . . . . .
      TBE = TF(HEX)
      TBETR = TBE
      ROL = ROLTF(TBE)
      MUL = MULTF(TBE)
      IF(XEXTR .GT. 0.0) GO TO 201
C
C     IN THE CASE OF SUBCOOLED BOILING AT THE EXIT MARNEL IS CALLED AND,
C     FOR SIMPLICITY, SOME PROPERTIES ARE EVALUATED AT THE SATURATION
C     TEMPERATURE INSTEAD  OF THE BULK TEMPERATURE
C
      BE = (-1.6628E-11)*G*G/ROL
      ALFA = 0.0
      ALFAEX = ALFA
C     EXIT PRINTOUT  . . . . . . . . . . . . . . . . . . . . . . . . .
      IF((KCOMP+1 .GE. KITER) .OR. (IP .GT. 0))
     1WRITE (6,8) XEX, XEXTR, ALFA, TBE, TBETR, PEX
      CALL SUBLIQ(ISUBC)
      GO TO 210
C     CASE OF POSITIVE EXIT QUALITY  . . . . . . . . . . . . . . . . .
  200 TBE = TSATF(PEX)
      ROL = ROLF(PEX)
      MUL = MULF(PEX)
  201 ROG = ROGF(PEX)
      MUG = MUGF(PEX)
      XTT = XTTF(XEXTR)
      ALFA = ALFAF(XTT)
      ALFAEX = ALFA
      BE = BF(XEXTR)
      TBETR = TF(HEX - XEXTR * HFGEX)
C     EXIT PRINTOUT  . . . . . . . . . . . . . . . . . . . . . . . . .
      IF((KCOMP+1 .GE. KITER) .OR. (IP .GT. 0))
     1WRITE (6,8) XEX, XEXTR, ALFA, TBE, TBETR, PEX
      RELPEX = RELPF(XEX)
      IF (RELPEX .LT. 2000.0) WRITE (6,9) RELPEX
      CALL MARNEL(ISUBC)
      IF(XI .GE. 0.0) GO TO 210
C
C     THE BOILING BOUNDARY IS DETERMINED BY BOBDRY ONLY IF NO SUBCOOLED
C     BOILING IS ASSUMED. WITH SUBCOOLED BOILING, THE TRANSITION OVER
C     THE BOILING BOUNDARY IS SMOOTH AND IT IS NO MORE NECESSARY TO
C     DETERMINE ITS POSITION ACCURATELY
C
      IF (ISUBC .LE. 0) CALL BOBDRY(ZBB,TBB,TBBTR,PBB,0,EBB)
  210 DPFREX = DPFR
      DPGREX = DPGR
      DPACEX = DPAC
      DPTOTX = DPTOT
      PNETEX = PI - .2604* ROLIN / 144.0 - PEX
C     POINT  8  PRINTOUT . . . . . . . . . . . . . . . . . . . . . . .
      IF((KCOMP+1 .GE. KITER) .OR. (IP .GT. 0))
     1WRITE (6,10) DPFR, DPGR, DPAC, DPTOT, XI, XITR, ALFA,TBI,TBITR,PI,
     2       PNETEX, DPFREX, DPGREX, DPACEX, DPTOTX
C
C     HEATED SECTIONS ************************************************
C
      DL = (15.5/12.0) / N
      L = 7 * N
C     VALUES AT POINT 8  . . . . . . . . . . . . . . . . . . . . . . .
      H(1) = HI
      X(1) = XI
      XTR(1) = XITR
      P(1) = PI
      T(1) = TBI
      TTR(1) = TBITR
      A(1) = ALFA
      SUMFR(1) = DPFREX
      SUMGR(1) = DPGREX
      SUMAC(1) = DPACEX
      SUMTOT(1) = DPTOTX
      PNET(1) = PNETEX
C
      DO 800 K = 1,L
      M = 7 - (K-1)/N
      QTS = QNET(M)
      DH = QNET(M)/ (W * N)
      HE = H(K)
      XE = XTR(K)
      PE = P(K)
      BE = BI
      TBE = TTR(K)
      IF (X(K) .GT. 0.0) GO TO 300
      CALL SUBLIQ(ISUBC)
      GO TO 310
  300 CALL MARNEL(ISUBC)
      IF(XI .GE. 0.0) GO TO 310
```

```
      IF (ISUBC .LE. 0) CALL BOBDRY(ZBB,TBB,TBBTR,PBB,K,EBB)
310   H(K+1) = HI
      X(K+1) = XI
      XTR(K+1) = XITR
      P(K+1) = PI
      T(K+1) = TBI
      TTR(K+1) = TBITR
      A(K+1) = ALFA
      FR(K) = DPFR
      GR(K) = DPGR
      AC(K) = DPAC
      TOT(K) = DPTOT
      SUMFR(K+1) = SUMFR(K) + FR(K)
      SUMGR(K+1) = SUMGR(K) + GR(K)
      SUMAC(K+1) = SUMAC(K) + AC(K)
      SUMTOT(K+1) = SUMTOT(K) + TOT(K)
      PNET(K+1) = P(K+1) - ROLIN * (.2604+ K * DL)/144.0 - PEX
C
C     DETERMINE THE POSITION OF THE BOILING BOUNDARY BY LINEAR INTERPOLA
C     TION (ONLY WITH SUBCOOLED BOILING, WHEN BOBDRY IS NOT USED)
C
      IF(ISUBC)330,330,331
 331  IF (X(K+1) * X(K)) 332,330,330
 332  PROP = X(K) / (X(K) - X(K+1))
      ZBB = 3.125 + 12.0 * DL * (PROP + K - 1.0)
      TBB = T(K) + (T(K+1)-T(K)) * PROP
      TBBTR = TTR(K) + (TTR(K+1) - TTR(K)) * PROP
      PBB = P(K) + (P(K+1)-P(K)) * PROP
C
C     DETERMINE THE POINT OF NET VAPOR GENERATION BY LINEAR INTERPOLATION
C
 330  IF (XTR(K+1)*XTR(K)) 320,800,800
 320  XDP = XD
      IF(XD .GE. 0.0) XDP = 0.0
      PROP = (XDP- X(K)) / (X(K+1) - X(K))
      ZD = 3.125 + 12.0 * DL * (PROP + K - 1.0)
      TD = T(K) + (T(K+1) - T(K)) * PROP
      TDTR  = TTR(K) + (TTR(K+1) - TTR(K)) * PROP
      PD = P(K) + (P(K+1) - P(K)) * PROP
      KNETVG = K
 800  CONTINUE
C
C     CHECK THE SUBCOOLED INLET CONDITION ******************************
C
      TSATIN = TSATF(P(L+1))
      IF(TSATIN .LT. TIN) GO TO 997
C
C     PRINTOUT AT SELECTED POINTS, SPACED NP STEPS **********************
C     CALCULATE FRICTION, GRAVITY, ACCELERATION AND TOTAL PRESSURE DROP
C     BETWEEN PRINTOUT POINTS
C
      IF((KCOMP+1 .GE. KITER) .OR. (IP .GT. 0))  GO TO 901
      GO TO 902
 901  LP = L / NP
      DO 900  I = 1,LP
      INI = NP * (I-1) + 1
      FIN = NP * I + 1
      SFR = SUMFR(FIN) - SUMFR(INI)
      SGR = SUMGR(FIN) - SUMGR(INI)
      SAC = SUMAC(FIN) - SUMAC(INI)
      STOT = SUMTOT(FIN) - SUMTOT(INI)
      IPOINT = 7 - (I - 1)/(N/NP)
      Z = 3.125 + ( NP * I) * DL * 12.0
      WRITE(6,11) SFR, SGR, SAC, STOT, IPOINT, Z, X(FIN), XTR(FIN),
     1      A(FIN), T(FIN), TTR(FIN), P(FIN), PNET(FIN), SUMFR(FIN),
     2      SUMGR(FIN), SUMAC(FIN), SUMTOT(FIN)
 900  CONTINUE
C
      WRITE(8,20) VIN, W,  QWAV, PEX, XEX, XEXTR, ALFAFX, P(FIN),        SUMMARY
     1      PNET(FIN), SUMTOT(FIN)
C
C     DETERMINE CONDITIONS AT BOILING BOUNDARY *************************
C
 902  IF(ZBB .EQ. 0.0) GO TO 808
      ZBBIN = 111.625 - ZBB
      TSUBBB = TBB - TIN
      IF((KCOMP+1 .GE. KITER) .OR. (IP .GT. 0))
     1WRITE (6,14) ZBB, ZBBIN, TBB, TBBTR, PBB, TSUBBB
C
C     TRANSFER TO SUBBOL POINT OF NET VAPOR GENERATION *****************
C
 808  IF (ZD .EQ. 0.0) GO TO 809
      ZDIN = 111.625 - ZD
      IF((KCOMP+1 .GE. KITER) .OR. (IP .GT. 0))
     1WRITE (6,17) ZD, ZDIN, KNETVG, TD, TDTR, PD
      PNVG = PD
      ITS = KNETVG
      PIN = P(L+1)
C
 809  KCOMP = KCOMP  + 1
      IF(KITER - KCOMP) 111,111,811
C
C     TRANSFER TO LOSSES BULK TEMPERATURES AND QUALITIES AT TEST SECTION
C     LIMITS (ARRAYS ORDERED FROM INLET TO EXIT)
C
 811  IF (LOSS) 112,112,812
 812  DO 810 I = 1,8
      TBST(I) = TTR(L+1-(I-1)*N)
 810  XST(I) = X(L+1-(I-1)*N)
      CALL LOSSES(TBST,XST,QNETW,G,TROOM,QLOSW)
      QTOTN = 0.0
      DO 820 I = 1,7
      QNETW (I) = QW(I) - QLOSW(I)
      QNET(I) = 3.412 * QNETW(I)
 820  QTOTN = QNET(I) + QTOTN
      GO TO 112
C
 997  WRITE (6,15) TSATIN
      GO TO 111
 998  WRITE(6,99) XEX
      GO TO 111
 999  STOP
      END


      SUBROUTINE SUBLIQ(ISUBC)
C     ------------------------
C
C     PRESSURE DROP CALCULATION FOR HEATED BUT SUBCOOLED LIQUID. THE
C     CALCULATIONS ARE EXECUTED WITH PROPERTIES EVALUATED AT THE AVERAGE
C     BULK SEGMENT TEMPERATURE, TBAV AND A CORRECTION IS MADE FOR THE
C     NON-ISOTHERMAL STATE
C
C     INPUT VARIABLES : D, DL, G, DH, QTS, HE, PE, BE, TBE, XD
C     OUTPUT VARIABLES : HI, XI, PI, BI, TBI, ALFA, DPFR, DPGR, DPAC,
C     DPTOT, XITR, TBITR
C
      REAL MULB, MULW, MULTF, MUL, MUG, MUGF, KLF
      COMMON D, DL, ERROR, G, DH, QTS, HE, HI, XE, XI, PE, PI,
     1      BE, BI, TBE, TBI, ALFA, DPFR, DPGR, DPAC, DPTOT, XITR, XD,
     2      TBITR
      COMMON /FLUID/ ROL, ROG, MUL, MUG
C
C     PRESSURE DROP FUNCTIONS ******************************************
C
      DPGRF(ALFA) = -DL*((ROG-ROL)*ALFA + ROL)/144.0
      BF(X) = (-1.662BE-11)*G*G*((1.0-X)**2/((1.0-ALFA)*ROL)+X**2/(ALFA
     1      *ROG))
C
```

```
C     CALCULATE TEMPERATURES . . . . . .
      HI = HE - DH
      TBI = TF(HI)
      TBAV = 0.5 * (TBF + TBI)
      MULB = MULTF(TBAV)
      DTFILM = 282.0*QTS*MULB**0.4/(G**0.8*KLF(TBAV)**0.6)
      TWAV = TBAV + DTFILM
C
C     CALCULATE PRESSURE DROP  . . . . . .
C
      MULW = MULTF(TWAV)
      ROL = ROLTF(TBAV)
      REL = G * D / MULB
      DPFR = (-3.3256E-11)*(DL/D)*FF(REL)*G*G*((MULW/MULB)**0.14)/ROL
      DPGR = - DL * ROL / 144.0
      IF((ISUBC .LE. 0) .OR. (XD .GE. 0.0)) GO TO 1
C
C     TO AVOID ITERATION THE PROPERTIES ARE EVALUATED AT APPROXIMATE
C     PRESSURES AND TEMPERATURES, PAVEST, PIEST
      DPEST = DPFR + DPGR
      PAVEST = PE - 0.5 * DPEST
      PIEST = PE - DPEST
      XI =(HI - HLF(PIEST))/ HFGF(PIEST)
      IF((XI .LE. XD) .OR. (XI/XD .LE. -25.0)) GO TO 1
      XITR = XI - XD * EXP(XI /XD -1.0)
      TBITR = TF(HI - XITR * HFGF(PIEST))
      PSATAV = PSATF(TBAV)
      ROG = ROGF(PSATAV)
      MUL = MULB
      MUG = MUGF(PSATAV)
      XTT = XTTF(0.5 * (XE + XITR))
      ALFA = ALFAF(XTT)
      DPGR = DPGRF(ALFA)
C
C     CALCULATE NOW FOR THE INLET  . . . . . .
      PSATI = PSATF(TBITR)
      ROL = ROLTF(TBITR)
      ROG = ROGF(PSATI)
      MUL = MULTF(TBITR)
      MUG = MUGF(PSATI)
      XTT = XTTF(XITR)
      ALFA = ALFAF(XTT)
      BI = BF(XITR)
      GO TO 4
 1    ROL = ROLTF(TBI)
      BI = (-1.6628E-11)*G*G/ROL
      XITR = -1.0E-20
      ALFA = 0.0
      ROG = 0.0
      TBITR = TBI
 4    DPAC = BE - BI
      DPTOT = DPFR + DPGR + DPAC
      PI = PE - DPTOT
      XI = (HI - HLF(PI))/HFGF(PI)
      RETURN
      END


      SUBROUTINE MARNEL(ISUBC)
C     ------------------------
C
C     CETTE SUBROUTINE EST DEDIEE A SUZANNE
C
C     SUBROUTINE MARNEL CALCULATES THE PRESSURE DROP ACCROSS A SHORT
C     SEGMENT DL ACCORDING TO THE LOCKHART-MARTINELLI MODEL FOR GIVEN EXIT
C     PRESSURE, PE(PSIA), AND EXIT QUALITY, XE. THE CALCULATION, EXCEPT
C     FOR THE ACCELERATION TERM IS DONE FOR THE AVERAGE PRESSURE, PAV
C     AND THE AVERAGE QUALITY, XAV.
C
C     THE CALCULATION IS ABANDONED IF NO CONVERGENCE IS OBTAINED WITHIN
C     30 ITERATIONS AND AVERAGE VALUES ARE USED FOR SUBSEQUENT CALCULATIONS
C
C     INPUT VARIABLES : D, DL, ERROR, G, DH, HE, XE, PE, BE, XD
C     OUTPUT VARIABLES : HI, XI, PI, BI, TBI, ALFA, DPFR, DPGR, DPAC,
C     DPTOT, XITR, TBITR
C
      REAL MULF, MUGF, MUL, MUG
      COMMON D, DL, ERROR, G, DH, QTS, HE, HI, XF, XI, PE, PI,
     1     BE, BI, TBF, TBI, ALFA, DPFR, DPGR, DPAC, DPTOT, XITR, XD,
     2     TBITR
      COMMON /FLUID/ ROL, ROG, MUL, MUG
      COMMON /NNN/ N
C
C     PRESSURE DROP FUNCTIONS ****************************************
C
      RELPF(X) = G*(1.0-X)*D/MUL
      DPLF(X) = (-3.3256E-11)*(DL/D)*FF(RELPF(X))*G*G*(1.0-X)**2/ROL
      DPGRF(ALFA) = -DL*((ROG-ROL)*ALFA + ROL)/144.0
      BF(X) = (-1.6628E-11)*G*G*((1.0-X)**2/((1.0-ALFA)*ROL)+X**2/(ALFA
     1       *ROG))
C
      NOITER = 0
C     CALCULATE FOR THE AVERAGE PRESSURE . . . . . .
      HI = HE - DH
      PIFIN = PE
 1    PI = PIFIN
      NOITER = NOITER + 1
      XI = (HI - HLF(PI)) / HFGF(PI)
      XITR = XI
      IF((ISUBC .GT. 0) .AND. (XI .GT. XD) .AND. (XD .LT. 0.0) .AND.
     1     (XI/XD .GT. -25.0)) XITR = XI - XD * EXP(XI/XD -1.0)
      XAV = 0.5 * (XF + XITR)
      PAV = 0.5 * (PE + PI)
      ROL = ROLF(PAV)
      ROG = ROGF(PAV)
      MUL = MULF(PAV)
      MUG = MUGF(PAV)
C
C     IN THIS SECOND MODIFIED VERSION OF MARNEL THE SEGMENT AROUND THE
C     BOILING BOUNDARY IS SUBDIVIDED (LINEARLY WITH X) INTO A BOILING
C     AND A NON BOILING REGION AND THE PRESSURE DROPS CALCULATED SEPARATELY
C     AND ADDED
C
      IF(XITR) 10,11,11
 10   XAVB = 0.5 * XF
      DLB = XF / (XE - XITR)
      XTT = XTTF(XAVB)
      DPFR = DLB * FI2LF(XTT) * DPLF(XAVB) + (1.0-DLB) * DPLF(0.0)
      ALFA = DLB * ALFAF(XTT)
      GO TO 12
 11   XTT = XTTF(XAV)
      DPFR = FI2LF(XTT) * DPLF(XAV)
      ALFA = ALFAF(XTT)
 12   DPGR = DPGRF(ALFA)
C     CALCULATE NOW FOR INLET PRESSURE. . . . . .
      ROL = ROLF(PI)
      ROG = ROGF(PI)
      IF (XITR .LE. 1.0E-30) GO TO 5
      MUL = MULF(PI)
      MUG = MUGF(PI)
      XTT = XTTF(XITR)
      ALFA = ALFAF(XTT)
      BI = BF(XITR)
      GO TO 6
 5    BI = (-1.6628E-11)*G*G/ROL
      ALFA = 0.0
      XITR = -1.0E-20
 6    DPAC = BE - BI
      DPTOT = DPFR + DPGR + DPAC
      PIFIN = PE - DPTOT
      IF(NOITER-30) 21,22,22
 22   WRITE(6,30) PI, PIFIN
 30   FORMAT('0******** MARNEL CONVERGENCE DIFFICULTY: AFTER 30 ITERATI'
     1     ,'ONS INLET PRESSURE VARIES BETWEEN', F8.3, '  AND', F8.3,
     2     '   PSIA'   /   20X, 'AVERAGE VALUE WAS USED FOR SUBSEQUENT'
     3     , ' CALCULATIONS **********'   /  )
      PI = 0.5 * (PI + PIFIN)
      GO TO 23
 21   ABSERR = ABS(PIFIN - PI)
      IF(((ABSERR/ABS(DPTOT)).GT.ERROR).AND.(ABSERR.GT.(ERROR/N)))
     1     GO TO 1
```

```
      PI = PIFIN
 23    IF(XI .GE. 0.0) TBI = TSATF(PI)
       IF(XI .LT. 0.0) TBI = TF(HI)
      TBITR = TBI
      IF(ISUBC .GT. 0.0) TBITR = TF(HI-XITR*HFGF(PI))
      RETURN
      END


      SUBROUTINE BCBDRY(ZBB,TBB,TBBTR,PBB,K,EBB)
C     ------------------------------------------
C
C     SUBROUTINE BOBDRY DETERMINES THE EXACT LOCATION OF THE BOILING
C     BOUNDARY AND THE PRESSURE DROP IN THE SEGMENT CONTAINING IT USING
C     BOTH MARNEL AND SUBLIQ.
C
C     INPUT VARIABLES : DL, DH, XE, XI, EBB, K PLUS INPUT VARIABLES OF
C     MARNEL AND SUBLIQ
C     OUTPUT VARIABLES : ZBB, TBB, TBBTR, PBB, DPFR, DPGR, DPAC, DPTOT,
C     PLUS OUTPUT VARIABLES OF SUBLIQ
C
      COMMON D, DL, ERROR, G, DH, QTS, HE, HI, XE, XI, PE, PI,
     1      BE, BI, TBE, TBI, ALFA, DPFR, DPGR, DPAC, DPTOT, XITR, XD,
     2      TBITR
C
C     CONSERVE STANDARD VALUES OF DL AND DH . . . . . .
      DLSTD = DL
      DHSTD = DH
C     DETERMINE BY ITERATION THE LOCATION OF THE BOILING BOUNDARY. . . .
      DDL = DLSTD
  1   DDL = 0.5 * DDL
      DL = DL + SIGN(DDL,XI)
      DH = (DL / DLSTD) * DHSTD
      CALL MARNEL(0)
C     CONVERGENCE IS ACHIEVED WHEN XI IS SLIGHTLY NEGATIVE (TO MAKE SURE
C     THE ACCELERATION TERM IS CORRECT) AND THE ERROR IN LENGTH SMALLER
C     THAN EBB
      IF((DDL .LT.EBB) .AND. (XI .LT. 0.0)) GO TO 2
      GO TO 1
  2   HE = HI
      PBB = PI
      TBB = TBI
      TBBTR = TBI
      PE = PI
      BE = BI
      TBE = TBI
      DPFR1 = DPFR
      DPGR1 = DPGR
      DPAC1 = DPAC
      DPTOT1 = DPTOT
      DL = DLSTD - DL
      DH = DHSTD - DH
C     CALCULATE LOCATION OF BOILING BOUNDARY . . . . . .
      ZBB = 3.125 + K*DLSTD*12.0 - DL*12.0
      CALL SUBLIQ(0)
C     SUM INCREMENTAL PRESSURE DROPS FROM MARNEL AND SUBLIQ  . . . . . .
      DPFR = DPFR + DPFR1
      DPGR = DPGR + DPGR1
      DPAC = DPAC + DPAC1
      DPTOT = DPTOT + DPTOT1
C     RESTORE STANDARD VALUES OF DL AND DH . . . . . .
      DL = DLSTD
      DH = DHSTD
      RETURN
      END
```

```
      SUBROUTINE LOSSES(T,X,QW,G,TROOM,QLOSW)
C     ---------------------------------------
C
C     SUBROUTINE LOSSES CALCULATES THE HEAT LOSSES FROM THE TEST SECTIONS
C     USING STANDARD CONVECTIVE AND RADIATIVE HEAT TRANSFER CORRELATIONS.
C     TEST SECTION O.D. = 0.527 IN, TEST SECTION EFFECTIVE LENGTH = 14 IN
C     THE ARRAYS ARE ORDERED FROM INLET TO EXIT
C
      REAL MULTF, KW, KLF
      DIMENSION T(8), X(8), QW(7), QLOSW(7), II(7)
C
C     CALCULATE AVERAGE BULK TEMPERATURES . . . . . .
C
      DO 9 J = 1,7
      II(J) = J
      TAV = 0.5 * (T(J) + T(J+1))
C
C     CALCULATE FILM TEMPERATURE DROP, DTF . . . . . .
C
      IF(X(J+1)) 1,1,2
C     WITHOUT BOILING:   NU = 0.023 * RE**0.8 * PR**0.4
  1   DTF = 1060.0 * QW(J) * MULTF(TAV) **0.4 /(G**0.8*KLF(TAV)**0.6)
      GO TO 3
C     WITH BOILING A HEAT TRANSFER COEFFICIENT OF 1000 BTU/HR-FT2-F
C     IS USED
  2   DTF = 0.026 * QW(J)
C
C     CALCULATE WALL TEMPERATURE DROP, DTW FOR AVERAGE WALL TEMPERATURE
C
  3   DTWFI =0.0
  4   DTW = DTWFI
C     HEAT CONDUCTIVITY OF THE PYREX GLASS WALL :
C           KW = 0.67 + 0.0005 * (T(F) - 100.0)  BTU/HR-FT-F
      KW = 0.67 + 0.0005 * (TAV + DTF + 0.5 * DTW - 100.0)
      DTWFI = 0.0952 * QW(J) / KW
      IF (ABS(DTW - DTWFI) - 0.1) 5,5,4
  5   DTW = DTWFI
C
C     CALCULATE OUTSIDE WALL TEMPERATURE . . . . . .
C
      TOUT = TAV + DTF + DTW
C
C     CALCULATE HEAT LOSSES IN WATTS USING THE FORMULA :
C           H = 0.29 * (DT/L)**0.25    FOR CONVECTIVE LOSSES
C     AND AN EMISSIVITY OF 0.95  FOR RADIATIVE LOSSES . . . . . .
C
  9   QLOSW(J) = 0.0132*(TOUT-TROOM)*(ABS(TOUT-TROOM))**0.25 + 0.00768*
     1       (((TOUT+459.6)*0.01)**4 - ((TROOM+459.6)*0.01)**4)
C
      WRITE (6,10) G, TROOM, II, T, X, QW, QLOSW
 10   FORMAT (/// 20X, 58HHEAT LOSSES CALCULATED FROM THE TEMP. DISTR.
     1BELOW         , 5X, 4H(G = , F10.1, 5X, 7HTROOM =, F6.1, 2H )  /
     1       22HOTEST SECTION NUMBER      , 7I10     /
     2       17HOTEMPERATURE (F)          , 8F10.1   /
     3       17HOEQUIL. QUALITY     , 8F10.3  /
     4       22HOPOWER (WATT)             , 7F10.1   /
     5       22HOPOWER LOST (WATT)      , 7F10.1     )
      RETURN
      END
```

```
      SUBROUTINE SUBBOL  (P,ITS,DTD,XD)                                  STAUB
C     ---------------------------------
C
C      THIS VERSION OF SUBROUTINE SUBBOL CALCULATES THE POINT OF NET
C      VAPOR GENERATION ACCORDING TO STAUB'S MODEL.
C
C     INPUT VARIABLES :     P, ITS, QNET(7), D, G
C     P : PRESSURE AT POINT OF NET VAPOR GENERATION (PSIA)
C     ITS : TEST SECTION NUMBER (SELECTS THE PROPER HEAT FLUX VALUE)
C     QNET(7) : NET POWER DISTRIBUTION (BTU/HR), INLET TO EXIT
C     (ITS AND QNET ARE ORDERED FROM INLET TO EXIT)
C     D : DIAMETER (FT)
C     G : MASS FLUX (LBM/HR-FT2)
C     OUTPUT VARIABLES : DTD, XD
C     DTD : TSAT - TBULK AT POINT OF NET VAPOR GENERATION (F)
C     XD : NEGATIVE EQUILIBRIUM QUALITY AT POINT OF NET VAPOR GENERATION
C
C     SUBBOL REQUIRES THE USE OF FUNCTIONS : ROLF(P), MULF(P), SIGMF(T),
C            TSATF(P) , ROGF(P) AND KLF(T)
C
      REAL MUL, MULF, KLF, KL
      COMMON D, DUM(2), G /SUBSUB/ QNET(7)
C
      FB = 0.030
      ROL = ROLF(P)
      ROG = ROGF(P)
      MUL = MULF(P)
      T = TSATF(P)
      SIGMA = SIGMF(T)
      KL = KLF(T)
      PR = 0.225 * MUL / KL
      REL = G * D / MUL
      A = (ROL-ROG)/(12.0*SIGMA*FB)
      B = G*G/(64.0*32.17*ROL*SIGMA*FB*3600.0*3600.0)
      ROUGH = 0.0
      DDSAVE = 0.0
C
C     THE FRICTION FACTOR IS OBTAINED FORM AN EMPIRICAL RELATION
    3 F = 0.0055*(1.0+(2.0E+04*ROUGH+1.0E+06/REL)**0.33333)
      BP = F * B
      DD = (-BP+SQRT(BP*BP+A))/A
      IF(ABS(DD-DDSAVE)/DD-0.001)2,2,1
    1 ROUGH = 0.5*DD/D
      DDSAVE = DD
      GO TO 3
    2 YD = 0.5*DD*G*SQRT(F/8.0)/MUL
      YCL = (D/DD)*YD
      Q = 86.1 * QNET(ITS) / (G * SQRT(F))
      IF(YD .LE. 5.0)      DTD = Q*(PR*(5.0-YD)+5.0*ALOG(1.0+5.0*PR)+
     1       2.5*((ALOG(YCL/30.0))/(1.0-30.0/YCL)-1.0))
      IF((YD .GT. 5.0) .AND. (YD .LE. 30.0))       DTD = Q*(5.0*ALOG((1.
     1     +5.0*PR)/(1.0+PR*(YD/5.0-1.0)))+2.5*(ALOG(YCL/30.)/(1.0-30.0
     2      /YCL)-1.0))
      IF(YD .GT. 30.0)         DTD = 2.5*Q*(ALOG(YCL/YD)/(1.0-YD/YCL)-1.0
     1      )*(1.0-YD/YCL)
      XD = -0.00364 * DTD
C
      WRITE(6,7) FB,REL,F,DD,YD,DTD,XD
    7 FORMAT('0POINT OF NET VAPOR GENERATION ACCORDING TO STAUB''S MODEL
     1'/  ' F(BETA) =', F6.3, 4X, 'RE =', F10.1, 4X, 'F =', F7.4,
     2      4X, 'DD =', F9.6, ' FT', 4X, 'YD =', F8.2, 7X, 'DTD =', F7.2
     3      , ' F' , 4X, 'XD =', F8.4)
      RETURN
      END
```

```
      SUBROUTINE SUBBOL  (P,ITS,DTD,XD)                                  LEVY
C     ---------------------------------
C
C     SUBROUTINE SUBBOL CALCULATES THE POINT OF NET VAPOR GENERATION
C     USING LEVY'S MODEL.
C
C     INPUT VARIABLES :     P, ITS, QNET(7), D, G
C     P : PRESSURE AT POINT OF NET VAPOR GENERATION (PSIA)
C     ITS : TEST SECTION NUMBER (SELECTS THE PROPER HEAT FLUX VALUE)
C     QNET(7) : NET POWER DISTRIBUTION (BTU/HR), INLET TO EXIT
C     (ITS AND QNET ARE ORDERED FROM INLET TO EXIT)
C     D : DIAMETER (FT)
C     G : MASS FLUX (LBM/HR-FT2)
C     OUTPUT VARIABLES : DTD, XD
C     DTD : TSAT - TBULK AT POINT OF NET VAPOR GENERATION (F)
C     XD : NEGATIVE EQUILIBRIUM QUALITY AT POINT OF NET VAPOR GENERATION
C
C     SUBBOL REQUIRES THE USE OF FUNCTIONS : ROLF(P), MULF(P), SIGMF(T),
C            TSATF(P) AND KLF(T)
C
      REAL MUL, MULF, KLF, KL
      COMMON D, DUM(2), G /SUBSUB/ QNET(7)
C
      ROL = ROLF(P)
      MUL = MULF(P)
      T = TSATF(P)
      SIGMA = SIGMF(T)
      KL = KLF(T)
      PR = 0.225 * MUL / KL
      REL = G * D / MUL
      F = 0.0055 * (1.0 + (2.0 + 1.0E 06/REL)**0.33333)
C     THE FRICTION FACTOR IS OBTAINED FORM AN EMPIRICAL RELATION FOR
C     A RELATIVE ROUGHNESS OF E-04
      Q = 86.1 * QNET(ITS) / (G * SQRT(F))
      YBPLUS = 308.0 * SQRT(SIGMA * D * ROL) / MUL
      DTFILM = 282.0*QNET(ITS)*MUL**0.4/(G**0.8*KL**0.6)                 D=0.43''
      IF (YBPLUS .LE. 5.0) DTD = DTFILM - Q * PR * YBPLUS
      IF ((YBPLUS .GT. 5.0) .AND. (YBPLUS .LE. 30.0)) DTD =
     1      DTFILM - 5.0 * Q * (PR + ALOG(1.0 + PR * (YBPLUS/5.0 -1.0)))
      IF (YBPLUS .GT. 30.0)  DTD =
     1   DTFILM - 5.0 * Q * (PR+ALOG(1.0+5.0*PR)+0.5*ALOG(YBPLUS/30.0))
      XD = -0.00364 * DTD
C
      WRITE(6,1) REL, F, YBPLUS, DTFILM, DTD, XD
    1 FORMAT('0POINT OF NET VAPOR GENERATION ACCORDING TO LEVY''S MODEL'
     1 /    ' RE =', F10.1, 5X, 'F =', F7.4, 5X, 'YBPLUS = ', F8.2, 5X,
     2      'DTFILM = ', F7.2, ' F', 15X, 'DTD =', F7.2, 10X, 'XD =',
     3      F8.4)
      RETURN
      END
```

Appendix B

The Physical Properties of Freon-113

The physical properties of Freon-113 as a function of saturation pressure or temperature were taken from references [41] and [42]. These functions were fitted in the least squares sense to polynomials (using IBM-360 Scientific Subroutine Package subprograms) with an excellent accuracy. The resulting FORTRAN FUNCTION subprograms are given in the following pages. To evaluate the accuracy of the fits the entire thermodynamic tables in the range 40 - 170°F, with an increment of 10°F, were reconstructed from these functions and compared to the original ones. The resulting r.m.s. errors were between 0.0002 and 0.2 percent.

```
C     F R E O N - 1 1 3    P R O P E R T I E S
C     ___________________________________
C     ARGUMENTS IN DEGREES F (T) OR PSIA (P).
C


      FUNCTION TSATF(P)
C     SATURATION TEMPERATURE (F)
      X       = 1.0 / (ALOG(P) - 13.47)
      TSATF = - .3609185E 03 - .4069273E 04*X + .1174451E 05*X*X
      RETURN
      END


      FUNCTION ROLF(P)
C     LIQUID DENSITY          (LBM/FT3)
      X = ALOG(P)
      ROLF     =     .1033078E  03 - .2657116E  01*X
     1         - .3389485E -01*X*X        - .8307981E -01*X*X*X
      RETURN
      END


      FUNCTION ROGF(P)
C     VAPOR DENSITY           (LBM/FT3)
      X = ALOG(P)
      ROGF     = EXP(      - .3267308E 01  + .9181820E 00 *X
     1         + .3519715E-02 *X*X )
      RETURN
      END


      REAL FUNCTION MULF(P)
C     LIQUID VISCOSITY        (LBM/HR FT)
      X = ALOG(P)
      MULF     = EXP(          .1064657 E 01 - .3255410 E 00*X
     1       + .6064336 E-02*X*X          - .1726090 E-02*X*X*X )
      RETURN
      END


      REAL FUNCTION MUGF(P)
C     VAPOR VISCOSITY         (LBM/HR FT)
      X = ALOG(P)
      MUGF     =              .1967795 E-01 + .7899068 E-02*X
     1       - .5630545 E-02*X*X          + .2141095 E-02*X*X*X
     2       - .3536185 E-03*X*X*X*X      + .1974262 E-04*X*X*X*X*X
      RETURN
      END


      FUNCTION HLF(P)
C     LIQUID ENTHALPY         (BTU/BLM)
      X       = 1.0 / (ALOG(P) - 13.54888)
      HLF                = - .3302970 E 02 + .2946777 E 00*X
     1       + .7782507 E 04*X*X
      RETURN
      END


      FUNCTION DHLF(P)
C     DHLF IS THE SLOPE OF THE LIQUID SATURATION ENTHALPY VS ABSOLUTE PR
C     ESSURE (OBTAINED FROM DIRECT DIFFERENTIATION OF HLF)
C     UNITS : BTU/LBM-PSIA
      X = 1.0 / (ALOG(P) - 13.54888)
      DHLF = -(0.2946777 + 15545.014 * X) * X *X / P
      RETURN
      END


      FUNCTION HEGF(P)
C     LATENT HEAT OF VAPORISATION  (BTU/LBM)
      HEGF                =    .7058670 E 02 - .9218673 E 00*P
     1       + .4283483 E-01*P*P          - .1186139 E-02*P*P*P
     2       + .1250690 E-04*P*P*P*P
      RETURN
      END


      FUNCTION PSATF(TF)
C     SATURATION PRESSURE     (PSIA)
      T = TF + 459.6
      PSATF = 10.0 **(33.0655 - 4330.98/T -9.2635*ALOG10(T) +
     1       0.0020539 * T)
      RETURN
      END


      FUNCTION ROLTF(T)
C     LIQUID DENSITY          (LBM/FT3)
      ROLTF    =    .1035453 E 03 - .7105255 E-01*T
     1       - .6448694 E-04*T*T
      RETURN
      END


      REAL FUNCTION MULTF(T)
C     LIQUID VISCOSITY        (LBM/HR FT)
      X = 1.0 /(T + 459.6)
      MULTF    = EXP( - .5483695 E 01  + .5585921 E 04*X
     1       - .1950534 E 07*X*X        + .3577018 E 09*X*X*X)
      RETURN
      END


      FUNCTION HLTF(T)
C     LIQUID ENTHALPY         (BTU/LBM)
      HLTF               =    .8119482 E 01 + .1961794 E 00*T
     1       + .1261047 E-03*T*T
      RETURN
      END


      REAL FUNCTION KLF(T)
C     LIQUID THERMAL CONDUCTIVITY  (BTU/HR FT F)
      KLF = 0.0475 - 6.7667E-05*T
      RETURN
      END


      FUNCTION SIGMF(T)
C     SURFACE TENSION         (LBF/FT)
      SIGMF = 1.27E-03 - 4.45E-06 * (T - 80.0)
      RETURN
      END


      FUNCTION TF(HL)
C     SATURATION TEMPERATURE (F)
      TF                  = - .4082034 E 02 + .5196681 E 01*HL
     1       - .1141203 E-01*HL*HL
      RETURN
      END
```

Appendix C

Auxiliary Functions for Pressure Drop Calculations

This appendix describes the evaluation and use in the computer programs of the friction factor, and the Lockhart-Martinelli two-phase friction multiplier $\Phi^2_{\ell tt}$ and void fraction α.

C.1 The Friction Factor, f

The Fanning friction factor, f for smooth pipes was obtained from Ref. [48] and approximated by a polynomial in the least squares sense. The resulting FORTRAN FUNCTION subprogram is listed at the end of this appendix, and the r.m.s. accuracy of the fit is given in Table C.1.

C.2 The Lockhart-Martinelli Two-Phase Friction Multiplier, $\Phi^2_{\ell tt}$

The values of $\Phi^2_{\ell tt}$ as a function of X_{tt} are tabulated in Ref. [49]. A least squares fit by a sixth order polynomial gave a satisfactory accuracy as shown in Table C.1. It was, however, necessary to extend the range of the function to very low and very high qualities:

By definition:

$$\left(\frac{dp}{dL}\right)_{2fr} = \Phi^2_{\ell tt}\left(\frac{dp}{dL}\right)_{\ell} = \Phi^2_{gtt}\left(\frac{dp}{dL}\right)_{g}$$

with

$$X_{tt} = \frac{\Phi_{gtt}}{\Phi_{\ell tt}}$$

At x approaching zero, X_{tt} tends towards infinity and $\Phi^2_{\ell tt}$ must obviously approach the unity. Therefore:

$$\lim_{\substack{X_{tt} \to \infty \\ x \to 0}} \Phi^2_{\ell tt} = 1$$

When x approaches the unity, X_{tt} tends towards zero and Φ^2_{gtt} now must have the limiting value of 1. As $\Phi_{\ell tt} = \Phi_{gtt}/X_{tt}$, it follows that

$$\lim_{\substack{X_{tt} \to \infty \\ x \to 1}} \Phi^2_{tt} = \frac{1}{X^2_{tt}}$$

These limiting cases are reflected in the FORTRAN listing of this subprogram.

C.3 The Lockhart-Martinelli Void Fraction Correlation

A numerical fit of the void fraction, α, as a function of X_{tt} was obtained in exactly the same way as for $\Phi^2_{\ell tt}$. The value of α was arbitrarily set equal to 0.97 for X_{tt} values smaller than 0.07 (corresponding to qualities a few percent below unity). At the other end of the range, for X_{tt} larger than 100 (x smaller than 0.007) an asymptotic expression, suggested by the homogeneous model, was used.

Table C.1

Range and Accuracy of the Numerical Fits of the Auxiliary Functions

Variable	FORTRAN FUNCTION name	Range of fit	Spacing of the input and test pts.	Relative rms error* (%)	Maximum observed relative error* (%)
Friction factor, f(Re)	FF(RE)	$3500 \leq Re \leq 300{,}000$	9 values per decade	0.20	0.48 @ Re=5000
Lockhart and Martinelli's friction multiplier $\phi^2_{\ell tt}(X_{tt})$	FI2LF(XTT)	$0.01 \leq X_{tt} \leq 100$	4 values per decade	0.80	1.53 @ X_{tt} = 0.02
Lockhart and Martinelli's void fraction, $\alpha(X_{tt})$	ALFAF(XTT)	$0.07 \leq X_{tt} \leq 100$	4 values per decade	2.01#	4.86 @ X_{tt} = 70

* using spacing of test points given in this table.

\# fit better than 1% for $X_{tt} < 10$ or $\alpha > 0.47$.

```
C     AUXILIARY FUNCTIONS FOR PRESSURE DROP CALCULATIONS
C     --------------------------------------------------
C
      FUNCTION FF(RE)
C     FANNING FRICTION FACTOR FOR SMOOTH PIPES
      X = ALOG(RE)
      FF     = EXP(      - .1805868 E 00 - .8502377 E 00*X
     1        + .4752425 E-01*X*X          - .1134451 E-02*X*X*X )
      RETURN
      END

      FUNCTION XTTF(X)
C     LOCKHART-MARTINELLI XTT PARAMETER
      REAL MUL, MUG
      COMMON /FLUID/ ROL, ROG, MUL, MUG
      IF(X .GT. 1.0E-30) XTTF =
     1          (((1.0 -X)/X)**0.9)*((ROG/ROL)**0.5)*(MUL/MUG)**0.1
      IF(X .LE. 1.0E-30)  XTTF = 1.0E 30
      RETURN
      END

      FUNCTION ALFAF(XTT)
C     LOCKHART-MARTINELLI VOID FRACTION CORRELATION
      IF(XTT .LT. 0.07) ALFAF = 0.97
      IF(XTT .GE. 100.0) ALFAF = 10.2661 / XTT
      X = ALOG(XTT)
      IF((XTT .GE. 0.07) .AND. (XTT .LT. 100.0)) ALFAF =
     1           EXP(      - .2543521 E 00 - .1478533 E 00*X
     2       - .3270721 E-01*X*X          + .1222962 E-02*X*X*X
     3       + .4128012 E-03*X*X*X*X      - .4598919 E-03*X*X*X*X*X )
      RETURN
      END

      FUNCTION FI2LF(XTT)
C     LOCKHART-MARTINELLI TWO-PHASE PRESSURE DROP MULTIPLIER
      IF(XTT  .LT. 0.01) FI2LF = 1.0 /(XTT*XTT)
      IF(XTT  .GE. 210.0) FI2LF = 1.0
      X = ALOG(XTT)
      IF((XTT .GE. 0.01) .AND. (XTT .LT. 210.0)) FI2LF =
     1          ( EXP(        .1445175 E 01 - .5039395 E 00*X
     2       + .5783838 E-01*X*X          - .1157590 E-02*X*X*X
     3       - .4390361 E-03*X*X*X*X      + .3007357 E-04*X**5 ))**2
      RETURN
      END
```

Appendix D

SUMMARY OF EXPERIMENTAL RUNS

RUN NO	GROSS POWER PER TEST LENGTH WATT	HEAT FLUX DISTRIBUTION	AVERAGE INLET TEMPERATURE F	CONDENSER PRESSURE PSI
4A	200	UNIFORM	96.0	29.95
5			95.2	30.24
6	400	UNIFORM	94.6	30.24
7	600	UNIFORM	94.6	30.24
8	200	COSINE	94.8	30.21
9	400	COSINE	94.8	30.21
10	200	UNIFORM	115.0	29.86
11	400	UNIFORM	114.8	29.86
12	600	UNIFORM	115.0	29.75
13	400	COSINE	114.5	29.76
14	200	COSINE	115.2	30.40
15	600	UNIFORM	115.2	30.40
16	400	UNIFORM	114.8	30.01
17	400	ROOFTOP	115.1	29.62
19	400	UNIFORM	95.3	29.98
22	400	UNIFORM	95.0	30.80

STEADY-STATE PRESSURE DROP DATA

V - INLET VELOCITY (FT/S)
TO - INLET TEMPERATURE (F)
P1 TO P8 - ABSOLUTE PRESSURE MINUS HYDROSTATIC HEAD AT NOMINAL RUN TEMPERATURE AT STATIONS 1 TO 8 (PSI)

RUN NUMBER 4A AT 200 W/TL, UNIFORM HEAT FLUX DISTRIBUTION

V	TO	P1	P2	P3	P4	P5	P6	P7	P8
7.43	96.5	3.12		2.20		1.35	0.81		
6.92	96.5	2.50		1.77		1.06	0.65		
6.32	96.3	2.12		1.51		0.92	0.56		
4.89	96.5	1.35		0.96		0.58	0.34		
3.82	96.4	0.87		0.60		0.36	0.20		
2.94	96.3	0.52		0.35		0.20	0.10		
2.08	96.0	0.23		0.13		0.07	0.02		
1.71	96.0	0.09		0.05		0.01	-0.02		
1.55	95.8	-0.14		-0.17		-0.22	-0.22		
1.43	95.8	-0.55		-0.55		-0.56	-0.54		
1.14	95.5	-1.12		-1.13		-1.07	-0.93		
0.87	95.5	-1.92		-1.98		-1.52	-1.02		

RUN NUMBER 5 AT 0 W/TL

V	TO	P1	P2	P3	P4	P5	P6	P7	P8
1.35	93.0	0.08		0.06	0.05	0.03	0.02	0.01	
1.81	93.0	0.17		0.14	0.11	0.08	0.06	0.03	
2.51	93.6	0.40		0.28	0.21	0.16	0.12	0.06	
2.98	94.0	0.52		0.39	0.30	0.22	0.16	0.08	
3.84	95.0	0.87		0.64	0.50	0.38	0.26	0.13	
4.85	95.5	1.28		0.94	0.77	0.56	0.38	0.18	
5.77	96.5	1.75		1.30	1.05	0.77	0.51	0.25	
6.55	96.5	2.19		1.64	1.20	0.97	0.65	0.31	
7.16	97.0	2.61		1.96	1.48	1.18	0.76	0.37	
7.76	97.2	3.10		2.33	1.73	1.40	0.92	0.44	
7.29	97.5	3.65		2.70	2.01	1.63	1.05	0.51	
1.08	97.2	0.07		0.05	0.01	0.02	0.02	0.01	

RUN NUMBER 6 AT 400 W/TL, UNIFORM HEAT FLUX DISTRIBUTION

V	TO	P1	P2	P3	P4	P5	P6	P7	P8
0.95	92.8	-1.21		-0.92	-0.71	-0.27	0.02	0.10	
1.56	92.8	0.10		0.07	0.03	0.15	0.30	0.30	
1.74	93.2	0.25		0.26	0.22	0.30	0.37	0.36	
1.95	94.0	0.43		0.54	0.45	0.47	0.50	0.41	
2.30	94.8	0.84		0.91	0.75	0.72	0.74	0.50	
2.93	95.1	1.36		1.28	1.04	1.12	1.07	1.02	
2.74	95.0	1.10		1.07	1.02	0.96	0.96	0.66	
3.70	95.7	1.27		1.09	0.96	0.87	0.78	0.64	
4.48	96.4	1.10		0.83	0.69	0.51	0.39	0.23	
4.15	96.0	0.99		0.77	0.65	0.51	0.38	0.28	
5.04	96.0	1.28		0.93	0.76	0.56	0.38	0.18	
5.73	95.6	1.61		1.19	0.98	0.71	0.49	0.23	
6.60	95.5	2.11		1.57	1.29	0.93	0.63	0.30	
7.23	95.7	2.48		1.83	1.50	1.12	0.74	0.35	
1.35	95.0	-0.27		-0.29	-0.17	0.08	0.28	0.29	
1.69	94.8	0.19		0.19	0.19	0.27	0.42	0.38	

RUN NUMBER 7 AT 600 W/TL, UNIFORM HEAT FLUX DISTRIBUTION

V	TO	P1	P2	P3	P4	P5	P6	P7	P8
1.26	93.5	1.49		1.56	1.61	1.88	1.72	1.70	
2.13	94.5	2.78		2.76	2.54	2.74	2.51	1.82	
2.65	96.5	3.41		3.40	2.88	3.15	3.15	2.23	
3.29	96.2	3.73		3.66	2.50	3.39	3.31	2.84	
4.42	93.7	3.08		3.01	2.58	2.53	2.24	2.60	
4.86	96.2	3.61		3.22	2.53	2.81	2.80	2.23	
4.50	96.7	4.04		3.78	2.50	3.38	3.36	2.86	
5.39	95.0	2.72		2.44	2.25	1.94	1.55	1.85	
5.65	97.5	2.54		2.12	1.76	1.64	1.34	1.32	
5.89	93.0	2.45		1.99	1.50	1.50	1.28	0.93	
6.41	96.0	2.80		2.29	1.76	1.71	1.44	1.08	
7.34	96.0	2.82		2.15	1.61	1.35	0.80	0.58	

RUN NUMBER 8 AT 200 W/TL, COSINE HEAT FLUX DISTRIBUTION

V	TO	P1	P2	P3	P4	P5	P6	P7	P8
1.25	94.3	-1.04		-1.10	-1.07	-1.01	-0.89	-0.50	
1.64	94.5	-0.44		-0.53	-0.51	-0.49	-0.49	-0.40	
1.85	94.5	-0.14		-0.24	-0.23	-0.23	-0.23	-0.20	
2.18	95.3	0.16		0.09	0.00	-0.01	-0.03	-0.04	
2.79	95.3	0.40		0.22	0.18	0.14	0.08	0.05	
3.70	94.5	0.76		0.49	0.40	0.30	0.20	0.11	
4.48	95.0	1.08		0.71	0.61	0.44	0.31	0.16	
5.37	95.4	1.54		1.06	0.88	0.64	0.44	0.22	
6.43	95.3	2.13		1.49	1.20	0.90	0.61	0.31	
7.36	94.5	3.28		2.39	1.74	1.43	0.94	0.47	
2.17	93.7	0.22		0.14	0.11	0.06	0.05	0.03	

RUN NUMBER 9 AT 400 W/TL, COSINE HEAT FLUX DISTRIBUTION

V	TO	P1	P2	P3	P4	P5	P6	P7	P8
1.05	94.5	-0.40		-0.43	-0.27	-0.01	0.12	0.09	
1.35	95.0	0.34		0.28	0.30	0.41	0.60	0.46	
1.69	94.8	0.47		0.38	0.37	0.48	0.48	0.32	
2.50	95.0	0.99		0.90	0.82	0.76	0.78	0.28	
3.58	95.2	1.48		1.26	1.03	1.05	0.95	0.89	
4.43	95.2	1.29		0.97	0.84	0.67	0.56	0.41	
3.15	95.0	1.18		1.00	0.94	0.85	0.79	0.73	
4.81	94.9	1.30		0.92	0.77	0.59	0.42	0.26	
5.61	95.2	1.59		1.15	0.94	0.69	0.47	0.24	
6.44	95.2	1.75		1.49	1.21	0.90	0.59	0.29	
3.62	94.5	0.64		0.49	0.38	0.31	0.23	0.15	

RUN NUMBER 10 AT 200 W/TL, UNIFORM HEAT FLUX DISTRIBUTION

V	T0	P1	P2	P3	P4	P5	P6	P7	P8
1.22	115.0	-1.35		-1.58	-1.36	-1.04	-0.58	-0.26	
1.42	115.2	-1.06		-1.23	-1.09	-0.75	-0.42	-0.10	
1.64	115.0	-0.67		-0.84	-0.79	-0.52	-0.32	-0.12	
1.90	114.5	-0.25		-0.42	-0.40	-0.36	-0.22	-0.03	
2.41	115.0	0.51		0.40	0.37	0.34	0.30	0.17	
3.12	115.0	0.75		1.38	1.19	1.24	1.13	1.08	
3.75	115.2	1.26		1.82	1.55	1.61	1.50	1.39	
4.29	114.8	0.96		1.49	1.23	1.20	0.98	0.96	
5.33	115.0	1.35		1.76	1.42	1.36	1.12	0.94	
6.22	115.2	1.02		2.16	1.70	1.63	1.36	1.03	

RUN NUMBER 11 AT 400 W/TL, UNIFORM HEAT FLUX DISTRIBUTION

V	T0	P1	P2	P3	P4	P5	P6	P7	P8
1.18	114.5	0.19		0.32		0.85	0.83	0.65	
1.45	114.8	0.83		0.87		1.26	1.16	0.85	
1.81	114.5	1.52		1.49		1.66	1.56	1.11	
2.35	114.8	2.63		2.60		2.54	1.78	1.68	
2.71	115.2	3.30		3.27		3.05	2.70	2.06	
3.70	114.8	4.48		4.38					
4.25	114.2	5.02		4.80					
5.01	115.0	5.20		4.94					
6.03	114.5	5.13		4.63					
6.28	114.8	5.18		4.58					
6.66	114.8	5.11		4.54					
7.38	114.0	5.04		4.34				2.52	
7.44	114.8	5.71		4.80				2.41	
10.30	114.5	6.16		5.17				2.58	
11.30	114.8	6.83		5.55			3.22	2.47	
12.70	115.0	7.06		5.92			2.80	2.38	
7.12	115.5	4.70		4.14		3.31	2.93	2.48	
5.15	115.0	4.63		4.45		3.48	3.70	2.90	
2.12	115.2	2.37		2.28		2.21	2.02	1.49	
1.80	115.0	1.59		1.58		1.70	1.58	1.16	

RUN NUMBER 12 AT 400 W/TL, UNIFORM HEAT FLUX DISTRIBUTION

V	T0	P1	P2	P3	P4	P5	P6	P7	P8
1.20	115.0	0.03	0.02	0.15	0.50	0.74	0.79	0.57	
1.47	115.0	0.64	0.65	0.72	0.99	1.21	1.15	0.82	
2.00	115.0	1.82	1.80	1.78	1.90	1.94	1.79	1.30	
2.73	115.0	3.24	3.16	3.15	3.13	3.06	2.64	2.08	
4.05	115.0	5.06	5.03	4.83	4.80	4.60	4.42	4.09	
4.90	114.8	5.29	5.24	4.98	4.88	4.65	4.39	4.15	
6.00	114.6	5.03	4.99	4.59	4.44	4.16	3.77	3.62	
4.96	115.0	5.30	5.25	4.99	4.88	4.68	4.35	4.06	
5.33	115.5	5.25	5.25	4.95	4.85	4.55	4.20	3.99	
7.24	114.2	5.29	5.27	4.66	4.39	3.97	3.51	3.23	
8.59	114.0	5.55	5.48	4.75	4.39	3.87	3.28	2.89	
10.50	113.5	6.43	6.25	5.31	4.68	4.05	3.26	2.89	
11.30	113.7	6.88	6.73	5.63	4.84	4.18	3.38	2.66	
12.15	114.0	7.40	7.26	5.98	5.10	4.35	3.43	2.69	

RUN NUMBER 13 AT 400 W/TL, COSINE HEAT FLUX DISTRIBUTION

V	T0	P1	P2	P3	P4	P5	P6	P7	P8
1.00	114.2	-0.17	-0.21	-0.06	0.26	0.68	0.65	0.25	
1.19	114.8	0.43	0.42	0.49	0.70	0.85	0.75	0.44	
1.50	114.9	1.15	1.17	1.19	1.34	1.40	1.17	0.70	
2.19	115.0	2.46	2.46	2.46	2.44	2.36	1.93	1.22	
2.90	114.6	3.50	3.43	3.45	3.37	3.34	2.67	1.84	
3.98	113.7	4.61	4.50	4.44	4.27	4.20	4.01	2.94	
4.17	115.0	4.97	5.01	4.80	4.70	4.54	4.33	3.67	
4.70	114.5	5.55	5.56	5.32	5.21	5.00	4.62	4.41	
7.25	114.5	5.51	5.38	4.84	4.51	4.16	3.67	3.44	
5.46	115.0	5.73	5.69	5.33	5.18	4.92	4.61	3.82	
6.35	115.0	5.29	5.24	4.85	4.61	4.25	3.84	3.77	
7.01	114.6	5.31	5.17	4.68	4.37	4.07	3.61	3.35	

RUN NUMBER 14 AT 200 W/TL, COSINE HEAT FLUX DISTRIBUTION

V	T0	P1	P2	P3	P4	P5	P6	P7	P8
0.82	115.2		-2.22	-2.18	-1.77	-1.25	-0.82	-0.43	
0.97	115.1		-1.93	-1.91	-1.61	-1.14	-0.72	-0.39	
1.32	115.1		-1.27	-1.28	-1.12	-0.81	-0.51	-0.26	
1.75	115.2		-0.67	-0.69	-0.66	-0.49	-0.28	-0.11	
2.30	115.7		0.10	0.04	0.07	0.10	0.04	0.07	
2.77	115.4		0.63	0.58	0.53	0.53	0.42	0.21	
3.90	115.3		2.04	1.91	1.83	1.71	1.59	1.47	
3.55	114.5		1.51	1.39	1.32	1.24	1.15	0.91	
4.99	115.4		2.57	2.35	2.29	2.00	1.75	1.75	
5.05	115.2		2.26	2.01	1.91	1.72	1.35	1.32	
5.50	115.4		2.33	1.99	1.79	1.65	1.41	1.16	
5.49	115.8		2.33	2.03	1.89	1.69	1.41	1.24	
6.11	115.9		2.65	2.29	2.07	1.78	1.48	1.29	
6.70	115.2		2.84	2.43	2.17	1.87	1.46	1.21	
7.26	114.7		3.08	2.61	2.24	1.89	1.46	1.12	
1.70	113.5		6.33	5.00		3.24	2.18	1.35	
1.10	115.2		3.00	2.53		1.84	1.44	1.12	
1.41	114.7		4.78	3.88		2.62	1.88	1.33	
1.62	114.9		5.56	4.44		2.96	2.11	1.36	
1.60	115.0		6.31	5.05		3.34	2.34	1.49	
3.35	115.4		1.54	1.48		1.28	1.21	1.16	
2.60	115.4		0.84	0.82		2.38	0.66	0.15	
2.22	115.7		0.29	0.25		0.19	-0.02	0.05	

RUN NUMBER 15 AT 600 W/TL, UNIFORM HEAT FLUX DISTRIBUTION

V	T0	P1	P2	P3	P4	P5	P6	P7	P8
0.67	115.0	-1.71	-1.37	-1.12	-0.74	-0.60	-0.63	-0.51	
0.73	115.0	-0.59	-0.40	-0.16	0.14	0.76	0.10	-0.14	
0.92	115.5	0.61	0.71	0.80	1.19	1.23	0.99	0.47	
1.28	115.5	2.29	2.30	2.20	2.68	2.53	2.24	1.39	
1.65	116.0	3.53	3.45	3.45	3.73	3.53	3.11	2.08	
2.34	116.0	5.15	5.07	4.96	5.15	4.85	4.35	3.11	
3.25	115.5	6.58	6.46	6.25	6.24	6.11	5.23	4.07	
4.05	115.0	7.59	7.47	7.17	6.95	6.68	5.95	4.47	
4.96	114.8	7.30	8.19	7.94	7.00	6.70	5.95	4.47	
5.45	115.5	7.34	8.17	7.94	7.00	6.70	5.95	4.47	
6.81	115.3	7.83	7.71	7.15	6.85	6.49	5.31	4.44	
8.60	114.7	7.53	7.23	6.41	6.13	5.52	4.95	4.41	
10.70	114.2	7.03	7.63	6.51	6.10	5.23	4.55	3.96	

RUN NUMBER 16 AT 400 W/TL, UNIFORM HEAT FLUX DISTRIBUTION

V	T0	P1	P2	P3	P4	P5	P6	P7	P8
0.40	115.5	-3.34	-2.90	-2.52	-2.01		-1.13	-0.71	
0.58	116.4	-1.14	-1.02	-0.72	-0.29		0.14	0.10	
2.62	115.0	2.80	2.81	2.86	2.75		2.41	1.81	
3.40	115.0	3.96	3.86	3.92	3.82		3.60	2.61	
6.16	115.0	5.03	4.91	4.64	4.32		3.81	3.46	
6.33	115.5	4.93	4.77	4.58	4.30		3.65	3.43	
9.00	114.8	5.30	5.26	4.64	4.16		2.62	2.48	
12.14	115.0	7.01	6.89	5.72	4.92		2.73	2.01	
13.06	115.1	7.94	7.77	6.44	5.44		2.93	2.01	
12.14	115.0	7.04	6.91	5.72	4.88		2.66	1.89	
9.16	115.0	4.86	4.65	4.03	3.48		2.22	1.68	
9.16	115.0	5.12	4.73	4.11	3.57		2.29	1.79	
9.11	115.0	5.11	4.90	4.16	3.68		2.23	1.87	
6.75	114.5	4.07	3.93	3.66	3.35		2.53	2.41	
4.02	114.4	4.62	4.56	4.53	4.43		4.05	4.02	
4.30	114.8	4.78	4.57	4.58	4.44		4.13	4.03	
3.31	114.6	3.85	3.75	3.82	3.72		3.46	2.33	
2.69	114.6	2.97	2.95	3.02	2.89		2.51	1.89	
2.23	114.2	2.15	2.14	2.13	2.13		1.82	1.36	
1.14	113.7	0.00	0.03	0.16	0.48		0.69	0.53	
0.47	112.2	-2.17	-1.99	-1.64	-1.15		-0.52	-0.29	

RUN NUMBER 17 AT 400 W/TL, ROOFTOP HEAT FLUX DISTRIBUTION

V	TO	P1	P2	P3	P4	P5	P6	P7	P8
0.80	115.5	-0.44	-0.38	-0.20	0.09	0.01	0.02	-0.03	
0.90	115.7	0.04	0.08	0.21	0.46	0.33	0.26	0.11	
1.20	116.0	0.89	0.88	0.93	1.12	0.86	0.73	0.41	
1.13	113.0	0.56	0.57	0.63	0.87	0.68	0.58	0.35	
1.52	114.1	1.30	1.23	1.31	1.45	1.19	0.99	0.62	
1.81	114.7	1.83	1.80	1.85	1.93	1.59	1.33	0.91	
2.22	115.0	2.60	2.55	2.64	2.64	2.13	1.79	1.18	
2.82	114.6	3.36	3.21	3.31	3.24	2.97	2.31	1.69	
3.42	115.2	4.00	3.86	3.91	3.83	3.65	3.06	2.25	
4.01	115.1	4.60	4.43	4.45	4.31	4.16	4.00	2.72	
4.57	115.0	5.30	5.19	5.14	4.94	4.73	4.57	4.21	
6.06	115.2	4.88	4.68	4.45	4.19	3.88	3.62	3.30	
5.92	115.5	4.99	4.89	4.64	4.43	4.06	3.75	3.58	
5.63	115.7	5.03	4.95	4.70	4.52	4.10	3.79	3.75	
7.12	114.5	4.92	4.77	4.36	4.01	3.49	3.00	2.78	
9.06	115.3	5.44	5.20	4.49	3.99	3.17	2.52	2.03	
10.80	115.5	6.67	6.38	5.37	4.62	3.50	2.62	1.93	
12.64	115.7	8.36	8.06	6.72	5.70	4.27	3.09	2.19	
9.48	115.3	5.25	5.04	4.27	3.74	2.76	2.08	1.66	
8.56	115.7	4.55	4.27	3.71	3.25	2.44	1.89	1.47	
7.12	115.0	3.43	3.19	2.82	2.43	1.94	1.58	1.24	
5.99	115.0	4.94	4.65	4.51	4.21	3.89	3.68	3.28	
3.64	115.5	4.32	4.17	4.23	4.13	3.94	3.64	2.37	
2.69	115.2	3.47	3.30	3.41	3.37	2.87	2.31	1.64	
2.45	115.0	3.05	2.97	3.07	3.01	2.44	2.06	1.41	
2.15	114.7	2.61	2.50	2.54	2.58	2.07	1.73	1.17	
1.60	114.5	1.61	1.57	1.63	1.76	1.40	1.19	0.76	

RUN NUMBER 22 AT 400 W/TL, UNIFORM HEAT FLUX DISTRIBUTION

V	TO	P1	P2	P3	P4	P5	P6	P7	P8
0.92	94.8	-0.96	-0.89	-0.84		-0.23	0.05		
1.50	94.6	-0.11	-0.16	-0.13		0.05	0.30		-0.04
1.80	95.2	0.20	0.16	0.19		0.22	0.45		-0.05
2.49	94.4	0.78	0.67	0.70		0.58	0.62		-0.14
3.02	94.6	1.19	1.06	1.08		0.84	0.83		-0.05
3.52	94.7	1.45	1.25	1.26		0.93	0.90		0.18
4.15	94.8	1.40	1.22	1.12		0.72	0.54		0.17
4.53	95.0	1.49	1.25	1.15		0.69	0.54		0.11
5.13	95.2	1.69	1.48	1.28		0.69	0.51		0.03
5.95	94.8	2.08	1.83	1.56		0.82	0.56		0.00
6.38	93.8	2.35	2.04	1.73		0.87	0.56		-0.02
6.38	93.8	2.35	2.04	1.73		0.89	0.56		-0.02
8.95	93.8	4.43	3.93	3.23		1.67	1.11		-0.03
10.18	93.8	5.62	5.07	4.15		2.15	1.41		-0.02
7.29	93.9	2.92	2.60	2.13		1.08	0.70		-0.03
6.02	93.0	2.04	1.77	1.47		0.73	0.48		-0.02
5.93	92.8	2.04	1.79	1.48		0.73	0.49		-0.02
5.50	95.0	1.78	1.56	1.29		0.63	0.43		-0.02
5.21	94.5	1.67	1.46	1.22		0.63	0.44		0.00
4.81	94.3	1.45	1.21	1.06		0.57	0.41		0.02
4.35	94.5	1.31	1.10	0.93		0.55	0.42		0.06
4.18	94.5	1.26	1.09	0.95		0.55	0.44		0.10
3.45	94.0	1.36	1.24	1.19		0.88	0.81		0.39
3.02	94.5	1.33	1.22	1.21		0.98	0.95		-0.05
2.39	94.0	0.80	0.73	0.73		0.60	0.63		-0.08

RUN NUMBER 19 AT 400 W/TL, UNIFORM HEAT FLUX DISTRIBUTION

V	TO	P1	P2	P3	P4	P5	P6	P7	P8
1.15	95.2	-0.41	-0.42	-0.41	-0.25	-0.01	0.23	0.24	
1.42	95.0	0.01	0.02	-0.02			0.38	0.33	
1.79	95.0	0.41	0.39	0.34	0.34	0.38	0.55	0.44	
2.36	94.8	1.02	0.96	0.88			0.83	0.62	
3.16	95.3	1.46	1.40	1.30			1.01	0.97	
3.93	95.2	1.44	1.32	1.14	1.01	0.81	0.65	0.55	
4.68	95.5	1.55	1.51	1.17			0.52	0.32	
5.72	95.5	2.03	1.87	1.48	1.19	0.80	0.51	0.24	
6.60	95.2	2.56	2.41	1.90	1.63	1.04	0.66	0.36	
6.46	95.3	2.55	2.41	1.90	1.54	1.03	0.66	0.30	
7.93	95.5	3.85	3.62	2.90	2.29	1.54	1.01	0.45	
10.59	95.1	6.57	6.27	4.96	4.04	2.68	1.76	0.81	
7.70	94.8	3.55	3.33	2.68	2.12	1.42	0.92	0.42	
6.42	95.3	2.61	2.35	1.86	2.13	1.01	0.65	0.30	
5.92	95.5	2.14	2.01	1.60	1.29	0.86	0.55	0.26	
5.88	95.8	2.15	2.03	1.60	1.29	0.85	0.55	0.26	
4.89	95.7	1.46	1.38	1.07	0.88	0.56	0.37	0.18	
4.60	95.5	1.33	1.27	0.97	0.78	0.52	0.34	0.18	
4.27	95.0	1.17	1.08	0.86	0.69	0.46	0.30	0.17	
3.72	94.7	0.96	0.87	0.71	0.58	0.43	0.30	0.20	
2.46	95.0	1.05	1.01	0.96	0.91	0.83	0.85	0.66	
1.73	95.4	0.37	0.37	0.35	0.33	0.33	0.50	0.46	
3.52	95.5	1.51	1.46	1.34	1.22	1.03	0.95	0.88	
3.53	95.5	1.49	1.45	1.31	1.19	1.02	0.93	0.86	
2.87	95.5	1.29	1.27	1.19	1.09	0.97	0.94	0.92	
2.54	95.7	1.07	1.06	1.01	0.95	0.84	0.86	0.71	
4.66	95.5	1.49	1.43	1.15	0.96	0.67	0.50	0.32	
4.21	95.6	1.38	1.35	1.12	0.96	0.74	0.59	0.45	
3.58	95.7	1.44	1.40	1.24	1.34	0.95	0.86	0.77	
6.83	95.4	2.72	2.59	2.04	1.66	0.52	0.73	0.35	
4.24	95.2	1.37	1.30	1.08		0.45	0.54	0.40	
2.84	95.4	1.36	1.35	1.24		0.75	1.02	0.98	
6.49	95.3	2.47	2.36	1.85		0.49	0.66	0.32	

Appendix E

STABILITY EXPERIMENTS

THRESHOLD AND TRANSITION POINT DATA

QW - AVERAGE GROSS POWER PER TEST LENGTH
TIN - INLET TEMPERATURE
W - AVERAGE MASS FLOW RATE
P0 - PRESSURE AT STATION 0
P1 - PRESSURE AT STATION 1
DP1EX - PRESSURE DROP FROM HEATED INLET TO EXIT (1 TO EX)
XEX - AVERAGE EXIT QUALITY
DTSUIN - INLET SUBCOOLING, TSAT(P1) - TO
DTSUBB - SUBCOOLING WITH RESPECT TO THE BOILING BOUNDARY, TSAT(PBB) - TO
Q/WHFG - TOTAL HEAT INPUT / MASS FLOW RATE TIMES LATENT HEAT
TAU - PERIOD OF THE OSCILLATION
WP/WA - PEAK TO AVERAGE FLOW RATIO
DPRAT - SINGLE-PHASE TO TOTAL PRESSURE DROP RATIO (0 TO BB / 0 TO EX)
ZRAT - SINGLE-PHASE TO TOTAL LENGTH RATIO (1 TO BB / 1 TO EX)
DHRAT - SINGLE PHASE TO TOTAL ENTHALPY RATIO
DELDH - DELAY OF ENTHALPY PERTURBATION AT BB, IN CYCLES (FROM DZDWTF)
ORDER - ORDER OF THE OSCILLATION

CODE FOR NUMBERING OF THE POINTS

80 SERIES - TRANSITIONS
90 SERIES - FIRST OCCURENCE OF OSCILLATIONS
100 SERIES - FREQUENCY OF NEXT UNSTABLE POINT WAS USED
200 SERIES - THRESHOLD OBTAINED BY INTERPOLATION
900 SERIES - TRANSITION TO FUNDAMENTAL MODE

UNIFORM HEAT FLUX DISTRIBUTION

RUN-PT	QW (W)	TIN (F)	W (LBM/HR)	PO (PSI)	P1 (PSI)	DP1EX (PSI)	XEX	DTSUIN (F)	DTSUBB (F)	Q/WHFG	TAU (S)	WP/WA	DPRAT	ZRAT	DHRAT	DELDH	ORDER	COMMENTS
TR2	91 100	121.5	279.0	18.54	17.51	2.96	0.152	5.6	3.7	0.136	4.20	1.10	0.403	0.094	0.097	0.657	0.256	BUBL HX
TR2A	91 100	123.0	419.0	19.61	18.53	3.98	0.112	7.3	4.2	0.090	4.65		0.409	0.161	0.165	0.686	0.262	BUBL HX
D12A	92 100	123.5	700.0	21.26	20.03	5.12	0.073	11.2	5.0	0.054	4.00	1.16	0.518	0.325	0.335	0.732	0.368	BUBL. HX
D12A	93 100	123.2	572.0	20.43	19.28	4.37	0.084	9.4	4.6	0.066	3.94	1.36	0.485	0.245	0.252	0.714	0.344	BUBL. HX
TR2B	92 100	119.2	168.5	18.34	17.34	2.64	0.231	7.4	5.6	0.225	3.60	1.27	0.420	0.087	0.090	0.734	0.456	OSC.DIES
TR2B	93 100	118.9	149.0	18.18	17.18	2.48	0.259	7.1	5.6	0.254	3.65	1.34	0.422	0.077	0.079	0.727	0.448	OSC.DIES
TR2B	94 100	118.3	131.0	18.05	17.06	2.36	0.292	7.4	5.9	0.289	3.80	1.33	0.425	0.071	0.073	0.725	0.455	
D4	294 100	116.6	285.8	19.23	18.20	3.46	0.129	12.6	8.3	0.132	2.95		0.529	0.219	0.225	0.936	0.827	INTERPOL
D5	932 100	103.6	85.0	17.82	16.82	1.98	0.394	21.3	18.3	0.446	8.65	6.05	0.627	0.142	0.146	0.947	0.622	W EST
D5	299 100	105.8	171.2	19.52	18.50	3.66	0.177	24.7	18.7	0.221	3.20		0.601	0.293	0.301	0.914	1.719	INTERPOL
D9	298 100	101.9	165.5	19.12	18.11	3.66	0.176	26.5	20.8	0.228	3.57		0.630	0.314	0.324	0.919	1.719	INTERPOL
D10A	90 100	91.5	47.9	17.62	16.61	1.95	0.699	32.7	29.9	0.790	7.25		0.612	0.130	0.134	0.621	1.220	TAU? PT?
D17	296 100	85.3	153.5	19.80	18.77	4.17	0.135	45.6	35.7	0.246	2.64		0.788	0.496	0.510	0.784	4.009	INTERPOL
D16	293 100	72.8	103.4	20.20	19.17	4.43	0.209	59.9	50.3	0.366	3.08		0.720	0.467	0.481	0.745	4.854	INTERPOL
D18A	196 100	62.5	102.0	20.02	18.98	4.61	0.184	69.1	58.4	0.371	3.90		0.772	0.532	0.547	0.935	4.464	
D18A	187 100	62.3	83.0	19.37	18.34	3.97	0.268	67.4	58.5	0.455	5.85		0.747	0.433	0.446	0.018	2.981	W ?
D20	98 100	44.3	113.0	21.80	20.74	5.84	0.081	92.4	77.4	0.335	3.80	1.30	0.858	0.773	0.795	0.755	6.095	W ?
D20	189 100	44.2	96.6	21.46	20.41	5.51	0.138	91.6	78.6	0.392	3.58	1.40	0.802	0.671	0.690	0.794	0.000	END OSC.
D20	90 100	44.8	88.8	21.12	20.07	5.17	0.174	90.1	78.1	0.427	4.20	1.20	0.787	0.613	0.631	0.719	5.565	
D20	82 100	45.1	75.9	20.54	19.49	4.59	0.248	88.1	77.8	0.499	3.30	1.40	0.767	0.522	0.537	0.150	7.055	TAU=5.80
D20	83 100	45.2	63.5	20.10	19.05	4.15	0.345	86.7	77.9	0.597	5.80	1.20	0.730	0.438	0.450	0.603	4.022	TAU=2.95

RUN-PT	QW (W)	TIN (F)	W (LBM/HR)	PO (PSI)	P1 (PSI)	DP1EX (PSI)	XEX	DTSUIN (F)	DTSUBB (F)	Q/WHFG	TAU (S)	WP/WA	DPRAT	ZRAT	DHRAT	DELDH	ORDER	COMMENTS
D12	98 200	125.1	516.0	21.10	19.98	5.17	0.172	9.5	6.6	0.147			0.333	0.157	0.162			BHX,THR?
TR3	92 200	120.0	262.0	19.15	18.13	3.43	0.298	9.1	7.3	0.289	3.00	1.15	0.351	0.089	0.091	0.697	0.359	
D4	917 200	118.0	281.0	19.39	18.36	3.62	0.271	11.7	9.4	0.269	3.52	1.21	0.382	0.122	0.125	0.719	0.392	
D6	199 200	115.6	265.0	19.38	18.35	3.51	0.277	14.1	11.4	0.286	3.96		0.415	0.140	0.144	0.752	0.424	
D6	196 200	114.0	211.0	19.06	18.05	3.21	0.344	14.8	12.5	0.359	3.81		0.414	0.121	0.124	0.754	0.480	
D5	294 200	107.0	223.5	19.95	18.90	4.06	0.799	24.7	20.4	0.339	5.00		0.456	0.210	0.216	0.831	0.603	INTERPOL
D9	94 200	103.2	202.5	18.86	17.84	3.39	0.326	24.9	21.1	0.373	5.40	1.68	0.503	0.195	0.201	0.823	0.576	TAU ?
D10A	93 200	94.0	194.5	19.09	18.06	3.40	0.307	34.9	29.6	0.389	2.74		0.597	0.262	0.269	0.785	1.598	TAU=6.60
D10A	284 200	93.8	142.8	18.57	17.55	2.89	0.446	33.4	29.6	0.530	6.60		0.563	0.192	0.198	0.865	0.662	INTERPOL
TR5	92 200	93.3	262.0	19.99	18.94	4.24	0.203	38.2	31.0	0.289	6.40	1.06	0.631	0.369	0.380	0.867	0.717	
D17	197 200	85.4	214.0	19.56	18.52	3.92	0.242	44.8	37.6	0.354	7.50		0.665	0.364	0.375	0.879	0.743	TAU ?
D17	182 200	84.9	87.0	17.85	16.83	2.23	0.756	40.0	37.0	0.870	7.25		0.590	0.145	0.150	0.910	0.755	
D18A	191 200	62.6	440.0	21.35	20.21	5.84	-0.014	72.6	49.8	0.172	6.15		1.051	1.000	1.000	0.707	1.233	W ESTEST
D18A	182 200	63.0	300.0	21.07	19.98	5.61	0.067	71.6	56.4	0.252	6.15		0.872	0.755	0.776	0.744	0.000	W?ENDOSC
D18A	93 200	63.4	197.0	19.82	18.76	4.39	0.200	67.6	57.4	0.384	2.84		0.774	0.504	0.519	0.427	3.006	
D18A	185 200	64.0	143.0	19.18	18.14	3.77	0.347	65.1	57.6	0.529	4.68		0.694	0.368	0.379	0.888	1.833	
D18A	287 200	64.1	122.5	17.36	16.32	3.43	0.453	64.0	57.4	0.617	9.05		0.672	0.314	0.323	0.929	0.945	INTERPOL
D18A	280 200	64.2	88.0	16.54	15.50	2.61	0.694	61.2	56.5	0.859	8.49		0.664	0.222	0.228	0.801	0.990	INTERPOL
D16	97 200	72.4	140.5	19.70	18.66	3.92	0.381	58.3	51.8	0.539	0.00		0.620	0.327	0.337		0.000	
D16	289 200	72.4	126.4	19.20	18.17	3.43	0.440	56.8	51.0	0.599	8.70		0.635	0.290	0.298	0.934	0.872	INTERPOL
D18	290 200	61.4	198.8	20.18	19.12	4.53	0.187	71.0	60.0	0.380	2.32		0.786	0.532	0.548	0.836	3.856	INTERPOL
D18	186 200	62.3	103.5	18.61	17.57	2.98	0.541	65.0	59.4	0.731	4.70		0.684	0.274	0.282	0.913	1.881	
D18	184 200	61.8	119.0	19.36	18.32	3.73	0.444	67.9	61.3	0.636			0.644	0.326	0.335			
D20	90 200	42.5	204.0	21.33	20.25	5.35	0.111	92.8	78.8	0.371	4.00	1.20	0.864	0.709	0.730	0.894	2.948	THR ?
D20	184 200	44.0	116.0	19.61	18.55	3.65	0.398	86.3	78.2	0.653	3.80	1.50	0.760	0.401	0.412	0.930	3.078	TAU CAHN
D20	186 200	45.1	81.3	18.78	17.73	2.83	0.680	82.7	77.0	0.932	6.00	2.50	0.718	0.277	0.285	0.936	1.919	TAU CHAN

UNIFORM HEAT FLUX DISTRIBUTION

RUN-PT	QW (W)	TIN (F)	W (LBM/HR)	PO (PSI)	P1 (PSI)	DP1EX (PSI)	XEX	DTSUIN (F)	DTSUBB (F)	Q/WHFG	TAU (S)	WP/WA	DPRAT	ZRAT	DHRAT	DELDH	ORDER	COMMENTS
D12	192	300	125.3	410.0	21.46	20.39	5.58	0.304	10.5	8.5	0.277	2.28	1.11	0.241	0.108	0.111	0.705	0.366	
TR1	91	300	121.0	336.0	20.68	19.63	5.08	0.352	12.6	10.6	0.338	2.62	1.13	0.281	0.110	0.113	0.718	0.395	
D4	299	300	120.3	387.2	20.88	19.81	5.07	0.302	13.8	11.4	0.293	3.25		0.310	0.136	0.140	0.709	0.342	INTERPOL
D5	296	300	107.4	331.4	20.54	19.48	4.64	0.305	26.0	21.6	0.343	4.75		0.422	0.219	0.224	0.760	0.447	INTERPOL
D9	197	300	103.2	312.0	19.73	18.68	4.23	0.316	27.5	23.3	0.364	3.75		0.458	0.221	0.228	0.829	0.610	
D10A	193	300	93.9	320.0	20.38	19.31	4.65	0.272	38.7	32.7	0.355	5.92		0.531	0.317	0.326	0.812	0.544	
D10	192	300	92.7	281.0	19.97	18.92	4.41	0.319	38.8	33.2	0.404	5.88		0.513	0.283	0.291	0.818	0.558	
TR6	92	300	92.0	317.0	20.37	19.30	4.60	0.268	40.6	34.3	0.358	6.35	1.08	0.549	0.329	0.339	0.806	0.533	
D17	199	300	85.3	295.0	20.19	19.13	4.53	0.273	46.8	39.9	0.385	6.50		0.585	0.355	0.366	0.832	0.607	TAU ?
TR7	92	300	74.5	261.0	20.17	19.11	4.41	0.285	57.5	49.9	0.435	8.20	1.07	0.639	0.391	0.402	0.828	0.603	
D16	193	300	73.0	225.0	19.88	18.83	4.09	0.349	58.2	51.4	0.503	7.75	1.26	0.624	0.347	0.357	0.853	0.658	
D13	90	300	65.7	204.5	19.96	18.90	4.09	0.374	65.7	58.7	0.555	8.76	1.75	0.640	0.358	0.369	0.854	0.666	
D18	193	300	57.9	200.0	19.61	18.55	3.96	0.363	72.4	64.7	0.567	9.30		0.691	0.384	0.396	0.858	0.693	W,P EST
TR8	92	300	58.1	251.0	20.35	19.28	4.58	0.247	74.4	64.9	0.452	1.74	1.10	0.727	0.483	0.497	0.664	3.708	
TR8	83	300	58.1	203.0	19.94	18.88	4.18	0.354	73.2	65.4	0.559	9.00	1.10	0.674	0.395	0.406	0.865	0.723	TAU CHAN
D20	197	300	42.4	264.0	20.65	19.56	4.66	0.170	91.0	78.7	0.430	2.88	1.27	0.862	0.611	0.628	0.852	2.723	
D20	188	300	42.6	216.0	20.34	19.26	4.36	0.266	89.4	79.8	0.526	2.06	1.25	0.787	0.507	0.522	0.770	3.863	TAU CHAN
D20	180	300	42.9	160.0	20.02	18.96	4.06	0.451	88.7	80.2	0.557	2.84	1.41	0.758	0.481	0.495	0.605	3.865	TAU CHAN
D20	198	300	42.9	221.0	20.57	19.49	4.59	0.255	90.3	80.0	0.514	2.88	1.30	0.769	0.520	0.535	0.818	2.771	
D20	180	300	42.7	204.0	20.33	19.25	4.35	0.298	89.8	81.1	0.710	2.07	1.72	0.677	0.382	0.393	0.878	2.850	TAU CHAN
D20	182	300	43.0	170.0	19.94	18.87	3.97	0.410	88.3	80.2	0.668	3.00	1.29	0.714	0.402	0.413	0.786	2.670	TAU CHAN
D20	185	300	43.9	121.0	19.30	18.24	3.34	0.694	85.5	79.7	0.939	2.57	5.40	0.647	0.284	0.293	0.949	3.097	TAU CHAN
D20	187	300	44.2	106.0	18.72	17.66	2.76	0.818	83.4	78.3	1.072	21.80	4.05	0.680	0.245	0.252	0.746	0.359	6 PEAKS
D19	191	300	40.0	234.0	20.25	19.17	4.81	0.224	92.2	80.9	0.484	2.90		0.790	0.556	0.572	0.851	2.782	
D19	182	300	40.0	207.0	19.85	18.77	4.41	0.287	91.0	81.0	0.548	2.01		0.763	0.492	0.506	0.764	4.018	
D19	183	300	40.2	176.5	19.47	18.40	4.04	0.382	89.7	81.0	0.642	2.90		0.728	0.420	0.432	0.887	2.787	
D19	184	300	40.8	145.0	19.28	18.22	3.86	0.524	88.5	81.4	0.782	4.46		0.660	0.347	0.357	0.924	1.821	
D19	185	300	41.3	136.5	18.94	17.88	3.52	0.574	87.0	80.3	0.831	2.57		0.674	0.322	0.331	0.645	3.116	
D19	986	300	42.0	118.5	18.32	17.26	2.90	0.703	84.3	78.5	0.957	8.50		0.702	0.273	0.281	0.887	0.920	

RUN-PT	QW (W)	TIN (F)	W (LBM/HR)	PO (PSI)	P1 (PSI)	DP1EX (PSI)	XEX	DTSUIN (F)	DTSUBB (F)	Q/WHFG	TAU (S)	WP/WA	DPRAT	ZRAT	DHRAT	DELDH	ORDER	COMMENTS
D12A	96	400	125.1	379.0	22.37	21.31	6.40	0.424	13.2	11.5	0.400	2.34	1.45	0.225	0.101	0.104	0.702	0.361	SMALLOSC
D9	195	400	103.8	344.0	21.57	20.41	5.96	0.233	32.0	26.0	0.278	4.77		0.448	0.324	0.334	0.748	0.403	
D10	195	400	92.8	360.0	21.06	19.98	5.47	0.336	41.7	36.3	0.420	5.82		0.447	0.297	0.306	0.779	0.462	
D17	90	400	85.5	350.0	21.03	19.95	5.35	0.321	49.0	42.7	0.432	6.90	1.30	0.496	0.339	0.348	0.776	0.460	TAU ?
D16	98	400	73.0	300.0	20.81	19.73	4.99	0.349	60.8	54.0	0.505	6.30		0.553	0.364	0.375	0.840	0.638	
D13	190	400	62.5	285.0	20.88	19.80	4.99	0.339	71.6	63.8	0.531	7.79		0.598	0.407	0.418	0.827	0.611	
D13	92	400	63.8	272.0	20.63	19.55	4.74	0.369	69.5	62.3	0.557	7.05		0.594	0.379	0.390	0.846	0.660	
D20	199	400	42.1	305.0	21.04	19.93	5.03	0.235	92.3	81.5	0.497	1.62	1.22	0.748	0.549	0.565	0.836	3.769	
D20	181	400	43.0	192.0	20.52	19.45	4.55	0.531	90.1	83.2	0.789	8.70	1.40	0.586	0.353	0.363	0.870	0.717	TAU CHAN
D19	97	400	40.0	235.0	20.10	19.01	4.65	0.383	91.7	83.1	0.643	9.25		0.664	0.430	0.443	0.865	0.673	= 7

RUN-PT	QW (W)	TIN (F)	W (LBM/HR)	PO (PSI)	P1 (PSI)	DP1EX (PSI)	XEX	DTSUIN (F)	DTSUBB (F)	Q/WHFG	TAU (S)	WP/WA	DPRAT	ZRAT	DHRAT	DELDH	ORDER	COMMENTS
D16	192	500	73.5	397.0	21.71	20.60	5.86	0.323	62.8	55.5	0.477	5.60		0.517	0.397	0.409	0.817	0.591	
D13	291	500	55.2	423.4	21.93	20.75	5.94	0.230	82.5	71.4	0.447	8.40		0.644	0.539	0.554	0.794	0.509	INTERPOL
D20	192	500	42.0	400.0	21.63	20.49	5.59	0.212	94.0	82.7	0.473	11.70	1.10	0.723	0.584	0.601	0.776	0.424	STEADY?
D20	92	500	42.0	295.0	21.48	20.38	5.48	0.380	93.7	85.3	0.642	11.70	1.24	0.595	0.445	0.458	0.780	0.438	
D20	194	500	41.7	396.0	21.77	20.63	5.73	0.216	94.7	83.5	0.478	11.20	1.08	0.708	0.584	0.601	0.784	0.447	
D19	192	500	39.0	420.0	21.25	20.10	5.74	0.186	95.9	83.6	0.450	6.15		0.741	0.619	0.637	0.885	0.814	W EST

COSINE HEAT FLUX DISTRIBUTION

RUN-PT	QW (W)	TIN (F)	W (LBM/HR)	PO (PSI)	P1 (PSI)	DP1EX (PSI)	XEX	DTSUIN (F)	DTSUBB (F)	Q/WHFG	TAU (S)	WP/WA	DPRAT	ZRAT	DHRAT	DELDH	ORDER	COMMENTS
D8	192	100	101.7	116.5	19.02	18.01	3.27	0.268	27.0	21.0	0.325	2.95		0.664	0.298	0.230	0.715	2.802	
D22	190	100	83.4	159.0	20.35	19.32	4.58	0.118	49.2	38.7	0.238	3.00		0.775	0.533	0.572	0.806	3.670	
D22	181	100	83.7	110.5	19.35	18.33	3.59	0.223	45.9	37.7	0.343	4.40		0.775	0.411	0.387	0.887	2.773	TAU CHAN
D23	198	100	70.8	227.0	21.87	20.81	6.08	0.004	66.1	47.3	0.167	8.00	1.01	0.980	0.948	0.989	0.911	1.731	
D23	180	100	70.8	196.0	21.37	20.32	5.59	0.030	64.7	49.3	0.193	5.39	1.30	0.898	0.785	0.890	0.802	2.464	
D23	82	100	70.8	192.0	21.18	20.13	5.40	0.034	64.2	49.1	0.197	5.50	1.10	0.903	0.763	0.868	0.816	2.396	OSC.DIES
D23	193	100	71.0	137.0	20.57	19.53	4.80	0.114	62.3	50.8	0.276	2.76	1.36	0.800	0.581	0.642	0.616	5.095	
D23	85	100	71.1	128.0	20.36	19.33	4.60	0.134	61.6	50.6	0.296	4.15	1.31	0.794	0.550	0.598	0.782	3.435	TAU CHAN
D23	96	100	71.3	121.5	20.19	19.16	4.43	0.150	60.9	50.4	0.312	3.75	1.33	0.793	0.528	0.565	0.835	3.844	
D23	189	100	72.5	70.4	19.32	18.29	3.56	0.380	57.0	49.6	0.538	5.60	1.35	0.720	0.365	0.373	0.826	3.066	TAU=2.90
D23	83	100	74.1	44.1	18.47	17.45	2.72	0.706	52.8	47.2	0.858	3.38	4.10	0.720	0.269	0.192	0.831	5.965	EMT.BYP.
D21	90	100	44.1	105.0	20.91	19.86	5.30	0.110	90.2	77.2	0.360	4.30	1.52	0.812	0.649	0.736	0.761	4.872	
D21	82	100	44.9	91.0	20.33	19.28	4.72	0.168	87.7	76.0	0.416	5.60	1.25	0.809	0.572	0.629	0.962	3.799	STEP DP
D21	85	100	45.1	71.7	19.72	18.67	4.11	0.281	85.6	75.7	0.528	3.50	1.95	0.794	0.482	0.493	0.768	6.495	STEP DP
D21	87	100	46.5	58.0	19.20	18.15	3.59	0.410	82.6	74.0	0.652	7.70	1.30	0.790	0.414	0.390	0.986	3.132	STEP DP

RUN-PT	QW (W)	TIN (F)	W (LBM/HR)	PO (PSI)	P1 (PSI)	DP1EX (PSI)	XEX	DTSUIN (F)	DTSUBB (F)	Q/WHFG	TAU (S)	WP/WA	DPRAT	ZRAT	DHRAT	DELDH	ORDER	COMMENTS
D7	198	200	112.9	275.0	19.82	18.79	3.96	0.257	18.2	13.4	0.275	3.38		0.514	0.250	0.174	0.748	0.861	
D8	196	200	103.3	240.0	19.82	18.79	4.05	0.264	27.7	21.8	0.315	4.22		0.578	0.310	0.246	0.798	0.986	
D11	191	200	93.5	276.0	19.99	18.94	4.28	0.190	38.0	29.9	0.274	4.80		0.675	0.410	0.385	0.777	1.007	
D11	190	200	92.0	260.0	20.59	19.54	4.88	0.202	41.3	33.2	0.291	5.50		0.619	0.422	0.403	0.809	0.963	
D22	98	200	83.4	325.0	20.54	19.46	4.72	0.113	49.7	38.9	0.233	5.00		0.773	0.543	0.587	0.785	1.097	
D23	97	200	70.9	262.0	20.70	19.63	4.90	0.126	62.7	51.4	0.289	7.56	1.08	0.776	0.567	0.622	0.832	0.950	UNST ?
D23	87	200	71.0	241.0	20.27	19.21	4.48	0.152	61.3	50.8	0.314	2.50	1.14	0.790	0.528	0.564	0.686	2.907	UNST ?
D23	88	200	71.5	161.5	19.56	18.52	3.79	0.308	58.7	50.6	0.469	2.00	1.28	0.739	0.404	0.377	0.700	4.149	OSC.DIES
D23	99	200	71.8	154.5	19.44	18.40	3.67	0.330	58.1	50.2	0.490	3.38	1.32	0.739	0.390	0.358	0.759	2.476	
D23	82	200	72.7	89.6	18.53	17.50	2.77	0.688	54.3	48.6	0.845	5.40	3.40	0.726	0.277	0.201	0.946	1.898	TAU=2.60
D23	194	200	73.2	265.0	20.47	19.40	4.67	0.131	59.7	48.7	0.286	3.60	1.09	0.787	0.549	0.597	0.766	1.906	
D23	86	200	73.5	218.0	20.02	18.97	4.24	0.193	58.1	48.5	0.347	2.05	1.25	0.765	0.479	0.489	0.634	3.544	TAU=3.70
D23	87	200	73.6	182.0	19.55	18.50	3.77	0.262	56.6	48.0	0.416	2.04	1.20	0.766	0.423	0.404	0.851	3.767	STABLE?
D21	94	200	42.5	286.0	21.95	20.85	6.29	0.009	94.5	75.8	0.264	7.00	1.03	0.950	0.932	0.982	0.889	1.578	TAU ?
D21	86	200	42.9	223.0	21.13	20.05	5.49	0.085	91.9	78.1	0.339	4.55	1.26	0.830	0.688	0.790	0.760	2.300	NVG 22''
D21	88	200	42.8	192.0	20.46	19.39	4.83	0.140	90.1	77.7	0.394	2.10	1.68	0.834	0.607	0.677	0.676	5.100	TAU=4.30
D21	80	200	42.9	171.0	20.16	19.09	4.53	0.188	89.1	77.7	0.442	3.65	1.17	0.818	0.553	0.603	0.751	3.006	TAU=2.05
D21	83	200	44.2	106.0	19.19	18.14	3.58	0.464	84.9	76.5	0.714	4.74	1.25	0.771	0.398	0.368	0.818	2.682	TAU=2.41
D21	188	200	47.0	56.5	18.10	17.05	2.49	1.098	78.6	72.9	1.339	2.50	1.25	0.767	0.264	0.187	0.881	0.000	OSC. END

COSINE HEAT FLUX DISTRIBUTION

RUN-PT	QW (W)	TIN (F)	W (LBM/HR)	PO (PSI)	P1 (PSI)	DP1EX (PSI)	XEX	DTSUIN (F)	DTSUBB (F)	Q/WHFG	TAU (S)	WP/WA	DPRAT	ZRAT	DHRAT	DELDH	ORDER	COMMENTS
D7	198 300	114.0	349.0	21.15	20.09	5.26	0.311	20.9	16.2	0.326	2.83		0.417	0.256	0.179	0.756	0.826	
D8	199 300	103.7	312.0	20.70	19.65	4.91	0.314	29.9	24.2	0.364	3.73		0.491	0.304	0.237	0.802	0.841	
D11	192 300	94.0	296.0	20.63	19.57	4.91	0.301	39.4	32.8	0.384	4.50		0.542	0.351	0.303	0.779	0.856	
D22	98 300	83.6	444.0	20.99	19.86	5.12	0.136	50.6	40.4	0.256	5.60	1.07	0.709	0.523	0.556	0.776	0.690	
D22	181 300	83.4	275.0	20.37	19.31	4.57	0.293	49.2	41.7	0.413	11.72	2.75	0.620	0.349	0.356	0.711	0.396	? PEAKS
D22	82 300	83.4	164.5	19.52	18.49	3.75	0.570	46.8	41.2	0.690	5.10	4.20	0.584	0.284	0.210	0.803	1.110	TAU CHAN
D23	195 300	69.8	410.0	20.91	19.79	5.06	0.110	64.2	52.4	0.277	6.40	1.15	0.791	0.595	0.560	0.809	0.752	
D23	88 300	71.0	189.0	19.72	18.67	3.94	0.438	59.7	52.6	0.601	3.00	4.60	0.654	0.353	0.306	0.618	2.065	TAU=6.05
D23	89 300	71.1	166.0	19.64	18.60	3.87	0.522	59.4	52.9	0.684	6.24	4.30	0.629	0.327	0.270	0.781	1.047	
D23	80 300	71.2	159.0	19.56	18.52	3.79	0.552	59.0	52.7	0.714	2.50	4.20	0.627	0.318	0.258	0.643	2.655	
D23	81 300	71.3	154.5	19.50	18.46	3.73	0.573	58.7	52.5	0.735	5.43	4.50	0.628	0.313	0.250	0.788	1.231	
D23	82 300	71.6	142.0	19.36	18.32	3.59	0.639	58.0	52.1	0.800	2.28	3.50	0.625	0.297	0.228	0.765	3.038	
D23	83 300	71.7	120.0	19.12	18.09	3.36	0.786	57.2	51.8	0.945	4.02	4.30	0.615	0.268	0.191	0.891	1.839	TAU=2.10
D23	86 300	72.6	84.1	18.32	17.29	2.56	1.193	53.8	49.6	1.350	6.15	7.50	0.643	0.205	0.128	0.663	1.314	TAU=3.07
D21	91 300	42.0	304.0	20.51	19.41	4.85	0.116	90.9	77.9	0.373	6.80	1.24	0.866	0.635	0.716	0.933	1.042	W? TAU?
D21	93 300	42.4	251.0	20.28	19.19	4.63	0.196	89.9	78.7	0.452	7.10	1.19	0.803	0.550	0.597	0.803	1.047	W? TAU?
D21	86 300	43.3	156.0	19.68	18.62	4.06	0.475	87.3	79.0	0.727	7.48	1.80	0.704	0.401	0.373	0.756	1.165	
D21	88 300	44.2	141.0	19.36	18.30	3.74	0.555	85.4	77.7	0.805	3.61	5.40	0.712	0.372	0.332	0.719	2.473	TAU=7.12
D21	92 300	42.5	320.0	20.99	19.88	5.32	0.099	91.8	78.4	0.355	6.00	1.09	0.834	0.665	0.758	0.812	1.175	W INCFAS

RUN-PT	QW (W)	TIN (F)	W (LBM/HR)	PO (PSI)	P1 (PSI)	DP1EX (PSI)	XEX	DTSUIN (F)	DTSUBB (F)	Q/WHFG	TAU (S)	WP/WA	DPRAT	ZRAT	DHRAT	DELDH	ORDER	COMMENTS
D8	191 400	104.2	470.0	22.17	21.05	6.31	0.274	33.4	27.1	0.322	3.29		0.444	0.349	0.301	0.769	0.728	
D11	193 400	94.6	385.0	21.63	20.54	5.88	0.313	41.6	35.0	0.393	4.50		0.479	0.360	0.316	0.759	0.676	
D22	82 400	83.5	268.0	20.52	19.46	4.72	0.445	49.6	43.3	0.565	9.72	3.00	0.536	0.327	0.270	0.713	0.412	TAU CHAN
D22	94 400	83.7	420.0	21.66	20.55	5.81	0.241	52.5	44.2	0.361	5.10	1.06	0.562	0.442	0.433	0.779	0.677	W ?
D22	86 400	83.5	283.0	20.94	19.88	5.14	0.415	50.8	44.3	0.535	10.40	2.90	0.516	0.343	0.292	0.705	0.382	TAU=5.08
D23	92 400	70.1	430.0	21.47	20.34	5.61	0.187	65.5	55.5	0.352	6.00	1.16	0.657	0.520	0.552	0.772	0.668	W? TAU?
D21	92 400	41.3	440.0	21.27	20.11	5.55	0.085	93.7	79.6	0.344	6.30	1.05	0.836	0.691	0.794	0.832	0.846	

SERIES E STABILITY EXPERIMENTS

ALL POINTS ARE TABULATED BELOW IN ORDER TAKEN

ALL TEST LENGTHS POWERED

RUN-PT	QW (W)	TIN (F)	W (LBM/HR)	PO (PSI)	P1 (PSI)	DP1EX (PSI)	XEX	DTSUIN (F)	DTSUBB (F)	Q/WHFG	TAU (S)	WP/WA	DPRAT	ZRAT	DHRAT	DELDH	ORDER	COMMENTS
E03	13 200	61.2	262.0	21.29	20.22	5.39	0.092	74.1	60.2	0.289	0.00	1.09	0.849	0.703	0.723			
E03	94 200	61.2	215.0	20.64	19.58	4.75	0.155	72.2	60.7	0.352	3.17	1.21	0.810	0.582	0.599	0.915	2.853	
E03	95 200	61.7	195.0	20.41	19.35	4.52	0.193	71.0	60.6	0.388	3.15	1.23	0.781	0.527	0.542	0.826	2.867	
E03	16 200	61.8	185.0	20.26	19.21	4.38	0.214	70.5	60.6	0.409	3.10	1.84	0.770	0.500	0.515	0.952	2.914	
E03	86 200	62.0	174.0	20.10	19.05	4.22	0.241	69.9	60.5	0.435	2.34	1.60	0.757	0.470	0.483	0.668	3.854	TAU CHAN
E03	17 200	62.0	164.0	19.88	18.83	4.00	0.267	69.2	60.3	0.462	2.31	2.30	0.755	0.442	0.454	0.605	3.894	
E03	88 200	62.1	145.0	19.68	18.63	3.80	0.328	68.5	60.7	0.522	5.00	1.24	0.722	0.393	0.404	0.846	1.808	TAU CHAN
E03	19 200	62.0	136.5	19.49	18.45	3.62	0.361	68.0	60.7	0.555	4.98	3.65	0.718	0.370	0.380	0.877	1.815	

TEST LENGTH 1 WITHOUT POWER

RUN-PT	QW (W)	TIN (F)	W (LBM/HR)	PO (PSI)	P1 (PSI)	DP1EX (PSI)	XEX	DTSUIN (F)	DTSUBB (F)	Q/WHFG	TAU (S)	WP/WA	DPRAT	ZRAT	DHRAT	DELDH	ORDER	COMMENTS
E04	1 171	78.5	255.5	20.95	19.89	5.07	0.115	55.8	43.3	0.253	0.00	1.11	0.824	0.638	0.599			
E04	92 171	78.6	235.0	20.72	19.67	4.85	0.138	55.1	43.3	0.276	3.50	1.17	0.812	0.598	0.551	0.918	2.396	UNST ?
E04	183 171	78.8	196.0	20.33	19.29	4.47	0.193	53.8	43.4	0.330	3.50	1.23	0.782	0.523	0.461	0.866	0.000	OSC.DIES
E04	94 171	78.7	185.0	20.17	19.13	4.31	0.212	53.4	43.4	0.350	2.40	1.38	0.780	0.502	0.435	0.741	3.722	
E04	5 171	78.8	174.0	20.07	19.03	4.21	0.235	53.0	43.4	0.372	2.52	2.35	0.769	0.480	0.410	0.647	3.608	
E04	6 171	78.8	150.5	19.78	18.75	3.93	0.293	52.2	43.4	0.430	2.40	2.50	0.754	0.434	0.354	0.825	3.959	
E04	87 171	78.5	130.0	19.58	18.55	3.73	0.360	51.9	43.9	0.498	7.65	1.61	0.736	0.397	0.309	0.889	1.314	TAU CHAN
E04	8 171	78.4	120.0	19.45	18.42	3.60	0.401	51.6	43.9	0.540	7.65	4.40	0.731	0.377	0.286	0.909	1.353	

TEST LENGTHS 1 AND 2 WITHOUT POWER

RUN-PT	QW (W)	TIN (F)	W (LBM/HR)	PO (PSI)	P1 (PSI)	DP1EX (PSI)	XEX	DTSUIN (F)	DTSUBB (F)	Q/WHFG	TAU (S)	WP/WA	DPRAT	ZRAT	DHRAT	DELDH	ORDER	COMMENTS
E05	1 143	94.5	343.0	21.26	20.19	5.37	0.075	40.7	27.0	0.158	0.00	1.05	0.844	0.698	0.605			
E05	92 143	94.3	245.5	20.73	19.69	4.87	0.137	39.4	27.9	0.221	5.00	1.14	0.796	0.589	0.448	0.922	1.559	UNST ?
E05	93 143	94.0	215.0	20.40	19.37	4.55	0.167	38.8	27.9	0.252	2.65	1.14	0.797	0.550	0.392	0.785	3.138	
E05	4 143	93.9	193.0	20.26	19.23	4.41	0.196	38.5	28.1	0.281	2.68	2.10	0.788	0.524	0.355	0.750	3.295	
E05	5 143	93.7	161.5	19.93	18.91	4.09	0.250	37.7	28.1	0.335	2.70	3.10	0.788	0.484	0.297	0.695	3.608	
E05	6 143	93.5	110.5	19.52	18.51	3.69	0.404	36.7	28.3	0.490	2.62	3.20	0.769	0.419	0.204	0.825	4.714	
E05	87 143	93.2	103.5	19.41	18.40	3.58	0.436	36.7	28.4	0.523	6.00	1.76	0.776	0.411	0.192	0.853	2.155	BB 33**
E05	8 143	93.0	96.5	19.31	18.30	3.48	0.473	36.6	28.4	0.561	6.10	6.80	0.781	0.402	0.179	0.836	2.222	
E05	9 143	93.0	148.0	19.90	18.88	4.06	0.278	38.3	29.0	0.366	2.75	3.70	0.778	0.472	0.280	0.685	3.775	FIL.BYP.
E05	10 143	93.0	145.0	19.82	18.80	3.98	0.285	38.1	28.8	0.373	2.74	3.45	0.784	0.467	0.273	0.679	3.825	
E05	11 143	92.9	123.0	19.61	18.60	3.78	0.352	37.6	28.8	0.440	2.68	3.40	0.779	0.438	0.231	0.795	4.328	
E05	82 143	92.8	96.5	19.43	18.42	3.60	0.472	37.1	29.0	0.561	6.06	2.20	0.764	0.404	0.183	0.843	2.252	D-8911**
E05	13 143	92.6	88.3	19.38	18.37	3.55	0.524	37.2	29.2	0.613	6.05	7.25	0.759	0.395	0.168	0.845	2.405	

TEST LENGTHS 1, 2 AND 3 WITHOUT POWER

RUN-PT	QW (W)	TIN (F)	W (LBM/HR)	PO (PSI)	P1 (PSI)	DP1EX (PSI)	XEX	DTSUIN (F)	DTSUBB (F)	Q/WHFG	TAU (S)	WP/WA	DPRAT	ZRAT	DHRAT	DELDH	ORDER	COMMENTS
E06	1 114	109.4	420.0	21.23	20.14	5.33	0.072	25.6	12.7	0.103	0.00	1.03	0.812	0.661	0.440			
E06	92 114	109.2	364.0	20.97	19.90	5.09	0.087	25.1	12.8	0.119	3.50	1.06	0.810	0.631	0.386	0.801	1.589	TAU ?
E06	93 114	109.3	785.0	20.64	19.60	4.79	0.121	24.2	12.8	0.151	3.55	1.14	0.748	0.584	0.301	0.810	1.851	
E06	4 114	109.1	276.0	20.55	19.51	4.70	0.125	24.1	12.8	0.156	3.66	1.80	0.804	0.578	0.291	0.803	1.837	
E06	5 114	108.1	200.0	20.28	19.26	4.45	0.181	24.4	13.7	0.216	3.75	3.10	0.798	0.542	0.227	0.778	2.323	
E06	6 114	108.8	102.0	19.68	18.68	3.87	0.391	22.0	12.5	0.423	3.38	5.20	0.805	0.475	0.105	0.751	4.422	

Appendix F

```
C     ********** ENTHALPY TRAJECTORY MODEL ********** VERSION 8.2  1/4/70
C
C     A COMPUTER PROGRAM FOR THE IBM-360 TO INVESTIGATE THE STABILITY
C     OF A BOILING CHANNEL.
C
C     ------------------------------------------------------------------
C
C     INPUT INFORMATION
C
C     -----------
C     FIRST CARD
C
C     ----------
C     ZPLOT(12) : COORDINATES ALONG THE CHANNEL (FT) AT WHICH THE TIME
C           VARIATIONS OF THE PRESSURE ARE TO BE ESTABLISHED; ANY
C           NUMBER OF VALUES UP TO 12.
C     AA :  VALUE OF THE COEFFICIENT A (CHAPTER5). THE DEFAULT VALUE IS 0.8
C     LCORR :IF .EQ. 1 USE LINEAR INTERPOLATION TO DETERMINE
C           PRESSURE AT EXIT; IF .EQ. 0 CALCULATE PRESSURE DROP IN LAST SEGMENT
C           SEPARATELY
C     NONLIN : IF .EQ. 0 USE LINEAR ESTIMATE OF PRESSURE DROP IN SINGLE-
C           PHASE REGION FROM DZDWTF; IF .EQ. 1 CALL DYNPR1 TO DETERMINE
C           PRESSURE DROP IN SINGLE-PHASE REGION.
C     WHEN THE SAME STEADY-STATE INFORMATION (W, AND DP1EX) IS SUPPLIED
C     FOR TWO SUBSEQUENT POINTS, THE STEADY-STATE CALCULATIONS ARE BYPAS-
C     SED FOR THE SECOND
C     IREPET =1 PERMITS TO REPEAT THE STEADY-STATE CALCULATIONS EVEN THOUGH
C           TAU DID NOT CHANGE
C     IOMIT =1 PERMITS TO BYPASS THE DZDWTF CALL WHEN THE SAME PERIOD TAU
C           AND THE SAME STEADY-STATE INFORMATION WAS SUPPLIED BUT CALC-
C           ULATIONS START AT A DIFFERENT PHASE, AS SPECIFIED BY TSKIP1
C     IWRITE: IF .EQ. 1 PRINTOUT OF THE PRESSURE, MASS FLUX, DZ/DT AND
C           COORDINATES OF THE MESH POINTS IS PRODUCED.
C     IPLOT1: IF .EQ. 1 A PLOT OF THE PRESSURE AT THE BB IS PRODUCED
C     IPLOT : IF .EQ. 1 A MAP OF THE COORDINATES OF THE MESH POINTS
C           SIMILAR TO FIGURE 6.3 OF THE TEXT IS PRODUCED
C
C     SECOND CARD
C
C     -----------
C     TIN : INLET TEMPERATURE (F)
C     QWAV : GROSS POWER (WATTS/TEST LENGTH)
C     PEX : EXIT PRESSURE (PSIA)
C     RELAMP : RELATIVE AMPLITUDE OF THE FLOW OSCILLATION (DW/WO)
C     YSC : IF .GT. 0 DETERMINES THE SCALE OF THE PLOTS(MAX COORD.)
C           IF .LE. 0 SUPPRESSES THE PLOTS. IN THIS CASE ONLY THE MAXIMA
C           ARE DETERMINED BY PRTPL3
C     CYCLES : NUMBER OF CYCLES TO BE INVESTIGATED
C     TSKIP : DETERMINES THE STARTING POINT OF THE CALCULATIONS; PHASE
C           OF FLOW PERTURBATION IN CYCLES
C     COMM(4) : COMMENTS
C
C     THIRD AND FOLLOWING CARDS
C
C     ------------------------
C     W : AVERAGE MASS FLOW RATE (LBM/HR)
C     DP1EX : PRESSURE DROP FROM STATION 1 TO EXIT (PSI)
C     TAU : PERIOD OF THE OSCILLATION  (S)
C     TSKIP1 : SAME AS TSKIP BUT FOR SUBSEQUENT POINTS. PERMITS TO BREAK
C           THE ENTIRE CYCLE INTO MORE THAN ONE CALCULATIONS (SPECIFY
C           ADEQUATE TSKIP,  TSKIP1 AND CYCLES)
C     PDZCOR : CORRECTION FACTOR TO MAXIMUM AMPLITUDE OF POSITION OF THE
C           BB PERTURBATION. DEFAULT VALUE IS 1.0
C     ADZCOR : CORREC TION (IN CYCLES) TO DELAY OF POSITION OF BB PERTUR-
C           BATION. DEFAULT VALUE IS 0.0
C     PEXCOR : VALUE OF THE EXIT PRESSURE TO BE USED WHEN THE PRESSURE DROP
C           IN THE LAST SEGMENT IS CALCULATED SEPARATELY. DEFAULT VALUE
C           IS EQUAL TO PEX. CAN BE USED TO SIMULATE THERMAL NON-EQUIL-
C           IBRIUM EFFECTS.
C
C
C
C
C
      IMPLICIT COMPLEX (C)
      REAL J, CCMM(4), COS, CPROP, CYCLES,CABS
      REAL MUL, MUG, MULF, MUGF
      INTEGER*2 NPLOT(60,350)
      INTEGER*4 NERASE(10500)
      DIMENSION BPLOT(120,4),ZPLOT(12), XEXK(120)
      EQUIVALENCE (NPLOT(1), NERASE(1))
      COMMON// D, QP, GC,ZBB,ZZMAX, PI , PBB, PEX, TIN, DTSUBB, DT
      COMMON /STA2OT/ DM(60), B(60), E(60), X(60), ZC(60), PO(60),
     1      DPDLFR(60), DPDLGR(60), DPAC(60), V(60), J(60)
      COMMON /DZDWOT/ PDHDW, ADHDW, SDHDW,     PDZDW, ADZDW, SDZDW,
     1      PDHDWP, ADHDWP, SDHDWP,  A
     2      , PDP1DZ, ADP1DZ, PDP1DG, ADP1DG, PDP1, ADP1
      COMMON /CCMPLX/ CDHDW, CDZDW, CDHDWP, CDP1DZ, CDP1DG, CDP1
      COMMON /DYNPR/ Z(40,120), DZDT(40,120), GI4C,120), P(40,120)
      COMMON/PLOTOT/ XMAXJ(9), YMAXJ(9), XMINJ(9), YMINJ(9), YRANJ(9)
C
      BGF(X,ALFA) = (-1.6628E-11)*((1.0-X)*(1.0-X)/((1.0-ALFA)*ROL) +
     1      X*X/(ALFA*ROG))
C
      DATA TWOPI/6.283185/
      DATA WOLD, DP1OLD, TAUOLD /3*0.0/
      D = 0.43/12.0
      AREA = TWOPI * D * D / 8.0
      ZZMAX = 13.0
      KMAX = 120
      KMAX1 = KMAX - 1
C     KMAX MUST BE .GE. 2 AND .LE. 120
      F = 25.0                                                    LINES/FT
C     F MUST BE SMALLER OR EQUAL THAN 25 LINES/FT FOR NPLOT(XX,350)
C
 1    FORMAT(12F5.2, F10.2, 3X, 7I1)
 2    FORMAT(7F10.2,  2X, 2A4)
 3    FORMAT('1' // 21X, 2A4, 5X, 2A4 /
     1          21X,'INPUT INFORMATION :   TIN =', F7.2, 5X, 'W =',
     2      F7.1, 5X, 'QWAV =', F7.1, 6X, 'DP1EX =', F7.2, 5X, 'P1 =',
     3      F7.2, 5X, /
     4      T44, 'TAU =', F7.2, 5X, 'DT(SEC) =', F8.5, 3X, F5.2,
     5      ' CYCLES EXAMINED STARTING AT', F5.2)
 4    FORMAT('OSUBCBB RESULTS :  ZBB =', F8.3, 5X, 'PBB =',
     1      F8.3, 5X, 'DTSUBB =', F8.2)
 5    FORMAT('OSTAPR2 RESULTS : IMAX =', I5)
 6    FORMAT('0',15X,'CM',10X,'B',10X,'E',10X,'X',10X,'Z',10X,'P',
     1      5X,'DPDLFR',5X,'DPDLGR',7X,'DPAC',10X,'V', 10X, 'J' /
     2      (I5, 5X, 3(1PE11.3), 0PF11.6, 2F11.3, 5(1PE11.3)))
 7    FORMAT('ODZDWTF RESULTS :', T20, 'DH   (NOD,ARG,DEL) :', T40  ,
     1      3F20.5, ' BTU/LBM'  /
     2      T20, 'DZ', T40, 3F20.5, ' FT'  /
     3      T20, 'DHP',    T40, 3F20.5, ' BTU/LBM'  /
     4      T20,  'DP1DZ', T40, 2F20.5, 20X, ' PSI'  /
     5      T20,  'DP1DG', T40, 2F20.5, 20X, ' PSI'  /
     6      T20,  'DP1  ', T40, 2F20.5,20X,' PSI',10X,'(A =',F5.2, ')' )
 8    FORMAT('ODGPEAK =', F10.1, ' LBM/HR-FT2', 5X, 'DZPEAK =', F8.5,
     1      ' FT', 5X, 'DDZDTP =', F10.5, ' FT/SEC' )
 9    FORMAT('ODYNPR1 : P(I,K) :' / (10F13.6))
 10   FORMAT('1', 5X, 3014 / )
 11   FORMAT('ODYNPR2 : P(I,K)  (PSIA)'  /
     1      8X, 2016  /  (I5, 5X, 20F6.2))
 12   FORMAT('1DYNPR2 : Z(I,K)  (FT) '  /
     1      8X, 2016  /  (I5, 5X, 20F6.3))
 13   FORMAT('O', 5X, 3014)
 14   FORMAT('ODYNPR2 : G(I,K)  10**5(LBM/HR-FT2)' /
     1      8X, 2016  /  (I5, 5X, 20(-5PF6.3)))
 15   FORMAT('ODZDWTF : BOILING BOUNDARY IS ON A COLD SPOT      ')
 16   FORMAT('ODYNPR2 : DZDT(I,K)   (FT/HR)'  /
     1      8X, 10I12 / (I5, 5X, 10F12.1))
```

```
 17   FORMAT('OREL. AMPLITUDE =', F6.3)
 18   FORMAT('O**********  FOR A RELATIVE AMPLITUDE OF', F5.2,
     1       '  THE RELATIVE CENTER OF VOLUME VELOCITY AT THE BOILING',
     2      / 12X,'BOUNDARY MIGHT BECOME NEGATIVE', '............',
     3      'CALCULATION DISCONTINUED')
 19   FORMAT('OBOILING TRANSIT TIME =', F8.3,  ' SEC')
 20   FORMAT(I5, 3X, 6012)
 21   FORMAT('1' //
     1       'OSAME STEADY STATE INFORMATION AND SAME DT USED NOW FOR ',
     2       'A DIFFERENT PERIOD OR TSKIP:'/'OTAU =', F6.2)
 22   FORMAT(7F10.2,  2X, 2A4)
 23   FORMAT(I5, 38X, F11.6, 2F11.3, 33X, 2(1PE11.3))
 24   FORMAT('0.........', 4A4, '.........'/)
 25   FORMAT('OPRESSURE AT THE EXIT FROM TIME', F7.4, ' CYCLES TO TIME',
     1       F7.4, ' CYCLES'/  (5X, 15F8.4))
 26   FORMAT(//'0********** DT(SEC) INCREASED BY A FACTOR OF 1.3 IN ',
     1       'ORDER TO REDUCE NUMBER OF MESH POINTS **********'//)
 27   FORMAT('OPEAK OF EXIT PRESSURE OUTSIDE RANGE, AT K =', I3)
 28   FORMAT('0**********  ZO(', I2, ') SMALLER THAN 9.30207,
     1       CALCULATION DISCONTINUED **********'//)
 29   FORMAT('0',   ' REL. AMPLITUDE =', F6.3, 20X, F5.2, ' CYCLES EXAMI
     1NED NOW STARTING AT', F5.2)
 30   FORMAT('OEXIT PRESSURE, PEX =', F7.3, 10X, 'PRESSURE DROP IN TWO-'
     1       , 'PHASE REGION, PBB-PEX =', F7.3 / 'OPEAK TO PEAK VARIATI',
     2       'ONS :    PEX :', F10.4, 5X, 'TWO-PHASE PRESSURE DROP :',
     3       F10.4,  ' PSI', 5X, 'EXIT FLOW :', F10.0, ' LBM/HR-FT2' )
 31   FORMAT('0************ MOVEMENT OF BOILING BOUNDARY CORRECTED',
     1       ' EXTERNALLY :')
 32   FORMAT(1X, 2A4, F6.1, F6.2, 2X, 6(F6.3, F5.3, 1X), 1X, -5PF6.3,
     1       0PF5.3, 1X, F6.3, 2X, F6.3, F5.3)                          SUMMARY
 33   FORMAT(/'OS U M M A R Y   O F   R E S U L T S , THRESHOLD POINT:',
     1       2A4, '  AT', F7.2, ' WATT/TS'//
     2       2X, 'POINT', T13, 'W', T18, 'TAU', T28, 'DHDW', T39, 'DZDW',
     3       T52, 'DP1DZ', T64, 'DP1DG', T76, 'DP1', T85, 'DP2(ENTH)',
     4       T99, 'DG(FBK)', T110, 'RATIO', T120, 'DPEX' /)
 34   FORMAT('OEXIT QUALITY : ' / (5X, 20F6.3))
 35   FORMAT('OEXIT PRESSURE DETERMINED BY LINEAR INTERPOLATION')
 36   FORMAT('OEXIT PRESSURE DETERMINED BY CALCULATION OF PRESSURE DROP
     1IN LAST SEGMENT'/
     2       ' IN ALL CASES SEGMENT STARTED BEFORE ZCORR =', F5.2,
     3       ' FT ;      ADJUSTED EXIT PRESSSURE, PEXCOR = ', F6.2, ' PSI
     4A')
C    ------------------------------------------------------------------
      CALL ERASE(Z,4800, DZDT,4800, G,4800, P,4800)
C
C     READ AND PROCESS INPUT INFORMATION . . . . . . . . . . . . . . .
C
      READ(5,2) ZCORR
1110  READ(5,1,END=9999) ZPLOT, AA,
     1                   LCORR, NONLIN, IOMIT, IREPET, IWRITE,
     2       IPLCT1, IPLOT
      READ(5,2,END=9999) TIN,QWAV,PEX,RELAMP,YSC,CYCLES,TSKIP,
     1       CCPM(1),COMM(2)
      IF(TIN .LE. 0.0) STOP
      A = 0.8
      IF(AA .NE. 0.0) A = AA
      WRITE(8,33) COMM(1), COMM(2), QWAV
1111  READ(5,22,END=9999) W, DP1EX, TAU, TSKIP1,   PDZCOR, ADZCOR,
     1       PEXCOR, COMM(3), COMM(4)
      IF(PEXCOR .LE. 0.0) PEXCOR = PEX
      IF(TAU .LE. 0.0) GO TO 1110
      IF(IOMIT .LE. 0) GO TO 117
      TSKIP = TSKIP1
 117  IF((W .NE. WOLD) .OR. (DP1EX .NE. DP1OLD) .OR. (IREPET .EQ. 1))
     1       GO TO 111
      WRITE(6,21) TAU
      WRITE(6,29) RELAMP, CYCLES, TSKIP
      GO TO 112
C
 111  P1 = PEX + DP1EX
      QP = (3.412/1.291667)*QWAV
      QTP = QP/AREA
      GO = W/AREA
C
C     DETERMINE POSITION OF BOILING BOUNDARY . . . . . . . . . . . . .
C
      CALL SUBC88
C    ------------------------------------------------------------------
C
      DTSEC = TAU * CYCLES / FLOAT(KMAX)
 113  DT = DTSEC/3600.0
C
      WRITE(6,3) COMM, TIN, W, QWAV, DP1EX, P1, TAU, DTSEC, CYCLES,TSKIP
      WRITE(6,17) RELAMP
      WRITE(6,4) ZBB, PBB, DTSUBB
C
C     DETERMINE REFERENCE STEADY-STATE CONDITIONS IN THE CHANNEL . . . .
C
      CALL STAPR2(IMAX)
C
      IF(IMAX .EQ. 1000) GO TO 114
      IMAX1 = IMAX - 1
      WRITE(6,5) IMAX
      WRITE(6,6) (I, DM(I),B(I),E(I),X(I),ZO(I),PO(I),DPDLFR(I),
     1       DPDLGR(I),DPAC(I),V(I), J(I), I=1,IMAX1)
      WRITE(6,23) IMAX, X(IMAX), ZO(IMAX), PO(IMAX), V(IMAX), J(IMAX)
C
C     CALCULATE THE TRANSIT TIME IN THE BOILING REGION . . . . . . . .
C
      DO 49 I = 1,IMAX
      IF(ZO(I) .GE. 9.30207) GO TO 48
 49   CONTINUE
      WRITE(6,28) IMAX
      GO TO 1111
 48   BOLTRT = ((I-1)*DT+ALOG(1.0+DM(I-1)*E(I-1)*(9.30207-ZO(I-1))
     1       /(ZO(I)-ZO(I-1))) / DM(I-1)) * 3600.0
      WRITE(6,19) BOLTRT
      IF(IMAX-40) 112,112,115
 114  DTSEC = DTSEC*1.3
 115  DTSEC = DTSEC*1.3
      CYCLES = KMAX*DTSEC/TAU
      IF(IOMIT .LE. 0)
     1TSKIP = 0.5*(1.0-CYCLES) - 0.5*BOLTRT/TAU
      WRITE(6,26)
      GO TO 113
C    ------------------------------------------------------------------
C
 112  IF((ICMIT.GT.0).AND.(TAU.EQ.TAUOLD).AND.(W.EQ.WOLD).AND.(DP1EX.EQ.
     1       DP1OLD))   GO TO 116
C
C     CALCULATE PERTURBATION OF THE POSITION OF THE BB AND SINGLE-PHASE
C     REGION DYNAMICS . . . . . . . . . . . . . . . . . . . . . . . . .
C
      CALL DZDWTF(TAU,ICOLD)
C
      IF(ICCLD .EQ. 1) WRITE(6,15)
      WRITE(6,7) PDHDW, ADHDW, SDHDW,       PDZDW, ADZDW, SDZDW,
     1       PDHDWP, ADHDWP, SDHDWP, PDP1DZ, ADP1DZ, PDP1DG, ADP1DG,
     2       PDP1, ADP1, A
C    ------------------------------------------------------------------
C
C     CORRECT IF NECESSARY THE AMPLITUDE OR THE PHASE OF THE POSITION OF BB
C     PERTURBATION . . . . . . . . . . . . . . . . . . . . . . . . . .
C
 116  IF(PDZCOR .EQ. 0.0) PDZCOR = 1.0
      IF((PDZCOR .EQ. 1.0) .AND.(ADZCOR .EQ. 0.0)) GO TO 118
      RDZ = TWOPI*ADZCOR
      CDZCOR = CMPLX(COS(RDZ),SIN(RDZ))*PDZCOR
      CDZDW = CDZDW*CDZCOR
      CDP1DZ = CDP1DZ*CDZCOR
      CDP1 = CDP1DZ + CDP1DG
C
      PDZDW = CABS(CDZDW)
      ADZDW = AMOD((1.0-ATAN2(AIMAG(CDZDW),REAL(CDZDW))/TWOPI),1.0)
      SDZDW = TAU + ADZDW
      PDP1DZ = CABS(CDP1DZ)
      ADP1DZ = AMOD((1.0-ATAN2(AIMAG(CDP1DZ),REAL(CDP1DZ))/TWOPI),1.0)  (CYCLES)
```

```
      PDP1   = CABS(CDP1   )                                                (PSI)
      ADP1   = AMOD((1.0-ATAN2(AIMAG(CDP1   ),REAL(CDP1   ))/TWOPI),1.0)  (CYCLES)
      WRITE(6,31)
      WRITE(6,7) PDHDW, ADHDW, SDHDW,       PDZDW, ADZDW, SDZDW,
     1       PDHDWP, ADHDWP, SDHDWP, PDP1DZ, ADP1DZ, PDP1DG, ADP1DG,
     2       PDP1, ADP1, A
C     ------------------------------------------------------------------
C
C     GENERATE G(I,K), Z(I,K) AND DZDT(I,K) . . . . . . . . . . . . . .
C
 118  DGPEAK = RELAMP*GC
      DZPEAK =  RELAMP*   PDZDW
      DDZDTP = DZPEAK*TWOPI*3600.0/TAU
      IF((GO-DGPEAK) * V(1)-DDZDTP) 50,50,51
  50  WRITE(6,18) RELAMP
      GO TO 1111
  51  T = TWOPI * ADZDW
      DTDIM = DTSEC/TAU
      DTIME = TWOPI*DTDIM
      TIME = -DTIME + TSKIP*TWOPI
C
      DO 99 K =1,KMAX
      TIME = TIME + DTIME
      G(1,K) = GO + DGPEAK*COS(TIME)
      Z(1,K) = ZBB + DZPEAK*COS(TIME - T)
  99  DZDT(1,K) = -DDZDTP*SIN(TIME-T)
C
      DDZDTP = DDZDTP/3600.0
      WRITE(6,8) DGPEAK, DZPEAK, DDZDTP
C     ------------------------------------------------------------------
C
C     IF A NONLINEAR TREATMENT OF THE SINGLE-PHASE REGION IS SPECIFIED'
C               DYNPR1 IS CALLED, OTHERWISE THE DZDWTF RESULTS ARE USED
C               TO CALCULATE THE PRESSURE DROP IN THE SINGLE-PHASE REGION
C
      IF(NONLIN) 60,60,61
C
  60  TP1 = TWOPI * ADP1
      TIME = - DTIME + TSKIP * TWOPI
      DO 63 K = 1,KMAX1
      TIME = TIME + DTIME
  63  P(1,K) = PBB + RELAMP*PDP1*COS(TIME-TP1)
      GO TO 62
C
  61  CALL DYNPR1(KMAX)
C     ------------------------------------------------------------------
  62  IF(IWRITE .GT. 0) WRITE(6,9)  (P(1,K), K = 1,KMAX)
C
C     PLOT THE PRESSURE AT THE BOILING BOUNDARY VERSUS TIME. . . . . .
C
      YSC1 = 1.0
      IF(IPLOT1 .LE. 0) YSC1 = -1.0
C
      DO 109 K = 1,KMAX1
      BPLOT(K,1) = (K - 1)*DTDIM + TSKIP
 109  BPLOT(K,2) = P(1,K)
      CALL PRTPL3(1,BPLOT,   KMAX1,2,    KMAX1,0,  KMAX,4,  YSC1)
C
C     USE THE ENTHALPY TRAJECTORY MODEL FOR THE DYNAMICS OF THE TWO-PHASE
C     REGION . . . . . . . . . . . . . . . . . . . . . . . . . . . . .
C
      CALL DYNPR2(IMAX, KMAX,KMAX2)
C
      KMAX3 = KMAX2 - 1
C     ------------------------------------------------------------------
      IF(IWRITE .LE. 0) GO TO 187
C
      KDK = KMAX1/20 + 1
      KDK2 = 2*KDK
      K20 = 19*KDK + 1
      K10 = 9*KDK2 + 1
      WRITE(6,12) (L, L =1,K20,KDK),
     1            (I, (Z(I,K), K=1,K20,KDK), I=1,IMAX)
      WRITE(6,11) (L, L =1,K20,KDK),
     1            (I, (P(I,K), K=1,K20,KDK), I=1,IMAX)
      WRITE(6,14) (L, L =1,K20,KDK),
     1            (I, (G(I,K), K=1,K20,KDK), I=1,IMAX)
      WRITE(6,16) (L, L =1,K20,KDK),
     1            (I, (DZDT(I,K), K=1,K10,KDK2), I=1,IMAX)
      WRITE(6,24) COMM
C     ------------------------------------------------------------------
 187  IF(IPLOT .LE. 0) GO TO 410
      ZMAX = -1.0E50
      ZMIN = 1.0E50
C
      DO 199 K =1,KMAX2
      IF(ZMAX-Z(IMAX,K)) 191,191,199
 191  ZMAX = Z(IMAX,K)
 199  CONTINUE
C
      DO 299 K =1,KMAX1
      IF(Z(1,K) - ZMIN)  291,291,299
 291  ZMIN = Z(1,K)
 299  CONTINUE
C
C     PRODUCE A MAP OF THE COORDINATES OF THE MESH POINTS . . . . . .
C
      CALL ERASE(NERASE,10500)
C     ERASE IS A CENTER SUPPLIED SUBROUTINE FOR ZEROING LENGTH #4 ARRAYS
C
      KDK = KMAX1/60 + 1
      KDK2 = 2*KDK
      IF(ZMAX - 13.96) 351,352,352
C
 352  DO 389 I = 1,IMAX
      KKK = KMAX - I
      DO 389 K = 1,KKK,KDK
      IF(Z(I,K) .GE. 13.96) GO TO 389
      NPLOT(K,Z(I,K)*F+1) = I + 10
 389  CONTINUE
      GO TO 400
C
 351  DO 399 I = 1,IMAX
      KKK = KMAX - I
      DO 399 K =1,KKK,KDK
 399  NPLOT(K,Z(I,K)*F+1) = I + 10
C
 400  IMIMIN = ZMIN*F - 1
      IMAMAX = ZMAX*F + 1
      IF(ZMAX .GT. 13.96) IMAMAX = IFIX(13.96*F)
      WRITE(6,10) (I, I =1,KMAX,KDK2)
      WRITE(6,20) (I, (NPLOT(K,I), K =1,60),   I = IMIMIN,IMAMAX)
      WRITE(6,13) (I, I =1,KMAX,KDK2)
      WRITE(6,24) COMM
C     ------------------------------------------------------------------
C     FIND TIME VARIATIONS OF PRESSURE AT GIVEN LOCATIONS ZPLOT(I)
C     FIND MIN VALUE OF Z(IMAX,K)
C
 410  ZMIN = 1.CE+50
      DO 479 K =1,KMAX2
      IF(Z(IMAX,K)-ZMIN) 471,471,479
 471  ZMIN = Z(IMAX,K)
 479  CONTINUE
C
      IF(ZPLOT(I) .LE. 0.0) GO TO 500
C
C     FIND MAX VALUE OF Z(1,K)
C
      ZMAX = -1.0E+50
      DO 489 K =1,KMAX2
      IF(ZMAX - Z(1,K))481,489,489
 481  ZMAX = Z(1,K)
 489  CONTINUE
C
      DO 499 L =1,12
      ZP = ZPLOT(L)
      IF(ZP .LE. 0.0) GO TO 500
      IF(ZP .GT. ZMIN) GO TO 499
      IF(ZP .LE. ZMAX) GO TO 499
C
```

```
      M = 0
      DO 498 K = 1,KMAX3
      M = M + 1
      DO 497 I = 1,IMAX
      IF(Z(I,K) - ZP) 497,496,496
  496 IF(Z(I-1,K+1) .GT. ZP) GO TO 494
C
C     DETERMINE PRESSURE AT ZP BY LINEAR INTERPOLATION
C
      BPLOT(M,2)=P(I-1,K+1)+(P(I,K)-P(I-1,K+1))*(ZP-Z(I-1,K+1))/(Z(I,K)
     1      - Z(I-1,K+1))
      BPLOT(M,1) = (K + I - 2) * DTDIM + TSKIP
      GO TO 498
  497 CONTINUE
  494 M = M - 1
  498 CONTINUE
      CALL PRTPL3(IFIX(100.*ZP+.5),BPLOT,    M,2,    M,0,    KMAX,4,  YSC)
  499 CONTINUE
  500 CONTINUE
C     ------------------------------------------------------------------
      WOLD = W
      DP1OLD = DP1EX
      TAUOLD = TAU
C
C     FIND FLOW AND PRESSURE VARIATIONS AT EXIT AND DP IN TWO-PHASE REGION
C
      ZP = 9.30207
      P88EX= P88-PEX
C
      IF(LCORR .EQ. 0) GO TO 550
      IF(ZP .GT. ZMIN) GO TO 550
C
C     USE LINEAR INTERPOLATION TO DETERMINE EXIT PRESSURE.
C
      WRITE(6,35)
      M = 0
      DO 548 K = 1,KMAX3
      M = M + 1
      DO 547 I = 1,IMAX
      IF(Z(I,K) - ZP) 547,546,546
  546 IF (Z(I-1,K+1) .GT. ZP) GO TO 544
      CPROP = (ZP-Z(I-1,K+1))/ (Z(I,K)-Z(I-1,K+1))
      BPLOT(M,1) = (K + I -2) *DTDIM + TSKIP
      BPLOT(M,2) = (P(I-1,K+1) + CPROP * (P(I,K)-P(I-1,K+1)))/PEX
      BPLOT(M,3) = (G(I-1,K+1) + CPROP*(G(I,K) - G(I-1,K+1)))/GO
      BPLOT(M,4) = (P(1,K+I-1)-BPLOT(M,2)*PEX)/(P88EX)
      GO TO 548
  547 CONTINUE
  544 M = M - 1
  548 CONTINUE
      CALL PRTPL3(930,BPLOT,       M,4,       M,0, KMAX,4,   YSC)
      WRITE(6,24) COMM
C     WRITE(6,25) BPLOT(1,1), BPLOT(M,1), (BPLOT(K,2), K =1,M)
      PEXRAN = YRANJ(1) *PEX
      GEXRAN = YRANJ(2) * GO
      DP2RAN = YRANJ(3) * P88EX
      WRITE(6,30) PEX, P88EX, PEXRAN, DP2RAN, GEXRAN
C     ------------------------------------------------------------------
C
  550 IF(LCORR .GT. 0) GO TO 600
C
C     EVALUATE PRESSURE DROP IN LAST SEGMENT INDEPENDENTLY
C     FIND ZMIN, ZMAX FOR IMAX, IMAX-1, ... UNTIL ZMAX .LE. CHANNEL
C     LENGTH.
C
      II = IMAX + 1
  551 II = II - 1
      ZMAX = 0.0
      DO 552 K = 1,KMAX2
      IF(Z(II,K) .GT. ZMAX) ZMAX = Z(II,K)
  552 CONTINUE
      IF((ZMAX.GT.ZCORR).AND.(II.GT.1)) GO TO 551
      IF(ZMAX .GT. ZP) GO TO 600
C
C     DETERMINE EXIT QUALITY ACCORDING TO PEXCOR, CORRECTED EXIT
C     PRESSURE TO TAKE INTO ACCOUNT SOME THERMAL NON-EQUILIBRIUM
C
      WRITE(6,36) ZCORR, PEXCOR
      HFGEX = HFGF(PEXCOR)
      HEX = HLF(PEXCOR)
      XII = X(II)
      HII = HLF(PO(III)) + XII *HFGF(PO(III))
      X1 = (HII - HEX)/HFGEX
C
C     ESTIMATE PROPERTIES AT AVERAGE PRESSSURE
C
      PAV = 0.5*(PO(II) + PEXCOR)
      MUL = MULF(PAV)
      MUG = MUGF(PAV)
      ROL = RCLF(PAV)
      ROG = ROGF(PAV)
      ROGROL = ROG - ROL
      XTT1 = (ROG/ROL)**0.5 * (MUL/MUG)**0.1
      XTTII = XTT1 * ((1.0-X(II))/X(II))**0.9
      ALFAII = ALFAF(XTTII)
      BGII = BGF(XII, ALFAII)
C
C     ADD ENTHALPY VARIATIONS AT ACTUAL POSITION OF BB TO ENTHALPY AT
C     MESH POINT II
C
      M = KMAX2 + IMAX - II - 1
      DO 559 K = 1,M
      GII =  G(II,K)
      DZ = ZP - Z(II,K)
      TIME = TWOPI*TSKIP + (K-1)*DTIME
      XEX = X1 + (QTP*(DZ-0.26)/GII  + RELAMP*PDHDWP*COS(TIME-ADHDWP*
     1      TWOPI))/HFGEX
      XEXK(K) = XEX
      XAV = 0.5*(XII + XEX)
      XTTEX = XTT1*((1.0-XEX)/XEX)**0.9
      XTTAV = 0.5*(XTTII + XTTEX)
      ALFAAV = ALFAF(XTTAV)
      ALFAEX = ALFAF(XTTEX )
      XDMUL = (1.0-XAV)*D/MUL
      DPFRIC = FI2LF(XTTAV)*(-3.3256E-11)*(DZ/D)*FF(GII*XDMUL)*GII**2
     1      *(1.0-XAV)**2 / ROL
      DPGRAV = -DZ*(ROGROL * ALFAAV + ROL)/144.0
      DPACCE = (BGF(XEX, ALFAEX) - BGII)*GII*GII
      BPLOT(K,1) = (K+I-2)*DTDIM + TSKIP
      BPLOT(K,2) = (P(II,K)+ DPFRIC + DPGRAV + DPACCE)/PEX
      BPLOT(K,3) = GII/GO
  559 BPLOT(K,4) = (P(1,K+II-1) - BPLOT(K,2)*PEX)/P88EX
C
      CALL PRTPL3(930,BPLOT,       M,4,       M,0, KMAX,4,   YSC)
      WRITE(6,24) COMM
      PEXRAN = YRANJ(1) *PEX
      GEXRAN = YRANJ(2) * GO
      DP2RAN = YRANJ(3) * P88EX
      WRITE(6,30) PEX, P88EX, PEXRAN, DP2RAN, GEXRAN
      WRITE(6,34)(XEXK(K),K = 1,M)
C
  600 CONTINUE
C     ------------------------------------------------------------------
C
C     CALCULATE OPEN LOOP TRANSFER FUNCTION
C
      ADP2E = XMAXJ(3)
      PDP2E = 0.5*DP2RAN / RELAMP
C
      RDP2 = TWOPI*ADP2E
      CDP2E = CMPLX(COS(-RDP2),SIN(-RDP2))*PDP2E
      CDP1E =-CDP2E
      CDP1G = CDP1E - CDP1DZ
      CDGFDB =-CDP1G*GO / CDP1DG
      PDGFDB = CABS(CDGFDB)
      ADGFDB = AMOD((1.0-ATAN2(AIMAG(CDGFDB),REAL(CDGFDB))/TWOPI),1.0)
      RATIO = PDGFDB / GO
      WRITE(8,32) COMM(3), COMM(4), W, TAU, PDHDW, ADHDW, PDZDW, ADZDW,
     1      PDP1DZ, ADP1DZ, PDP1DG, ADP1DG, PDP1, ADP1, PDP2E, ADP2E,
     2      PDGFDB, ADGFDB, RATIO, PEXRAN, XMAXJ(1)                    SUMMARY
      GO TO 1111
 9999 STOP
      END
```

```
      SUBROUTINE SUBCBB
C                                                    VERSION 3.1, 11/3/69
C     TAKES INTO ACCOUNT COLD SPOTS
C
C     CALCULATE SUBCOOLING WITH RESPECT TO BOILING BOUNDARY FOR EXPERIMENTAL
C     POINTS,STARTING PRESSURE DROP CALCULATIONS FROM INLET.
C     INPUT : CP (BTU/HR-FT), G (LBM/HR-FT2), PIN = P1 (PSIA), TIN (F)
C     OUTPUT : ZBB (FT), PBB (PSIA), DTSUBB (F)
C     FUNCTIONS REQUIRED : ROLTF, MULTF, HLTF, PSATF, TF, FF, KLF
C
      REAL MULB, MULW, MULTF, KLF
      REAL QDISTR(7)/7*1.0/                                          ********
      DIMENSION DISTR(15), Z(15), T(16), P(16), PSAT(16), H(16)
      COMMON /1/ D, QP, G, ZBB, ZMAX, PIN, PBB, PEX, TIN, DTSUBB, DT
      DATA DLH, DLU /1.125, .1666667/
C
C     *********  FREON - 113 PROPERTY FUNCTIONS  **********************
C
      TI(T) = 1.0 / (T + 459.6)
      ROLTF(T) =    .1035453 E 03 - .7105255 E-01*T - .6448694E-04*T*T   ROLTF1/1
      MULTF(T)= EXP( - .3483695 E 01  + .5585921 E 04*TI(T)
     1        - .1950534 E C7*TI(T)**2  + .3577018 E 09*TI(T)**3)        MULTF
      HLTF(T) = .8119482E 01 + .1961794E 00*T  + .1261047E-03*T*T       HLTF 1/1
      PSATF(T) = 10.0**(33.C655-4330.98/(T+459.6) - 9.2635*ALCG10(T+
     1      459.6)  + 0.0020539 * (T+459.6))                            PSATF
      TF(H) = - .4C82034E 02 + .5186681E 01*H  - .1141203E-01*H*H       TF   1/1
      KLF(T) = C.0475 - 8.76667E-05* T                                  KLF  1/1
C
      W = 0.7854*D*D*G
C
C     GENERATE CORRECTED HEAT FLUX DISTRIBUTION. . . . . . . . . . . .
C
      RATIO = (DLU + DLH)/DLH
      DO 98 J = 2,14,2
   98 DISTR(J) = QDISTR(J/2) * RATIO
C
C     GIVE INITIAL VALUES AT HEATED SECTION INLET . . . . . . . . . . .
C
      Z(1) = 0.0
      H(1) = HLTF(TIN)
      T(1) = TIN
      P(1) =PIN
      PSAT(1) = PSATF(TIN)
C
C     CALCULATE BULK TEMP. AND SATURATION TEMP. AT THE END OF EACH INTERVAL
C
      I = 0
    1 I = I + 1
      IF(MCC(I,2)) 3,3,4
    3 DL = DLH
      DH    = DL*QP*DISTR(I) / W
      H(I+1) = H(I) + DH
      T(I+1) = TF(H(I+1))
      TAV = 0.5 * (T(I) + T(I+1))
      ROL = ROLTF(TAV)
      MULB = MULTF(TAV)
      DTFILM = (282.0*DL)*QP*DISTR(I)*MULB**0.4/(G**0.8*KLF(TAV)**0.6)
      TWAV = TAV + DTFILM
      MULW = MULTF(TWAV)
      GO TO 5
    4 DL = DLU
      IF(I .EQ. 1) DL = 0.5*DLU
      DH = 0.0
      H(I+1) = H(I)
      TAV = T(I)
      T(I+1) = TAV
      ROL = ROLTF(TAV)
      MULB = MULTF(TAV)
      DTFILM = 0.0
      MULW = MULB
    5 REL = G * D / MULB
      DPFR = (-3.3256E-11)*(DL/D)*FF(REL)*G*G*((MULW/MULB)**0.14)/ROL
      DPGR = - DH  * ROL / 144.0
      P(I+1) = P(I) + DPFR + DPGR
      PSAT(I+1) = PSATF(T(I+1))
      Z(I+1) = Z(I) + DL
      IF(P(I+1) .LE. PSAT(I+1)) GO TO 2
      IF(I .LT.15) GO TO 1
      DTSUBB = T(16) - TIN
      PBB = P(16)
      ZBB = 9.041668
      WRITE(6,9)
    9 FORMAT('0********** SUBCBB  : BOILING BOUNDARY IS OUTSIDE HEATED'
     1      ,' SECTION'   //)
      RETURN
C
C     FIND EXACT LOCATION OF BOILING BOUNDARY BY ITERATION . . .. . . .
C
    2 DLP = DL
    6 DLP = DLP * (P(I) - PSAT(I)) / (P(I)-P(I+1)+PSAT(I+1)-PSAT(I))
      H(I+1) = DH     * DLP/DL + H(I)
      T(I+1) = TF(H(I+1))
      TAV = 0.5 * (T(I) + T(I+1))
      ROL = ROLTF(TAV)
      MULB = MULTF(TAV)
      TWAV = TAV + DTFILM
      MULW = MULTF(TWAV)
      REL = G * D / MULB
      DPFR = (-3.3256E-11)*(DLP/D)*FF(REL)*G*G*((MULW/MULB)**0.14)/ROL
      DPGR = -DLP *ROL /144.0
      P(I+1) = P(I) + DPFR + DPGR
      PSAT(I+1) = PSATF(T(I+1))
      IF(ABS(P(I+1)-PSAT(I+1)) .GT. 0.01) GO TO 6
      DTSUBB = T(I+1) - TIN
      PBB = P(I+1)
      ZBB = Z(I) + DLP
      RETURN
      END



      SUBROUTINE DZDWTF(TAU, ICOLD)
C                                                    VERSION 3.2,  12/30/69
C
C     SUBROUTINE DZDWTF CALCULATES THE AMPLITUDE AND PHASE OF THE
C     BOILING BOUNDARY OSCILLATION USING A LINEAR MODEL.
C
C     IN THIS VERSION THE COLD SPOTS IN THE WALLAND THE HEAT FLUX DISTR-
C     IBUTION ARE TAKEN INTO ACCOUNT
C     THE PRESSURE DROP VARIATIONS IN THE SINGLE-PHASE REGION ARE ALSO
C     CALCULATED.
C
C     INLET VARIABLES :
C     TIN : INLET TEMPERATURE (F)
C     DTSUBB: SUBCOOLING WITH RESPECT TO THE BOILING BOUNDARY SAT. TEMP (F)
C     PI: PRESSURE AT INLET OF HEATED LENGTH (PSIA)
C     QP : AVERAGE LINEAR HEAT RATE (BTU/HR-FT)
C     G : AVERAGE MASS FLUX (LBM/HR-FT2)
C     ZBB:   DISTANCE OF BOILING BOUNDARY FROM INLET (FT)
C     TAU : PERIOD OF SINUSOIDAL OSCILLATION (SEC)
C
C     QDISTR(7) : DIMENSIONLESS POWER DISTRIBUTION (INLET TO EXIT)
C     A : COEFFICIENT DEFINED BY DW/Q = A * DW/W
C
C     OUTPUT :
C     DHDW : INLET FLOW TO ENTHALPY AT STEADY STATE LOCATION OF BB
C     (WITH WALL EFFECT), (BTU/LBM)
C     DZDW : INLET FLOW TO POSITION OF BOILING BOUNDARY (ALL EFFECTS
C     INCLUDED)    (FT)
C     DHDWP : INLET FLOW TO ENTHALPY AT MOVING POSITION OF BB, (BTU/LBM)
C     DP1DZ : MOVEMENT OF THE BB TO PRESSURE DROP IN THE SINGLE-PHASE
C     REGION (PSI), FRICTION AND GRAVITY EFFECTS.
C     DP1DG : INLET FLOW TO PRESSURE DROP IN THE SINGLE-PHASE REGION
C      (PSI), FRICTION AND INERTIA EFFECTS
C     DP1 : INLET FLOW TO TOTAL  PRESSURE DROP IN THE SINGLE-PHASE REGION (PSI)
C     ICOLD : .EQ. 0 IF THE BB IS IN THE HEATED SEGMENT, .EQ. 1 IF THE BB
C             IS IN THE COLD WALL
```

```
C
C     THE PREFIX C DENOTES THE COMPLEX QUANTITY
C     THE PREFIX P DENOTES THE MAGNITUDE (PEAK VALUE)
C     THE PREFIX A DENOTES THE PHASE (IN CYCLES)
C     THE PREFIX S DENOTES THE DELAY (SEC)
C
      IMPLICIT COMPLEX (C)
      REAL MULTF, KW, CABS, KLF, MULB
      DIMENSION QDISTR(7), COEXP(16), DISTR(15), Z(16)
      COMMON// D, QP, G, ZBB, ZMAX, P1, PBB, PEX, TIN, DTSUBB, DT
      COMMON /CZDWOT/ PDHDW, ADHDW, SDHDW,     PDZDW, ADZDW, SDZDW,
     1      PDHDWP, ADHDWP, SDHDWP,  A
     2      , PDP1DZ, ADP1DZ, PDP1DG, ADP1DG, PDP1, ADP1
      COMMON /CCMPLX/ CDHDW, CDZDW, CDHDWP, CDP1DZ, CDP1DG, CDP1
      DATA DISTR/15*0.0/, QDISTR /7*1.0/                                ********
      DATA PI,TWOPI/3.141593, 6.283185/, CI/(0.0, 1.0)/,
     1      ALPHA, KW, THICK   /0.022, 0.75, 0.004/                     M.I.T.
     2      , DZH, DZL/1.125, .1666667/                                 M.I.T.
C
C     PROPERTY FUNCTIONS REQUIRED : ROLTF, MULTF, DHLF, KLF, HLTF
C
      TI(T) = 1.0 / (T + 459.6)
      MULTF(T)= EXP( - .5483695 E 01  + .5585921 E 04*TI(T)             MULTF1/2
     1      - .1950534 E 07*TI(T)**2  + .3577018 E 09*TI(T)**3)         MULTF2/2
      ROLTF(T) =   .1035453 E 03 - .7105255 E-01*T - .6448694E-04*T*T   ROLTF1/1
      HLTF(T) = .81194F2E 01 + .1961794E 00*T  + .1261047F-03*T*T       HLTF 1/1
      KLF(T) = 0.0475 - 6.76667E-05* T                                  KLF  1/1
C
C     AVERAGE TEMPERATURE AND DENSITY IN NON BOILING REGION
C
      TAV = TIN + 0.5*DTSUBB
      ROLAV = ROLTF(TAV)
      ROLIN = ROLTF(TIN)
      MULB = MULTF(TAV)
C
C     CALCULATE GRAVITY AND FRICTIONAL PRESSURE DROPS IN NON BOILING,
C     HEATED REGION  . . . . . .
C
      DPGR = -RCLAV * ZBB / 144.0                                       (PSI)
      DTFILM = (282.0*1.291667)*QP*MULB**0.4/(G**0.8*KLF(TAV)**0.6)
      DPFR= (-3.3256E-11 *ZBB/D)*FF(G*D/MULB)*G*G* (MULTF(TAV+DTFILM)/
     1      MULB)**0.14/ROLAV
      PBBCAL = P1 + DPFR + DPGR
      DHLBB = DHLF(PBBCAL)
C
      W = 0.7854 * D * D * G
      COMEGA = 3600.0*TWOPI*CI/TAU                                      (1/HR)
      SPEHEA = (HLTF(TAV + 5.0)-HLTF(TAV - 5.0)) * 0.1                  BTU/LB-F
      HFC = 0.0279*W**0.8*KLF(TAV)**0.6*SPEHEA**0.4 /
     1      (D**1.8*MULB**0.4)
C
      ABC = QP / H
      C1 = CSQRT(COMEGA/ALPHA)
      C2 = C1 * THICK * CI
      C3 = CI * CCOS(C2)/ (KW * CSIN(C2) * C1)
      C4 = PI * D /((1.0/HFC+C3)*W*SPEHEA)
      C5 = RCLAV*COMEGA/G
      CK = C5 + C4
      C6 = A * C3 /(1.0/HFC + C3)
      C7 = (1.0-A) * ABC
      C8 = C6 * ABC
      CL = C7 + C8
C
C
C     FIND IN WHICH TEST SECTION THE BOILING BOUNDARY IS LOCATED
C     GENERATE HEATED AND UNHEATED SECTION LIMIT COORDINATES AND CORRECTED
C     HEAT FLUX DISTRIBUTION
C
      RATIO = (DZU + DZH)/DZH
      Z(1) = 0.0
      Z(2) = 0.5*DZU
      DO 88 I = 2,14,2
      DISTR(I) = QDISTR(I/2) * RATIO
      Z(I+1) = Z(I) + DZH
      IF(ZBB-Z(I+1)) 881,881,882
  881 NTS = I
      GO TO 89
  882 Z(I+2) = Z(I+1) + DZU
      IF(ZBB-Z(I+2)) 883,883,88
  883 NTS = I + 1
      GO TO 89
   88 CONTINUE
   89 NTS1 = NTS + 1
      Z(NTS1) = ZBB
      COLD = MCD(NTS,2)
      DO 87 I = 2,NTS1
   87 COEXP(I) = CEXP(CK*Z(I))
C
C     EVALUATE INTEGRAL
C
      CSUM = 0.0
      DO 86 I = 2,NTS,2
   86 CSUM = CSUM + DISTR(I)*(COEXP(I+1) - COEXP(I))
C
C     CALCULATE THE INLET FLOW TO ENTHALPY TRANSFER FUNCTION . . . . . .
C
      CG1 = CL/CK
      CG2 = -CSUM/COEXP(NTS1)
      CDHDW = CG1 + CG2                                                 (BTU/LB)
C
      PDHDW = CABS(CDHDW)
      ADHDW = -ATAN2(AIMAG(CDHDW),REAL(CDHDW))/TWOPI
      IF(ADHDW .LT. 0.0) ADHDW = 1.0 + ADHDW
      SDHDW = TAU * ADHDW
C
C     CALCULATE THE INLET FLOW TO POSITION OF THE B.B. TRANSFER FUNCTION
C
      CFR= 1.8*(DPFR-1.735E-04*MULTF(TIN)**0.2*W**1.8/ROLIN)*DHLBB      (BTU/LB)
      CIN= -TWOPI*G*(ZBB+2.3)*DHLBB*CI/(TAU*3600.0*32.17*144.0)         (BTU/LB)
      B1 = ZBB * QP +  DISTR(NTS) / W                                   (BTU/LB)
      B2 = -DHLBB*(DPFR+DPGR)                                           (BTU/LB)
      CDZDW = (-CDHDW + CFR+ CIN)*ZBB / (B1 + B2)                        (FT)
C
      PDZDW = CABS(CDZDW)
      ADZDW = -ATAN2(AIMAG(CDZDW),REAL(CDZDW))/TWOPI
      IF(ADZDW .LT. 0.0) ADZDW = 1.0 + ADZDW
      SDZDW = TAU * ADZDW
C
C     CALCULATE THE INLET FLOW TO ENTHALPY AT THE ACTUAL POSITION OF
C     THE B. B. TRANSFER FUNCTION . . . . . .
C
      CDHDWP = CDPDW + B1 * CDZDW / ZBB                                 (BTU/LB)
      PDHDWP = CABS(CDHDWP)
      ADHDWP = -ATAN2(AIMAG(CDHDWP),REAL(CDHDWP))/TWOPI
      IF(ADHDWP .LT. 0.0) ADHDWP = 1.0 + ADHDWP
      SDHDWP = TAU * ADHDWP
C
C     CALCULATE THE PRESSURE DROP T.P.S. IN THE SINGLE-PHASE REGION.
C
      CDP1DZ = (-DPFR - DPGR)*CDZDW / ZBB                               (PSI)
      CDP1FR = -CFR/DHLBB                                               (PSI)
      CDP1IN = -CIN/DHLBB                                               (PSI)
      CDP1DG = CDP1FR + CDP1IN                                          (PSI)
      CDP1 = CDP1DZ + CDP1DG                                            (PSI)
C
      PDP1DZ = CABS(CDP1DZ)                                             (PSI)
      PDP1FR = CABS(CDP1FR)                                             (PSI)
      PDP1IN = CABS(CDP1IN)                                             (PSI)
      PDP1DG = CABS(CDP1DG)                                             (PSI)
      PDP1   = CABS(CDP1  )                                             (PSI)
      ADP1DZ = AMOD((1.0-ATAN2(AIMAG(CDP1DZ),REAL(CDP1DZ))/TWOPI),1.0)  (CYCLES)
      ADP1FR = AMOD((1.0-ATAN2(AIMAG(CDP1FR),REAL(CDP1FR))/TWOPI),1.0)  (CYCLES)
      ADP1IN = AMOD((1.0-ATAN2(AIMAG(CDP1IN),REAL(CDP1IN))/TWOPI),1.0)  (CYCLES)
      ADP1DG = AMOD((1.0-ATAN2(AIMAG(CDP1DG),REAL(CDP1DG))/TWOPI),1.0)  (CYCLES)
      ADP1   = AMOD((1.0-ATAN2(AIMAG(CDP1  ),REAL(CDP1  ))/TWOPI),1.0)  (CYCLES)
C
      RETURN
      END
```

```
      SUBROUTINE STAPR2(IMAX)
C                                                  VERSION 2.4    10/16/69
C
C     SUBROUTINE STAPR2 CALCULATES THE STEADY STATE CONDITIONS IN THE
C     BOILING CHANNEL STARTING AT THE BOILING BOUNDARY AND MARCHING
C     DOWNSTREAM.
C     ONLY FOR UNIFORM HEAT FLUX DISTRIBUTION.
C     SEGMENTS OF EQUAL TRANSIT TIME ARE CONSIDERED.
C
C     REQUIRED INPUT :
C           QP : LINEAR HEAT RATE (BTU/HR-FT)
C           G : MASS FLUX (LBM/HR-FT2)
C           ZBB : POSITION OF THE BOILING BOUNDARY (FT)
C           ZMAX : MAX VALUE OF COORDINATE ALONG THE CHANNEL TO BE
C                  REACHED (FT)
C           PBB : PRESSURE AT THE BOILING BOUNDARY (PSIA)
C           PEX : LIMITING EXIT PRESSURE VALUE (PSIA)
C           DT : TRANSIT TIME INCREMENT (HR)
C
C     OUTPUT :
C     IMAX : NUMBER OF SPACE POINTS
C           OM, B, E : COEFFICIENTS DEFINED IN TEXT
C           X : QUALITY VALUES
C           ZO: POSITION ALONG THE CHANNEL (FT)
C           J: VELOCITIES OF THE CENTER OF VOLUME (FT/HR)
C           PO: PRESSURE  VALUES (PSIA)
C           DPDLFR :  FRICTIONAL PRESSURE DROP SLOPE DIVIDED BY G**1.8
C                  (PSI/FT) / (LBM/HR-FT2)**1.8
C           DPDLGR : GRAVITATIONAL PRESSURE DROP SLOPE (PSI/FT)
C           DPAC : ACCELERATION PRESSURE DROP VALUES DIVIDED BY G**2
C                  (PSI/(LBM/HR-FT2)**2)
C           V : FLOWING SPECIFIC VOLUMES (FT3/LBM)
C
C     X, ZO, J AND PO ARE DEFINED FOR I = 1, IMAX
C     OM, B, E AND THE PRESSURE DROP TERMS ARE DEFINED FOR I = 1, IMAX-1
C
C     PROPERTY FUNCTIONS REQUIRED: RDLF, RDGF, MULF, MUGF, HFGF, HLF
C
      REAL MUL, MUG, MULF, MUGF, J
      COMMON// D, QP, G, ZBB, ZMAX, PIN, PBB, PEX, TIN, DTSUBR, DT
      COMMON /STA2DT/ OM(60), B(60), E(60), X(60), ZO(60), PO(60),
     1      DPDLFR(60), DPDLGR(60), DPAC(60), V(60), J(60)
C
C     *********  FREON - 113 PROPERTY FUNCTIONS  **********************
C
C     THE ARGUMENT OF RDLF, RDGF, MULF AND MUGF MUST BE ALOG(P)
C
      RDLF(X) =     .1033C78E  03 - .2657116E  01*X                        RDLF 1/2
     1      - .3389485E -01*X*X          - .8307981E -01*X*X*X             RDLF 2/2
      RDGF(X) = EXP(             - .3267308E 01  + .9181820E 00 *X         RDGF 1/2
     1      + .3519715E-02 *X*X )                                          RDGF 2/2
      MULF(X) = EXP(             .1064657 E 01 - .3255410 E 00*X           MULF 1/2
     1      + .6064336 E-02*X*X          - .1726090 E-02*X*X*X )           MULF 2/2
      MUGF(X) =                  .1967795 E-01 + .7899068 E-02*X           MUGF 1/3
     1      - .5630545 E-02*X*X          + .2141095 E-02*X*X*X             MUGF 2/3
     2      - .3936185 E-03*X*X*X*X      + .1974262 E-04*X*X*X*X*X         MUGF 3/3
C
      HFGF(P)              =  .7058670 E 02 - .9218673 E 00*P                HFGF 1/3
     1      + .4283483 E-01*P*P          - .1186139 E-02*P*P*P             HFGF 2/3
     2      + .1250690 E-04*P*P*P*P                                        HFGF 3/3
C
C     HLF MUST BE PROVIDED EXTERNALLY
C
C     PRESSURE DROP FUNCTIONS
C
      RELPF(X) = G*(1.0-X)*D/MUL
      DPDLFF(X) = (-3.3256E-11)*FF(RELPF(X))*G*G*(1.0-X)*(1.0-X)/(RDL*D)
      DPDLGF(ALFA) =-((RDG-RDL)*ALFA + RDL)/144.0
      BGF(X,ALFA) = (-1.6628E-11)*((1.0-X)*(1.0-X)/((1.0-ALFA)*RDL) +
     1      X*X/(ALFA*RDG))
      XTTF(X) = (((1.0 -X)/X)**0.9)*((RDG/RDL)**0.5)*(MUL/MUG)**0.1
C
      A = 0.7854 *D*D                                                   (FT2)
      QTP = QP/A                                                        B/HR-FT3
C
      PO(1) = PBB
      ZO(1) = ZBB
      X(1) = 0.0
      P = ALOG(PBB)
      V(1) = 1.0/RDLF(P)
      J(1) = G * V(1)
      OMI = QTP * (1.0/RDGF(P) - V(1))/HFGF(PBB)
      HE = HLF(PBB)
      XTTE = 1.0E+30
      ALFAE = 1.0E-10
C
      DO 999 I = 1,59
      HI = HE
      PI = PO(I)
      PEFIN = PI
  111 PE = PEFIN
      EI = (EXP(OMI*DT) - 1.0)/OMI
      DZ = J(I) * EI
      HE = HI + QTP*DZ/G
      XE = (HE - HLF(PE))/HFGF(PE)
      IF(XE .GE. 1.0) GO TO 997
C
C     CALCULATE PRESSURE DROP USING THE LOCKHART-MARTINELLI CORRELATION
C
      P = ALOG(PE)
      RDL = RDLF(P)
      RDG = RDGF(P)
      MUL = MULF(P)
      MUG = MUGF(P)
C
      XTTI = XTTE
      XTTE = XTTF(XE)
      DPDLF = FI2LF(0.5*(XTTI+XTTE))*DPDLFF(0.5*(X(I)+XE))
      DPDLFR(I) = DPDLF/G**1.8
      ALFAI = ALFAE
      ALFAE = ALFAF(XTTE)
      DPDLGR(I) = DPDLGF(0.5*(ALFAI+ALFAE))
      DPAC(I) = BGF(XE     , ALFAE) - BGF(X(I), ALFAI)
      DP = (DPDLF + DPDLGR(I))*DZ + DPAC(I)*G*G
      PEFIN = PI + DP
      IF(PEFIN .LE.PEX) PEFIN = PEX
      P = ALOG(PEFIN)
      VL = 1.0/RDLF(P)
      VG = 1.0/RDGF(P)
      V(I+1) = VL + XE*(VG-VL)
      OMI = ALOG(V(I+1)/V(I))/DT
      IF(ABS(PEFIN-PE)/PEFIN - 0.002) 112,112,111
  112 PO(I+1) = PEFIN
      OM(I) = OMI
      E(I) = (EXP(OMI*DT) - 1.0)/OMI
      B(I) = (E(I) - DT)/OMI
      X(I+1) = XE
      J(I+1) = G*V(I+1)
      ZO(I+1) = ZO(I) + DZ
      IF(ZO(I+1) - ZMAX) 999,998,998
  998 IMAX = I + 1
      RETURN
  999 CONTINUE
C     IMAX = 1000 IS USED AS A CODE TO INDICATE THAT EXIT WAS NOT REACHED
      IMAX = 1000
      DTSEC = 3600.0 * DT
      WRITE(6,1) ZO(60), DTSEC
    1 FORMAT('0************ STAPR2 ***** 60 ITERATIONS COMPLETED WITHOU
     1T REACHING ZMAX, ZO(60) =', F10.5 /
     2       '                 DT(SEC) = ', F10.5 //)
      RETURN
  997 IMAX = I
      WRITE(6,2) IMAX, ZO(IMAX)
    2 FORMAT('0********** STAPR2 ******** A QUALITY LARGER THEN 1.0 '
     1      , 'WAS OBTAINED BEFORE REACHING ZMAX, ZO(', I2, ') =',
     2      F8.5 //)
      RETURN
      END
```

```
      SUBROUTINE DYNPR1 (KMAX)
C                                                    VERSION 1.3  11/07/69
C     SUBROUTINE DYNPR1 CALCULATES THE PRESSURE DROP IN THE SINGLE-PHASE
C     REGION IN A NON-LINEAR FASHION
C
C     Z(I,K) AND G(I,K) FOR K =1,KMAX ARE INPUT TO THIS SUBROUTINE
C     P(I,K) FOR K =1,KMAX IS THE OUTPUT
C
      REAL MULB, MULTF, KLF, MULW
      COMMON // D, GP, GO, ZBB, ZMAX, P1 , PBB, PEX, TIN, DTSUBB, DT
      COMMON /DYNPR/ Z(40,120), DZDT(40,120), G(40,120), P(40,120)
C
C     PROPERTY FUNCTIONS REQUIRED : ROLTF, MULTF, KLF
C
      TI(T) = 1.0 / (T + 459.6)
      MULTF(T)= EXP( - .5483695 E 01  + .5585921 E 04*TI(T)              MULTF1/2
     1        - .1950534 E 07*TI(T)**2  + .3577018 E 09*TI(T)**3)        MULTF2/2
      ROLTF(T) =   .1035453 E 03 - .7105255 E-01*T - .6448694E-04*T*T    ROLTF1/1
      KLF(T) = 0.0475 - 6.76667E-05* T                                   KLF  1/1
C
      TAV = TIN + 0.5*DTSUBB
      RCL = ROLTF(TAV)
      ROLIN = ROLTF(TIN)
      MULB = MULTF(TAV)
      DTINCO = 1.0/((3600.0*3600.0*32.17*144.0)*DT)
      DTFILM = (282.0*1.291667)*GP*MULB**0.4/(GO**0.8*KLF(TAV)**0.6)
      TWAV = TAV + DTFILM
      MULW = MULTF(TWAV)
      RE = GO*D/MULB
      DPOLGR = -RCL/144.0
      DPOLFR = (-3.3256E-11)*FF(RE)*(GO**0.2)*(MULW/MULB)**0.14/(RCL*D)
C
      PBB2 = (DPOLFR*GO**1.8 + DPOLGR)*ZBB + P1
      IF(ABS(PBB2-PBB)/PBB .GE. 0.02) WRITE(6,1) PBB,PBB2
    1 FORMAT('0**********STEADY STATE SINGLE PHASE PRESSURE DROP AS '
     *       ,'CALCULATED BY DYNPR1 DOES NOT AGREE WITH SUBCBB VALUE :'/
     2       30X, 'PBB(SUBCBB) =', F10.4, 10X, 'PBB(DYNPR1) =', F10.4,
     3       '  PSIA' //)
      KMAX1 = KMAX -1
      DPFR01 = -7.01E-10*MULTF(TIN)**0.2/ROLIN
      P1P = P1 - DPFR01*GO**1.8
C
      DO 99 K = 1,KMAX1
      G18 = G(1,K)**1.8
      DGDT = (G(1,K+1)-G(1,K))*DTINCO
      DP01FI = DPFR01*G18 - DGDT*2.3
      DP = (DPOLFR*G18 + DPOLGR - DGDT)*Z(1,K) + DP01FI
   99 P(1,K) = P1P + DP
      RETURN
      END
```

```
      SUBROUTINE DYNPR2 (IMAX, KMAX, KMAX2)
C                                                    VERSION 1.5   11/07/69
C     SUBROUTINE DYNPR2 CALCULATES TIME DEPENDENT PRESSURE DROP IN A
C     TWO-PHASE CHANNEL ACCORDING TO THE ENTHALPY TRAJECTORY MODEL
C
C     INPUT : Z(I,K), P(I,K), DZDT(I,K), G(I,K), K=1,KMAX : VALUES AT THE
C                     STARTING POINT (USUALLY THE BB), AND
C                OM(I), E(I), B(I), DPDLFR(I), DPDLGR(I), DPAC(I),
C                     FOR I = 1, IMAX - 1
C                V(I) FOR I = 1, IMAX  AND DT. : REFERENCE STEADY-STATE
C                     PARAMETERS
C
      REAL  JI(120),  JZI(120), DZI(120)
      COMMON// D, GP, GO,ZBB, ZMAX, P1 , PBB, PEX, TIN, DTSUBB, DT
      COMMON /DYNPR/ Z(40,120), DZDT(40,120), G(40,120), P(40,120)
      COMMON /STA2DT/ OM(60), B(60), E(60), X(60), ZD(60), PD(60),
     1      DPDLFR(60), DPDLGR(60), DPAC(60), V(60), AJD(60)
C
      IMAX1 = IMAX - 1
      KMAX1 = KMAX
      DTINV = 1.0/DT
      DTINCO = 1.0/((3600.0*3600.0*32.17*144.0)*DT)
C
C     CALCULATE THE VOLUMETRIC FLUX DENSITIES AT THE B.B. . . . . .
C
      DO 89 K = 1,KMAX
   89 JI(K) = G(1,K) * V(1)
C
C     MAJOR LOOP
C
      DO 999 I =1,IMAX1
C
C       DETERMINE RELATIVE VELOCITIES AT INLET
C
      DO 99 K = 1, KMAX1
   99 JZI(K) = JI(K) - DZDT(I,K)
C
C     CALCULATE MASS FLUX, VELOCITIES AND COORDINATES OF MESH POINTS
C
      KMAX1 = KMAX1 - 1
C
      DO 98 K = 1,KMAX1
      SIK = (JZI(K+1) - JZI(K)) * DTINV
      DZI(K) = E(I) * JZI(K) + B(I) * SIK
C
C     CALCULATE VALUES FOR NEXT SPACE STEP . . . . . .
C
      JI(K) = JI(K+1) + OM(I) * DZI(K)
C     JI(K) HERE IS REDEFINED AS J(I+1,K)
      G(I+1,K) = JI(K) / V(I+1)
      Z(I+1,K) = Z(I,K+1) + DZI(K)
   98 DZDT(I+1,K) = DZDT(I,K+1) + E(I)*SIK
C
C     CALCULATE PRESSURE DROP AND PRESSURE . . . . . .
C
      KMAX2 = KMAX1 - 1
      GAVIK1 = (G(I+1,1) + G(I,2))*0.5
C
      DO 97 K =1,KMAX2
      GAVIK = GAVIK1
      GAVIK1 = (G(I+1,K+1) + G(I,K+2))*0.5
      DPIK = (DPDLFR(I)*GAVIK**1.8 + DPDLGR(I) - (GAVIK1-GAVIK)*DTINCO)
     1      *DZI(K) + DPAC(I)*GAVIK**2
   97 P(I+1,K) = P(I,K+1) + DPIK
  999 CONTINUE
      RETURN
      END
```

```
      SUBROUTINE PRTPL3(NO,B,   N,M,   NL,NS,    KX,JX,    YSC)          VERSION4
C
C     PRTPL3 IS A MODIFIED VERSION OF A SUBROUTINE SUPPLIED BY THE
C     INFORMATION PROCESSING CENTER AT MIT.  PRINTER PLOTS ARE PRODUCED
C     AND THE EXTREMA OF THE GIVEN FUNCTIONS ARE DETERMINED.
C
      DIMENSION CUT(101),YPR(11),IANG(9),A( 480), B(KX,JX)
      INTEGER  CUT,     IANG/'*','G','2','4','5','6','7','8','9'/
      COMMON/PLOTCT/ XMAXJ(9), YMAXJ(9), XMINJ(9), YMINJ(9), YRANJ(9)   VER. 4.1
C
    1 FORMAT(I1, 60X,7H CHART ,I3,/)
    2 FORMAT(1H, F11.4  , 5X, 101A1, I12)
    3 FORMAT(1H, 117X, I12)
    4 FORMAT('0PRTPL3 :  MIN ORDINATE =',   F12.5, ' AT ABSCISSA =',
     1        F12.5, '  (CURVE NO', I2, ')', 1X, A1 /
     2     11X, 'MAX ORDINATE =',   F12.5, ' AT ABSCISSA =',   F12.5,
     3                              30X, 'ORDINATE RANGE =', F12.5)
    7 FORMAT(1H ,16X,101H.         .         .         .         .
     1    .         .         .         .         .)
    8 FORMAT(1H ,9X,11F10.4)
C
      IADV = 0
      IF(YSC .GT. 0.0) IADV = 1
      WRITE(6,1) IADV, NO
      MY = M - 1
C
C     DETERMINE EXTREMA OF EACH CURVE. . . . . .
C
      DO 45 J = 2,M
      YMIN=1.0E75
      YMAX=-1.0E75
      DO 40 K = 1,N
      IF(B(K,J) - YMAX) 41,41,42
   42 YMAX = B(K,J)
      XMAX = B(K,1)
   41 IF(B(K,J) - YMIN) 43,40,40
   43 YMIN = B(K,J)
      XMIN = B(K,1)
   40 CONTINUE
      XMINJ(J-1) = XMIN
      XMAXJ(J-1) = XMAX
      YMINJ(J-1) = YMIN
      YMAXJ(J-1) = YMAX
   45 YRANJ(J-1) = YMAX - YMIN
C
C     PLOT THE DATA . . . . . .
C
      IF(YSC .LE. 0.0) GO TO 91
      YMAX=-1.0E75
      YMIN=1.0E75
      DO 49 J = 1,MY
      IF(YMAXJ(J) .GT. YMAX) YMAX = YMAXJ(J)
      IF(YMINJ(J) .LT. YMIN) YMIN = YMINJ(J)
   49 CONTINUE
      YRANGE = YMAX - YMIN
      I=1
      DO 39 J=1,M
      DO 39 K=1,N
      A(I)=B(K,J)
   39 I=I+1
      NLL=NL
      IF(NS) 16, 16, 10
   10 DO 15 I=1,N
      DO 14 J=I,N
      IF(A(I)-A(J)) 14, 14, 11
   11 L=I-N
      LL=J-N
      DO 12 K=1,M
      L=L+N
      LL=LL+N
      F=A(L)
      A(L)=A(LL)
   12 A(LL)=F
   14 CONTINUE
   15 CONTINUE
   16 IF(NLL) 20, 18, 20
   18 NLL=50
   20 WRITE(6,7)
      BLANK=0
      XSCAL=(A(N)-A(1))/(FLOAT(NLL-1))
      YSCAL = 0.01 * YRANGE
      IF(YSCAL .EQ. 0.0) YSCAL = 1.0
      IF((YSC .GT. YRANGE) .AND. (YRANGE .GT. YSC/10.0)) YSCAL=0.01*YSC
      XR=A(1)
      L=1
      DO 80 I=1,NLL
      F=I-1
      XPR=XR+F*XSCAL
      IF(A(L)-XPR-XSCAL*0.5) 50,50,70
   50 DO 55 IX=1,101
   55 CUT(IX)=BLANK
   57 CONTINUE
      DO 60 J=1,MY
   56 LL=L+J*N
      JP=((A(LL)-YMIN)/YSCAL)+1.0
      CUT(JP)=IANG(J)
   60 CONTINUE
      IF(L.EQ.N)  GO TO 61
      L=L+1
      IF(A(L)-XPR-XSCAL*0.5)  57,57,61
   61 CONTINUE
      WRITE(6,2)XPR,(CUT(IZ),IZ=1,101), I
      GO TO 80
   70 WRITE(6,3) I
   80 CONTINUE
      WRITE(6,7)
      YPR(1)=YMIN
      DO 90 KN=1,10
   90 YPR(KN+1)=YPR(KN)+YSCAL*10.0
      WRITE(6,8)(YPR(IP),IP=1,11)
C
C     WRITE THE VALUES OF THE MINIMUM AND MAXIMUM OF EACH CURVE
C
   91 DO 92 J = 1,MY
   92 WRITE(6,4) YMINJ(J),XMINJ(J),J,IANG(J),YMAXJ(J),XMAXJ(J),YRANJ(J)
      RETURN
      END
```

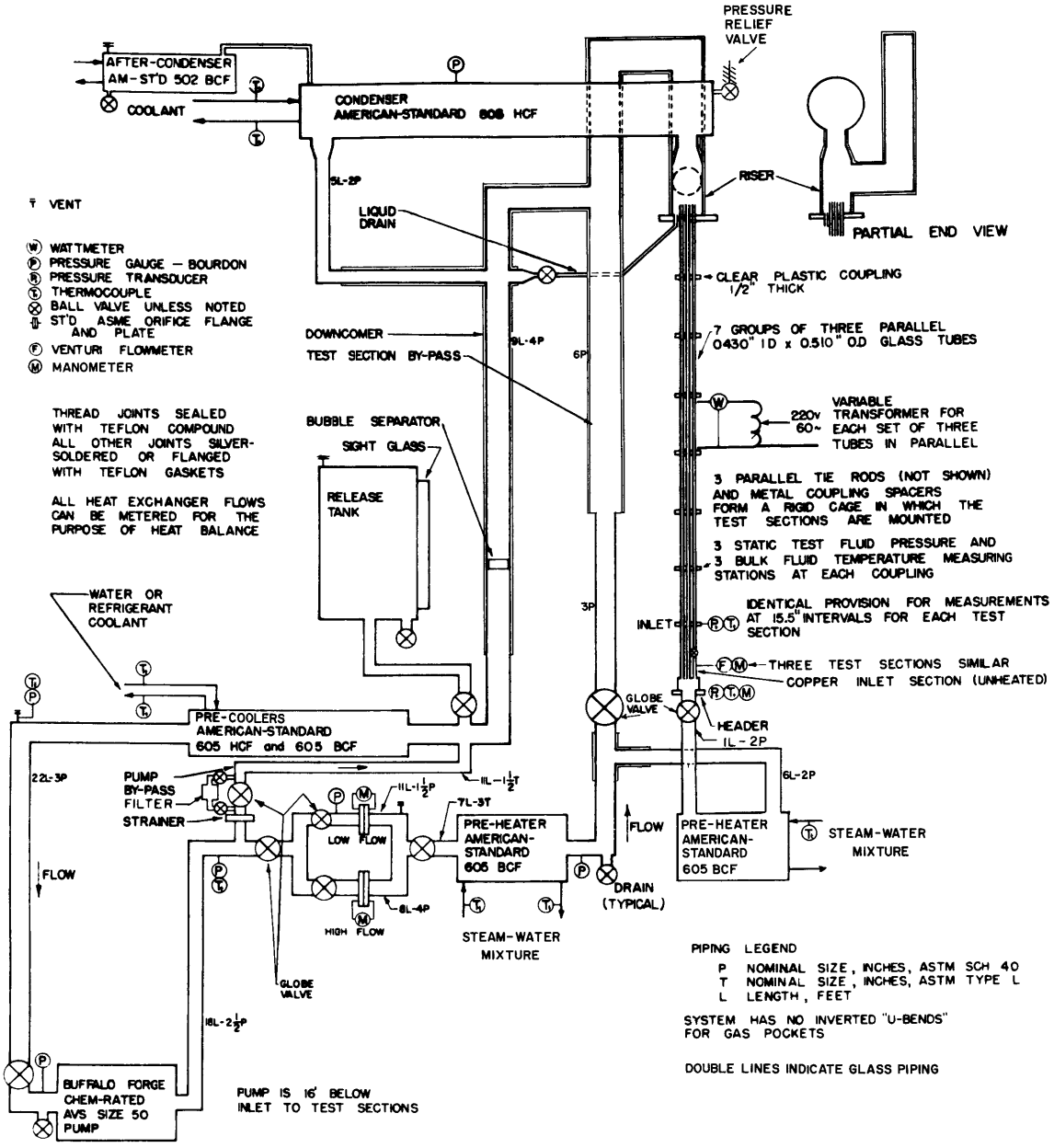

FIG 2.1 SCHEMATIC OF APPARATUS, WITH OVERALL DIMENSIONS

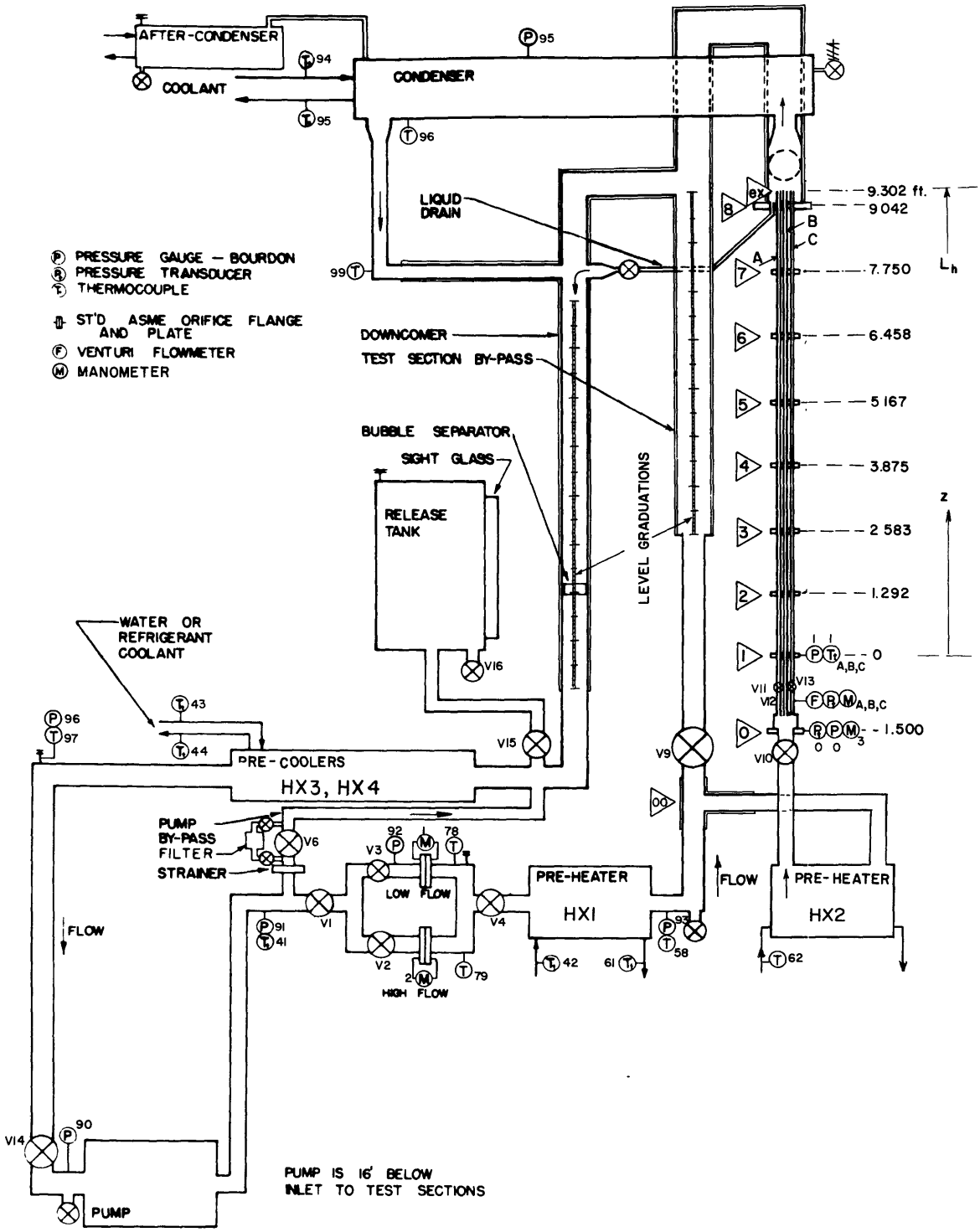

FIG. 2.2 CODING OF LOOP EQUIPMENT AND TEST SECTION DIMENSIONS

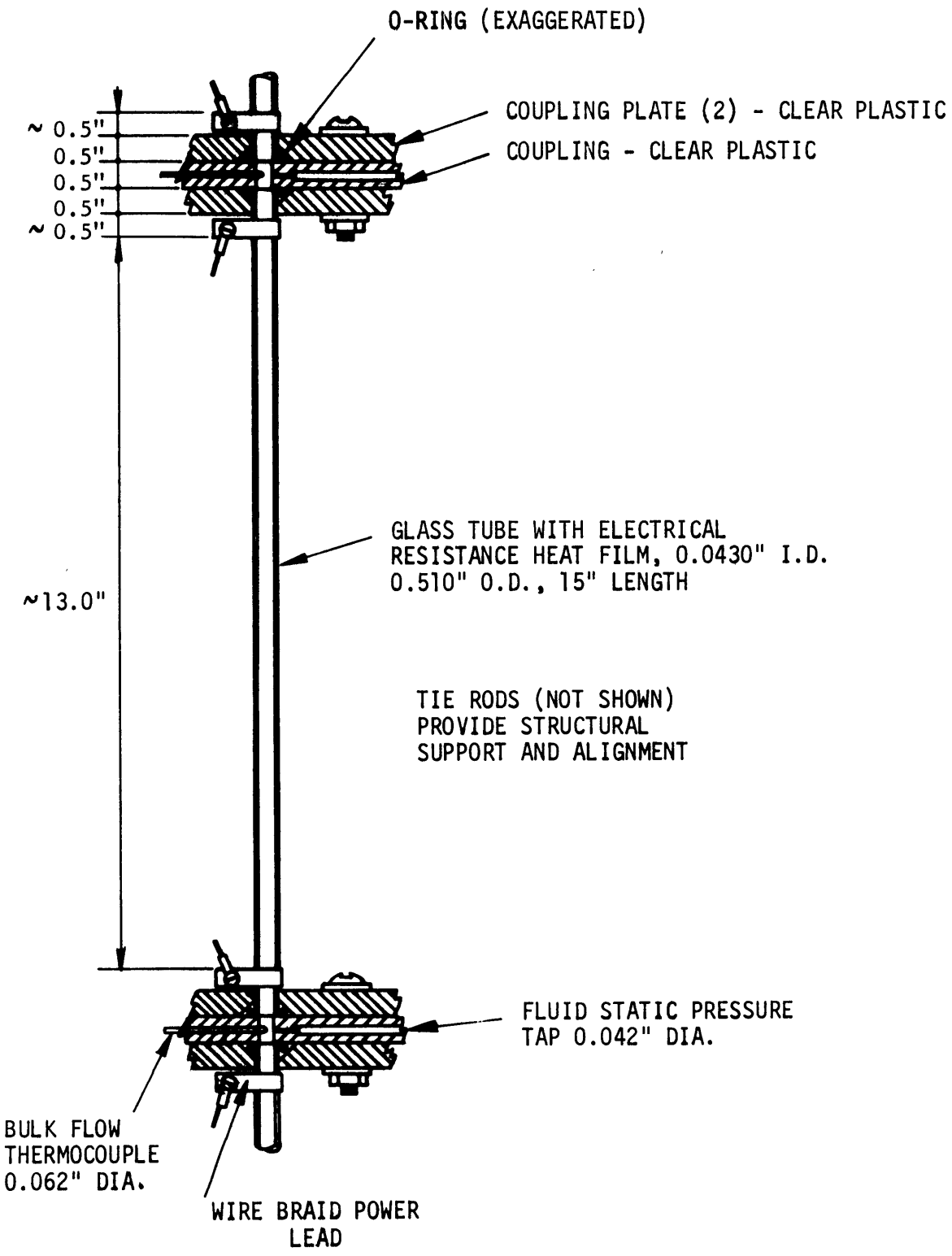

FIG. 2.3 CROSS-SECTIONAL DETAIL OF TEST LENGTH AND COUPLING

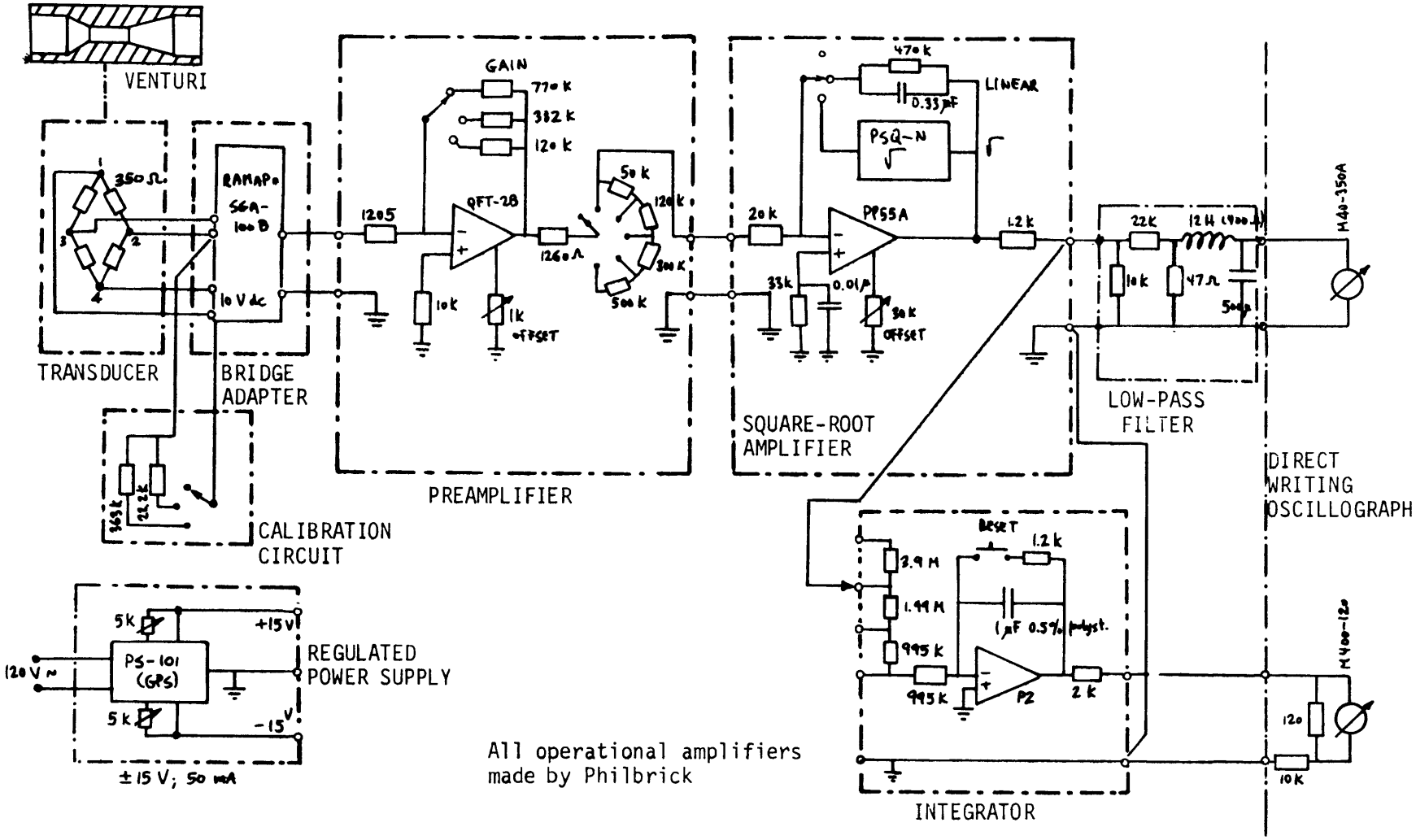

FIG. 2.4 FLOW MEASURING INSTRUMENTATION

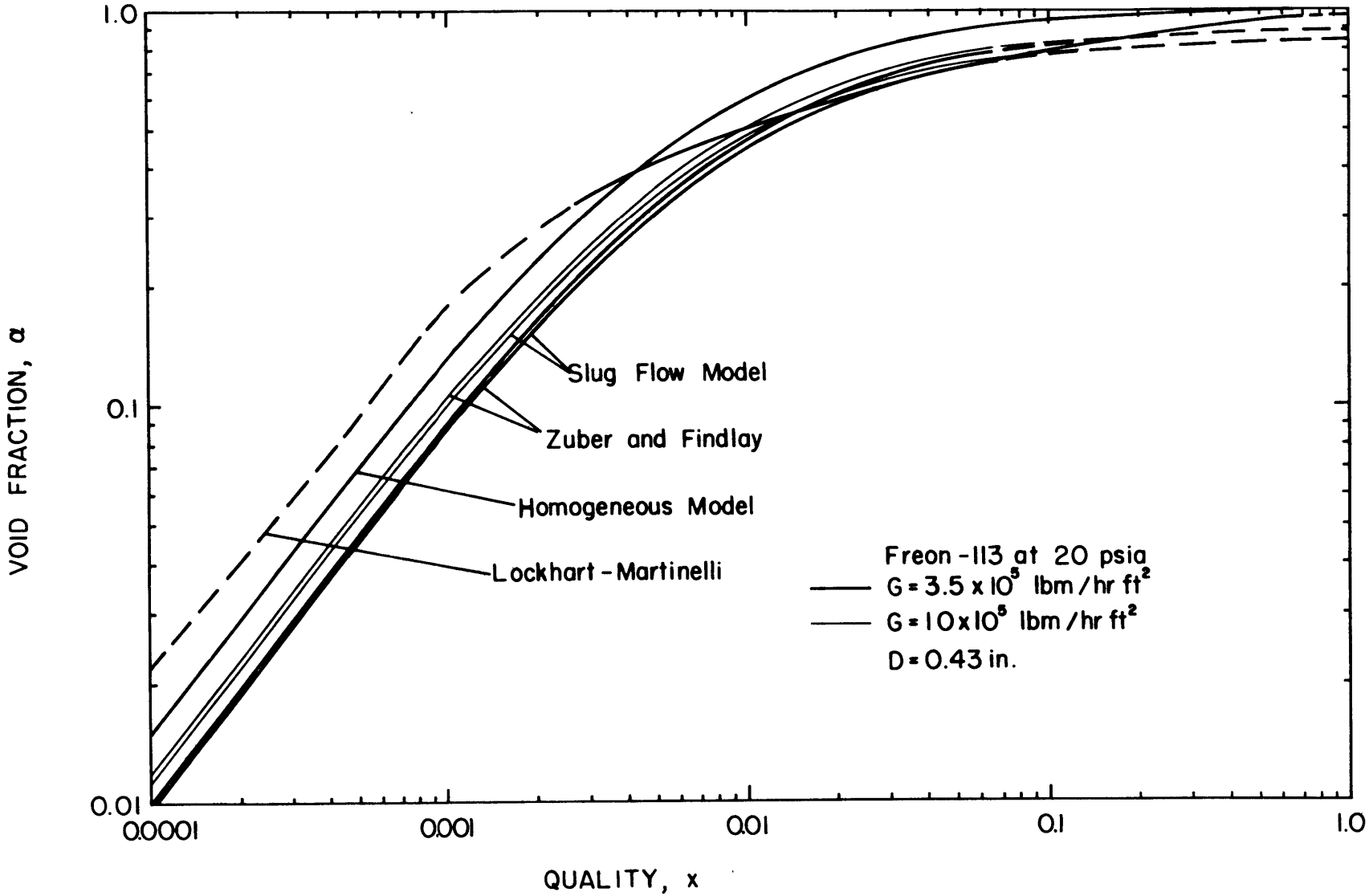

FIG. 3.1 COMPARISON OF VOID FRACTION CORRELATIONS

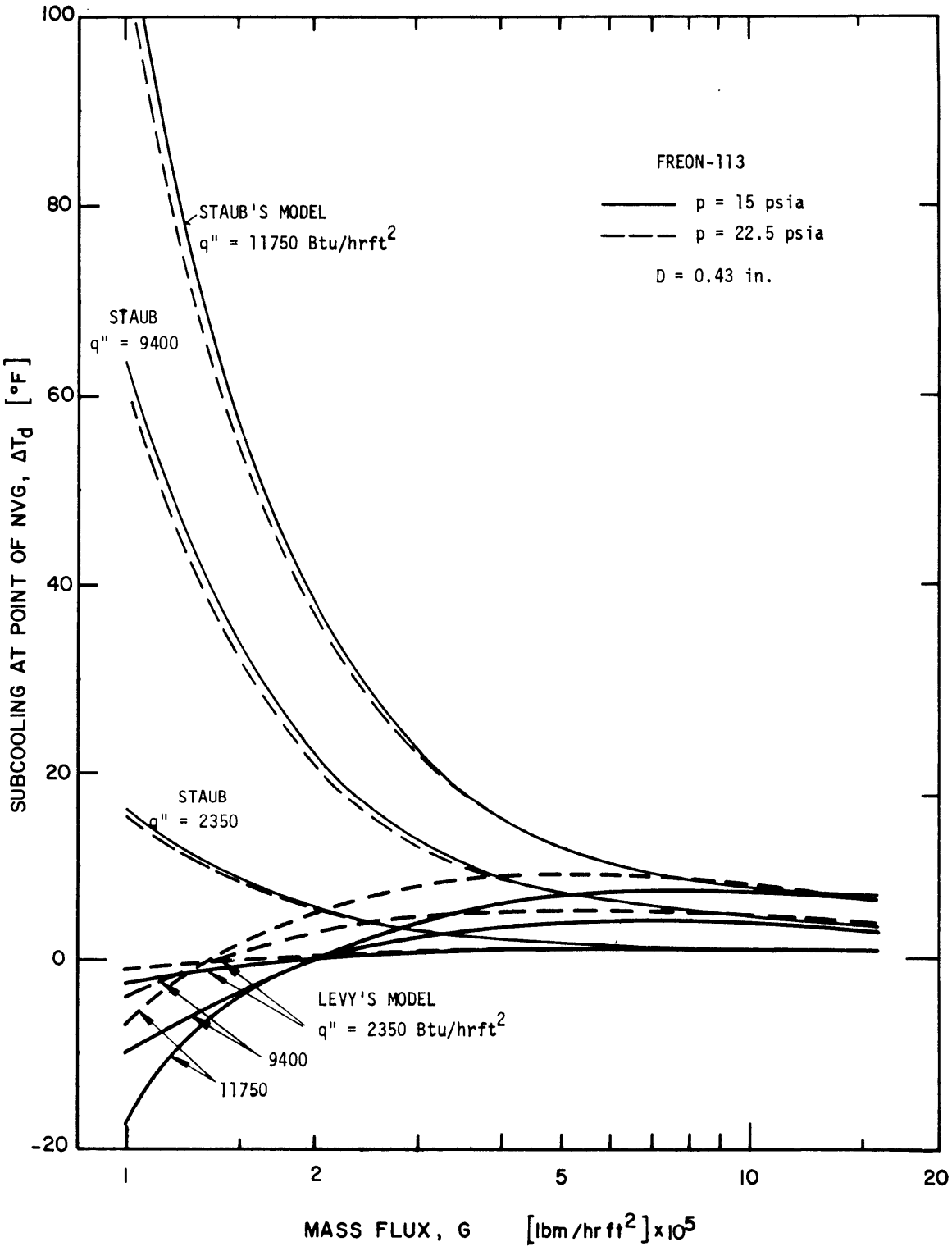

FIG. 3.2 POINT OF NET VAPOR GENERATION AS PREDICTED BY TWO MODELS

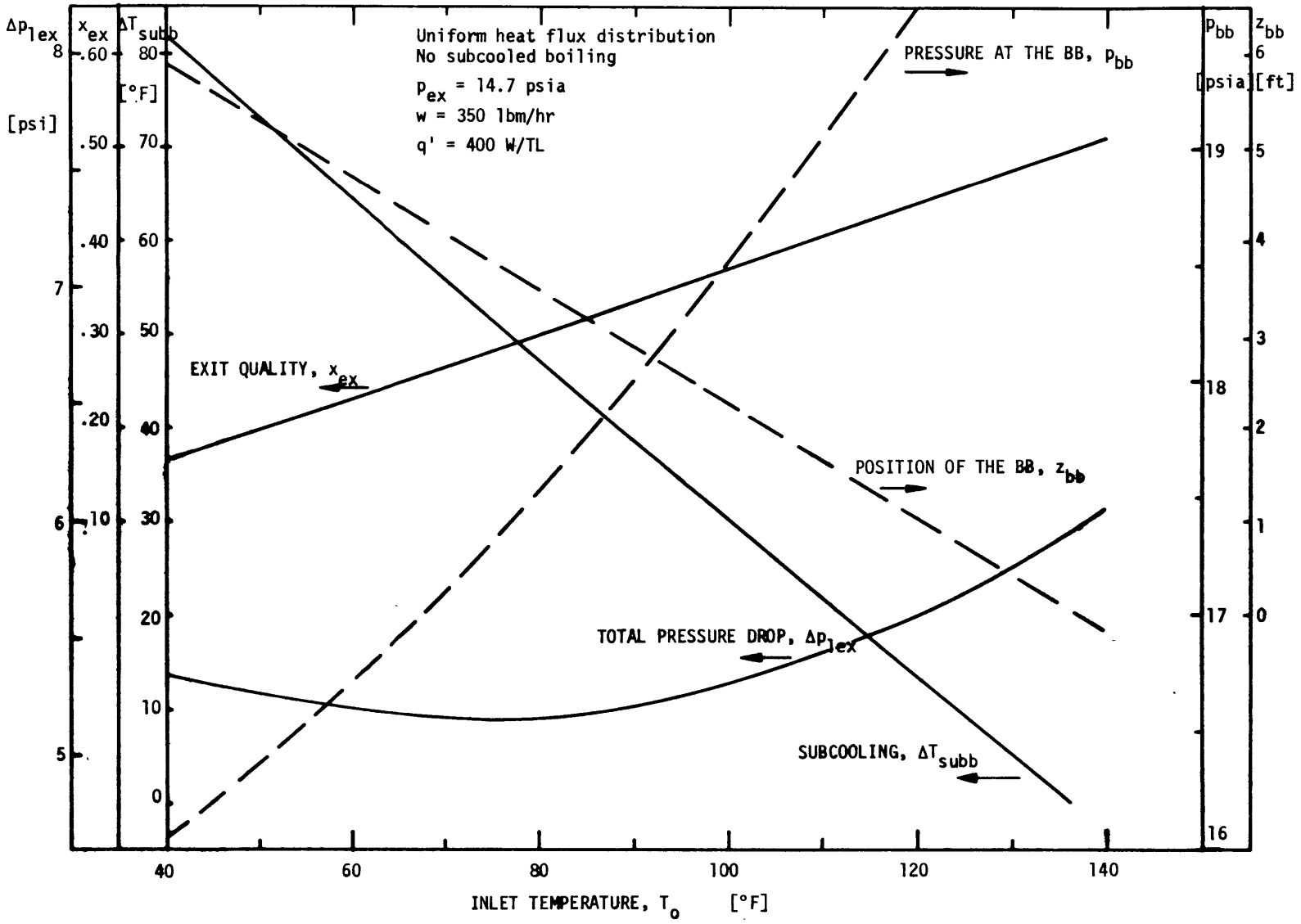

FIG. 3.3 EFFECT OF THE INLET TEMPERATURE ON VARIOUS PARAMETERS

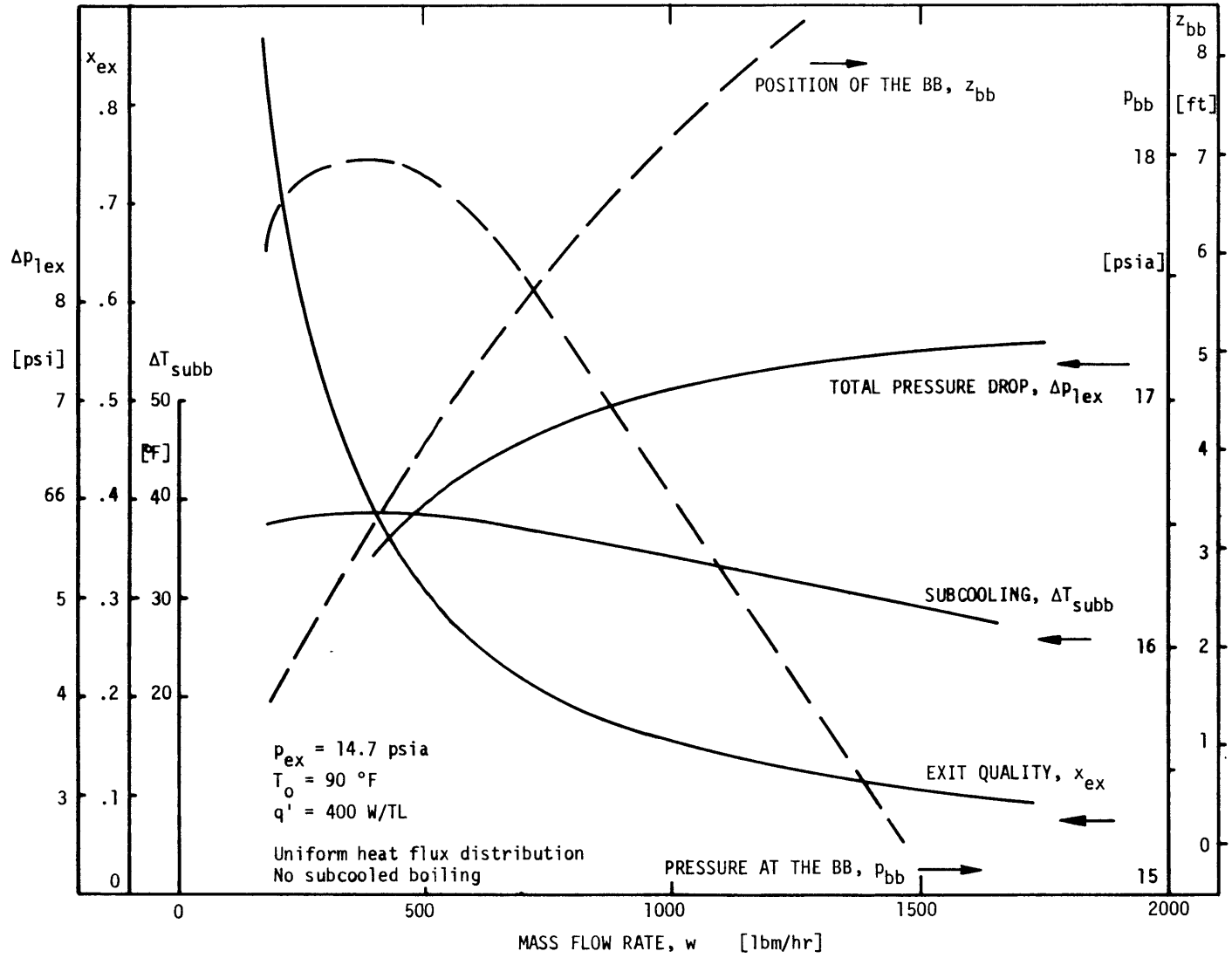

FIG. 3.4 EFFECT OF THE MASS FLOW RATE ON VARIOUS PARAMETERS

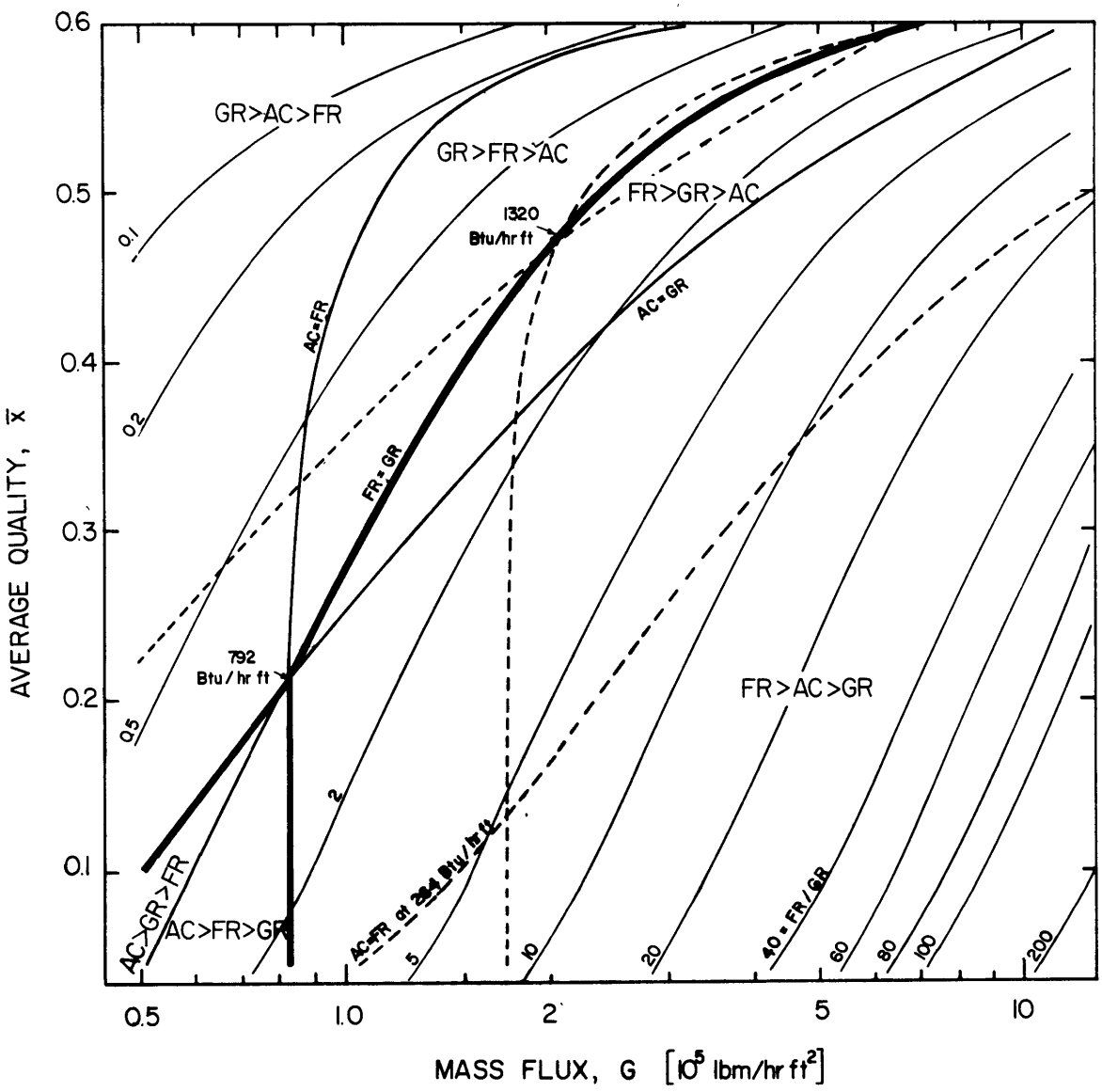

FIG. 3.5 RELATIVE IMPORTANCE OF THE FRICTION, GRAVITY AND ACCELERATION TERMS. CONTOUR MAP AT 792 Btu/hr ft

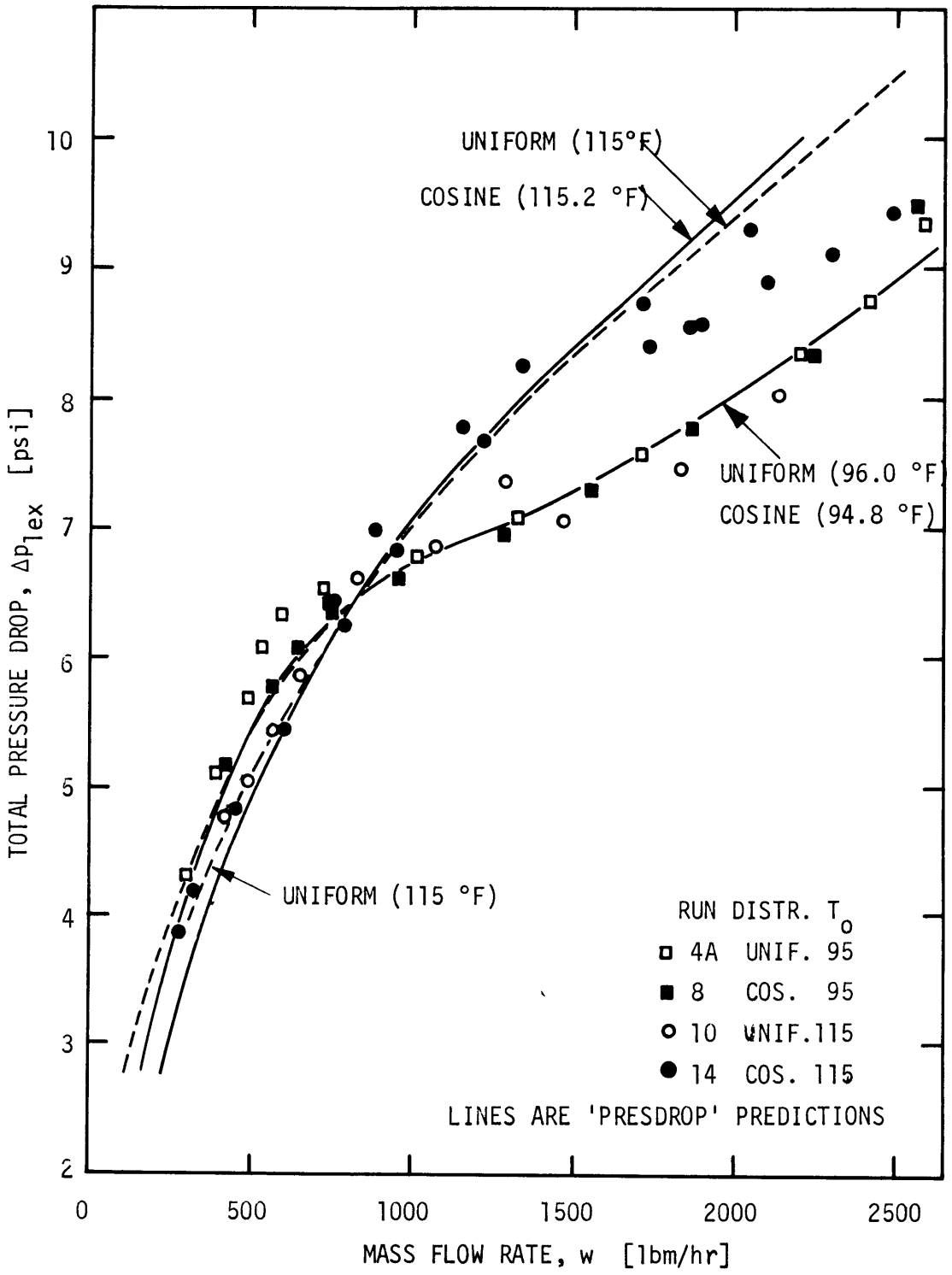

FIG. 4.1 PREDICTED AND MEASURED TOTAL PRESSURE DROP AT $q'' = 4700$ Btu/hrft^2

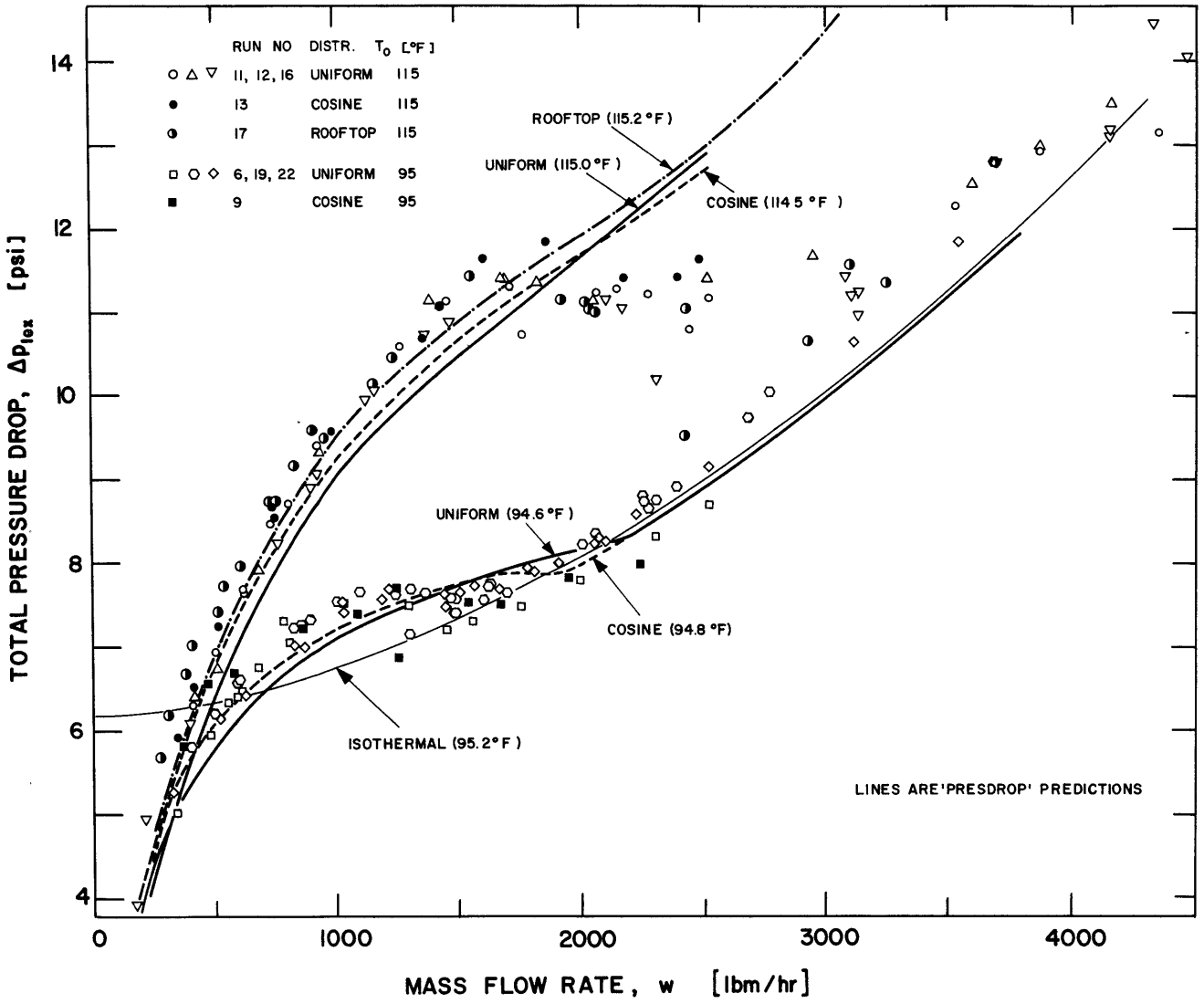

FIG. 4.2 PREDICTED AND MEASURED TOTAL PRESSURE DROP AT $q'' = 9400$ Btu/hrft^2

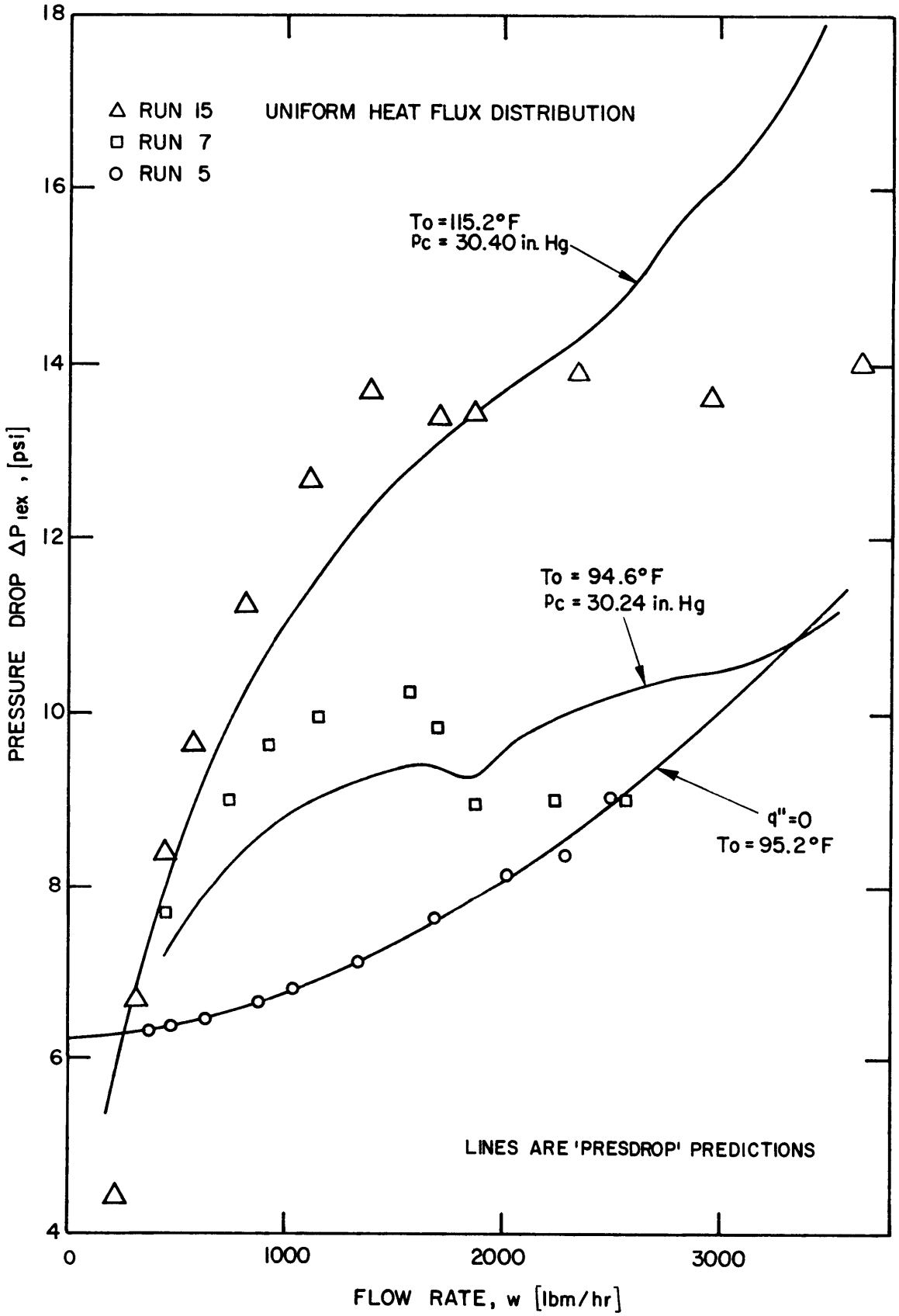

FIG. 4.3 PREDICTED AND MEASURED TOTAL PRESSURE DROPS AT $q'' = 14100$ Btu/hr ft^2

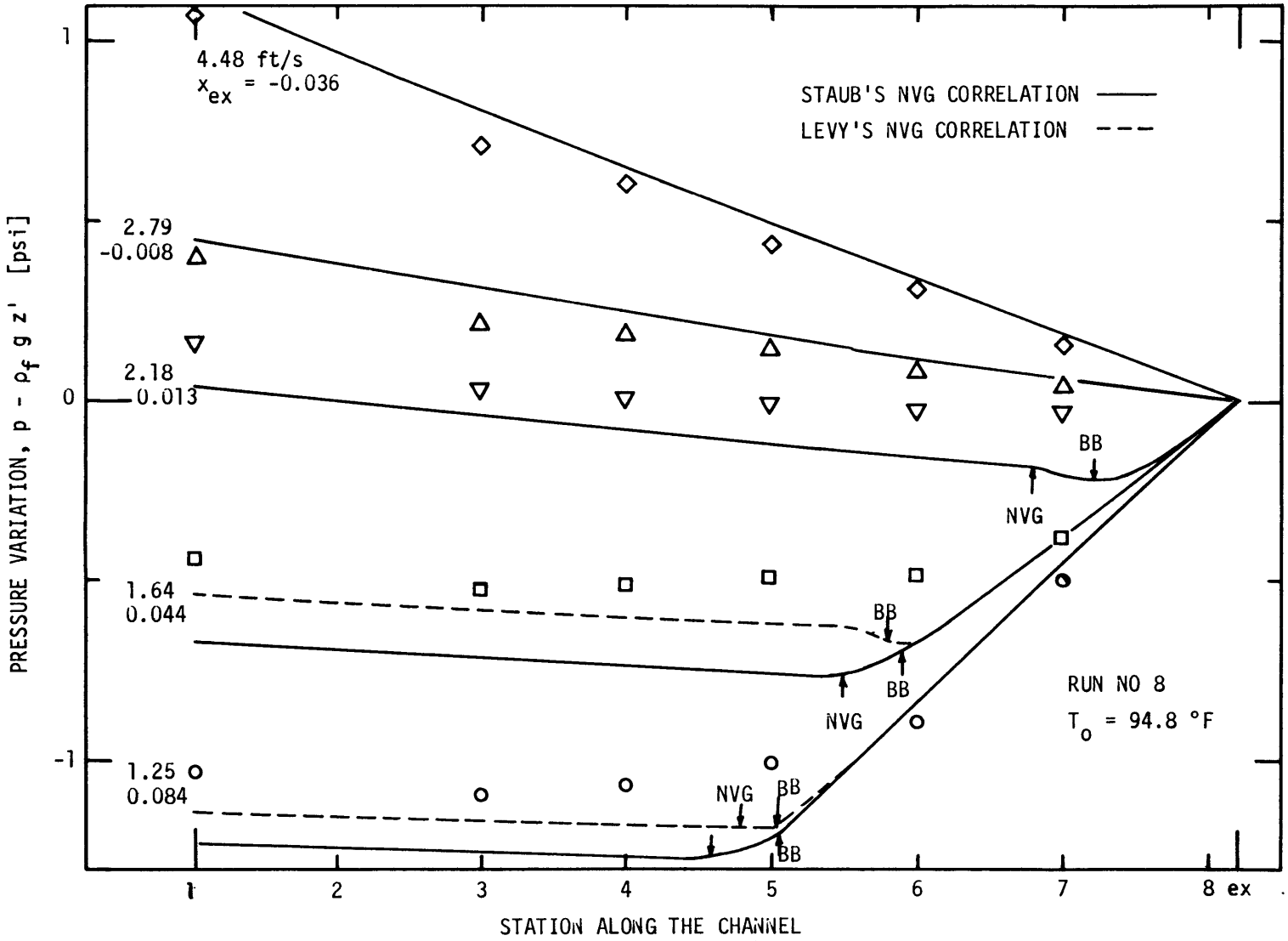

FIG. 4.4 PRESSURE PROFILES AT 4700 Btu/hrft^2, COSINE HEAT FLUX DISTRIBUTION

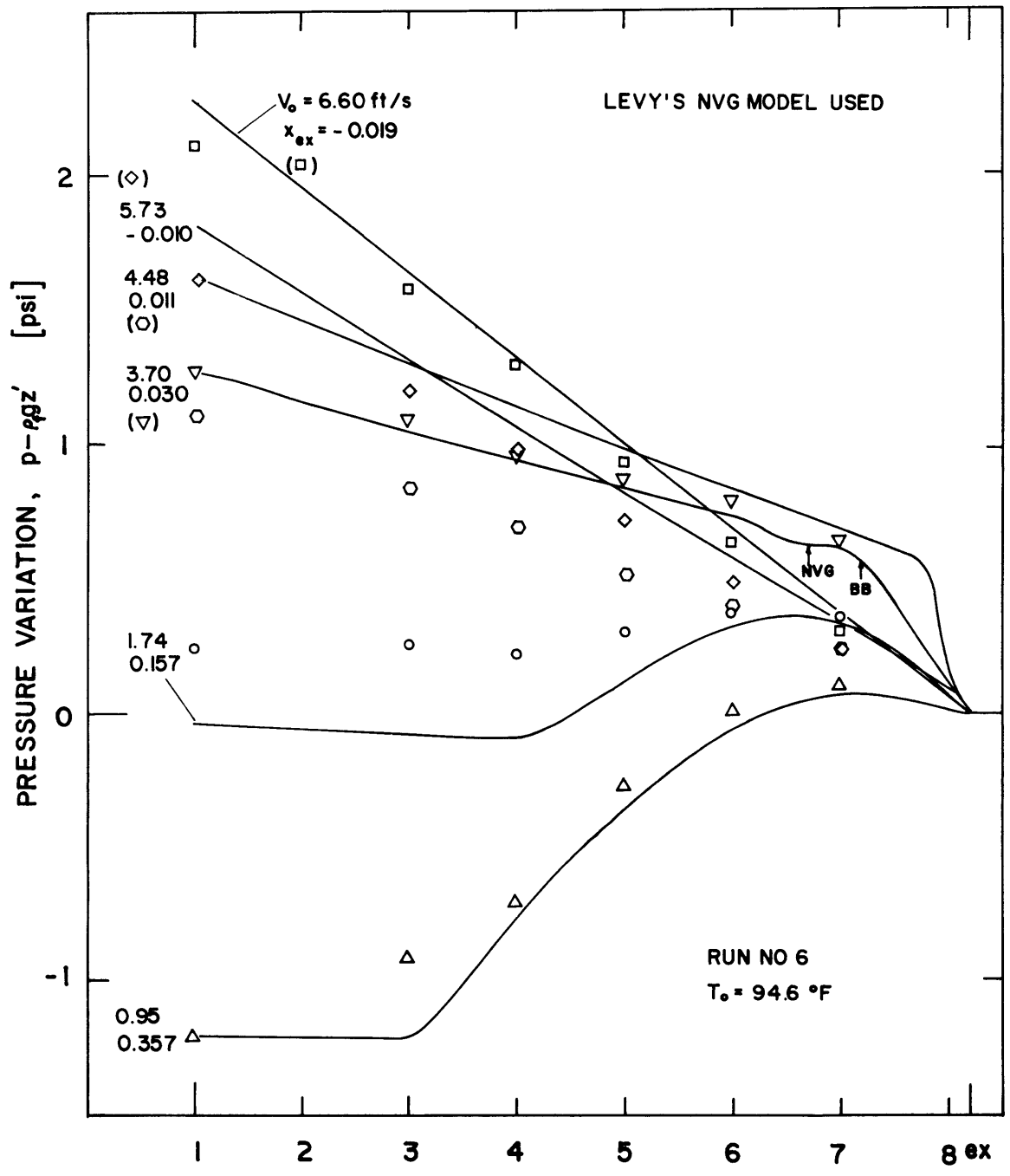

FIG. 4.5 PRESSURE PROFILES AT 9400 Btu/hr ft^2, UNIFORM HEAT FLUX DISTRIBUTION

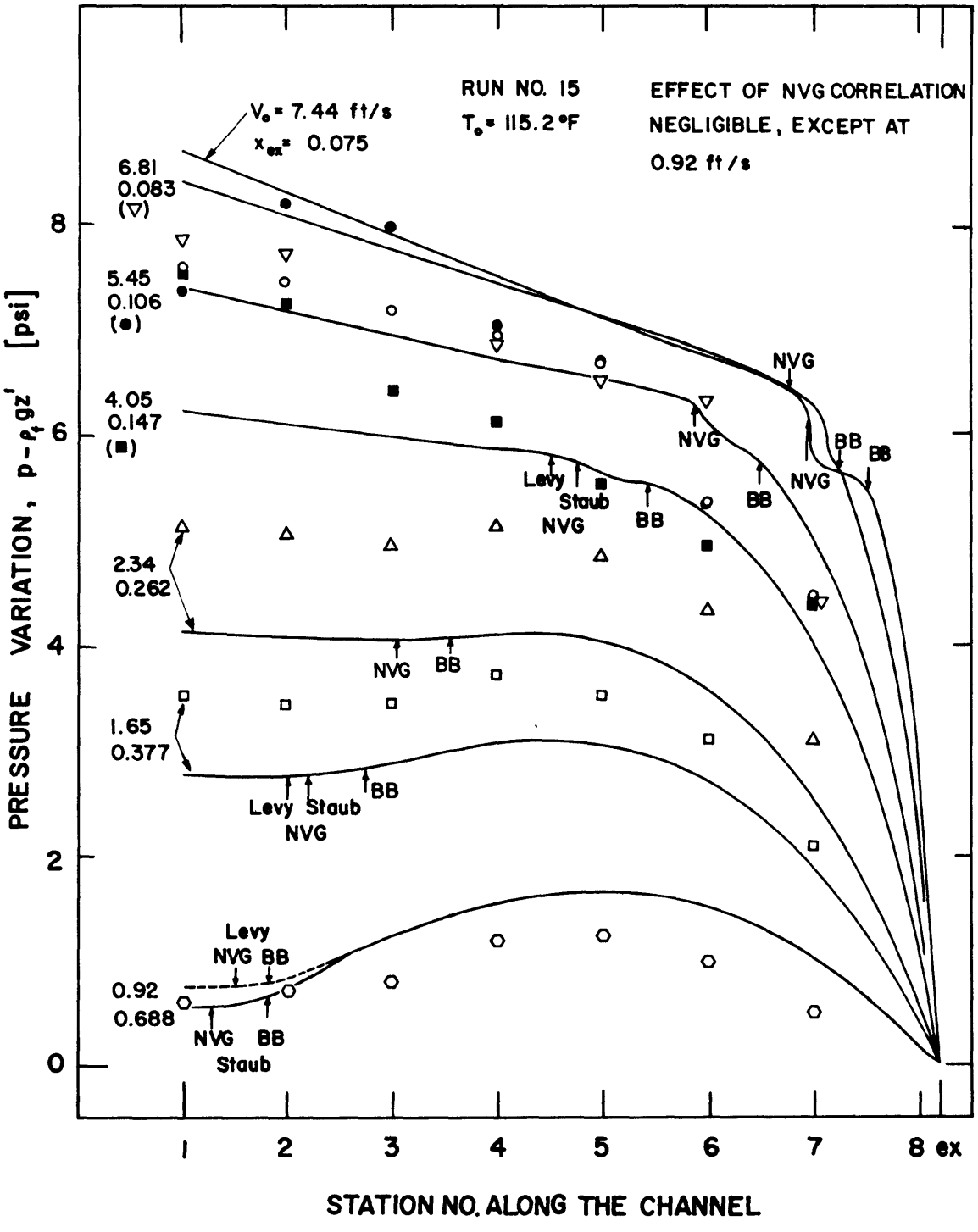

FIG. 4.6 PRESSURE PROFILES AT 14,100 Btu/hr ft^2, UNIFORM HEAT FLUX DISTRIBUTION

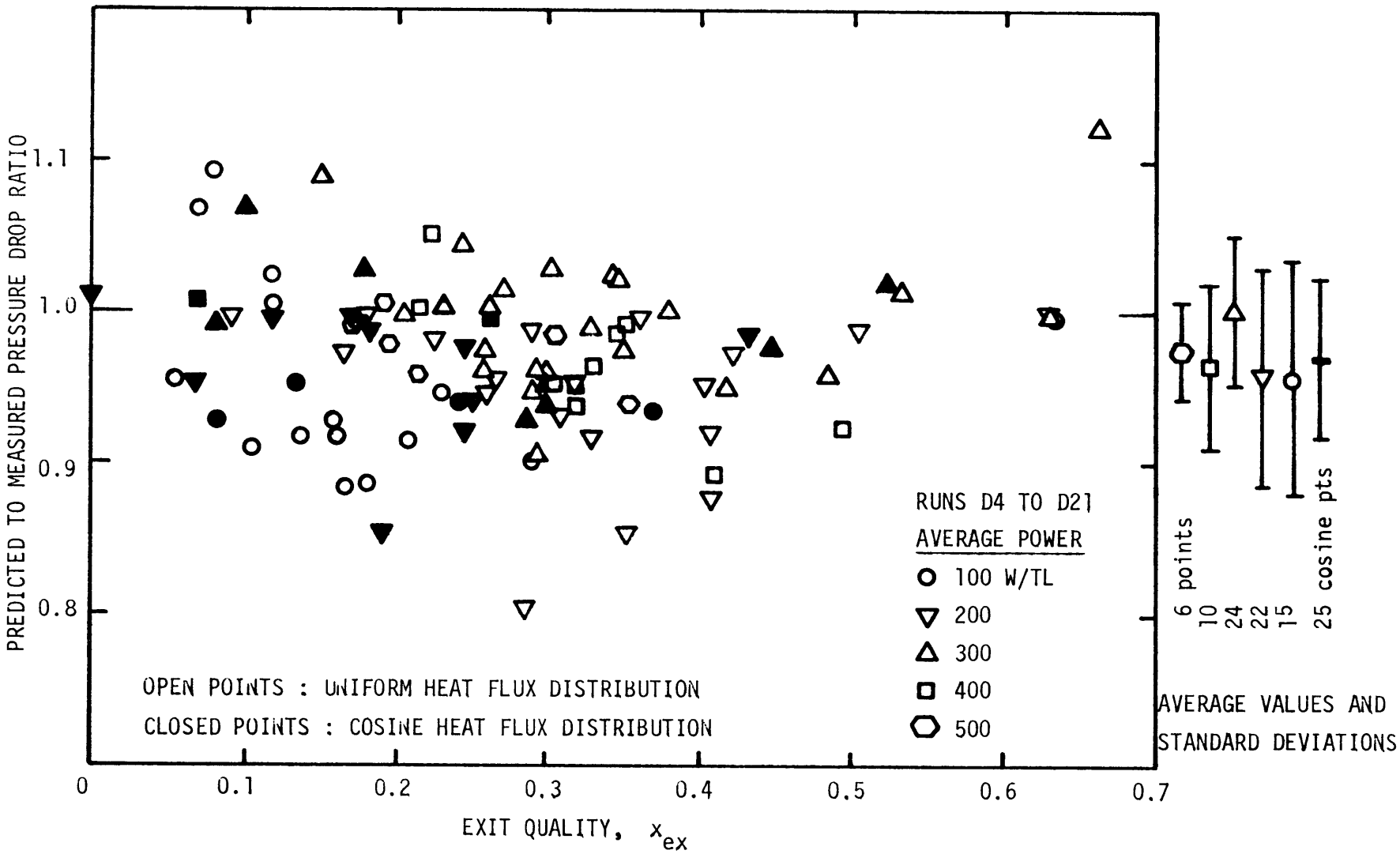

FIG. 4.7 ACCURACY OF THE PRESSURE DROP PREDICTIONS FOR ALL THRESHOLD AND TRANSITION POINTS

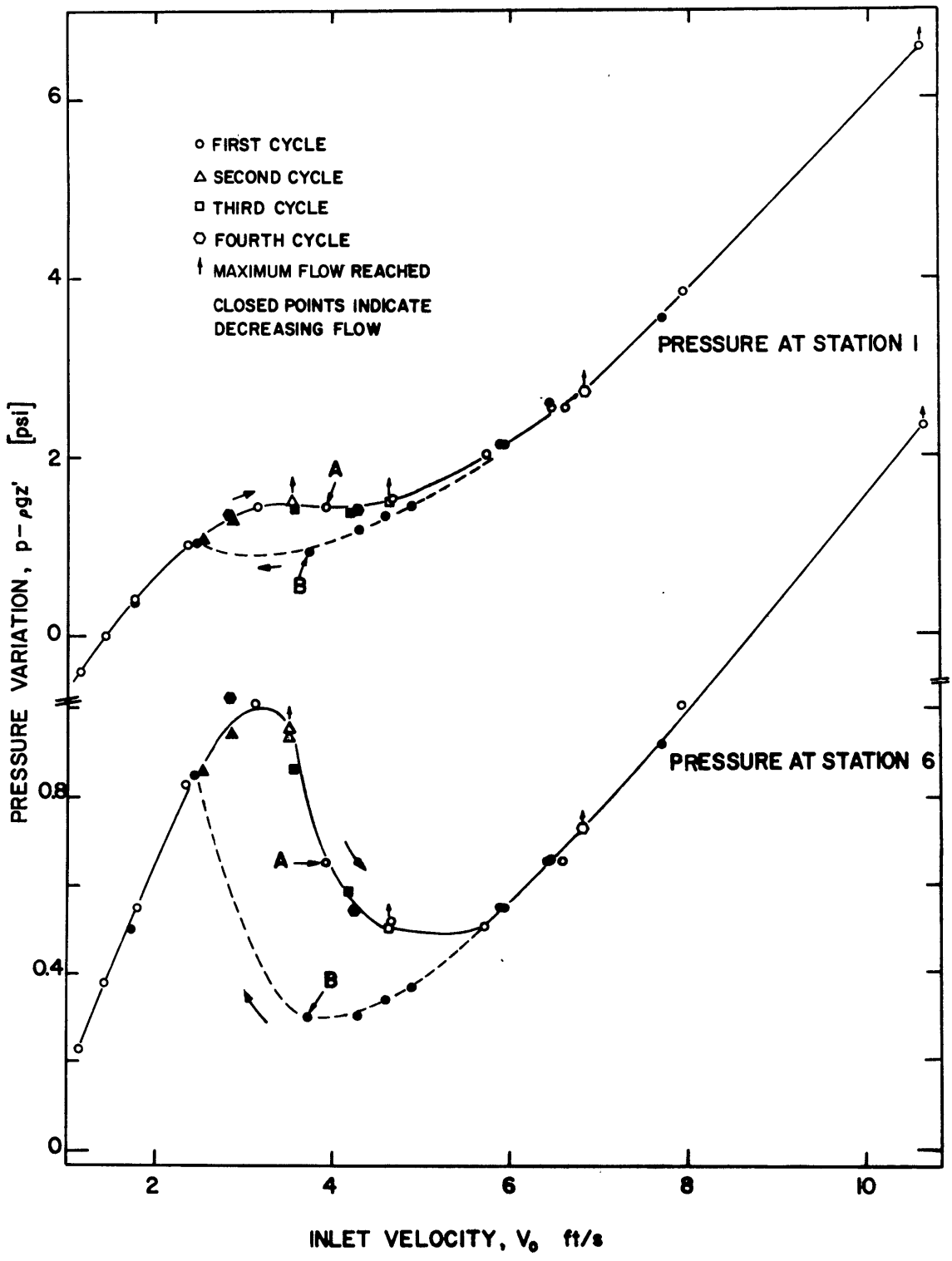

FIG. 4.8 PRESSURE DROP HYSTERESIS

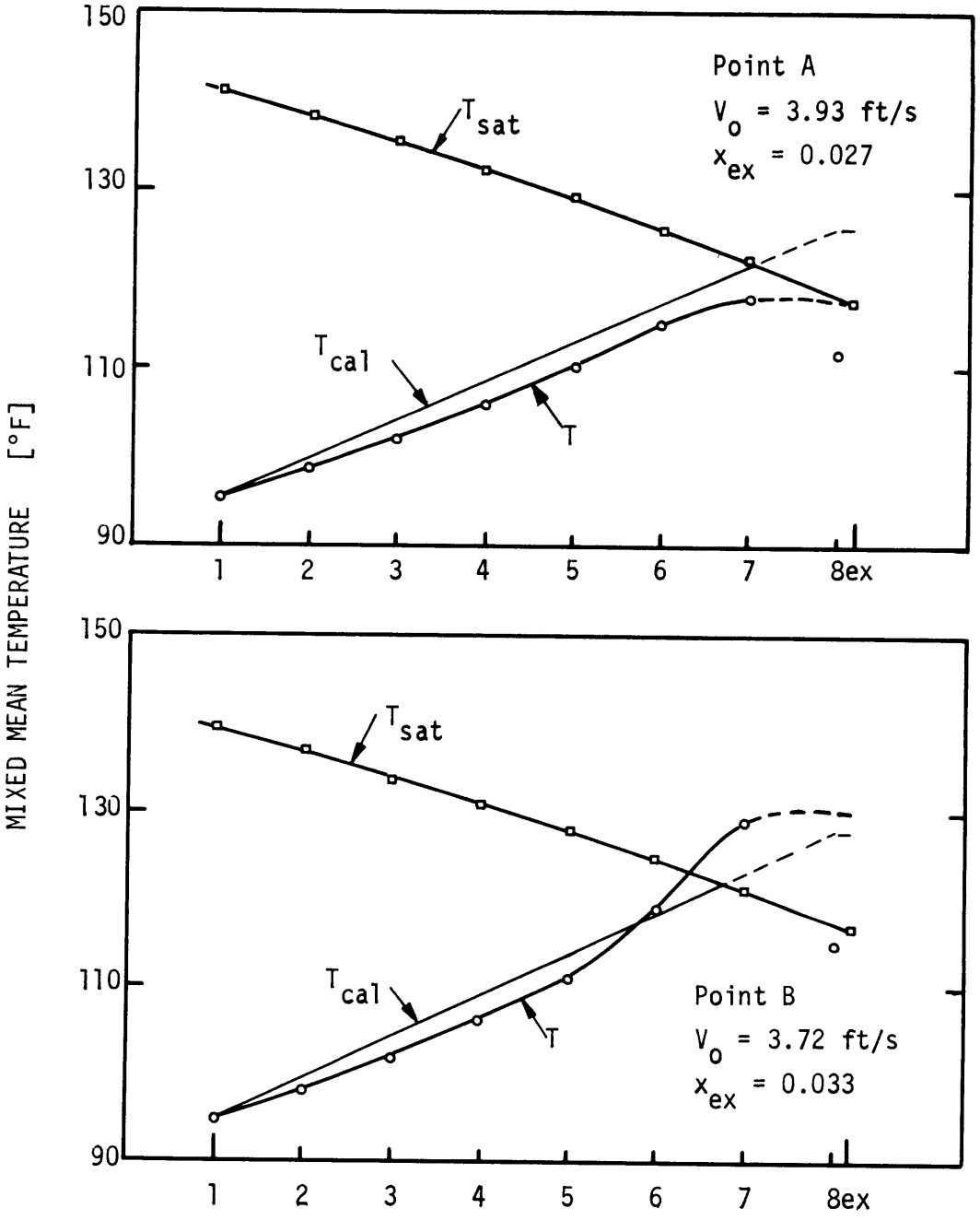

T_{sat} : Saturation temperature based on measured pressure

T_{cal} : Calculated single-phase temperature

T : Measured temperature (Low temperature reading at Station 8 is due to a thermocouple error)

FIG. 4.9 TEMPERATURE PROFILES FOR POINTS A AND B OF FIG. 4.8

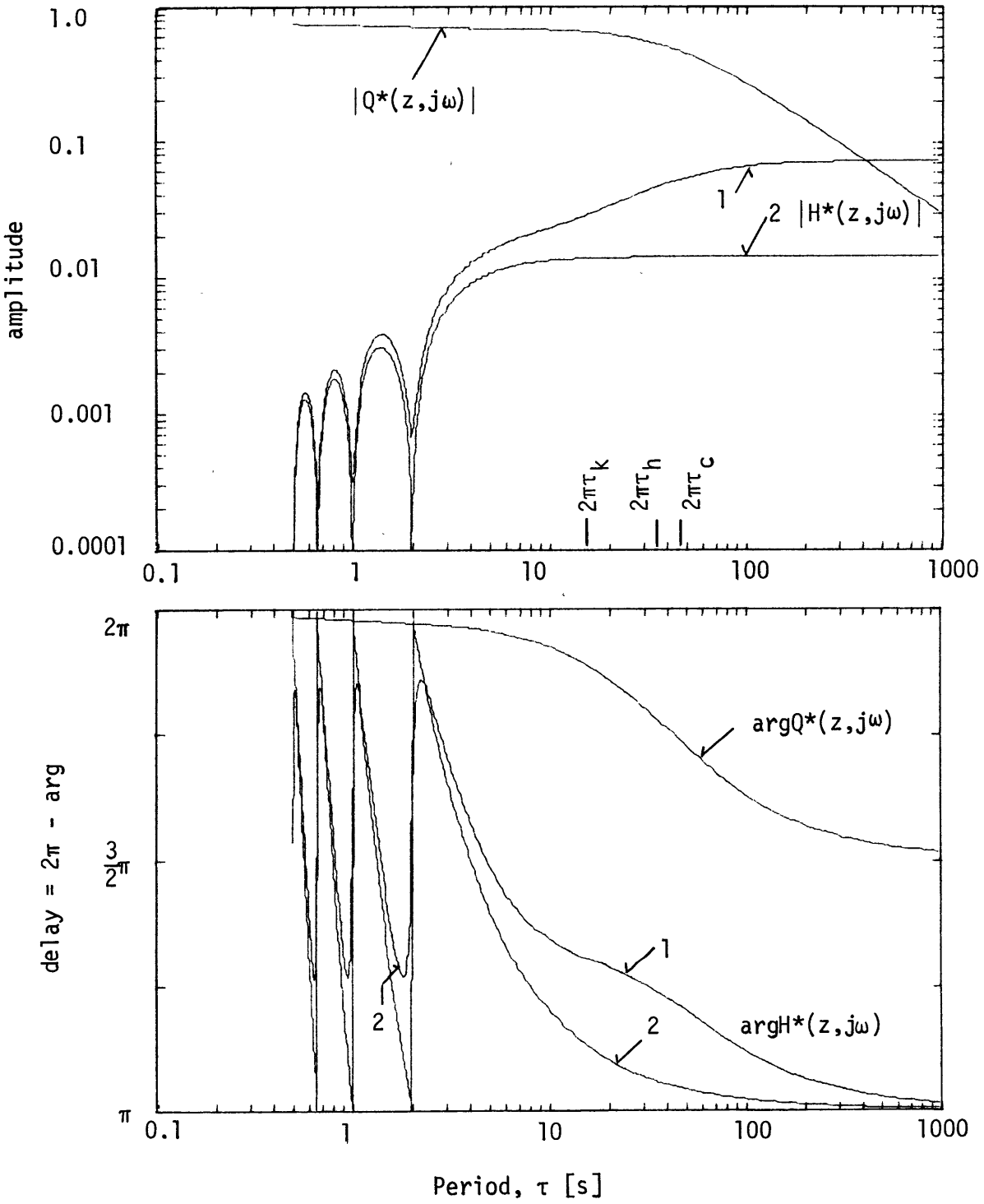

Uniform heat flux distribution; V_o = 1 ft/s, $\bar{T}$ = 100 °F;
q_o' = 800 Btu/hrft; a = 0.8.
Curve 2 is the high frequency approximation.
$2\pi\tau_k$ = 16.4 s; $2\pi\tau_h$ = 34.9 s; $2\pi\tau_c$ = 47.9 s.

FIG. 5.2 FLOW-TO-LOCAL-ENTHALPY AND FLOW-TO-HEAT-FLUX TRANSFER FUNCTIONS AT z = 2 ft.

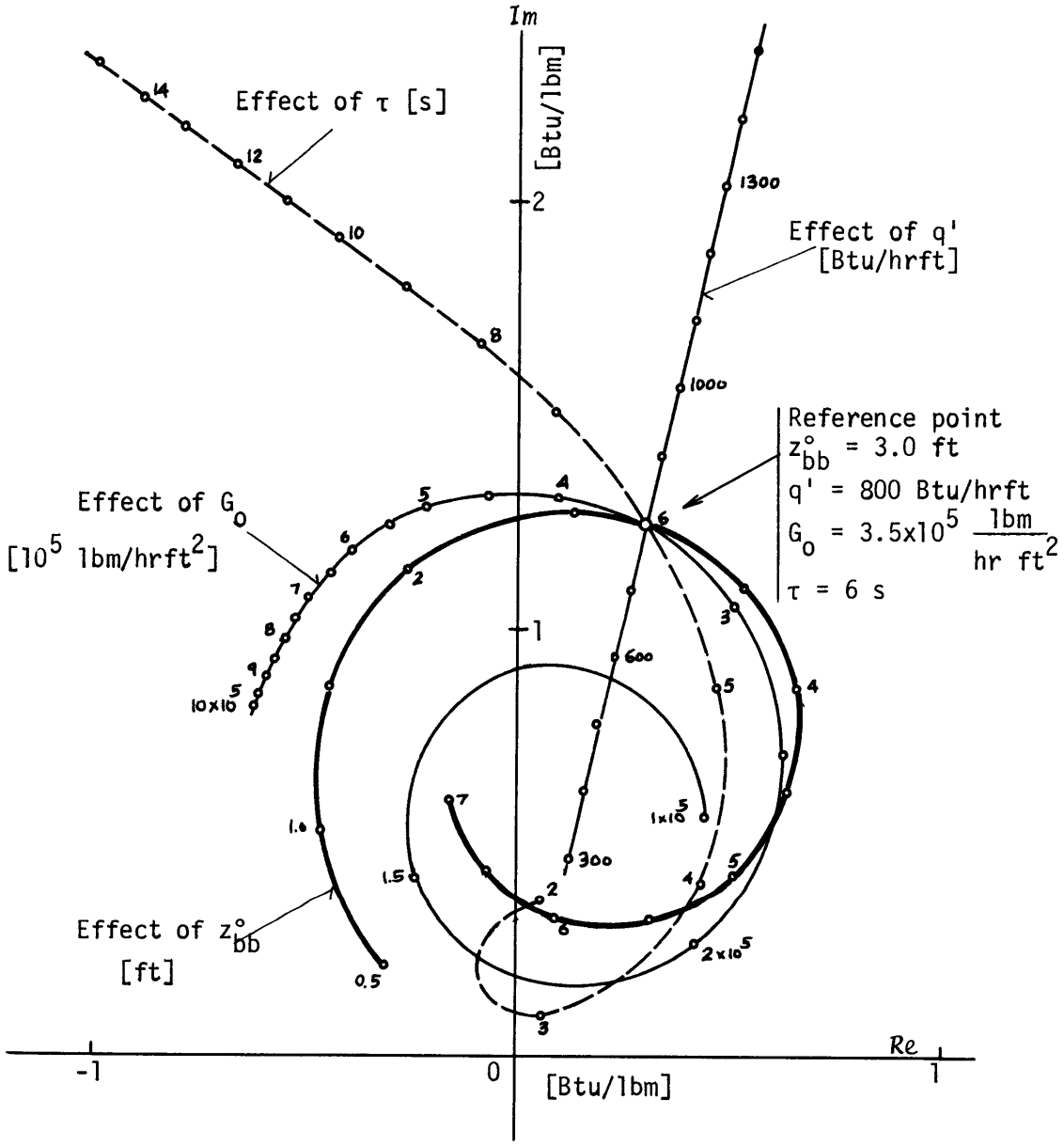

FIG. 5.4 PARAMETRIC STUDY OF THE ENTHALPY PERTURBATION AT THE BOILING BOUNDARY, δh°_{bb}

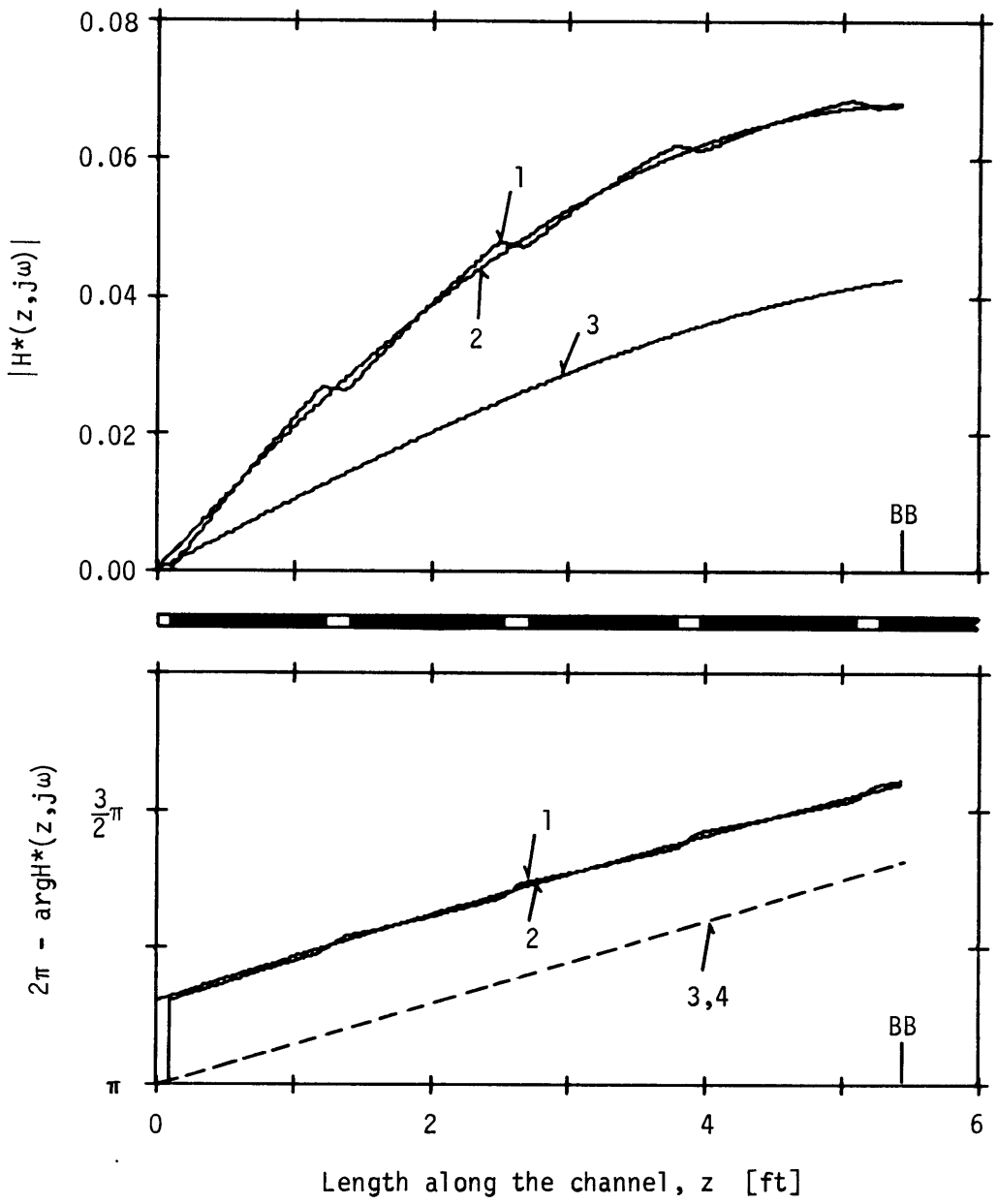

Experimental Point D20-192; τ = 11.70 s; V_o = 1.133 ft/s;
λ = 13.26 ft.

1: Wall heat storage and cold spots taken into account
2: Only wall heat storage taken into account; uniform heat input
3: High frequency approximation, Eq. (5.38)
4: Low frequency approximation. To get the amplitudes divide the amplitudes of 3 by (1 - a)
Heated and cold spots are shown by black and white line between the graphs.

FIG. 5.6 FLOW-TO-LOCAL-ENTHALPY TRANSFER FUNCTION ALONG THE CHANNEL. ZERO ORDER OSCILLATION.

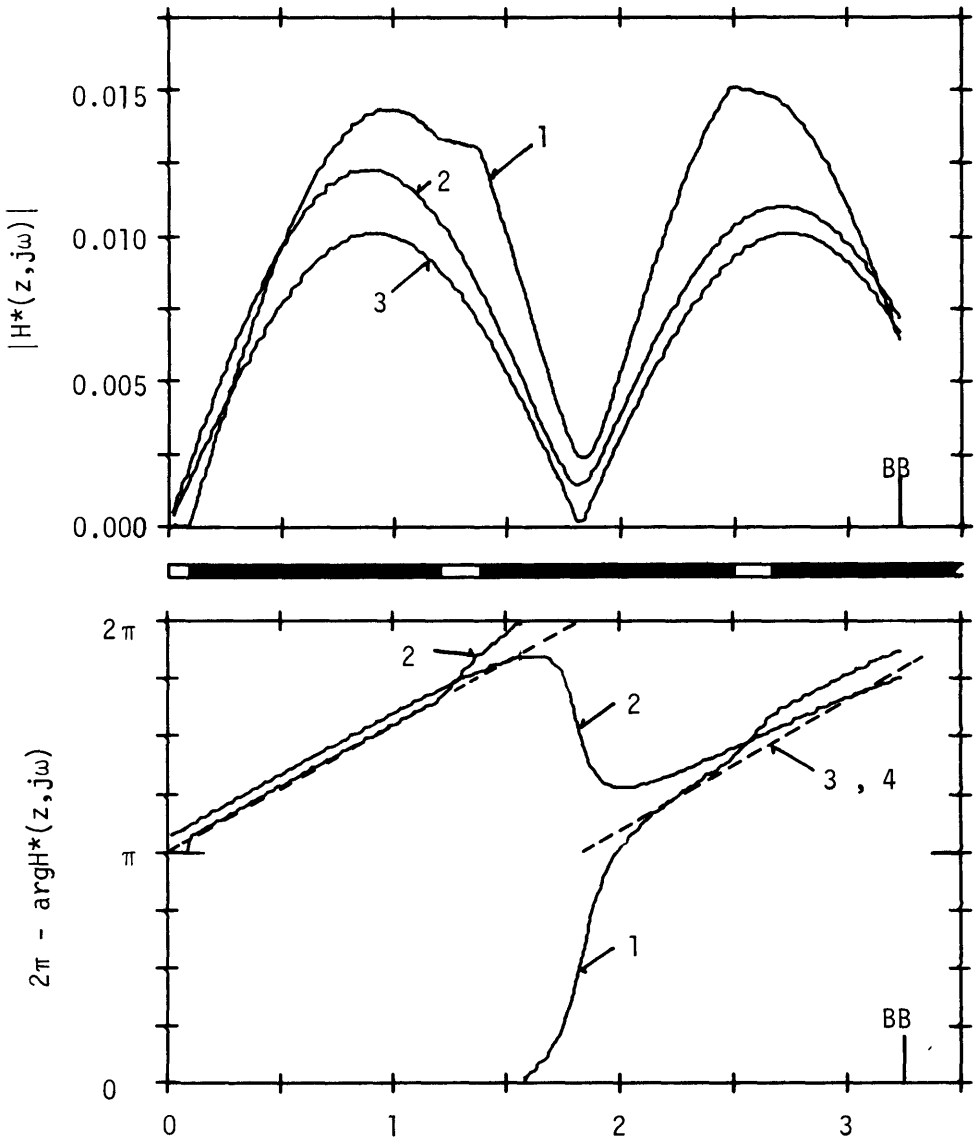

Length along the channel, z [ft]

Experimental Point D19-184; τ = 4.46 s; V_o = 0.410 ft/s;
λ = 1.83 ft.

1 , 2 , 3 , and 4 See Fig. 5.6

FIG. 5.7 FLOW-TO-LOCAL-ENTHALPY TRANSFER FUNCTION ALONG THE CHANNEL. FIRST ORDER OSCILLATION.

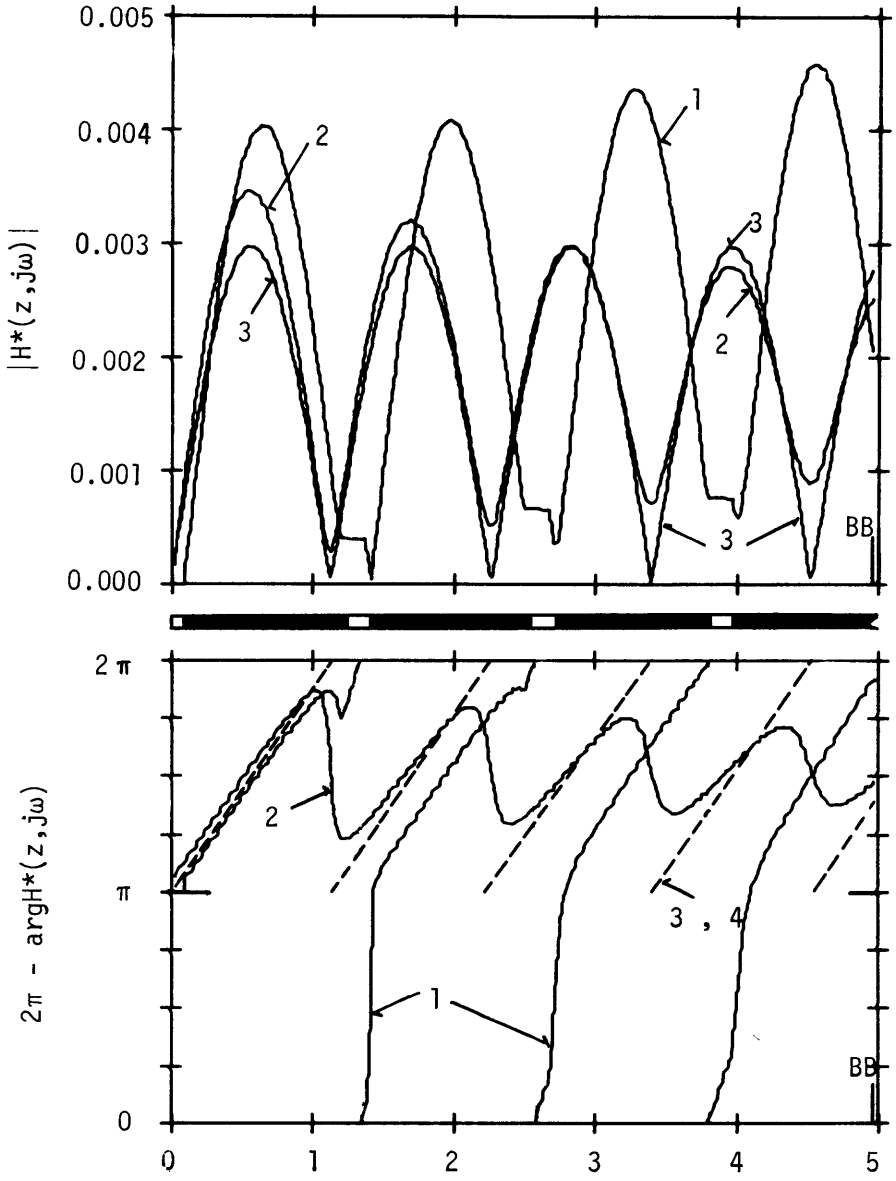

Experimental Point D18A-196; τ = 3.90 s; V_o = 0.291 ft/s; λ = 1.135 ft.

1 , 2 , 3 , and 4 See Fig. 5.6

FIG. 5.8 FLOW-TO-LOCAL-ENTHALPY TRANSFER FUNCTION ALONG THE CHANNEL. FOURTH ORDER OSCILLATION.

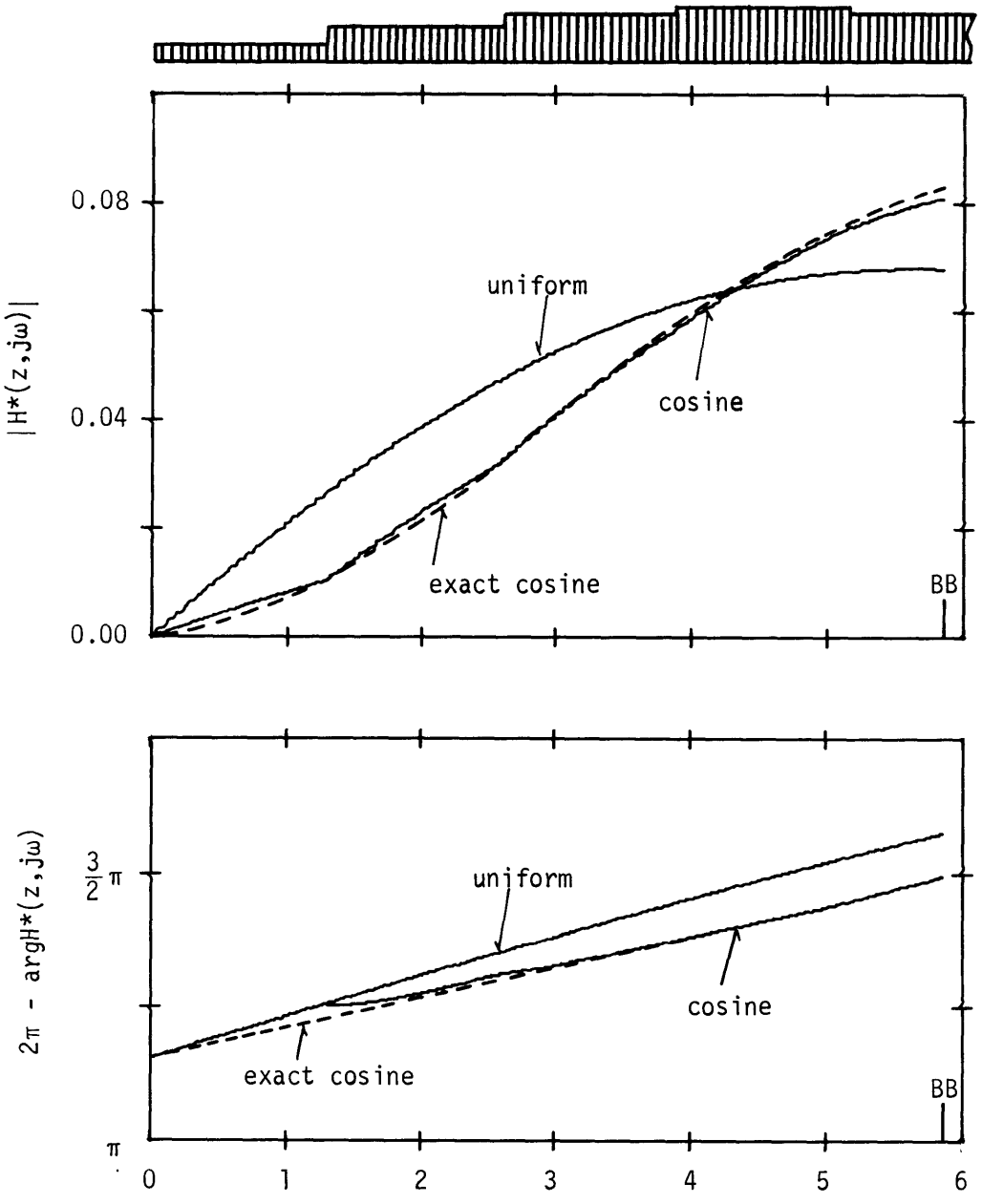

Experimental Point D20-192; τ = 11.70 s; V_o = 1.133 ft/s; λ = 13.26 ft.

Cosine heat flux distribution shown on top.

FIG. 5.9 COMPARISON OF THE-FLOW-TO-LOCAL-ENTHALPY TRANSFER FUNCTIONS FOR UNIFORM AND COSINE HEAT FLUX DISTRIBUTIONS. ZERO ORDER OSCILLATION.

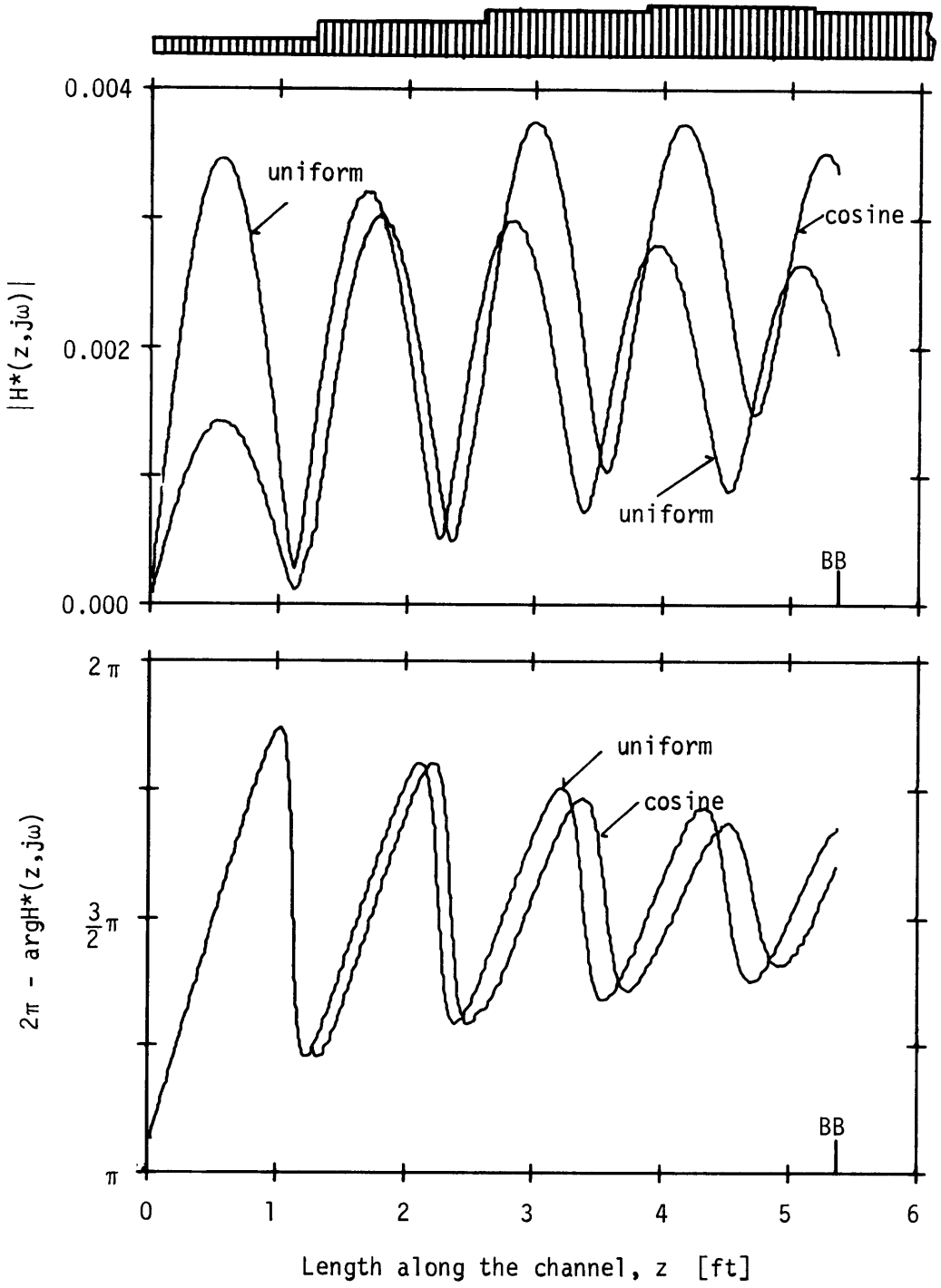

Experimental Point D18A-196; τ = 3.90 s; V_o = 0.291 ft/s; λ = 1.135 ft.
Cosine heat flux distribution shown on top.

FIG. 5.10 COMPARISON OF THE FLOW-TO-LOCAL-ENTHALPY TRANSFER FUNCTIONS FOR UNIFORM AND COSINE HEAT FLUX DISTRIBUTIONS. FOURTH ORDER OSCILLATION.

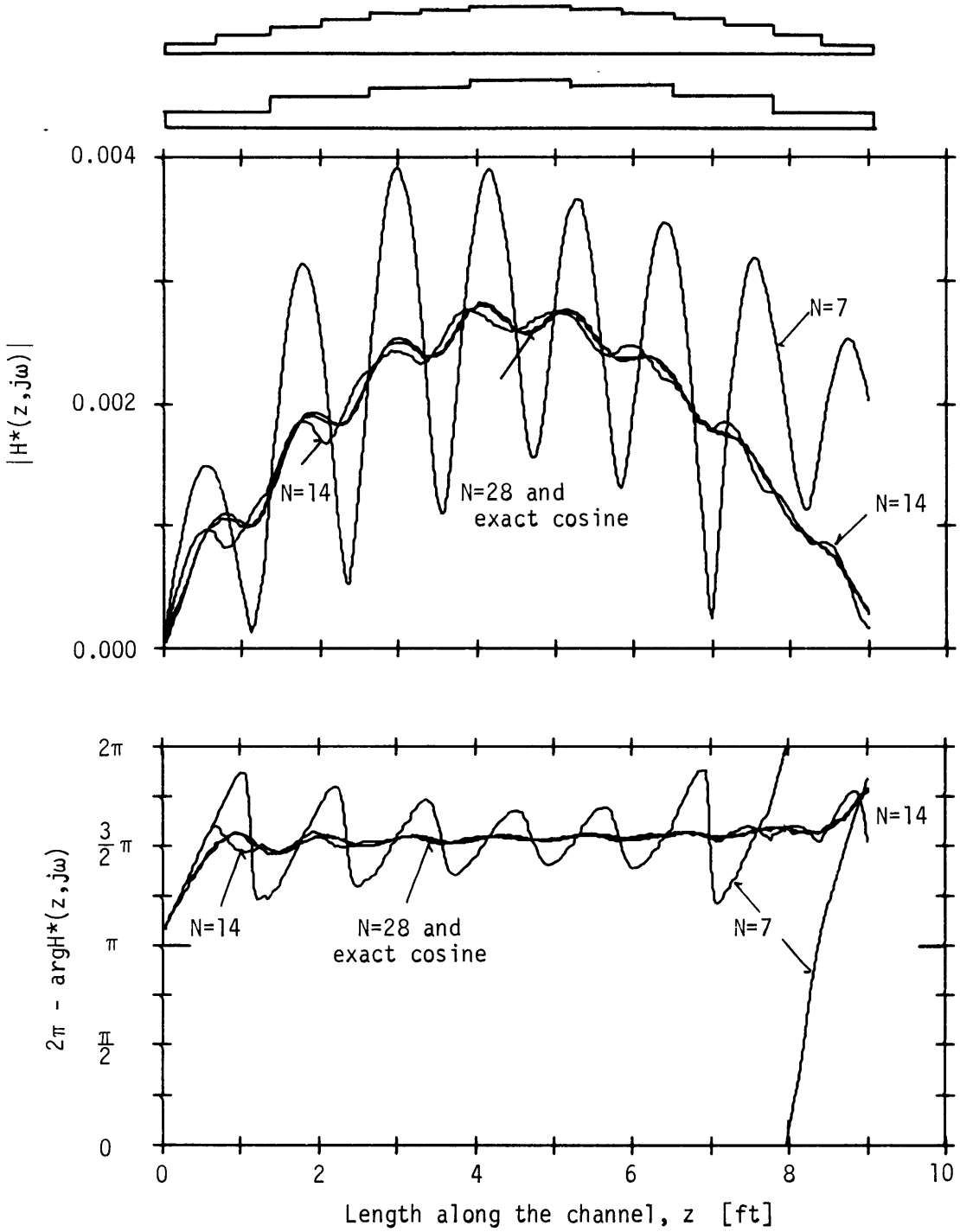

The cosine distribution is simulated by N = 7, 14, and 28 segments. Two corresponding heat flux distributions are shown at the top.

FIG. 5.11 EFFECT OF THE CHANNEL SEGMENTATION ON THE FLOW-TO-LOCAL ENTHALPY TRANSFER FUNCTION.

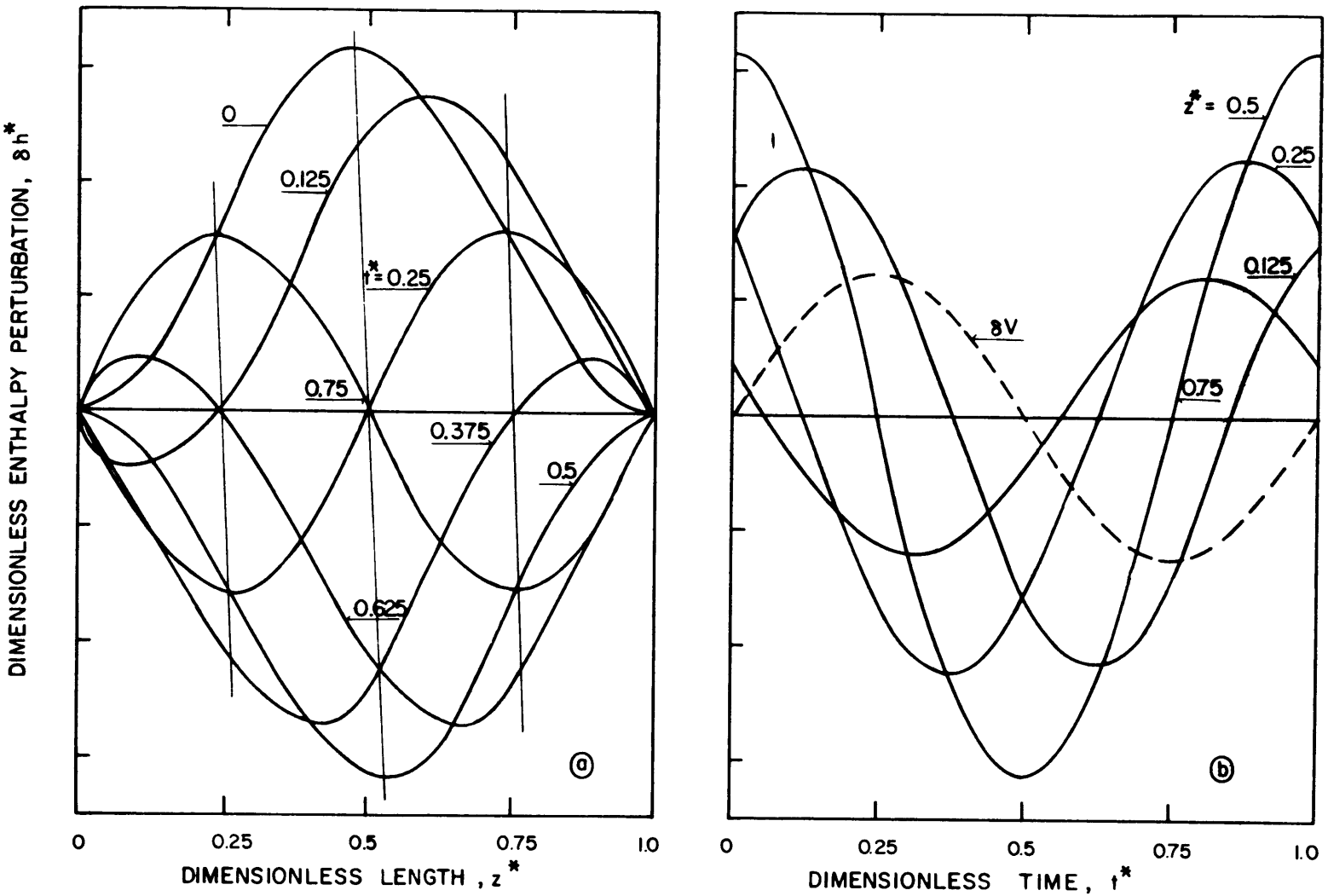

FIG. 5.12 ENTHALPY PERTURBATIONS ALONG THE CHANNEL, $\delta\hat{V}/V_0 = 0.1$

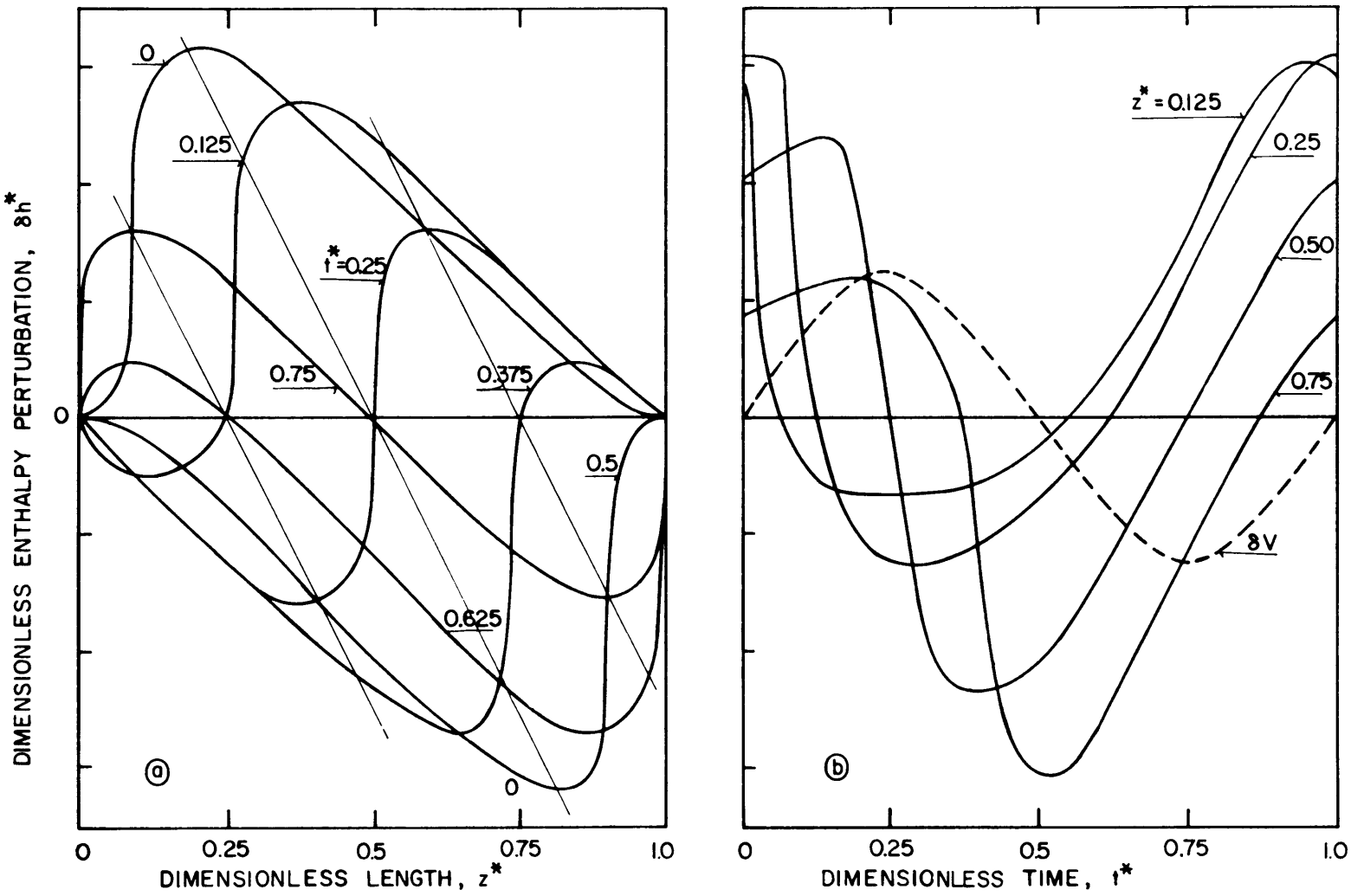

FIG. 5.13 ENTHALPY PERTURBATIONS ALONG THE CHANNEL, $\delta\hat{V}/V_0 = 1$

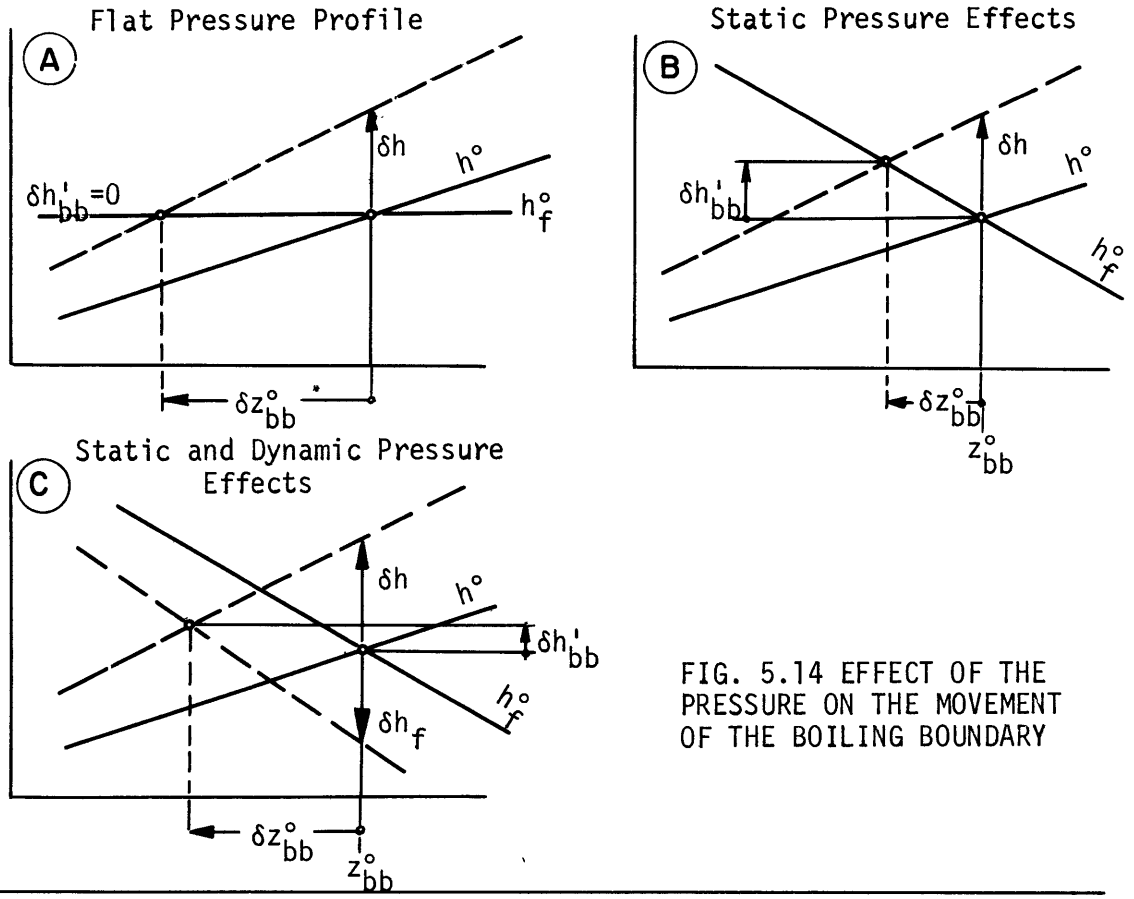

FIG. 5.14 EFFECT OF THE PRESSURE ON THE MOVEMENT OF THE BOILING BOUNDARY

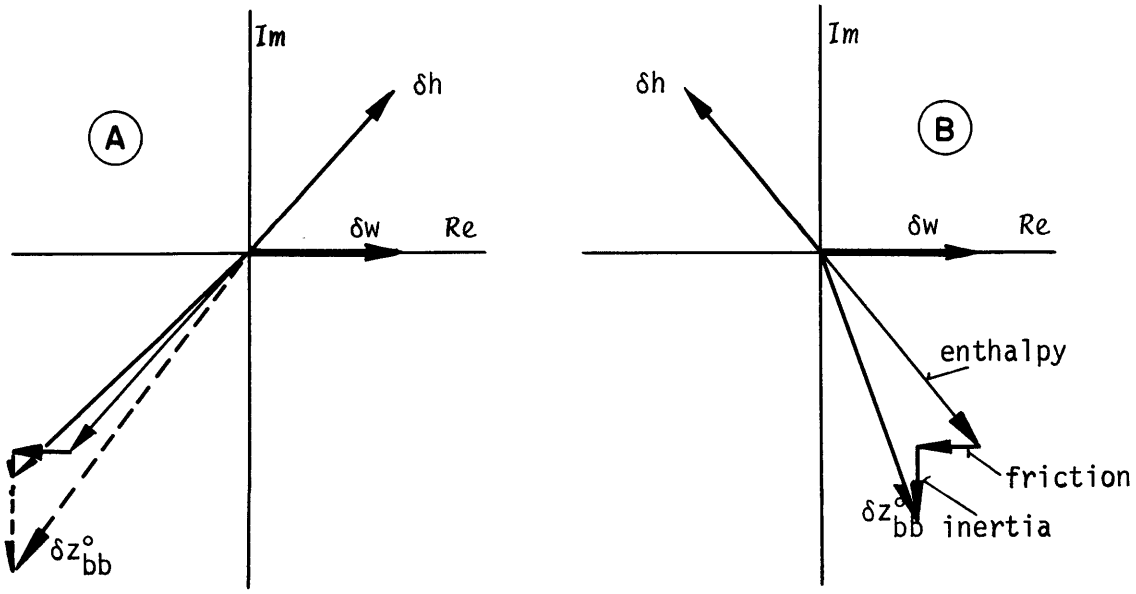

A. δh in First Quadrant B. δh in Second Quadrant

FIG. 5.15 EFFECT OF THE DYNAMIC PRESSURE VARIATIONS ON THE MOVEMENT OF THE BOILING BOUNDARY

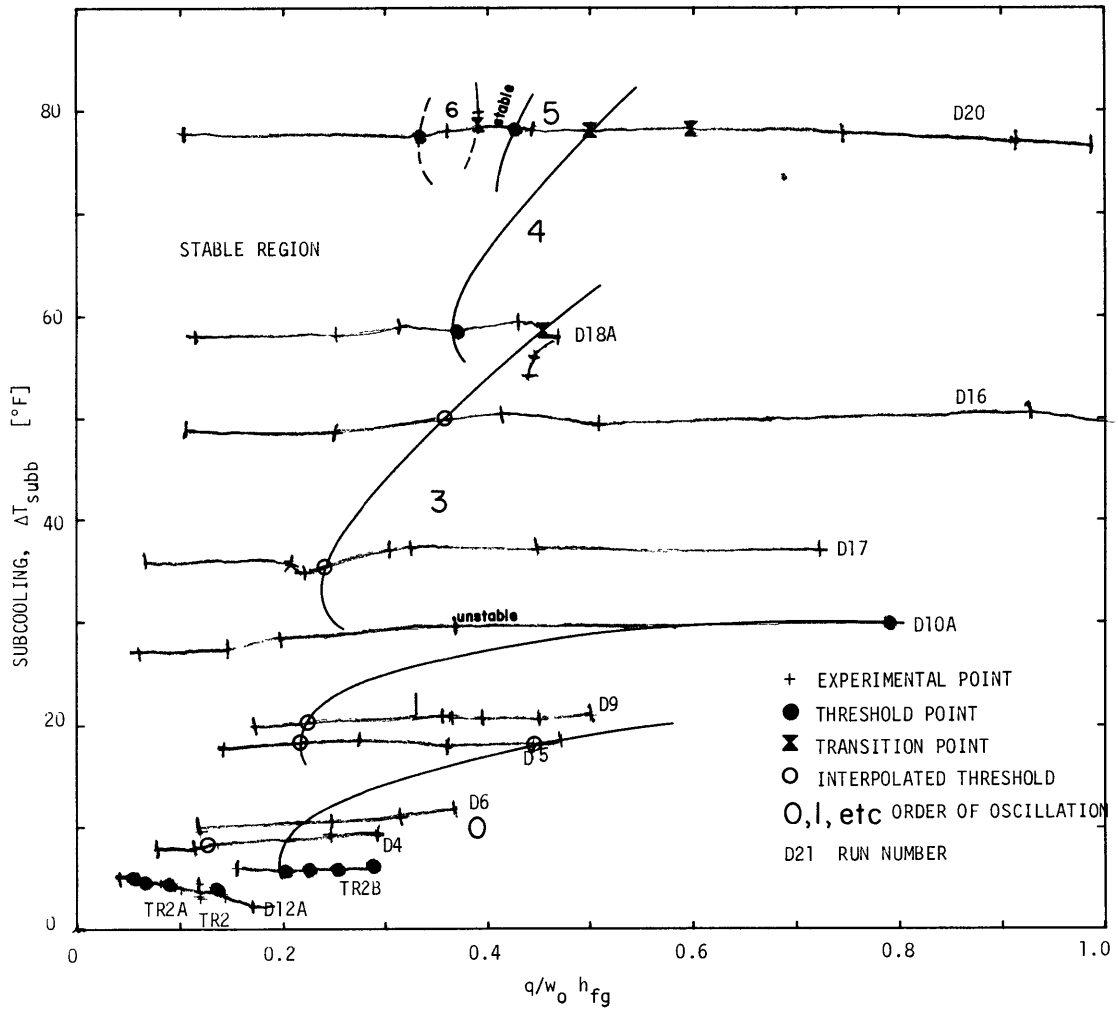

FIG. 7.1 STABILITY MAP AT 100 W/TL, UNIFORM HEAT FLUX DISTRIBUTION

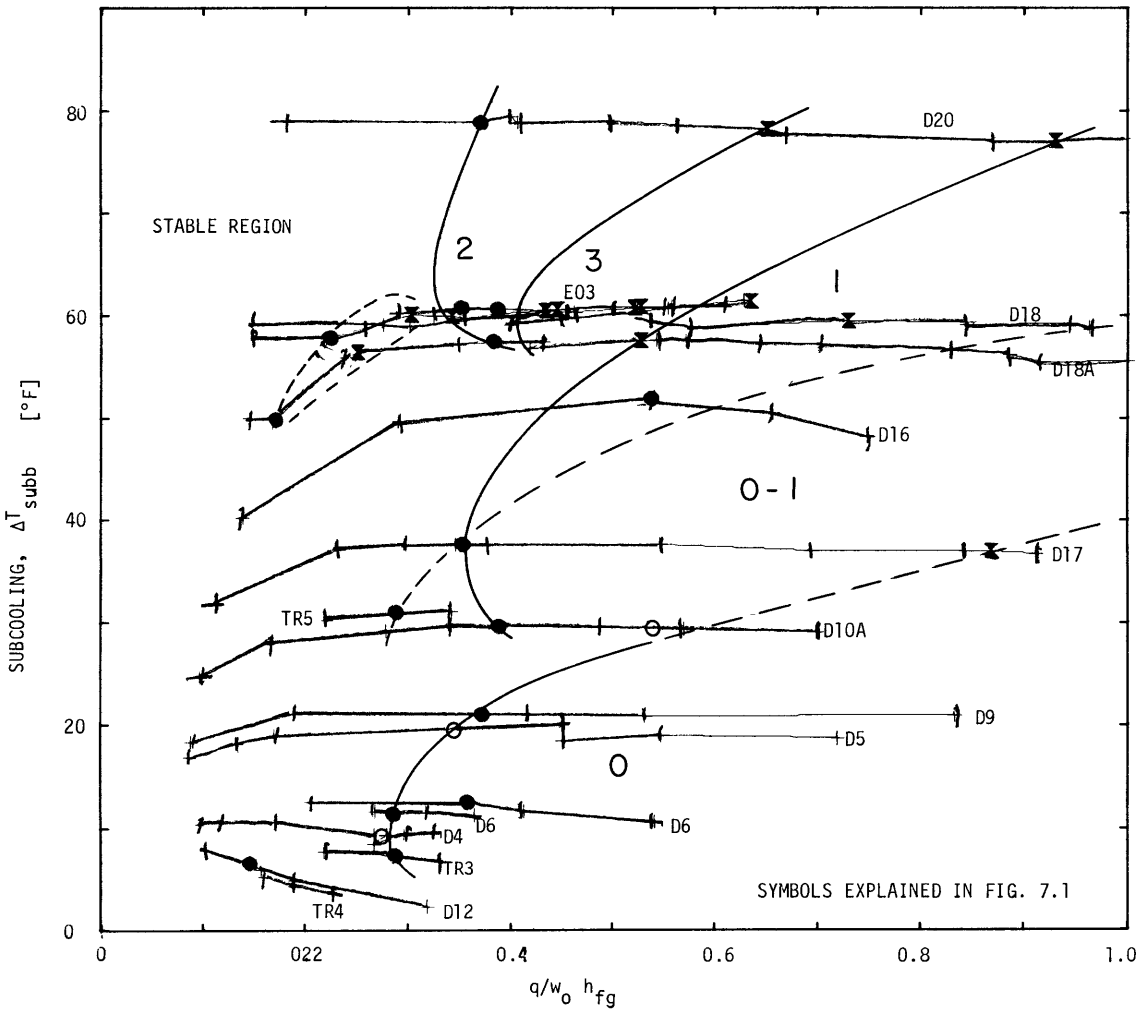

FIG. 7.2 STABILITY MAP AT 200 W/TL, UNIFORM HEAT FLUX DISTRIBUTION

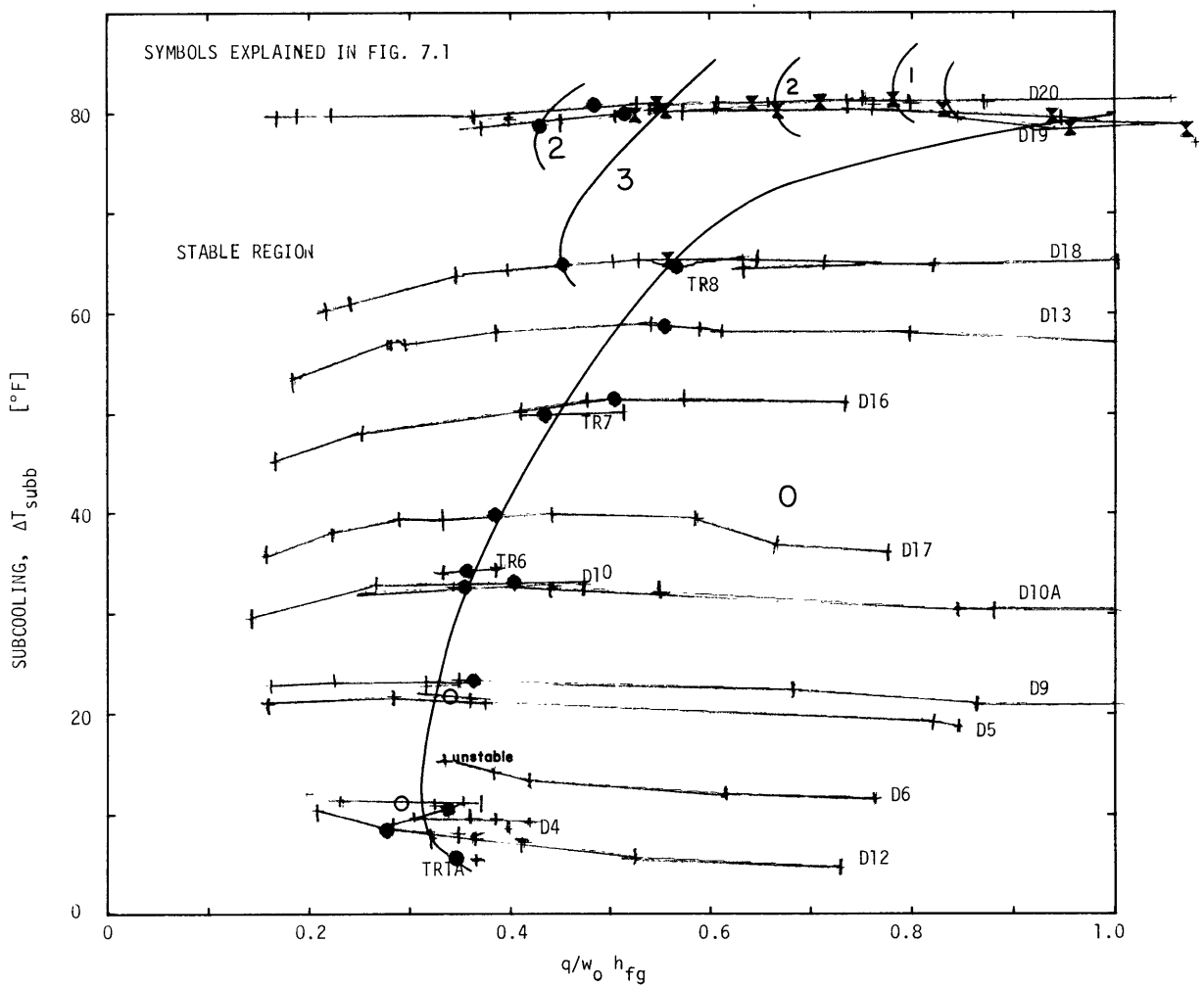

FIG. 7.3 STABILITY MAP AT 300 W/TL, UNIFORM HEAT FLUX DISTRIBUTION

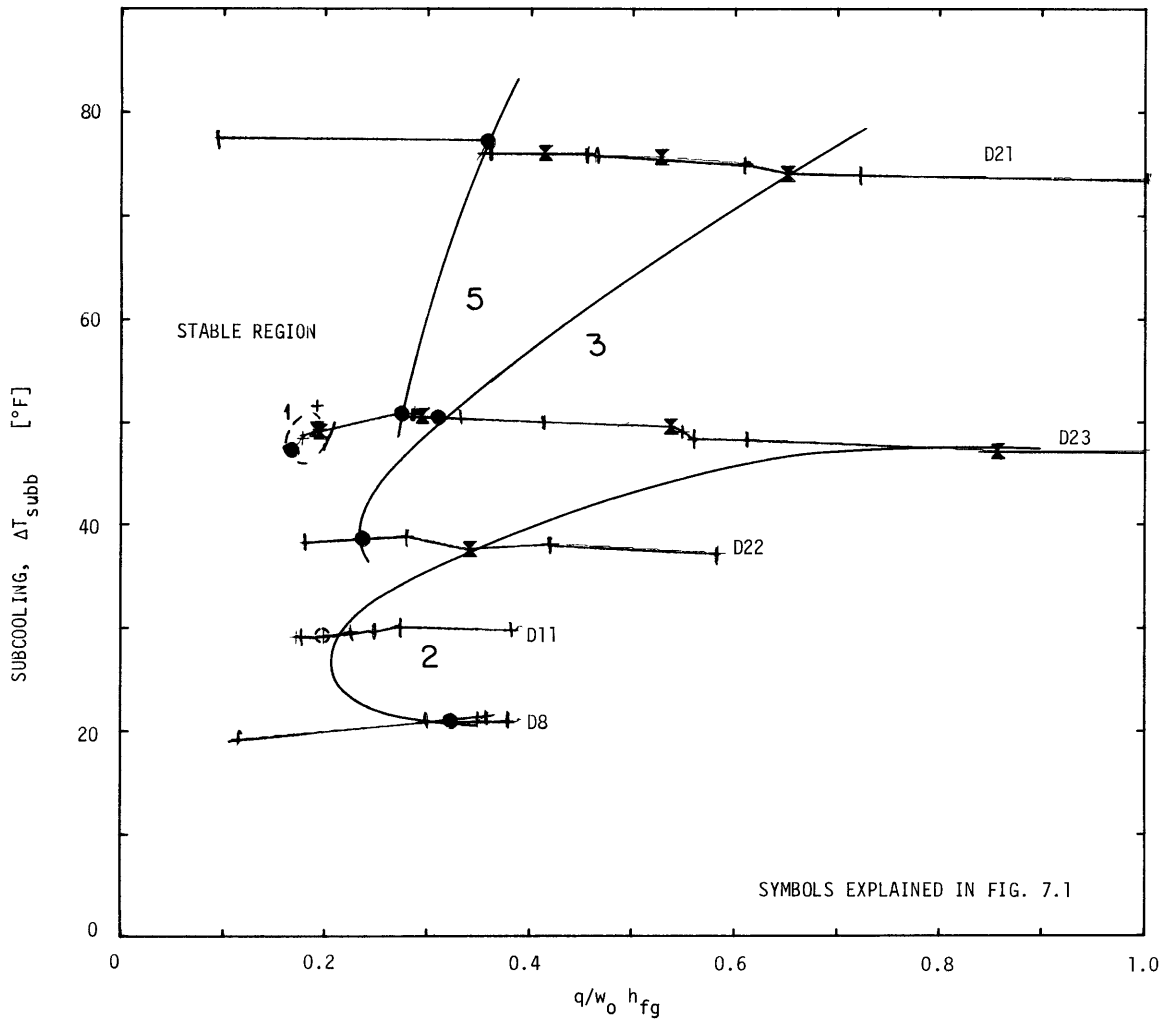

FIG. 7.4 STABILITY MAP AT 100 W/TL AVE., COSINE HEAT FLUX DISTRIBUTION

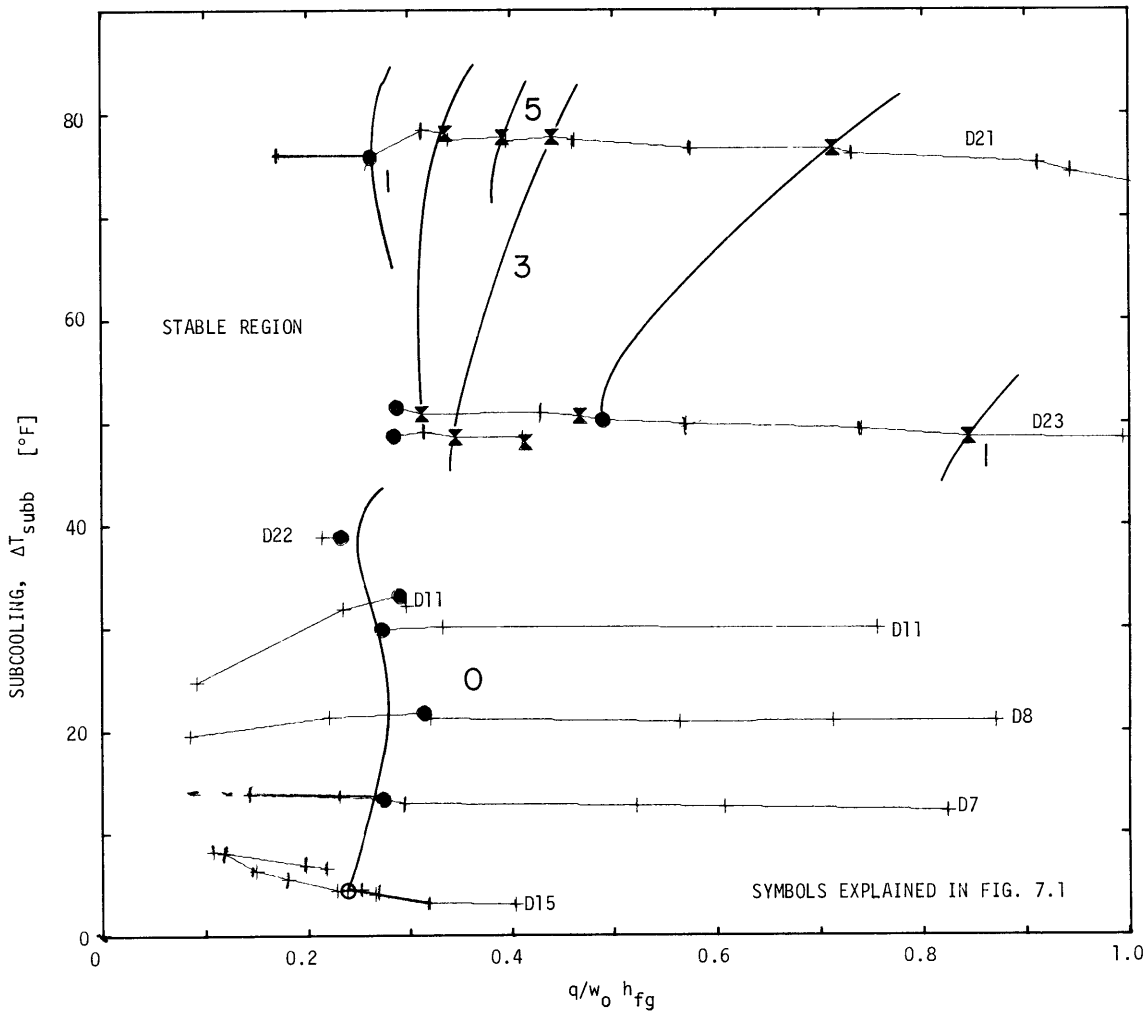

FIG. 7.5 STABILITY MAP AT 200 W/TL AVE., COSINE HEAT FLUX DISTRIBUTION

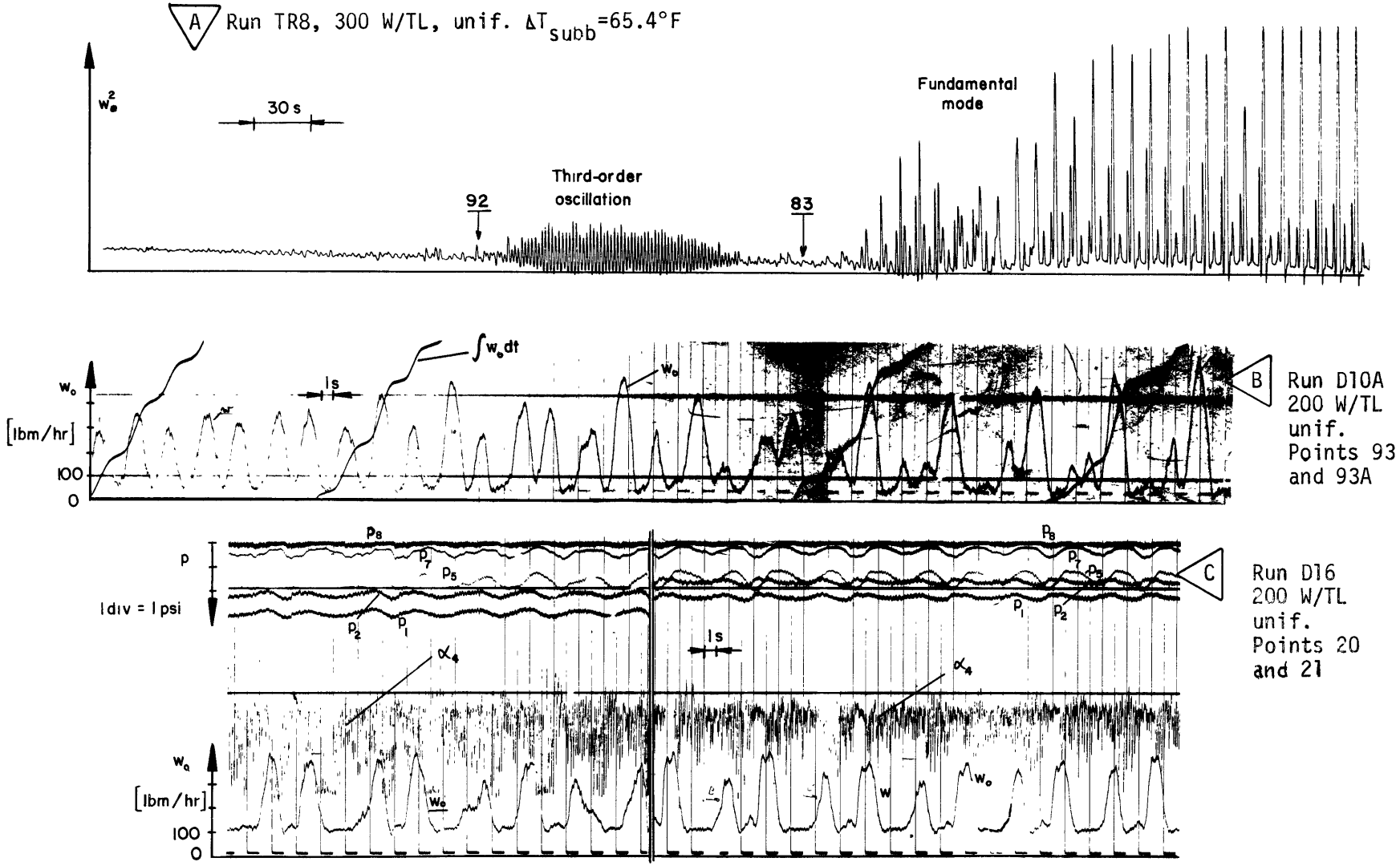

FIG. 7.6 RECORDINGS OF OSCILLATIONS - TRANSITION POINTS

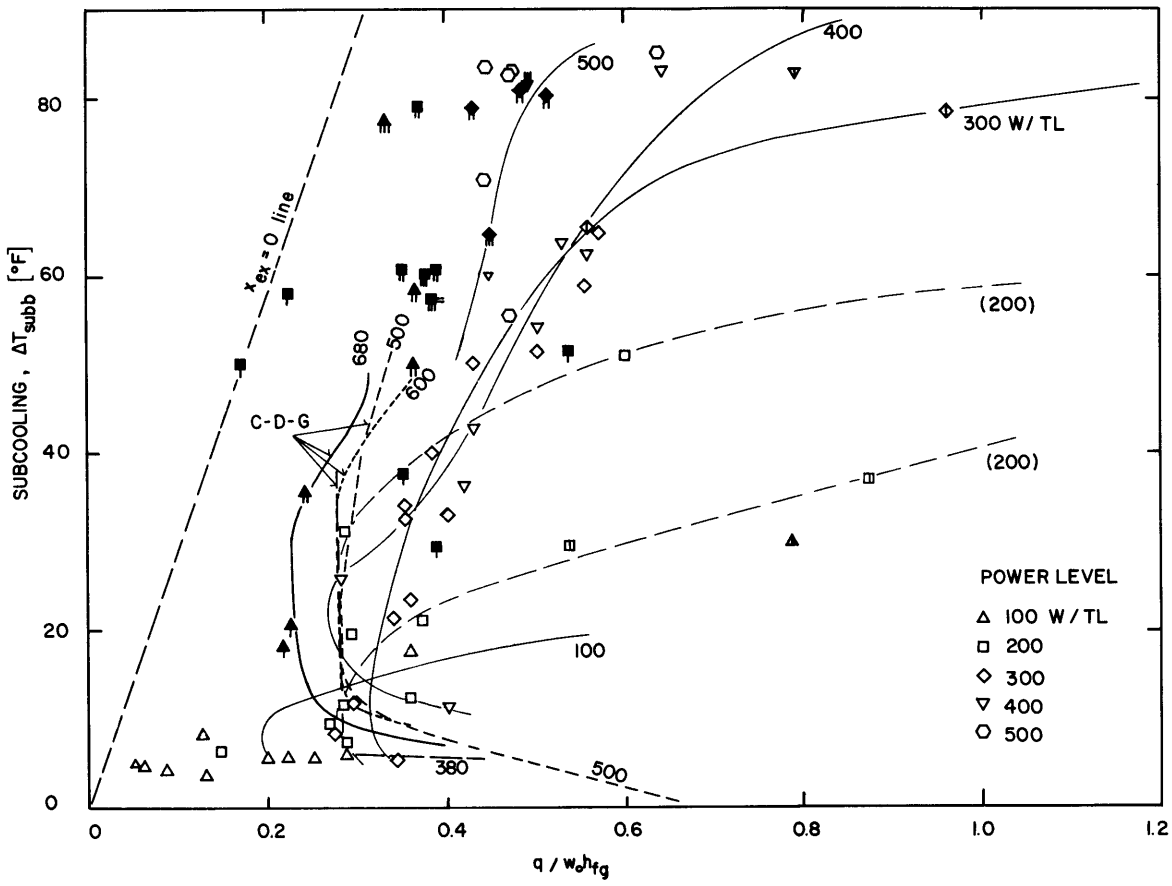

Open points: First occurrence of oscillation, zero order.
Closed points: First occurrence of oscillation , higher-mode
(Number of tails denotes order of oscillation).
Points with a bar: Transitions to fundamental model.
Crowley, Deane and Gouse's boundaries also shown.

FIG. 7.7 FIRST OCCURRENCE OF INSTABILITIES AND FUNDAMENTAL MODE OSCILLATION BOUNDARIES

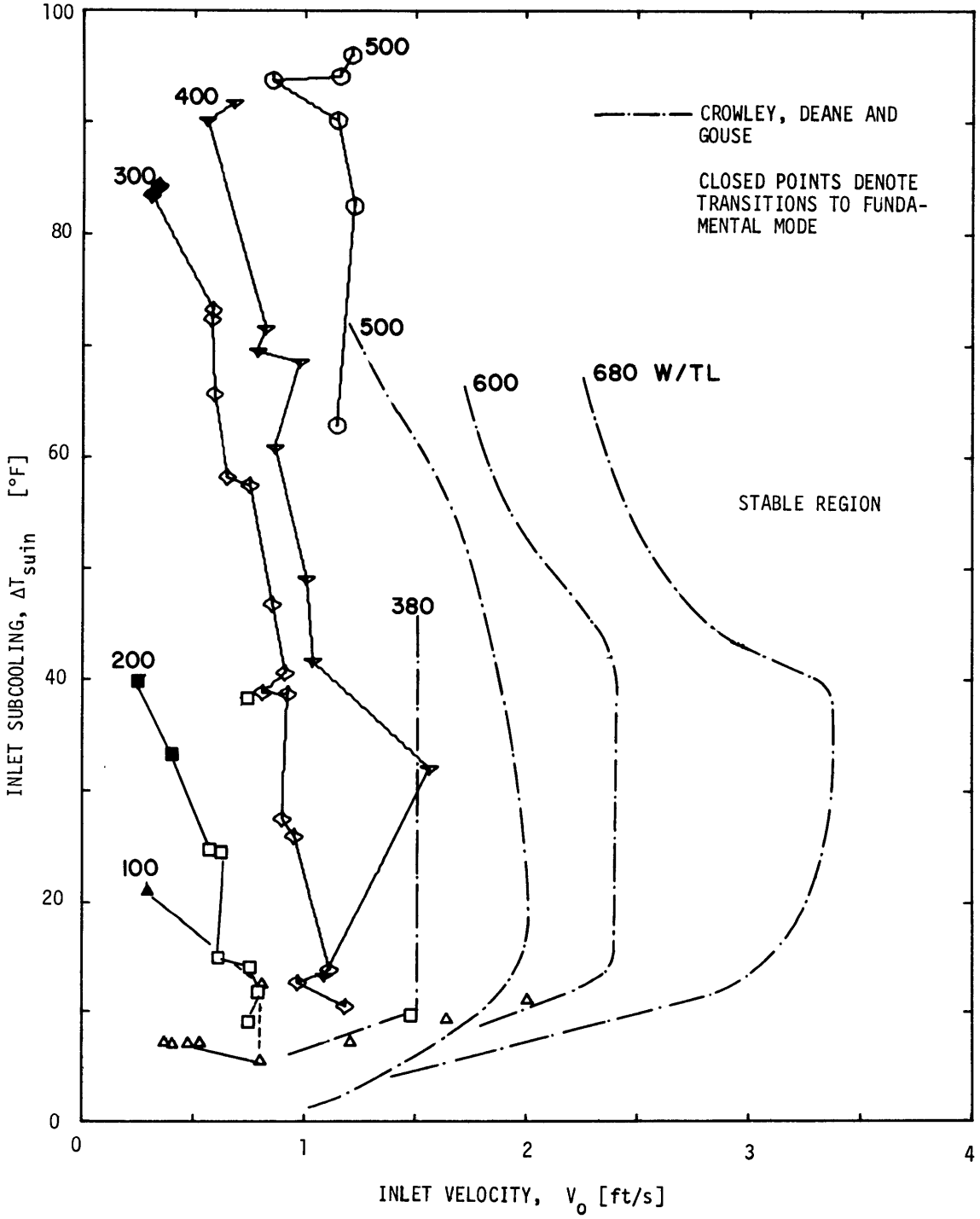

FIG. 7.8 STABILITY BOUNDARIES FOR UNIFORM POWER DISTRIBUTION, ZERO ORDER POINTS ONLY

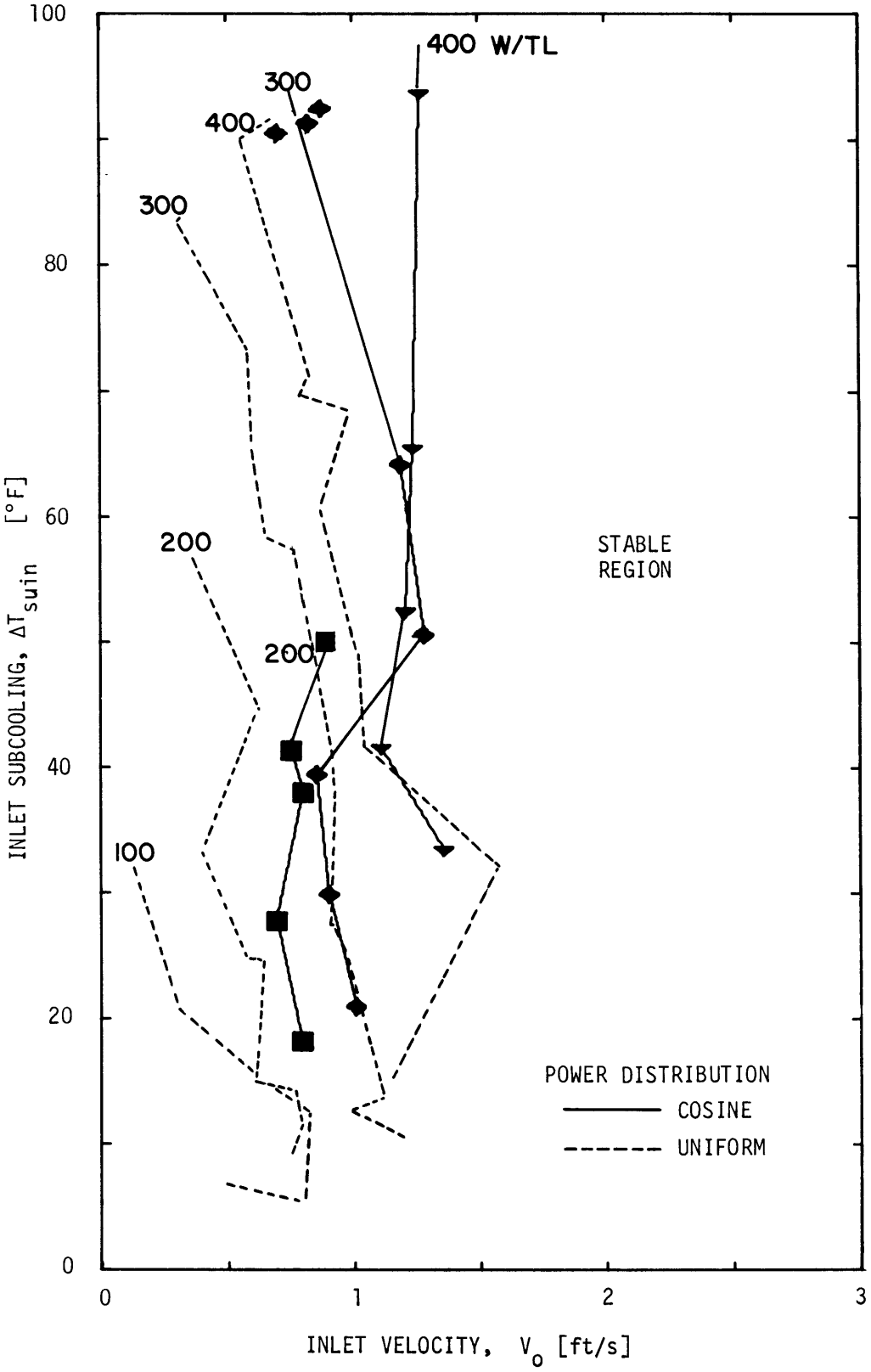

FIG. 7.9 STABILITY BOUNDARIES FOR COSINE POWER DISTRIBUTION - ZERO ORDER POINTS ONLY

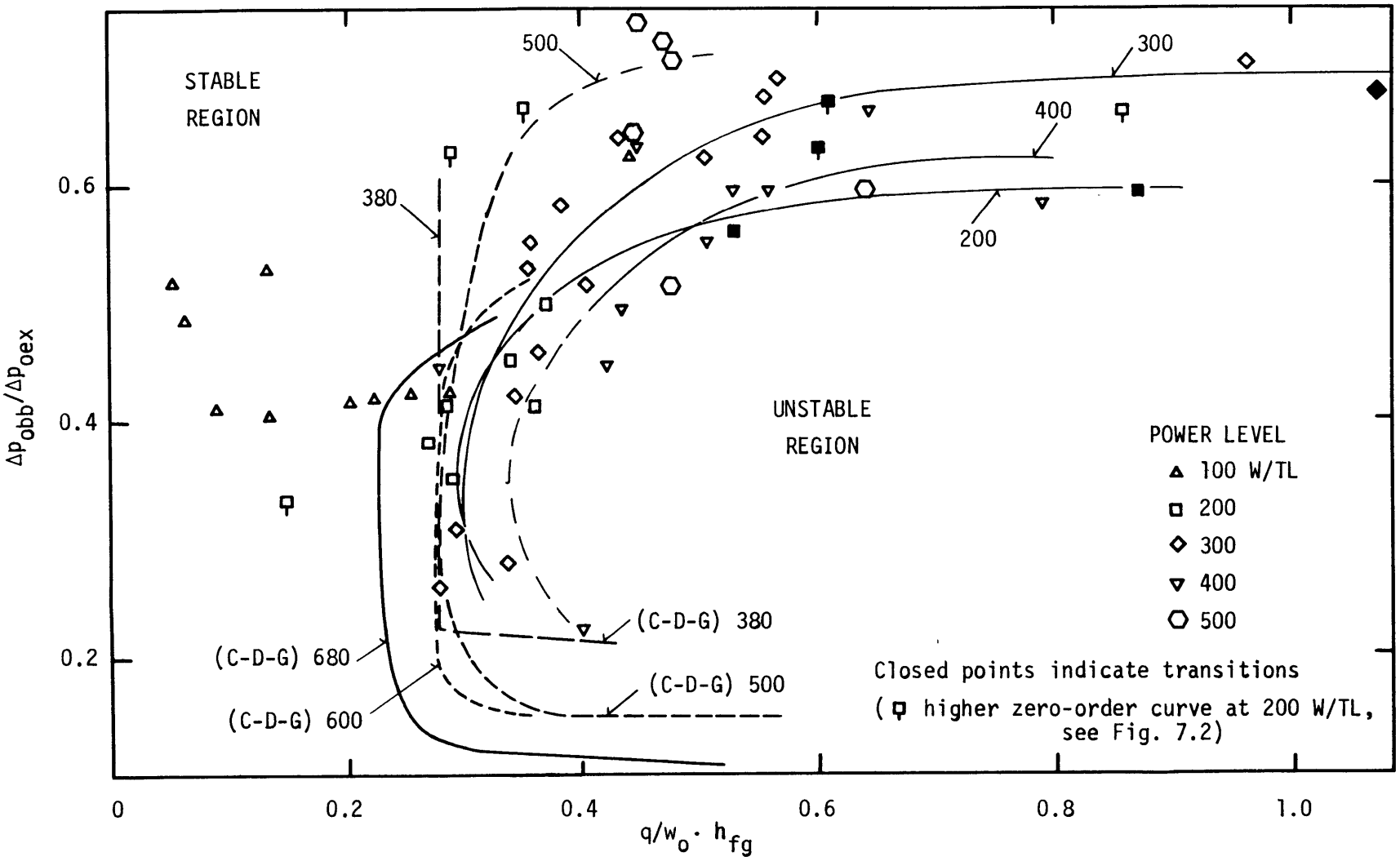

FIG. 7.10 STABILITY MAP IN THE DIMENSIONLESS ENTHALPY-PRESSURE DROP PLANE - ZERO ORDER POINTS ONLY

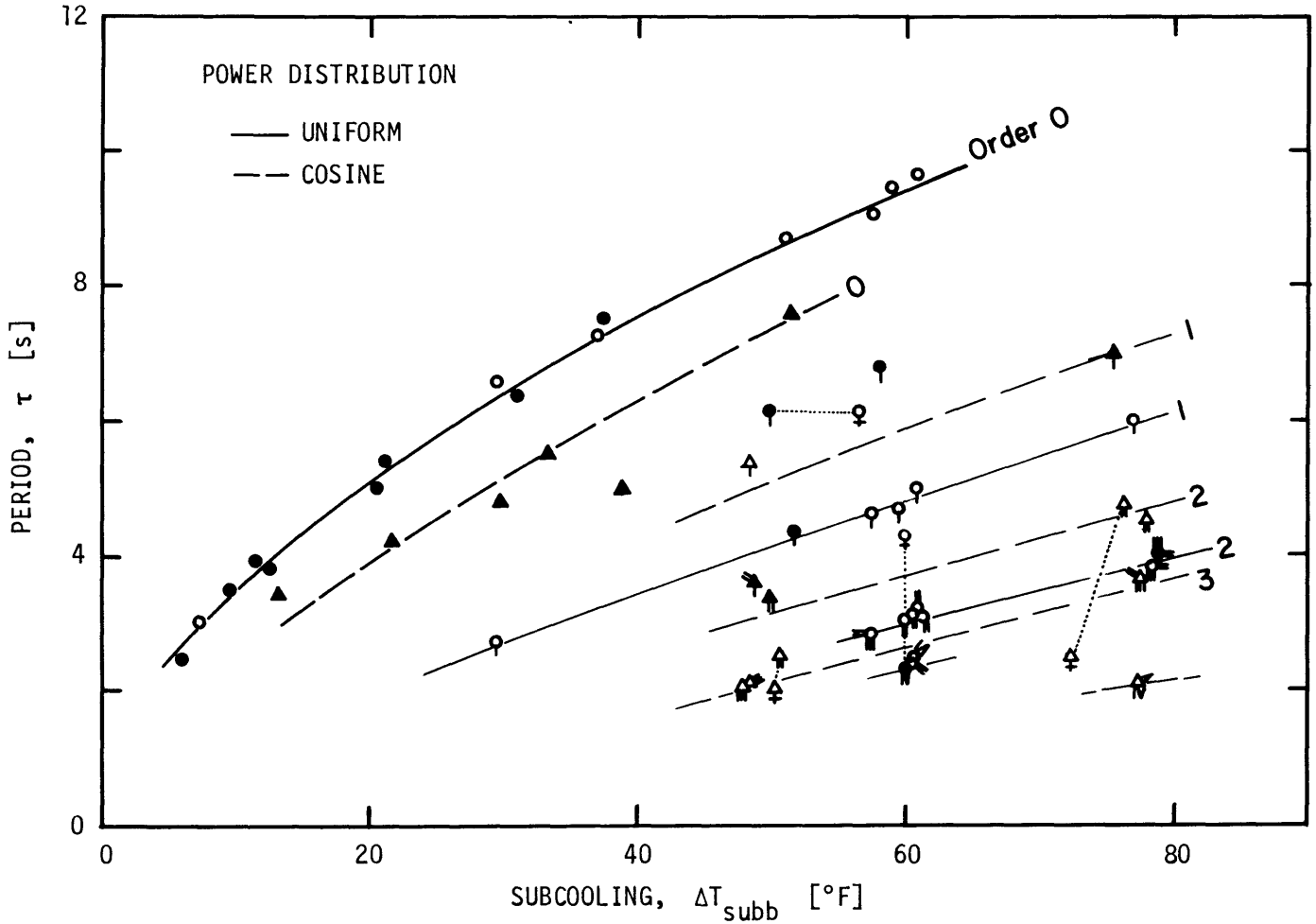

Open points denote transitions. Tails indicate order of oscillation.
Crosses mark decay of oscillations.

FIG. 7.11 PERIOD OF THE OSCILLATIONS AT THE THRESHOLD OF STABILITY - ALL ORDERS AT 200 W/TL

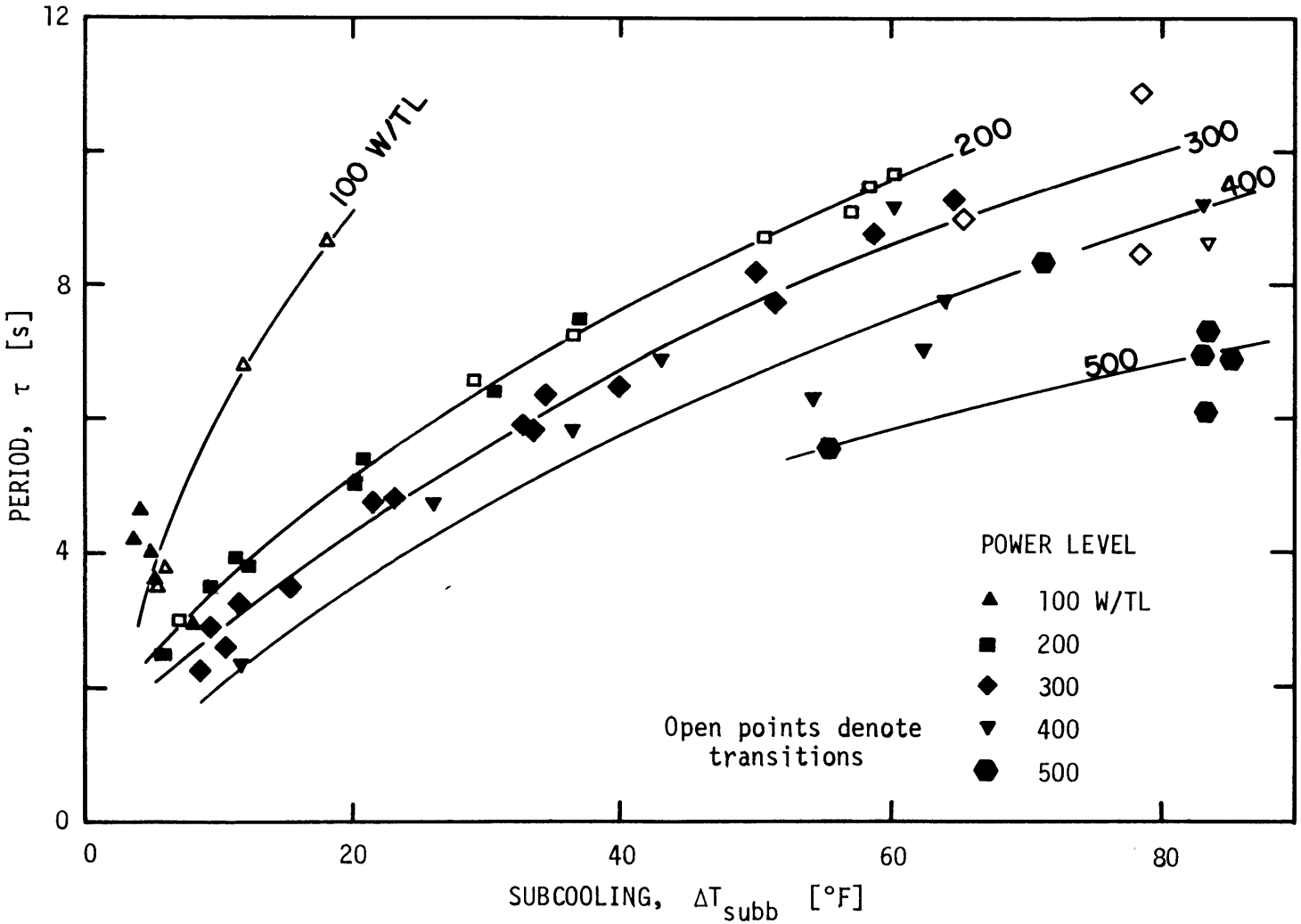

FIG. 7.12 PERIOD OF THE OSCILLATION AT THE THRESHOLD OF STABILITY - ZERO ORDER POINTS ONLY - UNIFORM HEAT FLUX DISTRIBUTION

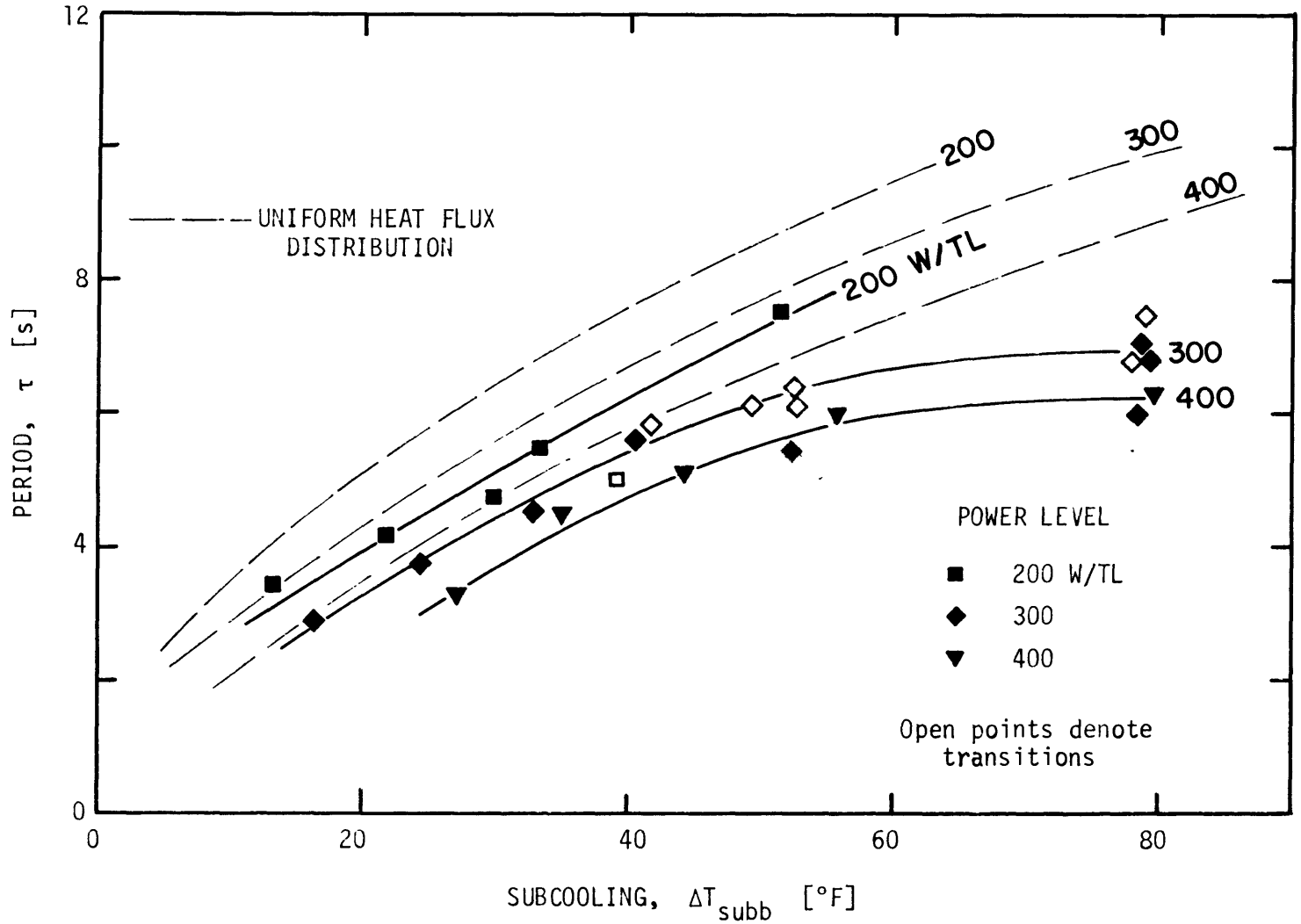

FIG. 7.13 PERIOD OF THE OSCILLATION AT THE THRESHOLD OF STABILITY - ZERO ORDER POINTS ONLY - COSINE HEAT FLUX DISTRIBUTION

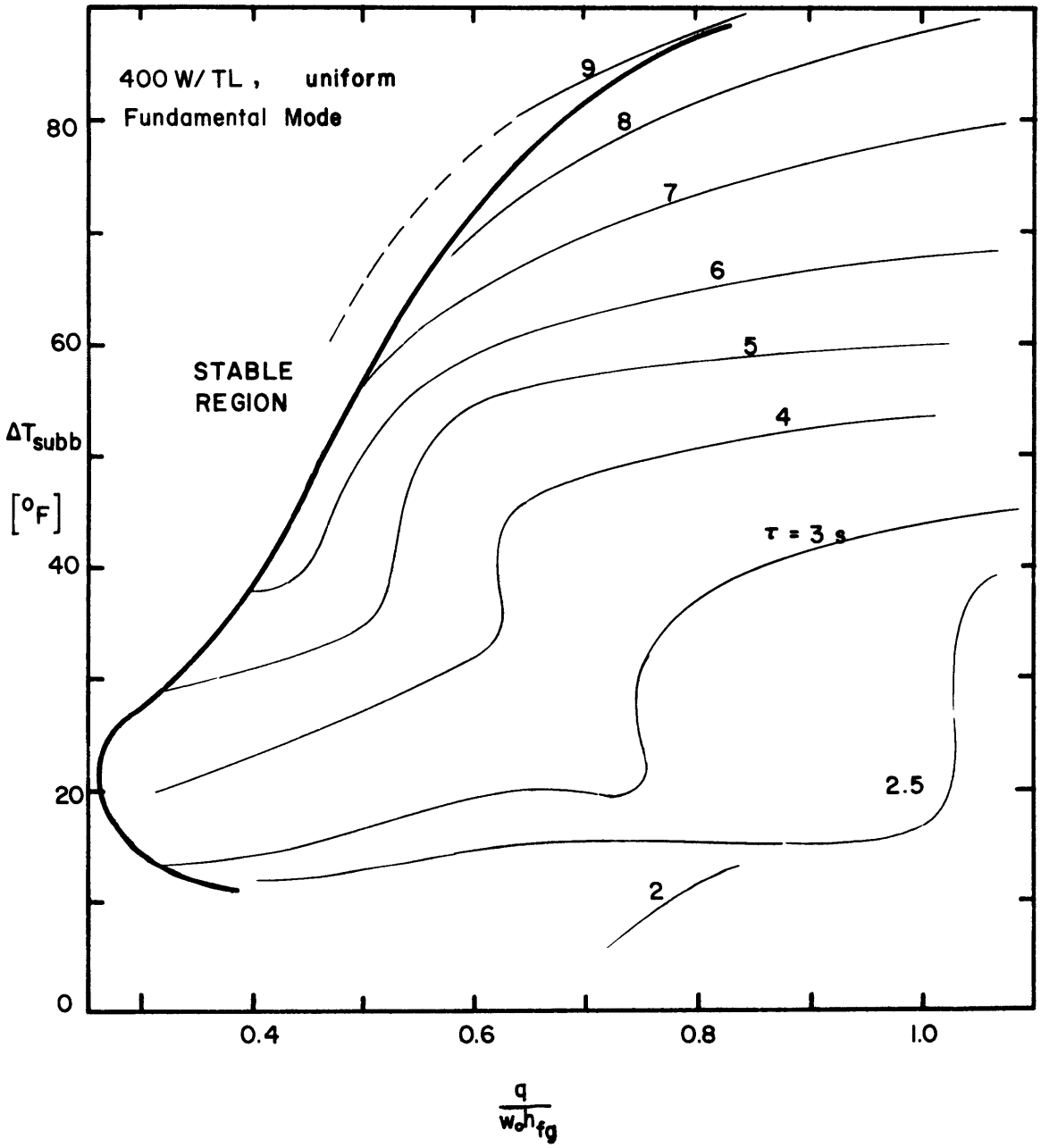

FIG. 7.14 PERIOD OF THE OSCILLATION WITHIN THE UNSTABLE REGION (CONTOUR MAP)

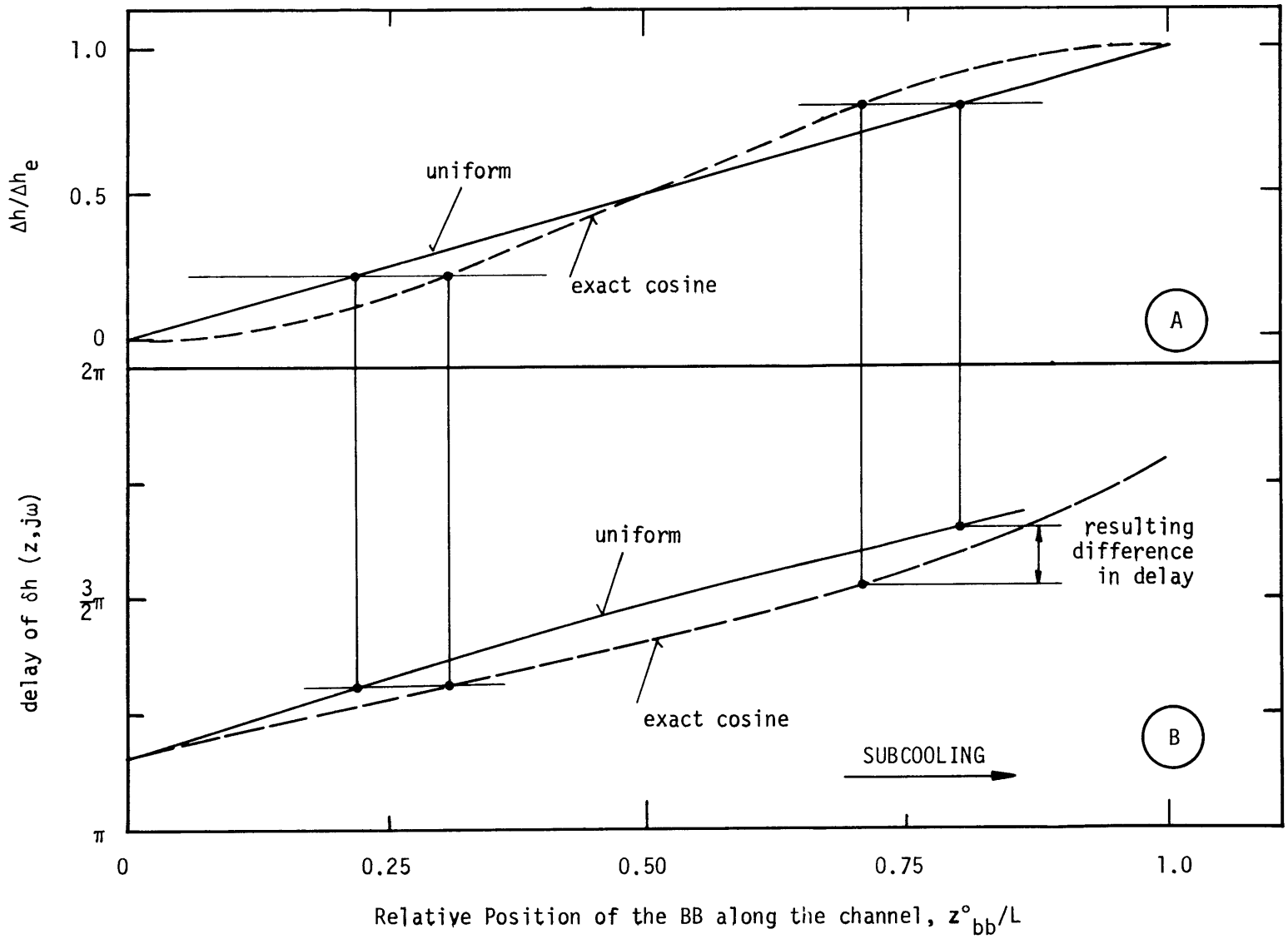

FIG. 7.15 ENTHALPY AND SINGLE-PHASE DELAYS - UNIFORM VERSUS COSINE HEAT FLUX DISTRIBUTION

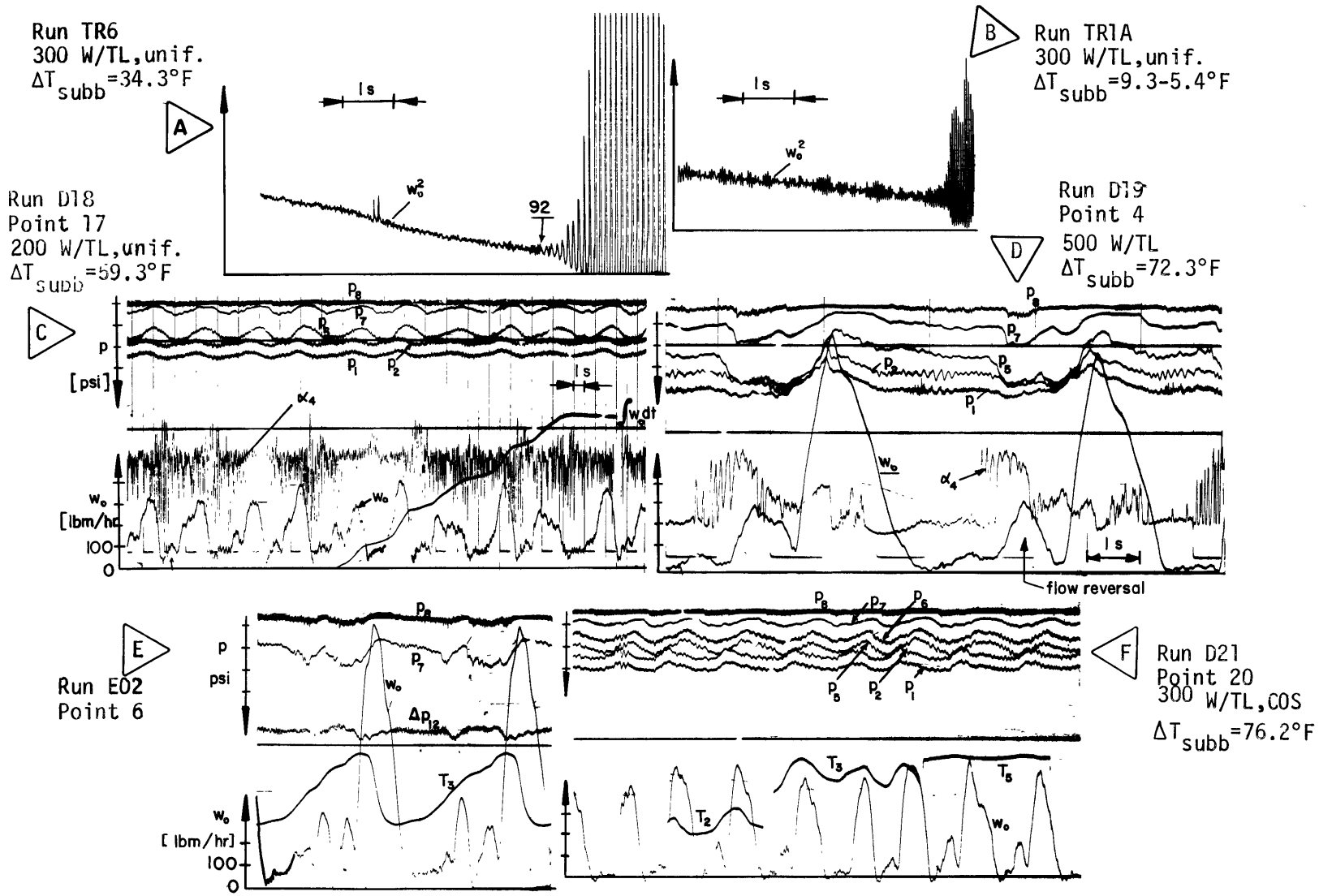

FIG. 7.16 TYPICAL OSCILLATION RECORDINGS

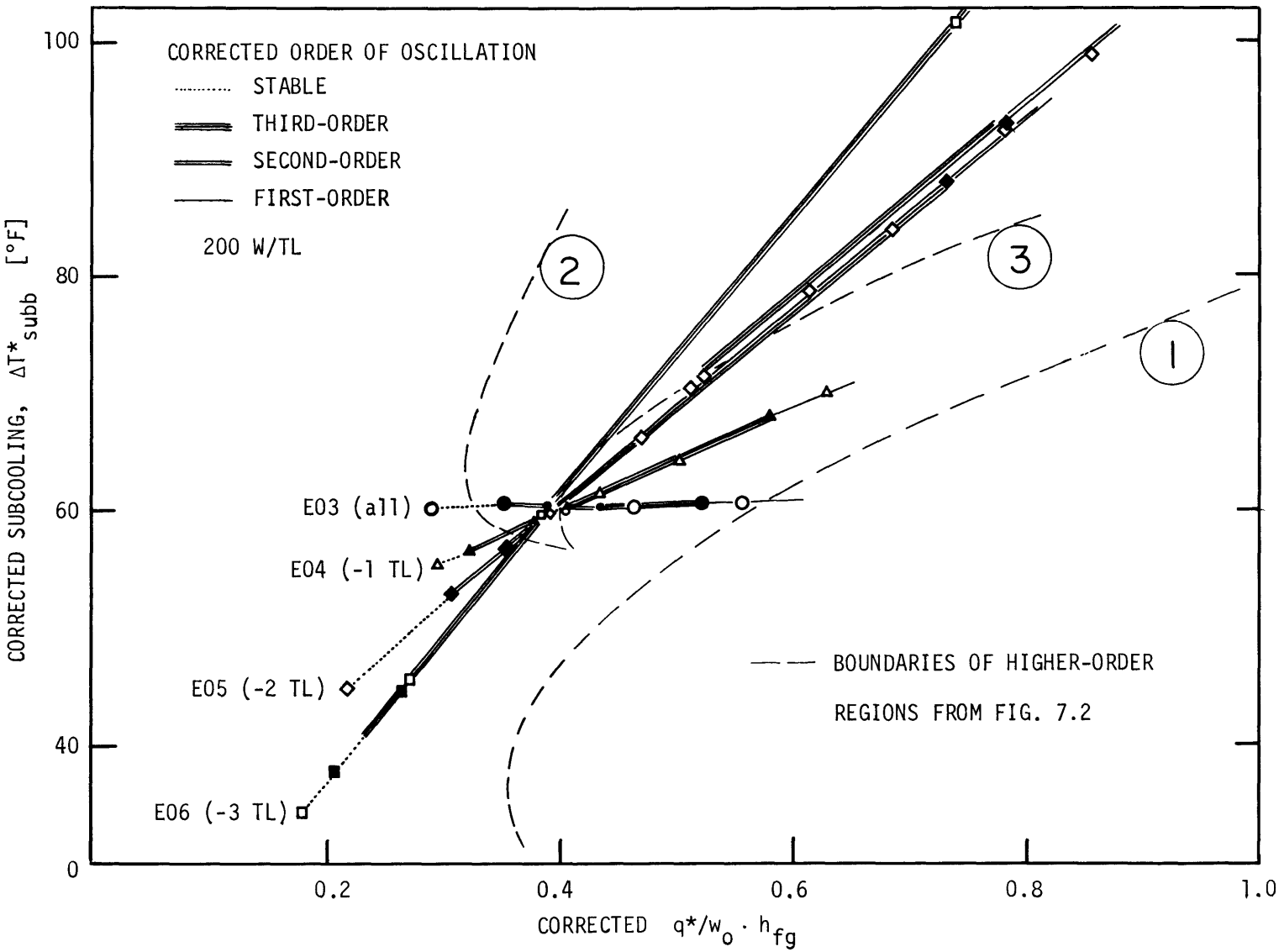

FIG. 7.17 STABILITY MAP IN THE ENTHALPY-SUBCOOLING PLANE - SERIES E EXPERIMENTS

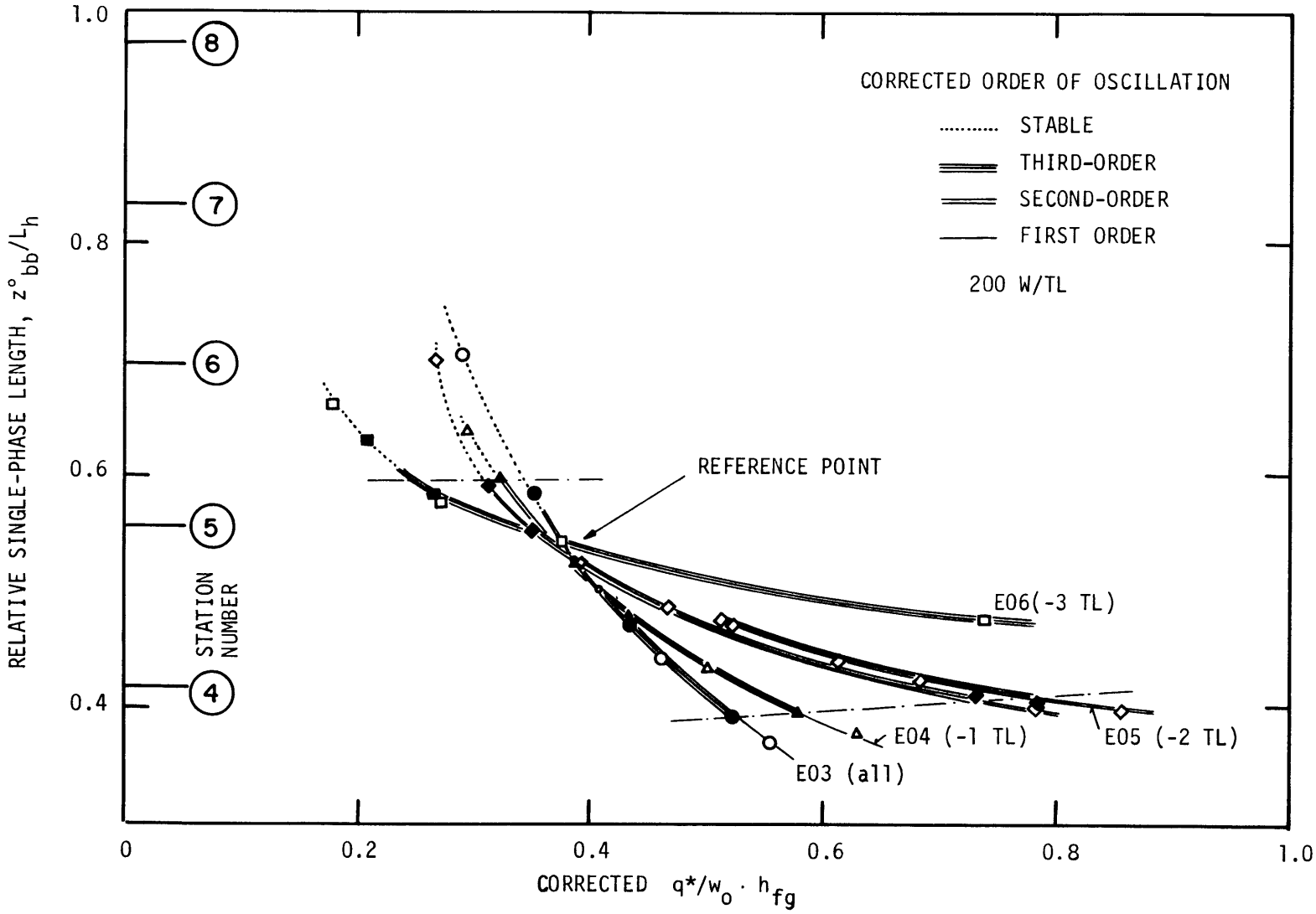

FIG. 7.18 STABILITY MAP IN THE ENTHALPY - SINGLE-PHASE-LENGTH PLANE-SERIES E EXPERIMENTS

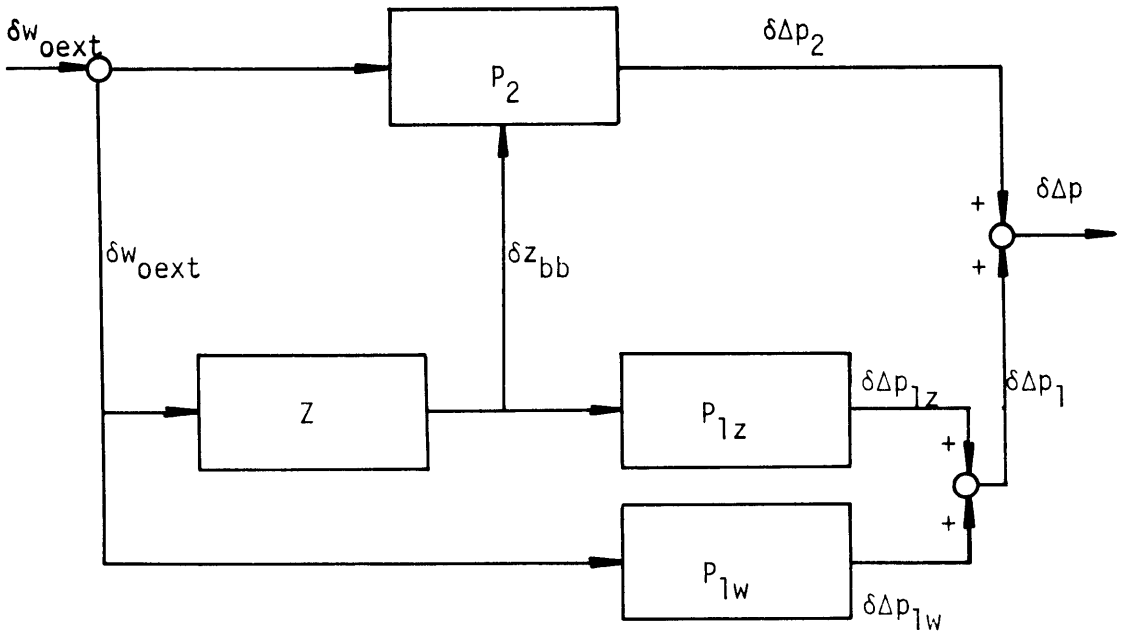

FIG. 8.1 OPEN LOOP BLOCK DIAGRAM OF THE BOILING CHANNEL

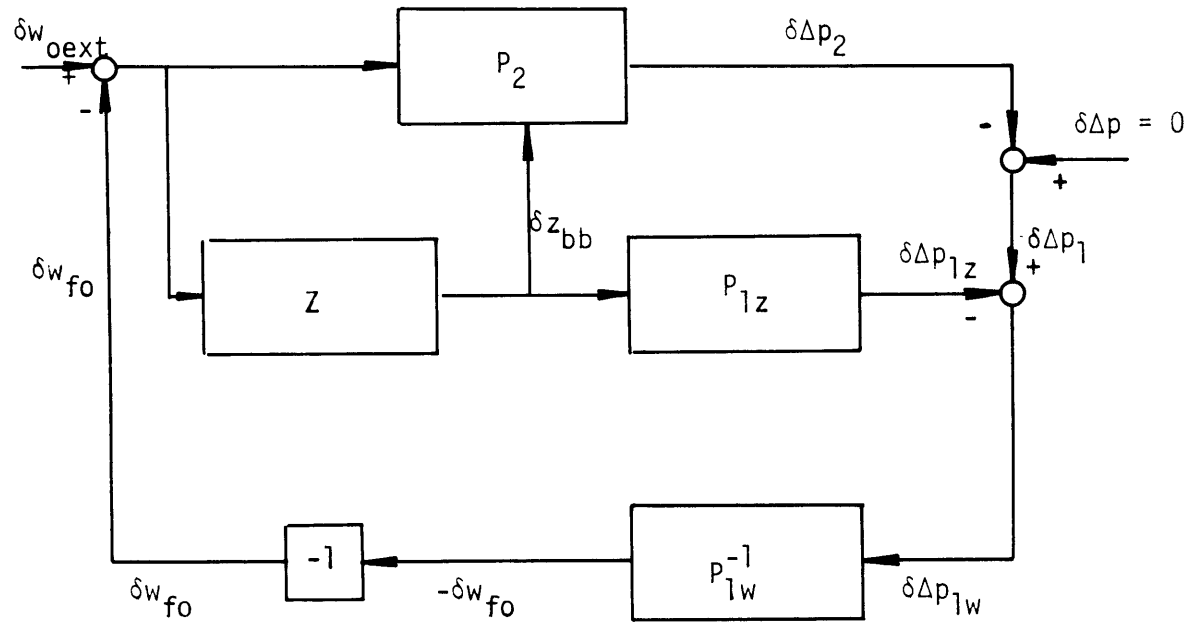

FIG. 8.2 CLOSED LOOP BLOCK DIAGRAM OF THE BOILING CHANNEL

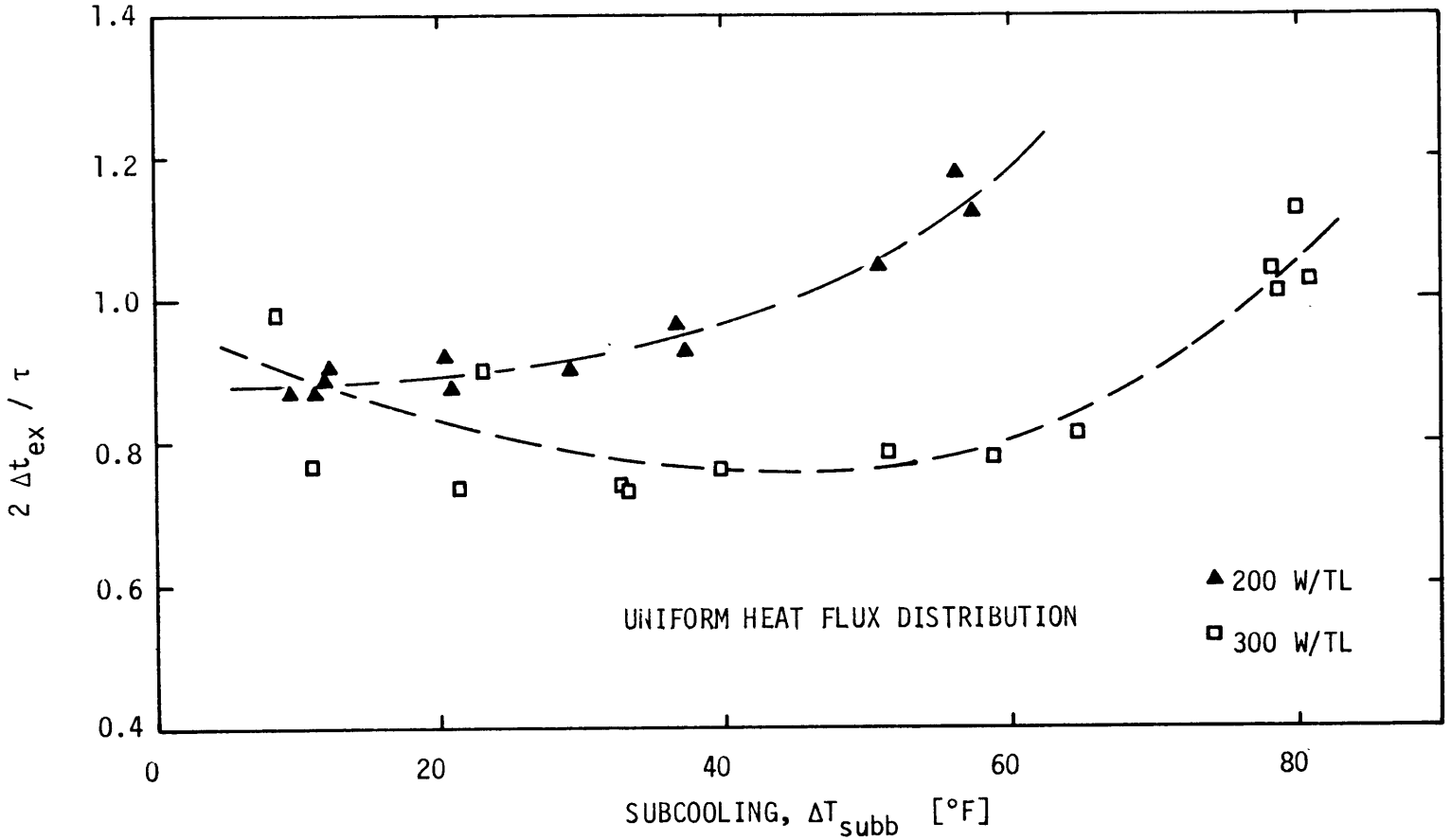

$\Delta t_{ex} = \Delta t_1 + \Delta t_2$; $\Delta t_1 = z^\circ_{bb}/2V_o$; $\Delta t_2 = \int_{z^\circ_{bb}}^{L_h} \frac{dz}{V_g(z)}$, calculated by stepwise integration; values of V_g from PRESDR results

All zero order threshold and transition pts.

FIG. 8.3 CORRELATION OF THE PERIOD OF THE OSCILLATION

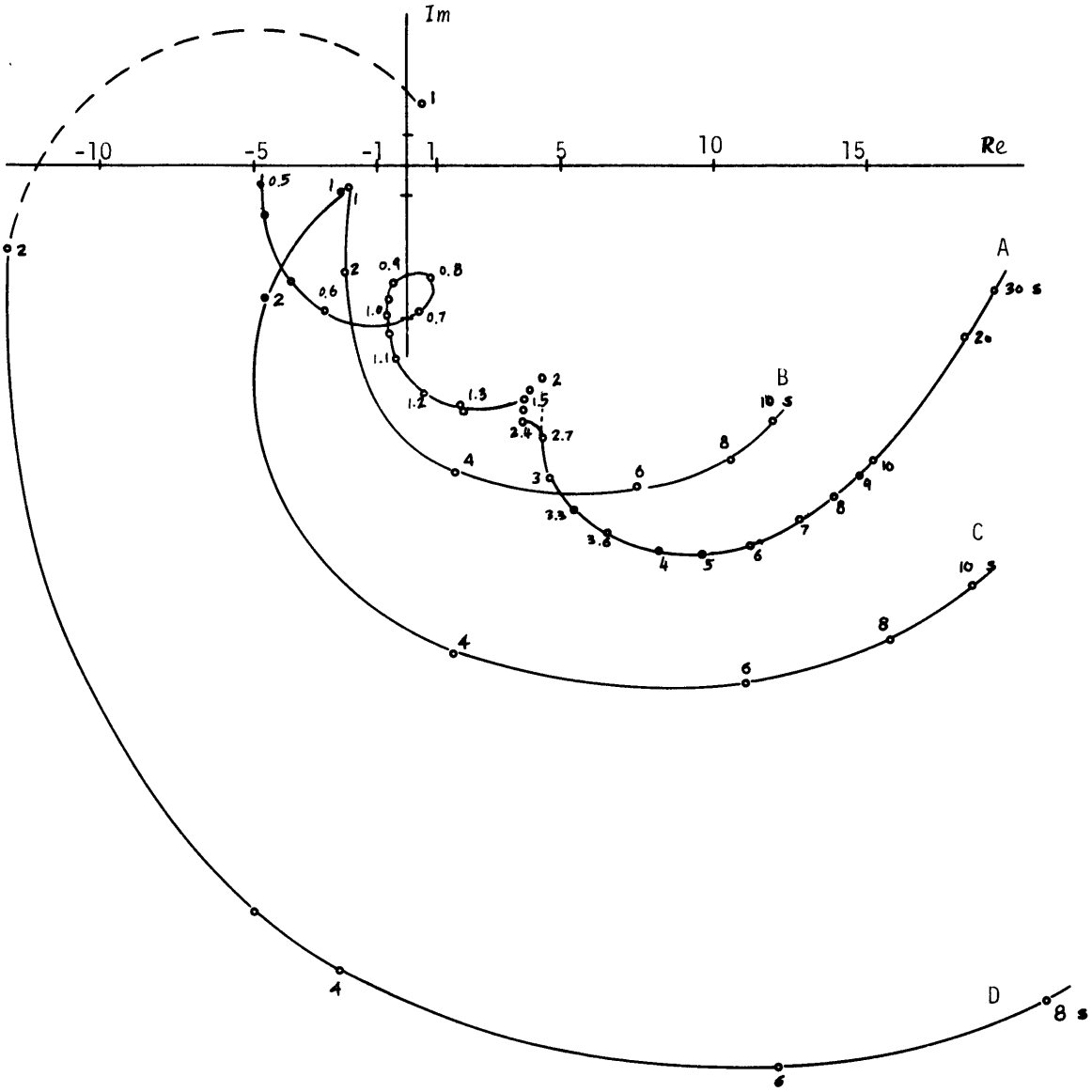

Curve	Point		w_o [lbm/hr]	τ [s]	z^o_{bb}/V_o [s]	
A	D12-01	Stable	547	-	0.960→	Plotted values
B	D12-92	Threshold	410	2.28	0.805	multiplied by 2
C	D12-03	Unstable	310	2.44	0.710	
D	D12-06	Unstable	216	2.43	0.426	

Subcooling, ΔT_{subb} = 8.5 to 5.7 °F ; Power, q_w = 300 W/TL, unif.

The curves are graduated in period [s].

FIG. 8.4 OPEN LOOP TRANSFER FUNCTIONS AT LOW SUBCOOLING

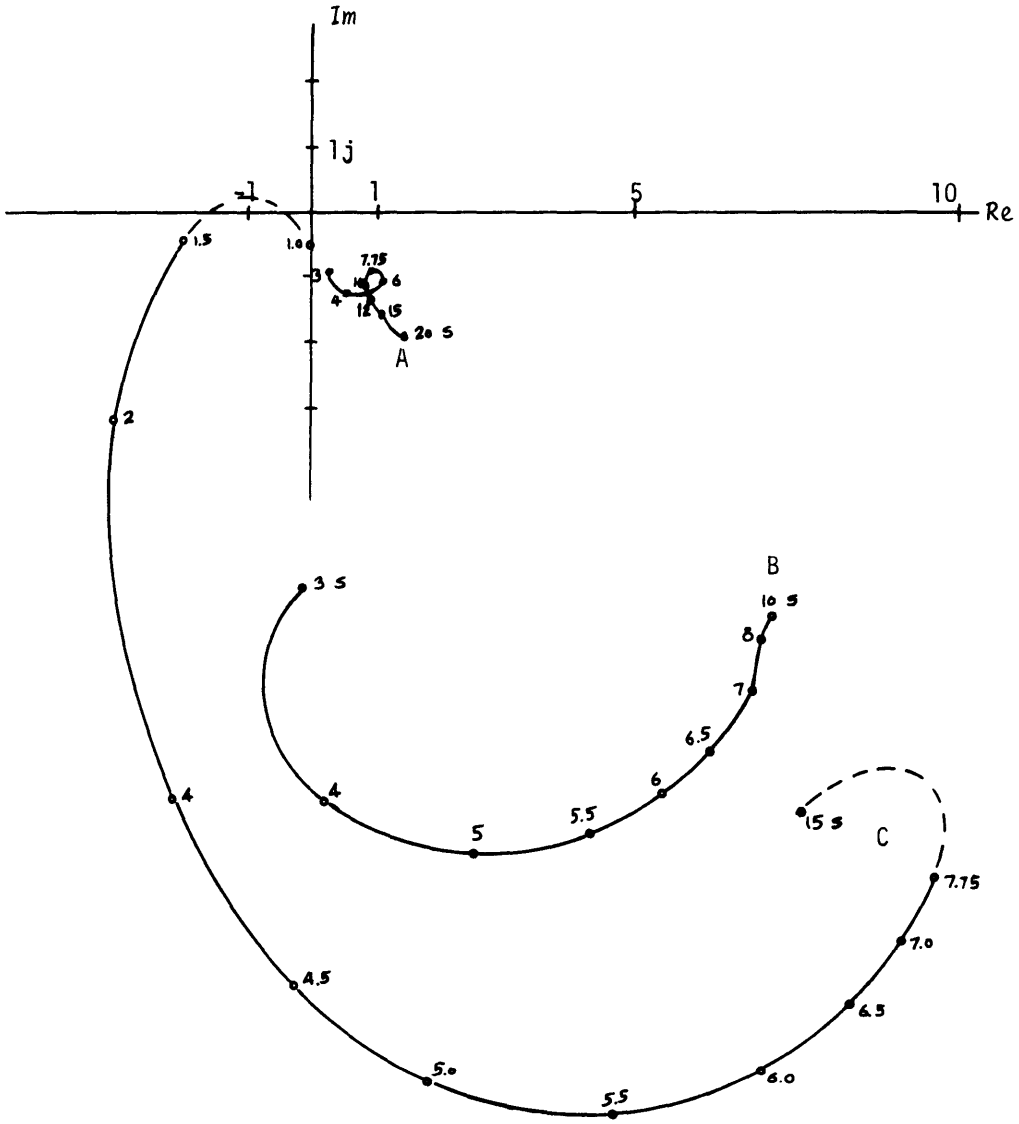

Curve	Point	w_o [lbm/hr]	τ [s]	z°_{bb}/V_o [s]
A	D16-12 Stable	445	-	4.80
B	D16-93 Threshold	225	7.75	5.07
C	D16-14 Unstable	197	7.75	5.18

Subcooling, ΔT_{subb} = 51.5 °F ; Power, q_w = 300 W/TL, unif.
The curves are graduated in periods [s].

FIG. 8.5 OPEN LOOP TRANSFER FUNCTIONS AT HIGH SUBCOOLING